Hinc patriam sustinet

Instituto Superior de Agronomia
Universidade de Lisboa

PROPRIEDADES HIDRÁULICAS DOS SOLOS E MODELAÇÃO PARA A OPTIMIZAÇÃO DA REGA CONSIDERANDO A DINÂMICA DO AZOTO E DOS SAIS

"Documento provisório"

TESE APRESENTADA PARA OBTENÇÃO DO GRAU DE DOUTOR EM ENGENHARIA DOS BIOSSISTEMAS

ORIENTADOR: DOUTOR LUIS ALBERTO SANTOS PEREIRA, PROFESSOR CATEDRÀTICO DO INSTITUTO SUPERIOR DE AGRONOMIA

CO-ORIENTADORA: DOUTORA MARIA DA CONCEIÇÃO PINTO BAPTISTA GONÇALVES, INVESTIGADORA AUXILIAR DO INSTITUTO DE INVESTIGAÇÃO AGRÁRIA E VETERINÁRIA

TIAGO CUNHA BRITO RAMOS

LISBOA

2013

U LISBOA | UNIVERSIDADE DE LISBOA

Agradecimentos

Ao Professor Catedrático Luís Santos Pereira, do Instituto Superior de Agronomia (ISA), um agradecimento muito especial por ter aceitado orientar este trabalho, pelo acolhimento concedido no Centro de Engenharia dos Biossistemas, pelos valiosos ensinamentos, ideias e sugestões transmitidas, pelos esclarecimentos, disponibilidade e apoio prestados e pela leitura e correcções do trabalho.

À Doutora Maria da Conceição Gonçalves, do Instituto Nacional de Investigação Agrária e Veterinária (INIAV), co-orientadora deste trabalho, por me ter aberto a porta para a física do solo e por me ter obrigado a realizar este trabalho.

Ao Investigador José Casimiro Martins, do INIAV, pelos conhecimentos transmitidos ao longo dos últimos doze anos, desde que aceitou acolher a realização de um estágio no Departamento de Ciência do Solo da Estação Agronómica Nacional e co-orientar o trabalho de fim de curso.

Ao Doutor Jiří Šimůnek, da Universidade da Califórnia, Riverside, pelos ensinamentos transmitidos, pela longa colaboração prestada, pela disponibilidade demonstrada e por me obrigar a viajar pelo mundo fora a apresentar os resultados obtidos.

À colega Nádia Castanheira, inicialmente da Universidade de Évora e actualmente do Instituto de Tecnologia Química e Biológica, pela condução dos trabalhos de campo realizados na Universidade de Évora e pela maneira apaixonada como discute os resultados obtidos.

Aos Engenheiros Fernando Pereira Pires e Luís Manuel Fernandes e à Doutora Ângela Prazeres, do INIAV, por todos os ensinamentos transmitidos, esclarecimentos e ajudas nos trabalhos de campo e laboratório.

Ao Professor Catedrático Amílcar Soares, do Instituto Superior Técnico (IST), e Doutora Ana Horta, da Universidade de Sidney, pelos ensinamentos e esclarecimentos na área da geoestatística.

Ao colega David Brito, do IST, pelas simulações realizadas com o modelo SWAT e ensinamentos transmitidos na área da modelação de bacias hidrográficas, à colega Paula Paredes, do ISA, pela disponibilidade e ajuda nos campos da burocracia, e à colega Ângela Moreno, também do ISA, pela colheita de material e ajuda no estudo das propriedades hidráulicas dos solos de Cabo Verde.

À Sr.ª Ana Maria Neves, Sr.ª Teresa Vales, Sr.ª Lurdes Cravo, Sr.ª Clara Pegado e Sr.ª Rosa Rocha, do INIAV, por todas as análises laboratoriais realizadas no âmbito deste trabalho e pela boa disposição manifestada ao longo dos últimos doze anos.

Aos Engenheiros Manuel Aires da Bica e Jesuína Bica, Sr. Romão, Sr. Gamito, Sr. Amaral, Sr. João e Sr. Victor Cunha, do INIAV, e ao Engenheiro João Reis, da Universidade de Évora, sem a ajuda dos quais o trabalho de campo apresentado nesta Tese seria muito difícil de ser realizado.

Agradece-se ainda à Fundação para a Ciência e Tecnologia, pela concessão da Bolsa de Doutoramento SFRH/BD/60363/2009 e pela aprovação dos Projectos PTDC/AGR-AAM/66004/2006 "Optimização da fertilização azotada em função do teor de sal na água de rega – NITROSAL" e PTDC/AGR-AAM/098100/2008 "Gestão Integrada de Fósforo para Controlo da Eutrofização de Bacias Hidrográficas – EUTROPHOS" e ao Programa AGRO, Medida 8,

Acção 8.1, pela aprovação do Projecto 727 “Demonstração e divulgação de gestão integrada da salinidade e da fertilização azotada em solos regáveis do Alentejo”, cujos financiamentos possibilitaram a realização deste trabalho.

Ao meu irmão, pelos programas que, volta e meia, me facilitam a vida e aos meus Pais e amigos por me darem grandes alegrias.

Resumo

A modelação do transporte reactivo de solutos no solo tornou-se numa ferramenta essencial para a implementação de melhores práticas de rega e de fertilização. O modelo HYDRUS é, presentemente, um dos poucos modelos capazes de considerar a componente geoquímica do solo e avaliar os diferentes problemas ambientais de forma integrada. Este modelo foi usado para simular o movimento da água e o transporte de solutos no solo, em duas experiências realizadas em condições de campo, entre 2004 e 2010. Estas experiências foram importantes para identificar os principais processos físicos e químicos que influenciam o movimento de água e o transporte reactivo de solutos nos solos regados com águas salinas. Foram também úteis na avaliação do efeito de diferentes cenários de qualidade de água de rega e de níveis de fertilização azotada na salinização/sodicização do solo, extracção e lixiviação de nutrientes e no rendimento das culturas. O modelo HYDRUS pode ser considerado como uma poderosa ferramenta na análise dos riscos de salinização do solo e do destino das formas azotadas aplicadas na fertilização. Contudo, o uso de modelos deste tipo no estabelecimento de políticas sustentáveis para o regadio é ainda limitado face à considerável necessidade de dados de entrada, nomeadamente a informação sobre as propriedades hidráulicas dos solos. Assim, foram desenvolvidas diferentes funções de pedotransferência (PTFs) para estimar indirectamente aquelas propriedades do solo a partir da informação reunida na base de dados PROPSOLO. Foi desenvolvido um conjunto de PTFs, para estimar as propriedades de retenção de água após agrupar os dados de acordo com a textura do solo, a profundidade e a massa volúmica aparente. Foram também desenvolvidas PTFs para estimar as propriedades de retenção de água a partir da granulometria das partículas e usando o diagrama textural e um método geoestatístico no processo. Finalmente, desenvolveram-se PTFs para os solos de Cabo Verde. As PTFs podem ter múltiplas aplicações na gestão da rega e de bacias hidrográficas. No entanto, é ainda necessário estender a informação de base a outras regiões de Portugal e de Cabo Verde, bem como aumentar o conhecimento sobre a função da condutividade hidráulica destes solos.

Palavras-chave: Águas salinas; Funções de pedotransferência; Lixiviação de azoto; Propriedades hidráulicas do solo; Transporte reactivo.

Abstract

Modeling has become an essential tool for implementing better irrigation and fertilization practices. The HYDRUS software package is currently one of the few models capable of considering multicomponent geochemistry and evaluating multiple environmental problems in an integrated way. The model was used to simulate water movement and solute transport in two complex experiments carried out under field conditions, between 2004 and 2010. The field experiments were helpful to identify the main physical and chemical processes influencing soil water flow and multicomponent solute transport in soils irrigated with saline waters. They were further useful for evaluating different irrigation water quality and fertilization scenarios while considering soil salinization/sodification risks, root nutrient uptake, nutrient leaching, and crop yield. HYDRUS proved to be a powerful tool for establishing sound irrigation policies. However, the considerable demand on input data, namely, soil hydraulic properties, has been limiting its use (and other reactive transport models). Different pedotransfer functions (PTFs) were thus established to indirectly estimate soil hydraulic properties from the soil information available in the PROPSOLO database. A set of class-PTFs were developed to estimate water retention properties after grouping data by soil texture, soil horizon, and bulk density. A different procedure was also presented to estimate water retention properties from particle size distribution using the soil texture triangle and ordinary kriging. Finally, a set of PTFs were established for Cape Verde soils. All these PTFs may have multiple applications in irrigation management and watershed modelling. However, it is still necessary to further extend those PTFs to other regions of Portugal and Cape Verde, and to gain more knowledge on the hydraulic conductivity functions of those soils so that they can be used in reactive transport modeling.

Keywords: Brackish waters; Nutrient leaching; Pedotransfer functions; Reactive transport modeling; Soil hydraulic properties.

Index

Chapter 1

Introduction

1. General Introduction

In the last few decades, modeling has become an essential tool for implementing better irrigation and fertilization practices, predicting groundwater quality, and quantifying salinization and sodification risks (e.g., Pereira et al., 1992, 1995; Cameira, 2005; 2007; Gonçalves et al., 2006; Xu et al., 2013). Various analytical and semianalytical solutions were made available for relatively simple applications, where specific boundary conditions need to be considered, and where the level of accuracy or detail may not be sufficient to answer specific management questions (Corwin et al., 2007; Romano et al., 2011). More complex numerical models have also been developed to allow considerations of a large number of simultaneous nonlinear transient processes, such as simulating subsurface water flow and the transport of major soluble ions in and below the root zone (Šimůnek and Bradford, 2008). However, these complex codes normally require large amounts of specialized input data that may not be directly available.

Most vadose zone models are typically based on the numerical solution of the Richards equation for variably-saturated water flow, and on analytical or numerical solutions of the Fickian-based convection–dispersion equation (CDE) for solute transport. A sink term is usually included in these equations to account for root water and nutrient uptake, and the effects of water and osmotic stresses (Feddes and Raats, 2004; Šimůnek and Hopmans, 2009). Solutions of the Richards equation require information on the soil hydraulic properties, i.e., the soil water retention, $\theta(h)$, and hydraulic conductivity, $K(h)$ or $K(\theta)$, functions, that are non-linear relationships between matric pressure head, h, soil water content, θ, and hydraulic conductivity, K. Solving the CDE equation in a steady-state, one dimensional water flow further requires information on the solute transport parameters, i.e., the dispersion coefficient, D, the mean pore-water velocity, v, and the retardation factor, R, when reactive solute transport is considered (van Genuchten and Wierenga, 1976). Because D depends upon v, most vadose zone models define an alternative mixing parameter, the dispersivity, λ, which describes spreading or dispersion of a surface-applied solute pulse (Perfect et al., 2002; Vanderborght and Vereecken, 2007).

Classical methods for direct measurement of soil hydraulic properties (Dane and Topp, 2002) and solute transport parameters (Mallants et al., 1994) are expensive, time-consuming, and impractical for large-scale applications in which many samples are required to quantify the

spatial and temporal variability of those properties. This has, in part, limited vadose zone modeling, especially when large scale applications are considered, but has also motivated the development of pedotransfer functions (PTFs), i.e., attempts to predict those properties from more easily obtained field data, such as soil texture information, soil bulk density, soil organic content, and other basic physical, chemical, and mineralogical properties (Pachepsky and Rawls, 2004). These relations are usually obtained by simply averaging the dataset after grouping data, by using regression analysis techniques or by applying more complex data mining tools. PTFs for determining soil hydraulic properties are now quite numerous (e.g., Gupta and Larson, 1979; Saxton et al., 1986; Gonçalves et al., 1997; Schaap et al., 2001; Bruand et al., 2003; Nemes et al., 2006; Al Majou et al., 2008; Haghverdi et al., 2012), but their application are normally limited to the regions were they were developed, i.e., PTFs should not be used to make predictions for soils that are outside the range of soils used to derive the PTFs (Wösten et al., 2001). In contrast, indirect determination of solute transport parameters is still quite rare (Gonçalves et al., 2001, Perfect et al., 2002). The main reason is that large databases have been and continue to be compiled for developing PTFs for estimating soil hydraulic properties (Wösten et al., 1999; Nemes et al., 2001; Weynants et al., 2013), while a large dataset containing solute transport parameters and other basic soil properties is still missing (Vanderborght and Vereecken, 2007).

Vadose zone modeling has been also limited by the quality of the models used, especially when reactive solute transport is to be considered. Solute partitioning between the solid and liquid phases has generally been treated in a simplistic way, by means of a linear distribution coefficient, K_d. Although reasonable for certain applications, numerous studies have demonstrated the inherent limitations in applying simplistic empirical expressions (e.g., K_d and linear kinetic terms) to describing solute transport at the field scale (Seaman et al, 2012). Only a few models have been able to consider that the soil liquid phase always contains a mixture of many ions that may interact, create complex species, precipitate, dissolve, and/or compete with each other for sorption sites on the solid phase (van Genuchten and Šimůnek, 2004; Seaman et al, 2012). These more complex vadose zone models allow for multiples solutes to be considered in an integrated way, thus avoiding giving particular emphasis to one environmental problem over others. Multicomponent solute transport, i.e., coupling of water flow, advective–dispersive transport, and multicomponent geochemistry into one integrated model thus provides a much-

needed tool for studying the interplay between different processes, including the various nonlinear feedbacks that occur between the different processes (Jacques et al., 2008) and helps to identify important data gaps and research priorities under more natural conditions (Seaman et al, 2012).

2. Problem Definition

In regions with scarce water resources, it is not always possible to irrigate with waters of good quality, and therefore even saline waters are seen as an important resource (Pereira et al., 2009). As a result, human-induced salinization and sodification are among the most important and widespread soil degradation processes, generally associated with irrigation practices and poor water management. As rainfall may not be sufficient to remove the salts accumulated during irrigation, it is often necessary to monitor soil and water quality, and to promote efficient leaching management to counteract soil salinization. Irrigation volume and frequency are therefore adjusted to remove salts from the root zone (e.g., Gonçalves et al., 2007; Pereira et al., 2007). However, promoting salt leaching also results in increased nitrogen leaching, which contributes to the degradation of groundwater reservoirs. As non-point source pollution from agricultural fertilization is considered to be a leading cause of water quality problems, especially in regions like those mentioned above, an integrated approach should always be considered to avoid emphasizing one problem over the other.

Assessing simultaneous soil salinization/sodification risks and non-point source pollution from agricultural fertilization can be achieved via multicomponent solute transport modeling. The HYDRUS software package (Šimůnek et al., 2008b) is one of the few state-of-the-art models capable of evaluating major ion chemistry in the subsurface, assessing the effects of irrigation water quality on groundwater recharge, and quantifying the amount of water and amendment required in order to reclaim sodic and saline soils to desired levels of salinity and exchangeable sodium percentage (Šimůnek and Suarez, 1997; Šimůnek and Valocchi, 2002; Gonçalves et al., 2006). The model can thus be used to predict the overall salinity given by the electrical conductivity of the soil solution (EC_{sw}), the concentration of individual ions (Na^+, Ca^{2+}, Mg^{2+}, K^+, and Cl^-), and sodium adsorption ratio (SAR), while also quantifying water uptake reductions

due to the use of saline waters, and nitrogen fate (NO_3^-, and NH_4^+ concentrations) in the soil and leaching (Gärdenäs et al., 2005). However, evaluation of these models under field conditions is still very limited, not only due to the lack of adequate field data necessary to calibrate/validate it, but mainly because of their need for a variety of input data, including soil hydraulic properties, solute transport parameters, parameters characterizing the partitioning between the solid phase and the soil solution, and meteorological and crop related information. Due to large need of information, it thus seems necessary to identify the main processes involved in multicomponent solute transport modeling, since not all applications need to be described while considering full model complexity. It is also essential to develop PTFs for estimating many of those parameters indirectly, allowing a wider application of multicomponent solute transport models for evaluating agricultural practices in different soils, climates, and land uses.

Many PTFs have been developed over the last few decades for estimating soil hydraulic properties (e.g., Gupta and Larson, 1979; Saxton et al., 1986; Vereecken et al., 1989; Wösten et al., 1999; Schaap et al., 2001; Bruand et al., 2003; Nemes et al., 2006). However, these 'external' or 'international' PTFs cannot be used lightly as they were never tested with Portuguese soil data, which means that the hydraulic characteristics of the Portuguese soils may fall outside the range of the original databases used to develop those PTFs (Wösten et al., 2001). Also, most of those PTFs were developed using different texture systems (normally the USDA texture system) from the one used in the Portuguese soil survey database (the International Soil Science Society system - ISSS). Interpolation techniques are thus necessary to convert the ISSS texture limits into those required by 'international' PTFs (Nemes et al., 1999; Shirazi et al., 2001; Nemes and Rawls, 2006). To this date, only the interpolation technique proposed by Gomes and Silva (1962) was used in national applications, which may lead to inaccurate results as interpolation was achieved by means of linear relationships between known limits of particle size distribution. Thus, there is currently a need to test some of the PTFs developed abroad while considering all the differences between PTFs needs and national datasets.

Gonçalves et al. (1997) proposed the first PTFs for estimating soil hydraulic properties of Portuguese soils. The water retention properties were described with the van Genuchten (1980) function, while the unsaturated hydraulic conductivity was defined with Gardner's model

(Gardner, 1958). Later, Gonçalves et al. (1999) developed new PTFs for obtaining the soil hydraulic parameters of the much more popular Mualem-van Genuchten functions (van Genuchten, 1980), while Paz et al. (2009) developed PTFs for point specific water retention values. Although these PTFs can be used to derive the necessary hydraulic information for vadose zone modeling, they require a large set of input parameters (texture information, bulk density, organic matter content, soil depth, and pH) that may not always be available in soil survey databases, as is the case of bulk density which cannot be found in national soil survey datasets prior to 2003.

Another important setback is the limited dataset used to derive Gonçalves et al. (1997; 1999) and Paz et al. (2009) PTFs, and their representativeness in generating soil hydraulic properties for the entire country. One has to have in mind that national soil survey datasets contain a significant amount of water retention information determined on undisturbed soil samples that could theoretically be included in the development of new PTFs (IDRHA, 2003; Geometral, 2004; DGADR, 2007). Unfortunately, most of that information is restricted to a few specific water retention points (usually, the field capacity and wilting point), making it impossible to describe $\theta(h)$ with a continuous function like the van Genuchten model. Also, methodologies used in those studies have long been considered less adequate when applied to certain pressure heads (Martins, 1989; ISO 11274:1998), thereby justifying not considering those dataset in the development of new PTFs. Therefore, the only reliable dataset available for developing PTFs for Portugal, which also follows standard methodologies (ISO 11274:1998), is the PROPSOLO database (Ramos et al., 2011). This database gathers all information on soil hydraulic and pedological properties from soil profiles obtained from research projects and academic studies performed at Estação Agronómica Nacional, in which Instituto Superior de Agronomia also contributed substantially. It is also the only database with information on the $K(h)$ functions of Portuguese soils. While earlier PTFs (Gonçalves et al., 1997; 1999) can provide reasonable estimates of soil hydraulic properties in Portugal, they need to be updated in order to take into account not only data available currently available, but also the need for simplifying the number of predictors necessary to estimate soil hydraulic properties.

The PROPSOLO database can potentially also be helpful to estimate water retention properties in other Mediterranean areas, and in the Macaronesia region, particularly in Cape Verde where the lack of information on soil hydraulic properties, mainly field capacity and wilting point, has limited the implementation of appropriate irrigation water management practices. As referred above, PTFs should not be used to make predictions for soils that fall outside the range of soils used to derive the PTFs (Wösten et al., 2001). While applying those PTFs to regions of the world with different soils and climates may reveal unsatisfactory results (van den Berg et al., 1997; Tomasella and Hodnett, 1998; Botula et al., 2012), the soil information available in PROPSOLO extends from dry temperate regions in southern Portugal's mainland to the volcanic Atlantic islands of Madeira and Azores. The database contains therefore a wider variety of information than the one normally found in other soil databases and could theoretically be helpful for estimating water retention properties in Cape Verde.

3. Objectives

The main objectives of this work are:

1. Identify the main physical and chemical processes influencing soil water flow and multicomponent solute transport in soils irrigated with saline waters;
2. Evaluate different irrigation water quality and fertilization scenarios by considering soil salinization/sodification risks, root nutrient uptake, nutrient leaching, and crop yield;
3. Develop a soil database capable of gathering reliable information on soil hydraulic properties of Portuguese soils;
4. Update and simplify the existing PTFs to estimate water retention properties to be used in soil modelling;
5. Extend the soil database to Cape Verde and gain knowledge on local water retention properties.

The PTFs here developed are limited to water retention properties as the information available on hydraulic conductivity of Portuguese soils continue to be very limited (300 soil horizons) taking into account the spatial variability of this parameter.

4. Outline of Thesis

This work is organized into nine chapters, including Chapter 1 were the main objectives of this work are given.

Chapter 2 evaluates the effectiveness of HYDRUS-1D (Šimůnek et al., 2008a) to simulate water flow and multicomponent solute transport in two soils irrigated with blended saline waters and waters with different nitrogen concentrations. Two modeling concepts based on the mechanisms describing solute partitioning between the liquid and solid phases, and the complex chemical reactions involved in solute transport are used. These modeling concepts allow simulating the transport and reactions of salts and nitrogen species in the soil profile in an integrated way, while also quantifying water and nutrient uptake reductions due to the use of saline waters. The approach followed shows how useful HYDRUS-1D can be in establishing sound irrigation policies in order to mitigate soil salinization/sodification and non-point source pollution from agricultural applications of fertilizers in irrigated areas located in water scarce regions.

Chapter 3 upgrades the previous work by applying the HYDRUS-2D model (Šimůnek et al., 2006) to simulate water flow and solute transport in a similar field experiment. The two-dimensional approach allows a better description of the drip irrigation system used, and also considers water and solute fluxes, and pressure head and concentration gradients in the horizontal direction. The modeling approach is applied to investigate sweet sorghum response to irrigation scenarios with different levels of nitrogen and different water qualities. The best irrigation and fertigation management practices are defined in order to increase nutrient uptake and reduce nutrient leaching.

Chapter 4 evaluates the combined effects of the irrigation water quality and fertilization scenarios described in Chapter 3 on sweet sorghum dry biomass, sugar content, and sugar yield functions. The yield relations are assessed with traditional multiple regression techniques as the HYDRUS

software package has no crop growth module incorporated to analyze the relations between soil processes and crop parameters.

Chapter 5 summarizes the development, structure, and contents of the novel version of the PROPSOLO (*PROPriedades do SOLO*) database. It is a searchable SQL-database that is compatible to many international databases and applications. Contents of PROPSOLO have already served as source data to a range of different studies. One example is here demonstrated where the variation of soil hydraulic properties within the ISSS texture classes is analyzed. Other applications have been the development of PTFs for estimating soil hydraulic properties and solute transport parameters from basic soil data. The database can be further used for scenario analyses where the modeling strategies presented in Chapters 2 and 3 are applied to different soils, crops, climates, and agricultural practice.

Chapter 6 describes a set of class-PTFs to estimate water retention properties after grouping data by soil texture, soil horizon, and bulk density. Class-PTFs are considered the simplest approach for presenting reliable soil hydraulic information to irrigation water managers and hydrological modelers due to the very basic data needs and comparable estimation accuracies to those obtained with more complex functions. A simple, inexpensive, and feasible approach is also presented in order to integrate the class-PTFs into soil survey maps and to derive maps of the available water capacity. These maps are then used for modeling the water balance in a small catchment area while also considering the spatial variability of soil retention properties.

Chapter 7 outlines a procedure to estimate water retention properties from particle size distribution using a geostatistical approach. Most PTFs use soil texture based information as the main predictor to estimate the hydraulic behavior of soils. The proposed method develops simplified tools for estimating the field capacity and wilting point from soil texture, and may eventually serve as an alternative to the traditional statistical regression and data mining techniques used to derive PTFs. The new method simplifies the number of input parameters necessary to estimate water retention properties and produces an estimation accuracy comparable to those found when using more complex methods.

Chapter 8 gains knowledge on the hydraulic behavior of the soils of Cape Verde and provides information for soil water balance modelling in the region. Most PTFs have been developed

based on the information collected in North American or European soils, and thus their use can hardly be extended to other regions of the world as Cape Verde. The water retention properties of Cape Verde soils are investigated and new PTFs are presented in order to improve irrigation water management practices in the region. Although care should be taken when using the new developed PTFs, the estimation accuracy is always better than when using reference PTFs, thereby justifying their development.

Chapter 9 presents the general conclusions and future perspectives for this work.

5. References

Al Majou, H., Bruand, A., Duval, O., Le Bas, C., Vautier, A., 2008. Prediction of soil water retention properties after stratification by combining texture, bulk density and the type of horizon. Soil Use Manage. 24, 383-391.

Botula, Y.-D., Cornelis, W.M., Baert, G., Van Ranst, E., 2012. Evaluation of pedotransfer functions for predicting water retention of soils in Lower Congo (D.R. Congo). Agric. Water Manage. 111, 1-10.

Bruand, A., Pérez Fernandez, P., Duval, O., 2003. Use of class pedotransfer functions based on texture and bulk density of clods to generate water retention curves. Soil Use Manage. 19, 232-242.

Cameira, M.R., Fernando, R.M., Ahuja, L.R., Ma, L., 2007. Using RZWQM to simulate the fate of nitrogen in field soil–crop environment in the Mediterranean region. Agric. Water Manage. 90, 121-136.

Cameira, M.R., Fernando, R.M., Ahuja, L.R., Pereira, L.S., 2005. Simulating the fate of water in field soil–crop environment. J. Hydrol. 315, 1-24.

Corwin, D.L., Rhoades, J.D., Šimůnek, J., 2007. Leaching requirement for soil salinity control: Steady-state versus transient models. Agric. Water Manage. 90, 165-180.

Dane, J.H., Topp, G.C., 2002. Methods of soil analysis. Part 4, Physical methods. Soil Science Society of America book Series, Madison, Wisconsin.

DGADR, 2007. Extensão do estudo de caracterização dos solos e esboço de aptidão das terras para o regadio à escala 1:25000 aos blocos de Serpa e Enxoé da área a beneficiar com o Empreendimento de Fins Múltiplos de Alqueva. Memória descritiva. Direcção Geral de Agricultura e Desenvolvimento Rural, Ministério da Agricultura, do Desenvolvimento Rural e das Pescas, Lisboa, 105 pp.

Feddes, R.A., Raats, P.A.C., 2004. Parameterizing the soil–water–plant–root system. In: Feddes, R.A., de Rooij, G.H., van Dam, J.C. (Eds.), Proceedings of the Unsaturated Zone Modelling: Progress, Challenges and Applications, pp. 95–141. Wageningen UR Frontis Series, vol. 6. Kluwer Academic Publishers, Dordrecht, The Netherlands.

Gärdenäs, A., Hopmans, J.W., Hanson, B.R., Šimůnek, J., 2005. Two-dimensional modeling of nitrate leaching for various fertigation scenarios under micro-irrigation. Agric. Water Manage. 74, 219-242.

Gardner, W.R., 1958. Some steady-state solutions of the unsaturated moisture flow equation with application to evaporation from water table. Soil Sci. 85, 228-232.

Geometral, 2004. Elaboração da carta de solos e de aptidão das terras da Zona Interior Centro. Memória descritiva. Instituto de Desenvolvimento Rural e Hidráulica, Ministério da Agricultura, do Desenvolvimento Rural e das Pescas, Lisboa, 289 pp.

Gomes, M.P., Silva, A.A., 1962. Um novo diagrama triangular para a classificação básica da textura do solo. Garcia da Orta 10, 171–179.

Gonçalves, J.M., Pereira, L.S., Fang, S.X., Dong. B., 2007. Modelling and multicriteria analysis of water saving scenarios for an irrigation district in the upper Yellow River Basin. Agric. Water Manage. 94, 93-108.

Gonçalves, M.C., Almeida, V.V., Pereira, L.S., 1999. Estimation of hydraulic parameters for Portuguese soils. In: van Genuchten, M.Th., Leij, F., Wu, L. (Eds.), Characterization and measurement of the hydraulic properties of unsaturated porous media. Part 2, pp 1199-1210. University of California Riverside, CA, USA.

Gonçalves, M.C., Leij, F.J., Schaap, M.G., 2001. Pedotransfer functions for solute transport parameters of Portuguese soils. Euro. J. Soil Sci. 52, 563-574.

Gonçalves, M.C., Pereira, L.S., Leij, F.J., 1997. Pedo-transfer functions for estimating unsaturated hydraulic properties of Portuguese soils. Euro. J. Soil Sci. 48, 387-400.

Gonçalves, M.C., Šimůnek, J., Ramos, T.B., Martins, J.C., Neves, M.J., Pires, F.P., 2006. Multicomponent solute transport in soil lysimeters irrigated with waters of different quality. Water Resour. Res. 42, 17, W08401, doi:10.1029/2005WR004802.

Gupta, S.C., Larson, W.E., 1979. Estimating soil water retention characteristics from particle size distribution, organic matter content, and bulk density. Water Resour. Res. 15, 1633-1635.

Haghverdi, A., Cornelis, W.M., Ghahraman, B., 2012. A pseudo-continuous neural network approach for developing water retention pedotransfer functions with limited data. J Hydrol. 442-443, 46-54.

IDRHA, 2003. Estudo de caracterização dos solos e esboço de aptidão das terras para o regadio à escala 1:25.000 na área a beneficiar com o Empreendimento de Fins Múltiplos de Alqueva. Relatório final. Divisão de Solos, Direcção de Serviços dos Recursos Naturais e Aproveitamentos Hidroagrícolas, Instituto de Desenvolvimento Rural e Hidráulica, Ministério da Agricultura, do Desenvolvimento Rural e das Pescas, Lisboa, 173 pp.

ISO 11274:1998. Soil quality – Determination of the water-retention characteristics – Laboratory methods.

Jacques, D., Šimůnek, J., Mallants, D., van Genuchten, M.Th., 2008. Modeling coupled hydrological and chemical processes: Long-term uranium transport following mineral phosphorus fertilization. Vadose Zone J. 7, 698-711.

Mallants, D., Vanclooster, M., Meddahi, M., Feyen, J., 1994. Estimating solute transport in undisturbed soil columns using time domain reflectrometry. J Cont. Hydrol. 17, 91-109.

Martins, J.C., 1989. Contribuição para a caracterização hidrológica dos solos de Portugal. Dissertação Elaborada para acesso à categoria de Investigador Auxiliar. Estação Agronómica Nacional, Instituto Nacional de Investigação Agrária, Oeiras, 304 pp.

Nemes, A., Rawls, W.J., 2006. Evaluation of different representations of the particle-size distribution to predict soil water retention. Geoderma 132, 47-58.

Nemes, A., Rawls, W.J., Pachepsky, Y.A., 2006. Use of a nonparametric nearest-neighbor technique to estimate soil water retention. Soil Sci. Soc. America J. 70, 327–336.

Nemes, A., Schaap, M.G., Leij, F.J., Wösten, J.H.M., 2001. Description of the unsaturated soil hydraulic database UNSODA version 2.0. J. Hydrol. 251, 151-162.

Nemes, A., Wösten, J.H.M., Lilly, A., Oude Voshaar, J.H., 1999. Evaluation of different procedures to interpolate particle-size distribution to achieve compatibility within soil databases. Geoderma 90, 187-202.

Pachepsky, Y.A., Rawls, W.J., 2004. Development of pedotransfer functions in soil hydrology. Elsevier, Amsterdam, The Netherlands.

Paz, A.M., Cipriano, D., Gonçalves, M.C., Pereira, L.S., 2009. Funções de pedo-transferência para a curva de retenção da água no solo. Rev. Ciências Agrárias 32, 337-343.

Pereira, L.S., Cordey, I., Iacovides, I., 2009. Coping with water scarcity. Addressing the challenges. Springer.

Pereira, L.S., Gonçalves, J.M., Dong, B., Mao, Z., Fang, S. X., 2007. Assessing basin irrigation and scheduling strategies for saving irrigation water and controlling salinity in the upper Yellow River Basin, China. Agric. Water Manage. 93, 109-122.

Pereira, L.S., Perrier, A., Ait Kadi, M., Kabat, P., 1992. Crop-Water Models. Special issue of the ICID Bulletin, ICID, New Delhi, 200 pp.

Pereira, L.S., van den Broek, B., Kabat, P., Allen, R.G., 1995. Crop-Water Simulation Models in Practice. Wageningen Pers, Wageningen, 332 pp.

Perfect, E., Sukop, M.C., Haszler, G.R., 2002. Prediction of dispersivity for undisturbed soil columns from water retention parameters. Soil Sci. Soc. America J. 66, 696-701.

Romano, N., Palladino, M., Chirico, G.B., 2011. Parameterization of a bucket model for soil-vegetation-atmosphere modeling under seasonal climatic regimes. Hydrol. Earth Syst. Sci. 15, 3877-3893.

Ramos, T.B., Gonçalves, M.C., Martins, J.C., Pires, F.P., Pereira,L. S., 2011. Propriedades hidráulicas dos solos para as diferentes classes texturais. Rev. Ciências Agrárias XXXIV (2): 252-264.

Saxton, K.E., Rawls, W.J., Romberger, J.S., Papendick, R.I., 1986. Estimating generalized soil water characteristics from texture. Soil Sci. Soc. America J. 50, 1031–1036.

Schaap, M.G., Leij, F.J., van Genuchten, M.Th., 2001. ROSETTA: a computer program for estimating soil hydraulic parameters with hierarchical pedotransfer functions. J. Hydrol. 251, 163-176.

Seaman, J.C., Chang, H., Goldberg, S., Šimůnek, J., 2012. Reactive Transport Modeling. Vadose Zone J. 11(2), doi:10.2136/vzj2012.0066.

Shirazi, M.A., Boersma, L., Johnson, C.B., 2001. Particle-size distributions: comparing texture systems, adding rock and predicting soil properties. Soil Sci. Soc. America J. 65, 300-310.

Šimůnek, J., Bradford, S.A., 2008 Vadose Zone Modeling: Introduction and importance. Vadose Zone J. 7, 581-586.

Šimůnek, J., Hopmans, J. W., 2009. Modeling compensated root water and nutrient uptake. Ecol. Model. 220, 505-521.

Šimůnek, J., Suarez D.L., 1997. Sodic soil reclamation using multicomponent transport modelling. J. Irrig. Drain. Engin. 123(5), 367–376.

Šimůnek, J., Šejna, M., Saito, H., Sakai, M., van Genuchten, M.Th., 2008a. The HYDRUS-1D software package for simulating the movement of water, heat, and multiple solutes in variably-saturated media. Version 4.0. HYDRUS Software Series 3, Department of Environmental Sciences, University of California Riverside, Riverside, CA, USA, 315 pp.

Šimůnek, J., Valocchi, A.J., 2002. Geochemical transport. In: Dane, J.H., Topp, G.C. (Eds.), Methods of Soil Analysis, part 1, Physical Methods, pp. 1511-1536. Soil Sci. Soc. of Am., Madison, Wis., USA.

Šimůnek, J., van Genuchten, M. Th., Šejna, M., 2006. The HYDRUS software package for simulating two- and three-dimensional movement of water, heat, and multiple solutes in

variably-saturated media, Technical manual. Version 1.0, PC Progress, Prague, Czech Republic, 241 pp.

Šimůnek, J., van Genuchten, M.Th., Šejna, M., 2008b. Development and applications of the HYDRUS and STANMOD software packages, and related codes. Vadose Zone J. 7, 587-600.

Tomasella, J., Hodnett, M.G., 1998. Estimating soil water retention characteristics from limited data in Brazilian Amazonia. Soil Sci. 163, 190-202.

van den Berg, M., Klamt, E., van Reeuwijk, L.P., Sombroek, W.G., 1997. Pedotransfer functions for the estimation of moisture content characteristics of Ferralsols and related soils. Geoderma 78, 161-180.

van Genuchten, M.Th., 1980. A closed form equation for predicting the hydraulic conductivity of unsaturated soils. Soil Sci. Soc. America J. 44, 892-898.

van Genuchten, M.Th., Šimůnek, J., 2004. Integrated modeling of vadose zone flow and transport processes. In: Feddes, R.A., de Rooij, G.H., van Dam, J.C. (Eds.), Unsaturated Zone Modeling: Progress, Challenges and Applications, pp. 37–69. Wageningen UR Frontis Series, vol. 6, Springer, New York.

van Genuchten, M.T., Wierenga, P.J., 1976. Mass transfer studies in sorbing porous media. I. Analytical solutions. Soil Sci. Soc. America J. 40, 473-480.

Vanderborght, J., Vereecken, H., 2007. Review of dispersivities for transport modeling in soils. Vadose Zone J. 6, 29-52.

Vereecken, H., Maes, J., Feyen, J., Darius, P., 1989. Estimating the soil moisture retention characteristics from texture, bulk density, and carbon content. Soil Sci. 148, 389-403.

Weynants, M., Montanarella, L., Tóth, G., Strauss, P., Feichtinger, F., Cornelis, W., Javaux, M., Matula, S., Daroussin, J., Hennings, V., Schindler, U., Bilas, G., Máki, A., Tóth, B., Romano, N., Iovino, M., Morari, F., Kværnø, S., Nemes, A., Børresen, T., Haugen, L.E., Slawinski, C., Lamorski, K., Gonçalves, M., Paryka, N.V., Shein, E., Houškivá, B., Anaya-Romero, M., Kätterer, T., Wösten, H., Hannam, J., Keay, C., Lilly, A., Laktionova, T.,

2013. European HYdropedological Data Inventory (EU-HYDI). JRC Technical Reports, Report EUR 26053. Institute for Environment and Sustainability, Joint Research Centre, European Commission, Ispra, Italy, 167 pp.

Wösten, J.H.M., Lilly, A., Nemes, A., Le Bas, C., 1999. Development and use of a database of hydraulic properties of European soils. Geoderma 90, 169-185.

Wösten, J.H.M., Pachepsky, Y.A., Rawls, W.J., 2001. Pedotransfer functions: bridging the gap between available basic soil data and missing soil hydraulic characteristics. J. Hydrol. 251, 123-150.

Xu, X., Huang, G., Sun, C., Pereira, L. S., Ramos, T. B., Huang, Q., Hao,Y., 2013. Assessing the effects of water table depth on water use, soil salinity and wheat yield: Searching for a target depth for irrigated areas in the upper Yellow River basin. Agric. Water Manage. 125, 46-60.

Chapter 2

Field evaluation of a multicomponent solute transport model in soils irrigated with saline waters

(Published in: Journal of Hydrology 407, 129-144. 2011)

Field evaluation of a multicomponent solute transport model in soils irrigated with saline waters

T. B. Ramos[1], J. Šimůnek[2], M. C. Gonçalves[1,3], J. C. Martins[3], A. Prazeres[3], N. L. Castanheira[3] and L. S. Pereira[1]

[1] CEER-Biosystems Engineering, Institute of Agronomy, Technical University of Lisbon, Tapada da Ajuda, 1349-017 Lisbon, Portugal

[2] Department of Environmental Sciences, University of California, Riverside, CA, 92521, USA.

[3] Estação Agronómica Nacional, L-INIA, Instituto Nacional de Recursos Biológicos, 2784-505 Oeiras, Portugal.

Abstract

Soil salinization, sodification, and non-point source pollution are among the most important and widespread environmental problems in agricultural regions with scarce water resources. Models evaluating these environmental problems should therefore consider an integrated approach to avoid favoring one problem over the other. The HYDRUS-1D software package was used to simulate water movement and solute transport in two complex experiments carried out under field conditions in Alvalade and Mitra, Portugal. The experiments involved irrigating maize with synthetic saline irrigation waters blended with fresh irrigation waters and waters with different nitrogen concentrations. The major ion chemistry module of HYDRUS-1D was used to model water contents (RMSE $\leq$ 0.04 cm^3 cm^{-3}), the overall salinity given by the electrical conductivity of the soil solution (EC_{sw}) (RMSE $\leq$ 2.35 dS m^{-1}), the concentration of soluble cations Na^+ (RMSE $\leq$ 13.86 $mmol_{(c)}$ L^{-1}), Ca^{2+} (RMSE $\leq$ 5.66 $mmol_{(c)}$ L^{-1}), Mg^{2+} (RMSE $\leq$ 4.16 $mmol_{(c)}$ L^{-1}), and SAR (RMSE $\leq$ 6.27 $(mmol_{(c)}L^{-1})^{0.5}$) in different experimental plots. RMSE were always lower for the soil with coarse texture of Mitra. The standard HYDRUS solute transport module was used to model $N\text{-}NH_4^+$ (RMSE $\leq$ 0.07 $mmol_{(c)}$ L^{-1}) and $N\text{-}NO_3^-$ (RMSE $\leq$ 2.60 $mmol_{(c)}$ L^{-1}) concentrations in the soil solution while either including or neglecting the effects of the osmotic

stress on nutrient uptake. The model was able to successfully simulate root water and nutrient uptake reductions due to osmotic stress. Consequently, modeled fluxes of $N\text{-}NH_4^+$ and $N\text{-}NO_3^-$ leached from the soil profiles increased due to the effects of the salinity stress on water and nutrient uptake. Possible causes of disagreements between the modeling and experimental data are discussed. HYDRUS-1D proved to be a powerful tool for analyzing solute concentrations related to overall soil salinity and nitrogen species.

Keywords: HYDRUS-1D, field experiment, modeling, soil salinity, osmotic stress, nitrogen leaching.

1. Introduction

In recent decades, countries located in regions with arid, semi-arid, and even sub-humid conditions have developed irrigation areas to satisfy the growing demands for food and raw materials. In regions with scarce water resources, it is not always possible to irrigate with waters of good quality, and therefore even saline waters are seen as an important resource (Pereira et al., 2009). As a result, human-induced salinization and sodification are among the most important and widespread soil degradation processes, generally associated with irrigation practices and poor water management. As rainfall may not be sufficient to remove the salts accumulated during irrigation, it is often necessary to monitor soil and water quality, and to promote efficient leaching management to counteract soil salinization. Irrigation volume and frequency are therefore adjusted to remove salts from the root zone (e.g., Gonçalves et al., 2007; Pereira et al., 2007). However, promoting salt leaching also results in increased nitrogen leaching, which contributes to the degradation of groundwater reservoirs. As non-point source pollution from agricultural fertilization is considered to be a leading cause of water quality problems, especially in regions like those mentioned above, an integrated approach should always be considered to avoid emphasizing one problem over the other.

Over the last few decades the scientific community has invested considerable time and resources in the development of analytical and numerical models as tools to predict the long and short-term

effects of irrigation water quality on soil properties, crop yield, groundwater, and the environment (Wagenet and Hutson, 1987; Jarvis, 1994; van Dam et al., 1997; Ahuja et al., 2000; van den Berg et al., 2002; Šimůnek et al., 2006, 2008a). Most vadose zone models are based on the numerical solution of the Richards equation for variably-saturated water flow, and on analytical or numerical solutions of the Fickian-based convection-dispersion equation for solute transport. A sink term is usually included in these equations to account for root water and nutrient uptake, and the effects of water and osmotic stresses (Feddes and Raats, 2004; Šimůnek and Hopmans, 2009).

Perhaps the most significant difference among vadose zone models is how they describe solute partitioning between the liquid and solid phases and the complex chemical reactions involved in solute transport. Most vadose zone models consider the transport of only one solute, and severely simplify various chemical interactions. The relatively complex processes of adsorption and cation exchange are often accounted for by means of empirical adsorption isotherms. Other processes such as precipitation/dissolution and biodegradation are frequently ignored or simulated by invoking simplified first- or zero-order rate equations. Only a few models have been developed that can consider multiple solutes and their various interactions, such as precipitation/dissolution and competition for sorption sites (Šimůnek and Valocchi, 2002).

The HYDRUS-1D software package (Šimůnek et al., 2008a) uses several modeling concepts for evaluating solute transport, two of which will be used in our study. The standard solute transport module, already available with earlier versions of HYDRUS, considers the transport of one or multiple solutes, which can be either independent or involved in sequential first-order decay reactions. This module has been used for a wide range of applications in research and irrigation management of poor quality waters (e.g., Hanson et al., 2008; Roberts et al., 2008, 2009; Forkutsa et al., 2009). It has also been used to simulate the fate of nutrients in soils by evaluating and comparing fertilization strategies for different crops (e.g., Cote et al., 2003; Gärdenäs et al., 2005; Hanson et al., 2006; Ajdary et al., 2007; Crevoisier et al., 2008). While salinity studies have typically been limited to estimating the electrical conductivity of the soil solution (EC_{sw}), the studies addressing fertilization strategies have been mainly theoretical, or when experimental data existed, limited to very short periods of time, while evaluating nutrient leaching

independently of irrigation water quality. As far as we know, no integrated studies using HYDRUS exist where both problems have been considered at the same time.

The major ion chemistry module adapted from the UNSATCHEM model (Šimůnek et al., 1996) has been used much less often than the standard solute transport module. We refer here to the comprehensive study carried out by Gonçalves et al. (2006), who analyzed transient water flow and solute transport in three soil lysimeters irrigated with waters of different quality over 4 years. The study made full use of the major ion chemistry module, which allowed comparisons between model-simulated and experimental soil water contents, concentrations of Na^+, Ca^{2+}, and Mg^{2+}, EC_{sw}, the sodium adsorption ratios (SAR), and the exchangeable sodium percentages (ESP). This study demonstrated how the major ion chemistry module of UNSATCHEM is a better tool for evaluating saline water management and for assessing the effects of irrigation water quality on groundwater recharge (Gonçalves et al., 2006).

While it has been shown that these two solute transport modules of HYDRUS-1D can be helpful tools for developing management irrigation strategies in regions with water scarcity, there is still a need to conduct studies where model predictions are compared against field experimental data in order to lend greater credibility to both the simulations and extrapolations to different soil types, crops, climatic conditions, tillage operations, and water management schemes. As arid and semi-arid regions are particularly vulnerable to soil salinization and non-point source pollution, there is also a need for these studies to consider an integrated approach, as the solution of one problem can easily aggravate the other problems.

The objective of this study was to use the HYDRUS-1D software package to evaluate soil salinization and sodification risks by analyzing experimental data collected in two agricultural fields (Ramos et al., 2009) irrigated with synthetic saline waters, and to quantify the effects of the salinity stress on nitrogen leaching. We further evaluated the effectiveness of HYDRUS-1D (i) to predict water contents and fluxes, (ii) to predict salinization and sodification risks by estimating the overall salinity given by EC_{sw}, individual cations Na^+, Ca^{2+}, and Mg^{2+}, and SAR, (iii) to quantify water uptake reductions due to the use of saline waters, and (iv) to predict $N\text{-}NH_4^+$ and $N\text{-}NO_3^-$ concentrations in the soil and their leaching under field conditions.

2. Material and methods

2.1. Field experiment

Since the experimental data used in this study was presented by Ramos et al. (2009), only information relevant to our modeling study will be given here.

2.1.1. Experimental fields

Two field plot experiments were conducted from June 2004 to February 2007 in Southern Portugal. One was a soil classified as Typic Xerofluvent with a medium texture in the Alentejo region at the Alvalade Experimental Station (37º 56' 48'' N and 8º 23' 40'' W), and the other a Typic Haplanthrept soil with a coarse texture found in Herdade da Mitra (38º 31' 55'' N and 8º 00' 59'' W) (Soil Survey Staff, 2006). The climate in this region is mostly dry sub-humid to semi-arid, with hot dry summers, and mild winters with irregular rainfall. In both experimental fields, maize was irrigated with synthetic saline waters, obtained by adding NaCl to the available irrigation water in the region. The irrigation water was also used to deliver NH_4NO_3 to the crop.

2.1.2. Experimental design and treatments

A triple emitter source irrigation system was used to deliver water, salts (e.g., Na^+), and fertilizer (N) to the crop. This system, adapted from Beltrão et al. (2002), consisted of three trickle laterals placed along each maize line (Fig. 1). The first lateral was connected to the salt stock solution, the second to the nitrogen reservoir, and the third to the source of fresh water. This last lateral was used to obtain a constant water application rate at each dripping point. Gradients of applied salt and nitrogen concentrations were produced by varying discharge rates at different laterals. Table 1 lists the different discharge rates of the emitters applying salts, nitrogen, and fresh water in each experimental plot while maintaining an overall constant cumulative discharge of 18 L h^{-1} m^{-1} (24 mm h^{-1}).

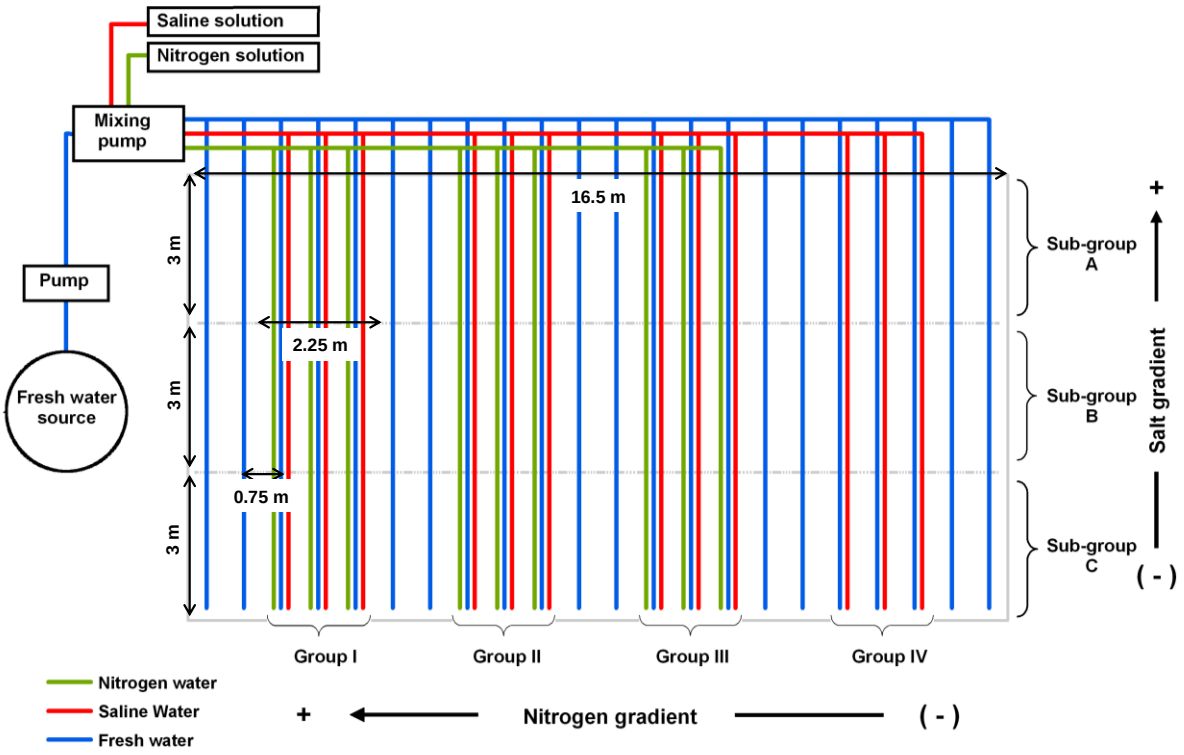

Fig. 1. Layout of the triple emitter source design (adopted from Ramos et al., 2009). The salt gradient decreases from sub-group A to C and the fertilizer gradient decreases from group I to IV.

Table 1. Discharge rates of the laterals applying salt (Na^+), nitrogen (N) and fresh water (*W*) in each experimental plot. There is an overall constant cumulative discharge at each dripping point of 18 L/h/m (Ramos et al., 2009).

Treatment	Application Rates (L/h/m)											
	Group I			Group II			Group III			Group IV		
	Na^+	N	*W*	Na^+	N	*W*	Na^+	N	*W*	Na^+	N	*W*
A	12	6	0	12	4	2	12	2	4	12	0	6
B	6	6	6	6	4	8	6	2	10	6	0	12
C	0	6	12	0	4	14	0	2	16	0	0	18

Each experimental field was divided into four groups (I to IV) with three triple joint laterals each, establishing a N gradient decreasing from group I to IV. Each group was then divided into 3 sub-groups, A, B, and C each with a surface area of 6.75 m^2 (2.25 m wide x 3 m long; 0.75 m between maize lines), and the Na^+ gradient decreasing from A to C. Synthetic saline waters (with

EC varying between 7.5 and 14.6 dS m^{-1}) were blended with the locally available water (*EC*≤1.2 dS m^{-1}). The amount of nitrogen applied to various plots varied from 0 to 65 g m^{-2} y^{-1}, while the amount of Na^+ varied from 0 to 2800 g m^{-2} y^{-1}. Table 2 presents the total amount of water applied in each year at both experimental fields, independent of its quality. A more detailed description of the trickle irrigation scheme used can be found in Ramos et al. (2009).

Table 2. Total amount of water applied (fresh water + saline water + water with fertilizer) in Alvalade and Mitra during the three irrigation seasons.

Experimental field	Water applied (mm)		
	2004	**2005**	**2006**
Alvalade	997	1012	1028
Mitra	1067	725	729

2.1.3. Observations and analysis

In the plots with the highest application of the synthetic saline waters (sub-group A), and in the plots irrigated only with the locally available water (sub-group C), TDR probes and ceramic cups were installed at 20, 40, and 60 cm depths to measure soil water contents and collect soil solutions. The soil solution was monitored for the concentrations of soluble Na^+, Ca^{2+}, Mg^{2+}, N-NO_3^-, N-NH_4^+, EC_{sw}, and SAR. Soil water content measurements and soil solutions were taken twice a week during irrigation seasons, generally 24 hours after an irrigation event, and twice a month during the rest of the year. Large periods with no data were due to low soil water contents, which made it impossible to collect soil solutions with the ceramic cups used in our experiments.

Modeling of water flow and solute transport was carried out for the worst case scenario, where potential root water uptake was reduced due to water and osmotic stresses, increasing the risk of salt and nitrogen leaching to the groundwater (group I, sub-group A, i.e., plot I-A). Results for this worst-case scenario were then compared with results for plots where it was assumed that the potential root water uptake was affected only by the water stress, and that osmotic stress could be neglected (groups I and IV, sub-groups C, i.e., plots I-C and IV-C).

We used the HYDRUS-1D software package to simulate one-dimensional water flow and solute transport in the plots where the observations were carried out. The major ion chemistry module

UNSATCHEM was used to simulate water contents, overall salinity given by EC_{sw}, concentrations of individual ions (Na^+, Ca^{2+}, and Mg^{2+}), and SAR. The standard HYDRUS solute transport module, run for every plot in sub-groups A and C, was used to simulate water contents, EC_{sw}, and concentrations of the nitrogen species. Potential and actual root water uptakes obtained using the two HYDRUS-1D modules were compared for each experimental plot.

2.2. HYDRUS-1D simulation model

The HYDRUS-1D software package (Šimůnek et al., 2008a) numerically simulates one-dimensional (1D) water flow, solute, and heat transport in variably-saturated porous media. Although other HYDRUS models (Šimůnek et al., 2008b) can simulate two- and three-dimensional transport, the 1D version simplifies the processes involved in our experiments by neglecting water and solute fluxes, and pressure head and concentration gradients in the horizontal direction. Below we give an overview of the main HYDRUS-1D processes that were involved in our experiments.

2.2.1. Water flow

Variably-saturated water flow is described using the Richards equation:

$$\frac{\partial \theta}{\partial t} = \frac{\partial}{\partial z}\left[K(h)\frac{\partial h}{\partial z} - K(h) \right] - S(z,t) \qquad (1)$$

where θ is the volumetric soil water content [L^3L^{-3}], t is time [T], z is the vertical space coordinate [L], h is the pressure head [L], K is the hydraulic conductivity [LT^{-1}], and S is the sink term accounting for water uptake by plant roots [$L^3L^{-3}T^{-1}$]. The unsaturated soil hydraulic properties are described using the van Genuchten-Mualem functional relationships (van Genuchten, 1980).

2.2.2. Root water uptake

The sink term, S, is calculated using the macroscopic approach introduced by Feddes et al. (1978). In this approach, the potential transpiration rate, T_p [LT^{-1}], is distributed over the root zone using the normalized root density distribution function, $\beta(z,t)$ [L^{-1}], and multiplied by the dimensionless stress response function, $\alpha(h, h_\phi, z, t)$, accounting for water and osmotic stresses (Feddes et al., 1978; van Genuchten, 1987; Šimůnek and Hopmans, 2009):

$$S\left(h,h_\phi,z,t\right)=\alpha\left(h,h_\phi,z,t\right)S_p\left(z,t\right)=\alpha\left(h,h_\phi,z,t\right)\beta\left(z,t\right)T_p\left(t\right) \tag{2}$$

where $S_p(z,t)$ and $S(h, h_\phi, z, t)$ are the potential and actual volumes of water removed from unit volume of soil per unit of time [$L^3L^{-3}T^{-1}$], respectively, and $\alpha(h, h_\phi, z, t)$ is a prescribed dimensionless function of the soil water (h) and osmotic (h_ϕ) pressure heads ($0 \le \alpha \le 1$). The actual transpiration rate, T_a [LT^{-1}], is then obtained by integrating Eq. (2) over the root domain L_R:

$$T_a=\int_{L_R}S\left(h,h_\phi,z,t\right)dz=T_p\int_{L_R}\alpha\left(h,h_\phi,z,t\right)\beta\left(z,t\right)dz \tag{3}$$

In our simulations, we assumed that the potential root water uptake was reduced due to water stress in all experimental plots. Water stress is a function of the adopted irrigation schedule, which may lead to insufficient (during early growth stages to allow the development of the rooting system) or excessive (due to over-irrigation during the remaining growth periods) supply of water to the crop. We also assumed that potential root water uptake was further reduced by osmotic stress resulting from the use of saline waters in the experimental plots irrigated with the synthetic saline waters (sub-group A in Fig. 1). We further assumed that the effects of the water and salinity stresses were multiplicative, i.e., $\alpha(h, h_\phi) = \alpha_1(h)\ \alpha_2(h_\phi)$ (van Genuchten, 1987), so that different stress response functions (as described below) could be used for the water and salinity stresses. It can be shown (e.g., Oster et al., 2012) that the combined effect of the two stresses is larger when the multiplicative (compared to additive) approach is considered.

Root water uptake reduction due to water stress, $\alpha_1(h)$, was described using the model developed by Feddes et al. (1978):

$$\alpha_1(h)=\begin{cases}0, & h>h_1 \text{ or } h\le h_4\\ \dfrac{h-h_1}{h_2-h_1}, & h_2<h\le h_1\\ 1, & h_3<h\le h_2\\ \dfrac{h-h_4}{h_3-h_4}, & h_4<h\le h3\end{cases} \tag{4}$$

where h_1, h_2, h_3, and h_4 are the threshold parameters. Water uptake is at the potential rate when the pressure head is between h_2 and h_3, drops off linearly when $h > h_2$ or $h < h_3$, and becomes zero when $h < h_4$ or $h > h_1$. Soil water pressure head parameters are available for maize in HYDRUS-1D internal database based on the work of Wesseling et al. (1991).

Root water uptake reduction due to salinity stress, $\alpha_2(h_\phi)$, was described using the Maas's (1990) threshold and slope function. The threshold-slope salinity stress model is implemented in the standard HYDRUS and UNSATCHEM solute transport modules as:

$$\alpha_2(h_\phi)=\begin{cases}1, & EC\le EC_T \text{ or } h_\phi\ge h_{\phi T}\\ 1-(EC-EC_T)\,0.01s & EC>EC_T\\ \text{or} & \text{or}\\ 1+(h_\phi-h_{\phi T})\,s^* & h_\phi<h_{\phi T}\end{cases} \tag{5}$$

respectively, where EC_T is the salinity threshold [dS m^{-1}], which corresponds to the value of the electrical conductivity (EC), below which root water uptake occurs without a reduction, $h_{\phi T}$ is the corresponding threshold value given in terms of the osmotic head [L], and s and s* are the slopes determining root water uptake decline per unit increase in salinity (in standard HYDRUS) or osmotic head (in UNSATCHEM) above or below the threshold, respectively. For the Alvalade and Mitra soils we found the relationship between EC_{sw} and h_ϕ to be:

$$\begin{aligned} h_\phi &= -3.8106\,EC_{sw}+0.5072 && (R^2=0.997)\\ h_\phi &= -3.8143\,EC_{sw}+0.6990 && (R^2=0.996)\end{aligned} \tag{6}$$

respectively. Equations (6) were determined by fitting a line to the computed values of EC_{sw} and h_ϕ obtained in the UNSATCHEM simulations. They are very similar to the relationship reported by the U.S. Salinity Laboratory Staff (1954) for estimating the osmotic pressure of soil solutions from *EC* measurements ($h_\phi = -3.7188\,EC$, if converted to S.I. units). HYDRUS-1D provides a database with the threshold-slope salinity parameters for different plants, including maize, based on work by Maas (1990). However, these values are given for the electrical conductivity of the saturation extract (EC_e). In our applications, EC_e values first had to be converted into EC_{sw}:

$$EC_e \times k_{EC} = EC_{sw} \tag{7}$$

where k_{EC} is the ratio of the electrical conductivity of the *in situ* soil water at field capacity and the *EC* of the soil water in the saturation extract. In our study we assumed a k_{EC} of 2, which is a common approximation (e.g., Ayers and Westcot, 1985) used for soil water contents near field capacity in medium-textured soils. Further details on k_{EC} variability can be found in Skaggs et al. (2006).

2.2.3. Solute transport

The partial differential equations governing one-dimensional advective-dispersive chemical transport under transient flow in a variably-saturated rigid porous medium are defined in HYDRUS-1D as:

$$\frac{\partial \theta c_k}{\partial t} + \rho \frac{\partial \bar{c}_k}{\partial t} = \frac{\partial}{\partial z}\left(\theta D \frac{\partial c_k}{\partial z} \right) - \frac{\partial q c_k}{\partial z} + \phi_k - S c_{r,k} \tag{8}$$

where θ is the volumetric water content [L^3L^{-3}], c, $\bar{c}$ and c_r are solute concentrations in the liquid phase [ML^{-3}], solid phase [MM^{-1}], and sink term [ML^{-3}], respectively, ρ is the soil bulk density [ML^{-3}], q is the volumetric flux density [LT^{-1}], D is the hydrodynamic dispersion coefficient [L^2T^{-1}], ϕ represents chemical reactions of solutes involved in a sequential first-order decay chain, such as nitrification of nitrogen species [$ML^{-3}T^{-1}$], and subscript k represents chemical species present in our study (e.g., Na^+, Ca^{2+}, and other major ions in the UNSATCHEM module

and *EC*, N- NO_3^-, and N- NH_4^+ in the standard HYDRUS solute transport module). The last term of Eq. (8) represents a passive root nutrient uptake (Šimůnek and Hopmans, 2009).

The parameter ϕ in Eq. (8), which is only considered in the standard HYDRUS solute transport module, represents nitrification of the N- NH_4^+ species to N- NO_3^-, and appears in Eq. (8) for N- NH_4^+ and N- NO_3^- species as follows, respectively:

$$\phi_{N-NH_4^+} = -\phi_{N-NO_3^-} = -\mu_{w,N-NH_4^+}\theta c_{N-NH_4^+} - \mu_{s,N-NH_4^+}\rho\bar{c}_{N-NH_4^+} \tag{9}$$

where μ_w and μ_s are the first-order rate constants for solutes in the liquid and solid phases [T^{-1}], respectively. In our study, we considered only the nitrification process from N- NH_4^+ - to N- NO_3^-, which resulted from the application of NH_4NO_3 fertilizer. Other reactions, such as the nitrification from N- NO_2^- to N- NO_3^-, the volatilization of N- NH_4^+ and subsequent N- NH_4^+ transport by gaseous diffusion, mineralization of crop residues and soil humus, and the denitrification of N- NO_3^- into N-N_2 or N-N_2O, were neglected. Some of these reactions, such as mineralization of crop residues and soil humus, simply cannot be described with sequential first-order decay chain reactions, while others occur at a rate so fast that they are often lumped, such is the case of the nitrification from N- NO_2^- to N- NO_3^- (e.g., Hanson et al., 2006).

The two different HYDRUS-1D modules used here apply two different approaches for relating solutes in the liquid and solid phases. The major ion chemistry module takes into account the fact that the soil liquid phase always contains a mixture of many ions that may interact, create complex species, precipitate, dissolve, and/or compete with each other for sorption sites on the solid phase (van Genuchten and Šimůnek, 2004). Thus, the UNSATCHEM module considers these interactions, including aqueous complexation, precipitation/dissolution, and cation exchange, described using the Gapon exchange equations (Šimůnek and Suarez, 1994).

The standard HYDRUS solute transport module accounts for the relatively complex processes of adsorption and cation exchange by means of empirical linear or nonlinear adsorption isotherms. In our application, the adsorption isotherm relating c and $\bar{c}$ in Eq. (8) is described using the following linear equation:

$$\overline{c_k} = K_{d,k}\, c_k \tag{10}$$

where $K_{d,k}$ [L^3M^{-1}] is the distribution coefficient of a chemical species *k*.

The electrical conductivity of the soil solution (EC_{sw}) is determined in the UNSATCHEM module from individual anions and cations following the method of McNeal et al. (1970), while in the standard HYDRUS solute transport module, EC_{sw} was run as an independent solute, available only in the liquid phase (i.e., K_d = 0 cm^3 g^{-1}). SAR, which is only determined in the UNSATCHEM module, was calculated as follows:

$$SAR = \frac{Na^+}{\sqrt{\frac{(Ca^{2+} + Mg^{2+})}{2}}} \tag{11}$$

2.2.4. Root nutrient uptake

The parameter c_r in the last term of Eq. (8) is the dissolved nutrient concentration taken up by plant roots in association with root water uptake, and is defined as:

$$c_r(z,t) = min[c(z,t), c_{max}] \tag{12}$$

where c_{max} is the *a priori* defined maximum concentration of the root uptake. We considered unlimited passive nutrient uptake for nitrogen species, which means that c_{max} was set to a larger concentration value than the dissolved concentrations, *c*, allowing all dissolved nutrients to be taken up by plant roots, and zero uptake for other species (*EC*, major ions), which means that c_{max} was set to zero. Since root nitrogen uptake likely involves both passive and active mechanisms (e.g., Šimůnek and Hopmans, 2009), considering only passive uptake will likely underestimate the total N uptake. By integrating passive nutrient uptake over the root domain, L_R, we obtained an equation similar to Eq. (3), given as:

$$P_a(t) = T_p(t) \int_{L_R} \alpha(h, h_\phi, z, t)\, \beta(z,t)\, min[c(z,t), c_{max}]\, dz \tag{13}$$

where P_a is the passive root nutrient uptake for the whole root domain ($ML^{-2}T^{-1}$) (Šimůnek and Hopmans, 2009).

2.3. Statistical analysis

In addition to a visual check, field measured values were compared with the results of the HYDRUS-1D simulations using the mean absolute error and the root mean square error. The mean absolute error (MAE) given by

$$MAE = \frac{1}{N}\sum_{i=1}^{N}\left|O_i - P_i\right| \tag{14}$$

describes the difference between observations (O_i) and model predictions (P_i) in the units of a particular variable, with N being the number of observations. The root mean square error (RMSE) given by

$$RMSE = \sqrt{\frac{\sum_{i=1}^{N}\left(O_i - P_i\right)^2}{N-1}} \tag{15}$$

is the square root of the mean square error, also given in the units of a particular variable. In general, RMSE ≥ MAE. The degree in which the RMSE value exceeds MAE is usually a good indicator of the presence and extent of outliers, or the variance of the differences between the modelled and observed values (Legates and McCabe, 1999).

3. Input data

3.1. Initial conditions

The initial soil water content was set to a uniform value of 0.25 cm^3cm^{-3} throughout both soil profiles. Initial conditions for the UNSATCHEM module were given in terms of concentrations of Na^+, Ca^{2+}, Mg^{2+}, and K^+ in the liquid and solid phases. Initial conditions for the standard HYDRUS solute transport module were specified in terms of EC_{sw}, and concentrations of N-NH_4^+ and N-NO_3^-. To obtain these values, chemical analyses were performed on soil samples collected in the beginning of the experiments. Concentrations of soluble cations Na^+, Ca^{2+}, Mg^{2+}, and K^+ were measured in the soil solutions collected from saturation extracts using atomic

absorption spectrophotometry. Exchangeable cations $\overline{Na}^{+}$, $\overline{Ca}^{2+}$, $\overline{Mg}^{2+}$, and $\overline{K}^{+}$ were determined with the Bascomb method (Bascomb, 1964), using a solution of $BaCl_2$+Triethanolamine at pH 8.1. The *CEC* was determined as defined in Šimůnek and Suarez (1994). *EC* was determined by electrometry, and converted to EC_{sw}. $N\text{-}NH_4^+$ was determined using a modified Bertholot method (Searle, 1984). $N\text{-}NO_3^-$ was determined by an automated segmented flow analyzer, using the cadmium reduction method to quantify nitrate-N (Hendrilsen and Selmer-Olsen, 1970). Table 3 presents the initial soluble and exchangeable cation concentrations determined in representative soil profiles of both experimental fields.

Table 3. Physical and chemical soil characteristics (initial conditions)[a].

	Alvalade			Mitra		
Depth (cm)	**0-30**	**30-75**	**75-100**	**0-30**	**30-50**	**50-90**
Coarse sand (g kg^{-1})	83	65	58	461	431	423
Fine sand (g kg^{-1})	329	245	215	284	306	323
Silt (g kg^{-1})	458	510	481	176	178	160
Clay (g kg^{-1})	13	18	246	79	85	9.4
Texture	Loam	Silty-loam	Loam	Sandy-loam	Sandy-loam	Sandy-loam
Bulk density (g cm^{-3})	1.49	1.51	1.61	1.51	1.70	1.69
EC (dS m^{-1})	0.42	1.22	0.96	0.48	0.63	0.25
SAR ($mmol_{(c)}\ L^{-1})^{0.5}$	3.25	3.87	2.96	0.41	0.56	0.57
pH (H_2O)	7.00	7.13	7.33	6.63	6.59	7.11
Soluble cations ($mmol_{(c)}\ L^{-1}$)						
Ca^{2+}	1.225	1.055	0.705	2.960	2.940	1.520
Mg^{2+}	0.978	0.830	0.590	1.278	1.175	0.640
Na^{+}	3.050	2.440	2.980	0.668	0.800	0.644
K^{+}	0.440	0.595	0.085	0.713	0.570	0.235
Cl^- ($mmol_{(c)}\ L^{-1}$),[b]	5.693	4.920	4.360	5.619	5.485	3.039
Exchangeable cations ($mmol_{(c)}\ kg^{-1}$)						
Ca^{2+}	60.01	61.64	62.77	98.10	78.10	71.07
Mg^{2+}	17.50	18.51	20.35	13.16	12.14	10.72
Na^{+}	2.53	2.28	3.49	0.99	1.03	1.11
K^{+}	5.71	7.1	2.95	6.16	4.68	3.63
CEC ($mmol_{(c)}\ kg^{-1}$),[c]	85.75	89.53	89.56	118.41	95.95	86.53
Gapon selectivity coefficients ($mol\ L^{-1})^{-1/2}$						
$K_{Ca/Na}$	2.92	2.87	2.85	1.73	1.58	1.51
$K_{Mg/Ca}$	0.33	0.34	0.35	0.20	0.25	0.23
$K_{Ca/K}$	0.11	0.11	0.10	0.09	0.10	0.09
$N\text{-}NO_3^-$ ($mmol_{(c)}\ L^{-1}$)	0.276	0.287	0.307	0.350	0.760	0.060
$N\text{-}NH_4^+$ ($mmol_{(c)}\ L^{-1}$)	0.001	0.001	0.001	0.001	0.001	0.001

[a] *EC*, electrical conductivity; SAR, sodium adsorption ratio; CEC, cation exchange capacity; *K*, Gapon selectivity coefficient.
[b] calculated to maintain the charge balance.
[c] calculated from the sum of ion exchange species.

3.2. Time-variable boundary conditions

Atmospheric and free drainage conditions were defined as boundary conditions at the surface and the bottom of each field plot, respectively. Atmospheric boundary conditions were specified using meteorological data, from which daily values of the reference evapotranspiration rate (ET_0) were calculated using the Penman-Monteith method (Allen et al., 1998). Crop evapotranspiration rates (ET_c) were then calculated using the product of ET_0 and K_c, where K_c is a crop coefficient accounting for both soil evaporation and crop transpiration. Values of K_c were taken from Allen et al. (1998). As required by HYDRUS-1D, ET_c daily values were divided into two components: crop transpiration (T) and soil evaporation (E) rates. These two components were estimated as a function of the Leaf Area Index (LAI) and the corresponding Soil Cover Factor (SCF), following Ritchie (1972).

LAI values were measured in each plot of both experimental fields during different stages of the maize cycle using a LI-COR area meter (Model LI-3100C, LI-COR Environmental and Biotechnology Research Systems, Lincoln, Nebraska), and were linearly interpolated between measurement dates. Although the combined effect of salinity and nitrogen fertilization is present in LAI values, in order to reduce the number of variables in our study, and to simplify the analysis of potential and actual root water uptake and solute leaching, we used only those LAI values measured at plot I-A (Fig. 1), where potential root water uptake was reduced due to water and osmotic stresses thereby increasing the risk of salt and nitrogen leaching to the groundwater, and plot IV-C (Fig. 1), where potential root water uptake was affected only by water stress, and where we assumed that osmotic stress could be neglected since osmotic heads in these plots were above the threshold value and thus $\alpha_2(h_\phi)$=1, i.e., no reduction occurred. For the nitrogen simulations, which were run for every plot in sub-groups A and C, we adopted LAI values measured in plots I-A and IV-C, respectively.

Experimental fields were irrigated three times per week between June and September. In Alvalade, application amounts averaged 23 mm per irrigation event, while in Mitra the mean

application amount was 18 mm per irrigation event. Daily values of precipitation, irrigation, and ET_0 for both experimental fields are presented in Fig. 2.

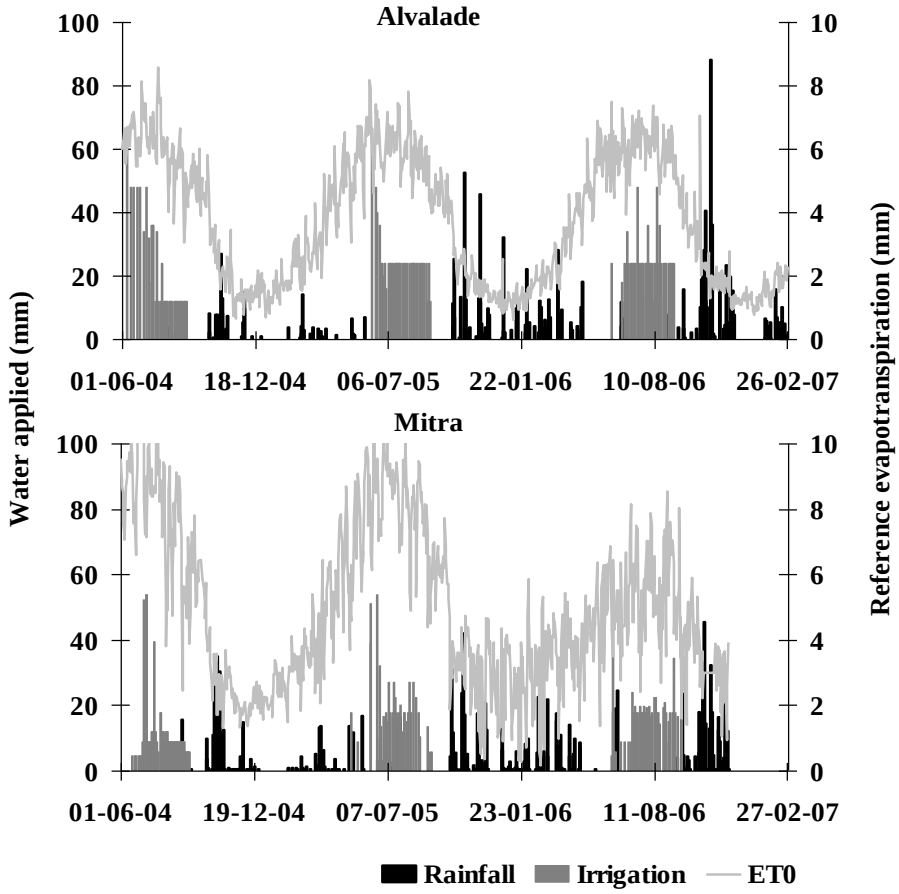

Fig. 2. Daily values of precipitation, irrigation and reference evapotranspiration rate in Alvalade (top) and Mitra (bottom) from 1st June 2004 and 27th February 2007.

3.3. Soil hydraulic properties

Undisturbed soil samples (100 and 630 cm^3) were collected at the beginning of the experiment from different soil layers of each soil profile to measure soil hydraulic properties. The soil water retention curve, $\theta(h)$, was determined in the laboratory using suction tables with sand or kaolin for suctions below 500 cm, and a pressure plate apparatus for suctions above 1000 cm. The

evaporation method (Wind, 1968; Halbertsma and Veerman, 1994) was further used to simultaneously estimate water retention and hydraulic conductivity data between pressure heads of approximately -50 and -800 cm. The same samples had been used previously to determine the saturated hydraulic conductivity K_s using a constant-head method (Stolte, 1997), completing the hydraulic conductivity function, $K(h)$. The parameters of the van Genuchten-Mualem equations were optimized using simultaneously retention and conductivity data determined by all three methods with the RETC computer program (van Genuchten et al., 1991). Table 4 lists the van Genuchten-Mualem parameters for the two field sites. Identical soil hydraulic parameters were considered for all experimental plots at each field, thus neglecting the probable effect of the spatial variability of soil hydraulic properties on water flow and solute transport.

Table 4. Soil hydraulic parameters of the van Genuchten-Mualem functions (van Genuchten, 1980) and solute transport parameters.

	Alvalade			Mitra		
Depth (cm)	**0-30**	**30-75**	**75-100**	**0-30**	**30-50**	**50-90**
θ_r (cm^3 cm^{-3})	0.050	0.108	0.000	0.000	0.000	0.000
θ_s (cm^3 cm^{-3})	0.380	0.380	0.375	0.340	0.319	0.312
α (cm^{-1})	0.027	0.115	0.045	0.238	0.091	0.077
η (-)	1.21	1.19	1.17	1.15	1.12	1.18
ℓ (-)	-4.41	-5.37	-6.48	-7.33	0.00	0.00
K_s (cm d^{-1})	16.6	84.4	21.0	57.0	52.4	98.9
λ (cm)	25.8	25.8	12.2	8.5	6.5	6.5

3.4. Solute transport parameters

Solute transport parameters were obtained from solute displacement experiments carried out on undisturbed 9040 cm^3 cylindrical samples with a cross-sectional area of 452 cm^2. A 0.05 M KCl pulse was applied during steady-state flow. The sampling and preparation of the soil columns were carried out according to the method described by Mallants et al. (1994). All experimental procedures are explained in Gonçalves et al. (2001). The chloride breakthrough curves were expressed using the dimensionless concentration as a function of the number of pore volumes leached through the soil column. Transport parameters were obtained using Toride et al's. (1995) non-linear parameter estimation code CXTFIT 2.1, implemented in the STANMOD software

package (Šimůnek et al., 1999) by fitting analytical solutions of the CDE to observed breakthrough data. Dispersivity (λ) values were calculated from the ratio D/υ and are presented in Table 4.

3.5. Relation between liquid and solid phases

The Gapon selectivity coefficients $K_{Ca/Na}$, $K_{Mg/Ca}$, and $K_{Ca/K}$ are presented in Table 3. They were calculated from the initial soluble and exchangeable cations concentrations presented in the same Table, according to the system of equations described by Šimůnek and Suarez (1994) for the case of exchange of the four cations simulated with UNSATCHEM.

In the standard HYDRUS solute transport module, nitrate ($N\text{-}NO_3^-$) and EC_{sw} were assumed to be present only in the dissolved phase (K_d = 0 $cm^3\ g^{-1}$), while ammonium ($N\text{-}NH_4^+$) was assumed to adsorb to the solid phase using a distribution coefficient K_d of 3.5 $cm^3\ g^{-1}$. The first-order decay coefficients μ_w and μ_s, representing nitrification from $N\text{-}NH_4^+$ to $N\text{-}NO_3^-$ in the liquid and solid phases, were set to be 0.2 d^{-1}. The parameters K_d, μ_w, and μ_s were taken from a review of published data presented by Hanson et al. (2006), and represent the center of the range of reported values.

3.6. Ionic concentration of irrigation waters

Irrigation water was monitored for concentrations of Na^+, Ca^{2+}, Mg^{2+}, electrical conductivity (EC_{iw}), $N\text{-}NH_4^+$, and $N\text{-}NO_3^-$. The average concentrations of individual ions in different irrigation waters (saline waters, waters with nitrogen, and fresh waters) mixed during application to the crop in the two experimental fields are presented in Table 5. Fertigation was limited to a certain number of irrigation events in the beginning of maize growing season. In Alvalade, fertigation was applied during 8, 6, and 6 irrigation events in the first, second, and third years, respectively. In Mitra, the fertilizer was applied during 4, 6, and 4 irrigation events during the three years of our experiment. During remaining irrigation events, the drip emitters that were first used to apply water with nitrogen applied only fresh irrigation water.

Table 5. Weighted average ionic composition of irrigation waters applied in the experimental fields.

Irrigation waters	Ca^{2+} $mmol_{(c)}\ L^{-1}$	Mg^{2+} $mmol_{(c)}\ L^{-1}$	Na^{+} $mmol_{(c)}\ L^{-1}$	K^{+} $mmol_{(c)}\ L^{-1}$	Cl^{-} [b] $mmol_{(c)}\ L^{-1}$	EC $dS\ m^{-1}$	SAR $(mmol_{(c)}\ L^{-1})^{0.5}$	USSL Classification[a]	$N\text{-}NH_4^{+}$ $mmol_{(c)}\ L^{-1}$	$N\text{-}NO_3^{-}$ $mmol_{(c)}\ L^{-1}$
Fresh waters:										
Alvalade	2.80	3.00	4.16	0.24	10.20	1.2	2.4	C_3S_1	0.03	0.15
Mitra	1.10	1.36	1.00	0.04	3.50	0.5	0.9	C_2S_1	0.03	0.24
Saline waters:										
Alvalade (2004)	2.80	3.00	66.13	0.24	72.17	7.8	38.8	C_4S_4	0.03	0.15
Alvalade (2005)	2.80	3.00	66.13	0.24	72.17	7.8	38.8	C_4S_4	0.03	0.15
Alvalade (2006)	2.80	3.00	136.66	0.24	142.70	14.6	80.2	C_4S_4	0.03	0.15
Mitra (2004)	1.10	1.36	74.23	0.04	76.73	8.1	66.9	C_4S_4	0.03	0.24
Mitra (2005)	1.10	1.36	68.57	0.04	71.07	7.5	61.8	C_4S_4	0.03	0.24
Mitra (2006)	1.10	1.36	68.33	0.04	70.83	7.5	61.6	C_4S_4	0.03	0.24
Waters with fertilizer:										
Alvalade (2004)	2.80	3.00	4.16	0.24	10.20	6.0	2.4	C_4S_1	46.1	46.1
Alvalade (2005)	2.80	3.00	4.16	0.24	10.20	6.0	2.4	C_4S_1	46.3	46.3
Alvalade (2006)	2.80	3.00	4.16	0.24	10.20	6.0	2.4	C_4S_1	45.6	45.6
Mitra (2004)	1.10	1.36	1.00	0.04	3.50	8.0	0.9	C_4S_1	80.4	80.4
Mitra (2005)	1.10	1.36	1.00	0.04	3.50	6.0	0.9	C_4S_1	49.5	49.5
Mitra (2006)	1.10	1.36	1.00	0.04	3.50	8.0	0.9	C_4S_1	83.0	83.0

[a] U.S. Salinity Laboratory Staff (1954). C_2, medium-salinity water (EC 0.25-0.75 dS m^{-1}); C_3, high-salinity water (EC 0.75-2.25 dS m^{-1}); C_4, very high salinity water (EC >2.25 dS m^{-1}); S_1, low-sodium water [SAR 0-10 $(mmol_{(c)}\ L^{-1})^{0.5}$]; S_4, very high sodium water [SAR >26 $(mmol_{(c)}\ L^{-1})^{0.5}$].

[b] Calculated to maintain the charge balance.

The EC_{iw} values used in the standard HYDRUS solute transport module were based on relations between EC and solute concentrations derived using UNSATCHEM. This was done in order to obtain similar osmotic stresses and actual root water uptake rates by the two modules. The relationships for Alvalade and Mitra were found to be:

$$\begin{aligned} EC_{sw} &= 0.1063 c_{sum} + 0.0915 \qquad \left(R^2 = 0.999\right) \\ EC_{sw} &= 0.1030 c_{sum} + 0.1585 \qquad \left(R^2 = 0.998\right) \end{aligned} \tag{16}$$

respectively, where c_{sum} is the sum of the solute concentrations [ML^{-3}] in the liquid phase as given by UNSATCHEM. The relations (16) are only slightly different from the common dilute-solution approximation EC=0.1c_{sum} (e.g., Bresler et al., 1982).

3.7. Root distribution and root water uptake

In each plot of both experimental fields, the root depth was set to 60 cm and the root density was assumed to decrease linearly with depth. These estimates were based on field observations made with the minirhizotron technique of Machado and Oliveira (2003). Soil water pressure head parameters in the Feddes et al. (1978) model were taken from the HYDRUS-1D internal database, which is based on Wesseling et al. (1991), i.e., h_1=-15, h_2=-30, h_3=-325 to -600, h_4=-8000 cm. In the Maas (1990) function, the salinity threshold (EC_T) for maize corresponds to a value of 1.7 dS m^{-1} for EC_e, and a slope (s) of 12. These values were converted into EC_{sw} using Eq. (7) and a k_{EC} of 2. The corresponding $h_{\phi T}$ and s* were obtained according to Eq. (6).

4. Results and discussion

The HYDRUS-1D simulations began on 22 April 2004 in Alvalade, and on 27 April 2004 in Mitra, at the beginning of the maize growing season. The actual experiments began later, on 6 June 2004 in Alvalade, and on 15 June 2004 in Mitra, when irrigation started. Beginning the HYDRUS-1D simulations long before irrigation events ensured that the initial soil water conditions were not a factor in solute transport simulations.

The amount of applied water (irrigation and rainfall), the irrigation schedule, and daily ET_c values were the same for all plots located in each experimental field. The effect of irrigation water

quality on root water uptake (transpiration) was assumed to be the main difference between experimental plots. Although measured and simulated data were compared at depths of 20, 40, and 60 cm, only results for the depth of 40 cm are presented graphically, in order to limit the number of figures and to maintain consistency. The statistical analysis presented in Table 6 involves results obtained for all three depths.

Table 6. Results of the statistical analysis between measured and simulated soil water contents, soluble Na^+, Ca^{2+}, Mg^{2+}, electrical conductivity of the soil solution (*ECsw*), N-NH_4^+, and N-NO_3^- obtained for all three studied depths (i.e., 20, 40, and 60 cm).

	Alvalade			Mitra		
	N	**MAE**	**RMSE**	**N**	**MAE**	**RMSE**
Water content	446	0.03	0.04	698	0.03	0.04
Na^+	239	10.65	13.86	356	3.78	6.44
Ca^{2+}	221	4.46	5.66	336	2.76	3.54
Mg^{2+}	223	3.28	4.16	342	1.32	1.75
SAR	216	4.68	6.27	333	2.14	3.91
EC_{sw} (UNSATCHEM)	244	1.91	2.35	361	0.61	0.87
EC_{sw} (HYDRUS)	244	1.60	2.04	361	0.62	0.99
N-NH_4^+	648	0.04	0.07	642	0.02	0.05
N-NO_3^-	637	1.53	2.60	771	0.84	2.01

N, number of observations; MAE, mean absolute error; RMSE, root mean square error. Units for MAE and RMSE are the units of a particular variables.

4.1. Volumetric water contents

Figure 3 shows the water contents measured with TDRs for the two experimental fields in plots I-A and IV-C, and compares these values with the results of the HYDRUS-1D simulations between 1st June 2004 and 26th February 2007 (i.e., 1000 days). During irrigation periods, the amount of water applied in both experimental fields (Table 2) was considerably higher than the usual amount of water used to irrigate maize in the Alentejo region (500 to 700 mm). The objective was to increase water contents above soil field capacity so that soil solution samples could be

easily collected using the installed ceramic cups. As a result, soil water content rapidly increased in the beginning of each irrigation season, and then varied between soil saturation and soil field capacity. Between the end of the irrigation seasons (September) and the beginning of rainy seasons (October or November), soil water contents gradually decreased, allowing maize to mature and be harvested. During rainy seasons, soil water contents were dependent on rainfall events (Fig. 2).

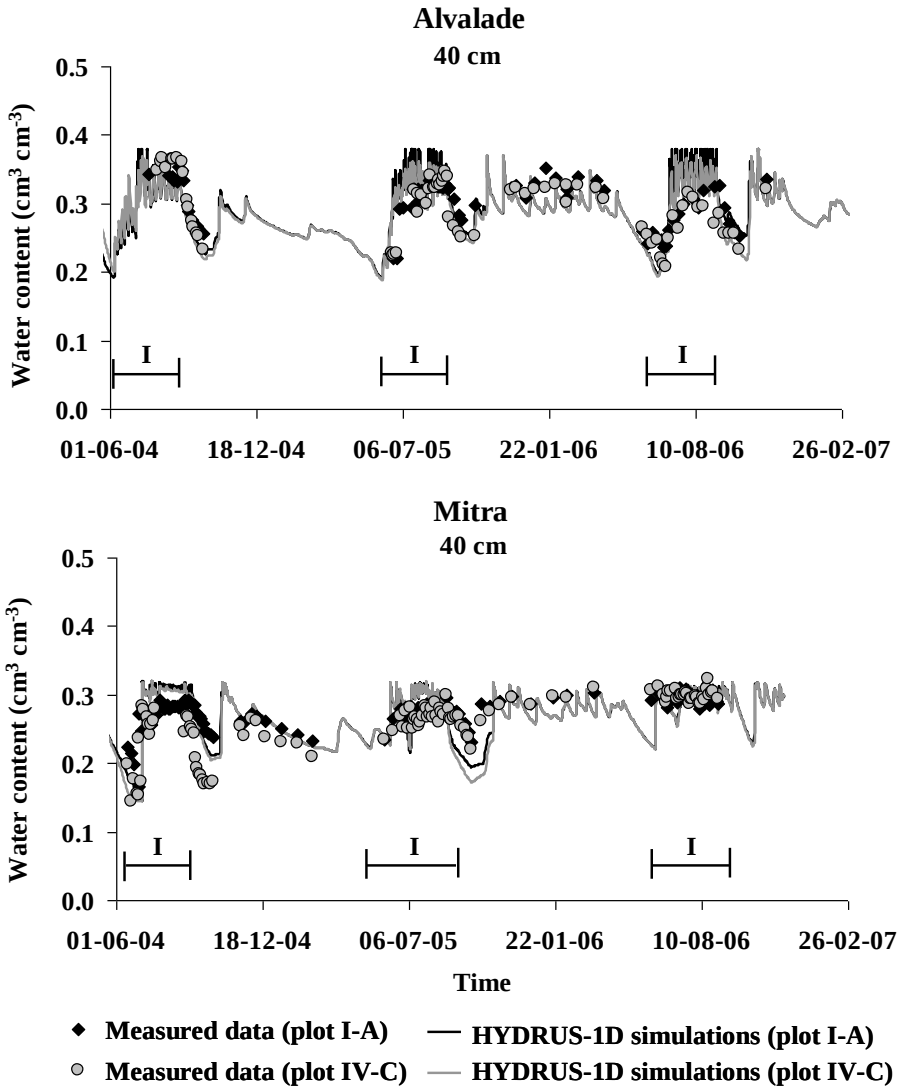

Fig. 3. Measured (TDR) and simulated (HYDRUS-1D) volumetric water contents at a 40-cm depth in Alvalade (top) and Mitra (bottom). Symbol I denotes the irrigation periods.

Some differences found between measurements and simulations during irrigation seasons can be explained by the fact that TDR measurements were usually taken 24 hours after an irrigation event, which means that the highest observed water content values correspond roughly to values close to soil field capacity, while HYDRUS-1D, which calculates water flow continuously, produced higher water contents during irrigation events. Mismatch between simulations and measurements depended on the time step used for specifying boundary conditions (1 day) and were more significant for depths near the soil surface, which reflected these inter-daily variations. While in the model we assume constant daily fluxes, soil evaporation varies during this time interval (has peaks during the day and very low during the night). Soil water content at the soil surface reflects these variations, which were not considered in the model, which focused on longer-term changes. Additionally, the distribution of water when drip emitters are used is known to be spatially non-uniform. Soil water content is highest near the drip line after water application and then water redistributes throughout the soil profile, as controlled by soil physical properties (Gärdenäs et al., 2005; Hanson et al., 2006). This non-uniformity could explain deviations between simulated and measured water contents, especially at the 20-cm depth, and a relatively high RMSE of 0.04 cm^3 cm^{-3} obtained for both soils. Also, in Mitra the apparently chaotic TDR data during irrigation periods may have caused larger deviations between observations and simulations. Using two-dimensional version of HYDRUS-1D would likely resulted in better agreement between experimental and modeled data, especially for shallower depths.

4.2. Root water uptake and transpiration

Figure 4 shows the cumulative potential root water uptake in Alvalade and Mitra during the three years of the experiment. It also shows the actual root water uptake during the same time period, while either considering only water stress (plots IV-C) or both water and salinity stress (plots I-A). In Alvalade, cumulative potential root water uptake rates (transpiration) in plots I-A and IV-C were 2074 and 2301 mm, respectively (Table 7). Since ET_c was assumed to be the same in all experimental plots, lower transpiration rates were balanced by higher evaporation rates. Variations in transpiration reflected the effects of the salinity and fertilization gradients on plant growth, characterized by LAI values measured in different plots. As an example, maximum LAI values (LAI_{max}) varied between 3.6 and 5.4 m^2 m^{-2} in plot I-A, and between 5.3 and 5.5 m^2 m^{-2} in

plot IV-C. Differences between LAI_{max} in the different plots were usually less than 1 m^2 m^{-2}, which means that the results obtained for the other experimental plots would not differ much from those presented here for plots I-A and IV-C, since transpiration was the only factor that was different between experimental plots.

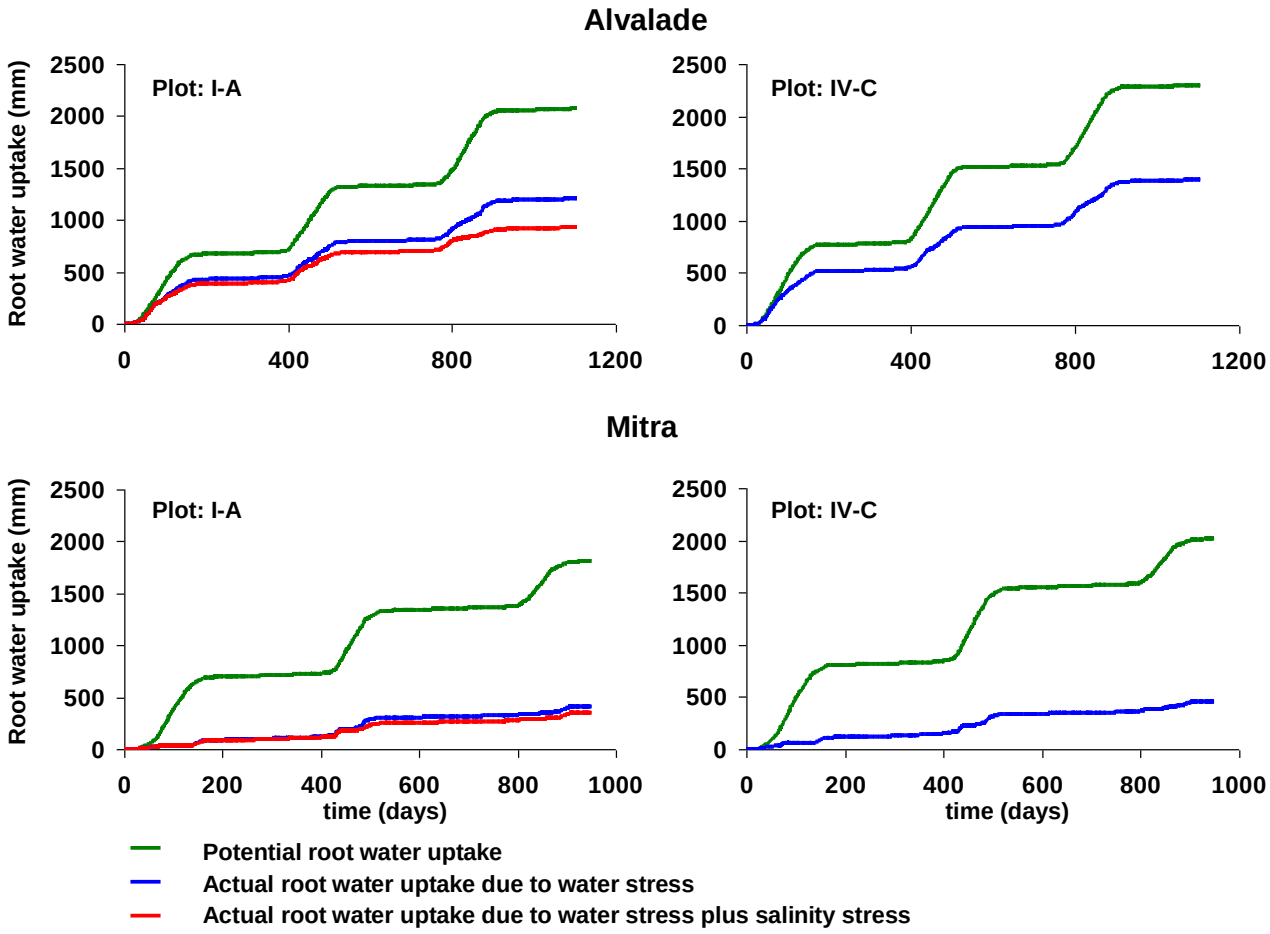

Fig. 4. Cumulative potential and actual root water uptake in plots I-A (left) and IV-C (right) in Alvalade (top) and Mitra (bottom).

Table 7. Cumulative potential and actual root water uptake determined in the experimental plots.[a]

Experimental plots	Alvalade		Mitra	
	Potential root water uptake (mm)	Actual root water uptake (mm)	Potential root water uptake (mm)	Actual root water uptake (mm)
I-A	2074 (2074)	949 (932)	1809 (1809)	362 (346)
II-A	2074	999	-	-
III-A	2074	1005	1809	368
IV-A	2074	1021	1809	374
I-C	2301	1418	2016	483
II-C	2301	1420	-	-
III-C	2301	1418	2016	482
IV-C	2301 (2301)	1422 (1396)	2016 (2016)	484 (458)

[a] Values obtained with the standard HYDRUS solute transport module. Values in brackets were determined with the UNSATCHEM module.

In all plots of sub-group C we assumed that potential root water uptake was reduced only due to water stress, since these plots were irrigated with fresh irrigation water (Table 5). Root water uptake (transpiration) was reduced from 2301 to 1396 mm when the UNSATCHEM module was used, and to 1420 mm when the standard HYDRUS solute transport module was used. These differences in cumulative actual transpiration were minimal (less than 3%). We also ran simulations with UNSATCHEM for plots IV-C while either considering or neglecting the effect of the salinity stress on the potential root water uptake. Osmotic heads in these plots were above the threshold value and thus $\alpha_2(h_\phi)$=1. As a result, the values for actual root water uptake were identical while considering or neglecting the salinity stress, confirming our initial assumption that no salinity stress reduction occurred in the plots in sub-group C.

In all plots of sub-group A we assumed that potential root water uptake was reduced due to water and osmotic stresses, since these plots were irrigated with saline waters. As EC_{sw} calculations in the two codes followed different methodologies, root water uptake reductions due to osmotic stress were slightly different. In the UNSATCHEM module, transpiration in plot I-A decreased from 2074 to 1208 mm due to water stress, and further to 932 mm due to the osmotic stress. In the standard HYDRUS solute transport module, cumulative actual root water uptake in plot I-A

was 949 mm, which is very close to the value obtained using UNSATCHEM. The effect of osmotic stress on water content can be observed in the simulation results (Fig. 3), in which HYDRUS-1D produced water content values slightly lower in plot IV-C than in plot I-A, where root water uptake reduction was higher, during irrigation periods.

In Mitra, cumulative potential transpiration in plots I-A and IV-C were 1809 and 2016 mm, respectively. Root water uptake was reduced to 458 mm in plot IV-C due to water stress, and to 346 mm in plot I-A due to water and osmotic stresses (values determined by the UNSATCHEM module). The reduction due to water stress was considerably higher than in Alvalade. This dramatic reduction was caused mainly by soil pressure heads being kept above the optimum range of the Feddes model (Feddes et al., 1978) for maize (h>-30 cm). The irrigation schedule was thus the main factor responsible for causing such high reductions in actual root water uptake. Also, soil hydraulic properties determined in Mitra resulted in some atypical values (e.g., the η parameter for different layers ranged from 1.12 to 1.18 and was lower than usual for coarse textured soils, and the ℓ parameter was 0.0 in layers under 30 cm), which may have contributed to errors in the water content and flux simulations. Underestimated values of the $K(h)$ function could cause HYDRUS-1D to predict longer periods of soil profile saturation than in reality, maintaining pressure heads above the optimum range of the Feddes stress response model, thus contributing to the lower root water uptake. Note that methods used to determine the $K(h)$ function (i.e., the evaporation and hot air methods) produce more precise $K(h)$ estimates for pressure heads below -50 cm and are less precise close to saturation. Nevertheless, cumulative actual transpiration agreed with lower maize yields as reported in Ramos et al. (2009). However, we were not able to relate yields with the T_a/T_p ratio.

4.3. Overall salinity

Soil salinity increased considerably in the plots irrigated with saline waters (Fig. 5). In Alvalade, measured EC_{sw} in plot I-A reached values higher than 6.0 dS m^{-1} during the first two irrigation seasons, and higher than 16.0 dS m^{-1} during the third year, as the applied waters became more saline. In the plots irrigated with the locally available water (IV-C), soil salinity remained below 5.0 dS m^{-1} throughout all irrigation seasons. Soil salinity decreased in all plots during rainfall periods, due to soil leaching. Only in the rainy season of 2004-2005, rainfall was not sufficient to

completely remove salts from the root zone in plot I-A, where EC_{sw} values between 2.0 and 6.3 dS m^{-1} were observed in the soil profile. In Mitra, irrigation with saline waters led to similar EC_{sw} peaks as in Alvalade, but with EC_{sw} values reaching only 9.0 dS m^{-1} during the final irrigation season. In plot IV-C, where the applied fresh irrigation water was of much better quality than in Alvalade, EC_{sw} was kept below 2.0 dS m^{-1} throughout irrigation seasons. Soil salinity also decreased in Mitra during rainfall periods, due to soil leaching. Since the saturated hydraulic conductivity of the top soil layer in Mitra (K_s = 57.0 cm d^{-1}) was higher than in Alvalade (K_s=16.6 cm d^{-1}), salts were more easily removed from the root zone, although during the rainy season of 2004-2005, EC_{sw} values above 2.0 dS m^{-1} were still observed in the deeper layers.

Figure 5 shows EC_{sw} values measured by electrometry in samples collected in plots I-A and IV-C, and EC_{sw} values simulated using the major ion chemistry module (UNSATCHEM module) and the standard HYDRUS solute transport module. Although EC_{sw} was calculated using different methodologies, the two modules produced very similar results during irrigation seasons. The main differences were found at the end of the irrigation seasons when soil water contents decreased significantly below field capacity, due to relatively high air temperatures and soil evaporation rates. During these periods, the standard HYDRUS solute transport module simply increased EC_{sw} linearly as the soil dried out, while the UNSATCHEM module produced a nonlinear increase of EC_{sw} as a result of cation exchange. The UNSATCHEM model also considers processes of precipitation/dissolution of solid phases, such as calcite and gypsum. However, the reported *pIAP* values (the negative logarithm of the ion activity product) indicated that conditions were undersaturated with respect to calcite and gypsum. In Alvalade, minimum calculated *pIAP* values for calcite and gypsum were 12.8 and 31.2, respectively. In Mitra, corresponding minimum *pIAP* values were 12.5 and 30.8. Since precipitation only occurs at values of 8.37 for calcite and 4.8 for gypsum (Truesdell and Jones, 1974), differences found between the two HYDRUS-1D modules were caused mainly by cation exchange. Consequently, during irrigation seasons the standard HYDRUS solute transport module produced higher peaks of EC_{sw} than the UNSATCHEM module. Similar trends were obtained during the rainy season of 2004-2005, when rainfall was not sufficient to remove salts from the root zone. During this season, the standard HYDRUS solute transport module clearly showed that high concentrations of salts remained in the soil profile of Alvalade, while the UNSATCHEM module produced lower simulated EC_{sw} values. RMSE between measured and simulated EC_{sw} values (Table 6)

were not sufficient to conclude which module produced better results. In addition, since it was difficult to collect soil solution samples with the ceramic cups during dry periods, model simulations could not be compared with measured data during these periods, which would have provided conclusive evidence regarding which module better fitted measured data. On the other hand, the statistical indicators showed that both modules reproduced EC_{sw} measured values equally well, with RMSE being similar for both modules for each soil.

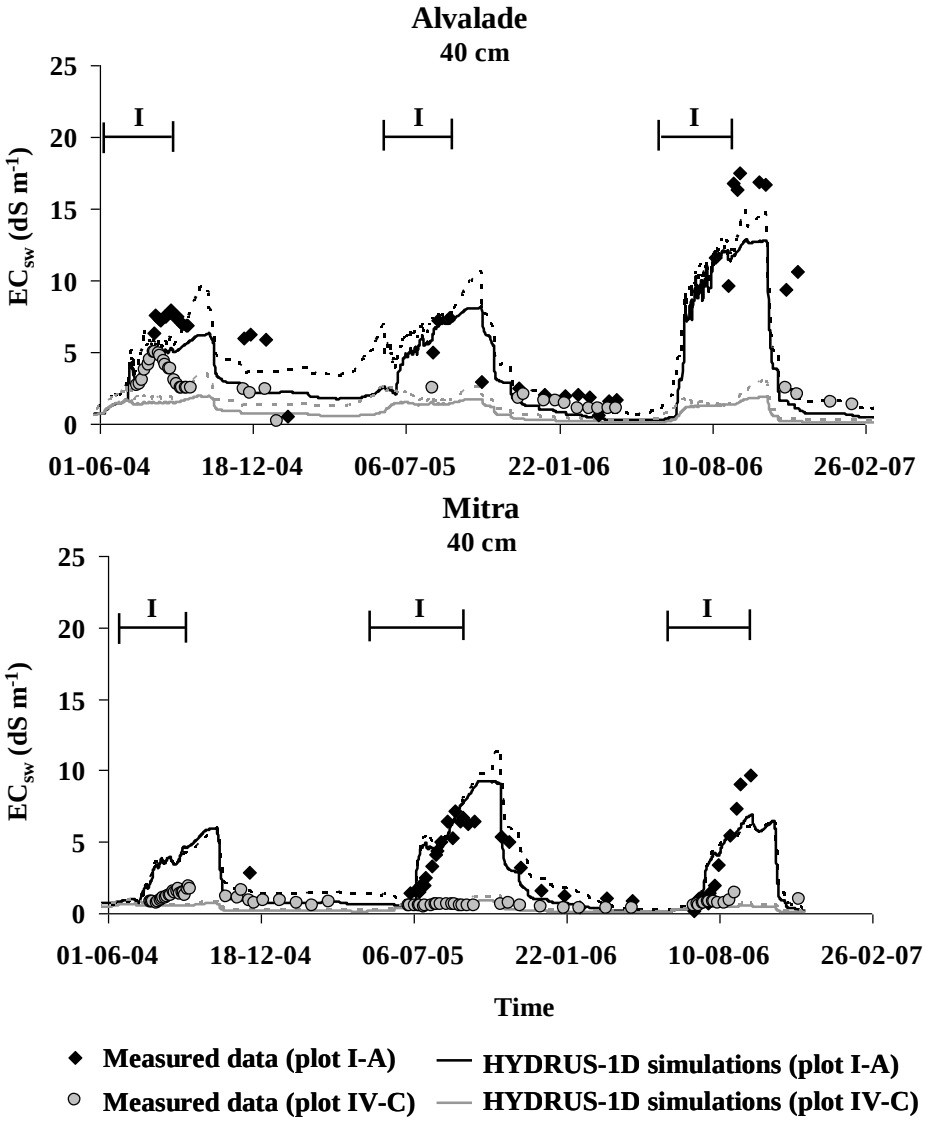

Fig. 5. Measured and simulated soil solution electrical conductivities at a 40-cm depth in Alvalade (top) and Mitra (bottom). Symbol I denotes the irrigation periods. Full lines represent the results of the major ion chemistry module (the UNSATCHEM module). Dashed lines represent the results obtained with the standard HYDRUS solute transport module.

Model simulations were very helpful in evaluating the management of irrigation with saline waters in the two experimental fields, allowing for a few additional observations. Based on model predictions, blending saline waters, in which EC_{iw} varied between 7.5 and 14.6 dS m^{-1}, with irrigation waters of good quality increased the amount of water available to meet crop water requirements while maintaining some level of maize yield (Ramos et al., 2009). Both measured and simulated values revealed that during irrigation seasons, EC_{sw} values became high enough to lead to significant maize yield reductions (e.g., Ayers and Westcot, 1985; Maas, 1990; Steppuhn et al., 2005), but never exceeded levels that would lead to zero yield, which for our crop would correspond to a EC_{sw} of 20 dS m^{-1} (EC_e=10 dS m^{-1}; k_{EC}=2). Additionally, variations in simulated EC_{sw} (Fig. 5), which increased and decreased regularly with irrigation events, showed the contribution of blending in providing some control on soil salinity status for both experimental fields. These variations were caused by blending saline waters with fresh waters, while keeping soil salinity relatively constant, which otherwise would have increased considerably.

4.4. Individual cations

Measured and simulated concentrations of soluble Na^+, Ca^{2+}, and Mg^{2+} for plots I-A and IV-C at a depth of 40 cm are presented in Figure 6. As the only cation being added to the synthetic saline irrigation waters, the general behavior of sodium was similar to EC_{sw} The highest concentrations were reached in plots I-A during the irrigation seasons. In Alvalade, the highest measured Na^+ concentrations were about 50 $mmol_{(c)}\,L^{-1}$ during the first two years and 130 $mmol_{(c)}\,L^{-1}$ during the third year. In Mitra, as saline waters were similar during the three irrigation seasons, measured Na^+ concentrations peaked always at about 50 $mmol_{(c)}\,L^{-1}$. During the rainy seasons, Na^+ concentrations decreased considerably due to soil leaching, similar to EC_{sw}. RMSE calculated for Na^+ concentrations (Table 6) resulted in 13.86 and 6.44 $mmol_{(c)}\,L^{-1}$ for Alvalade and Mitra, respectively.

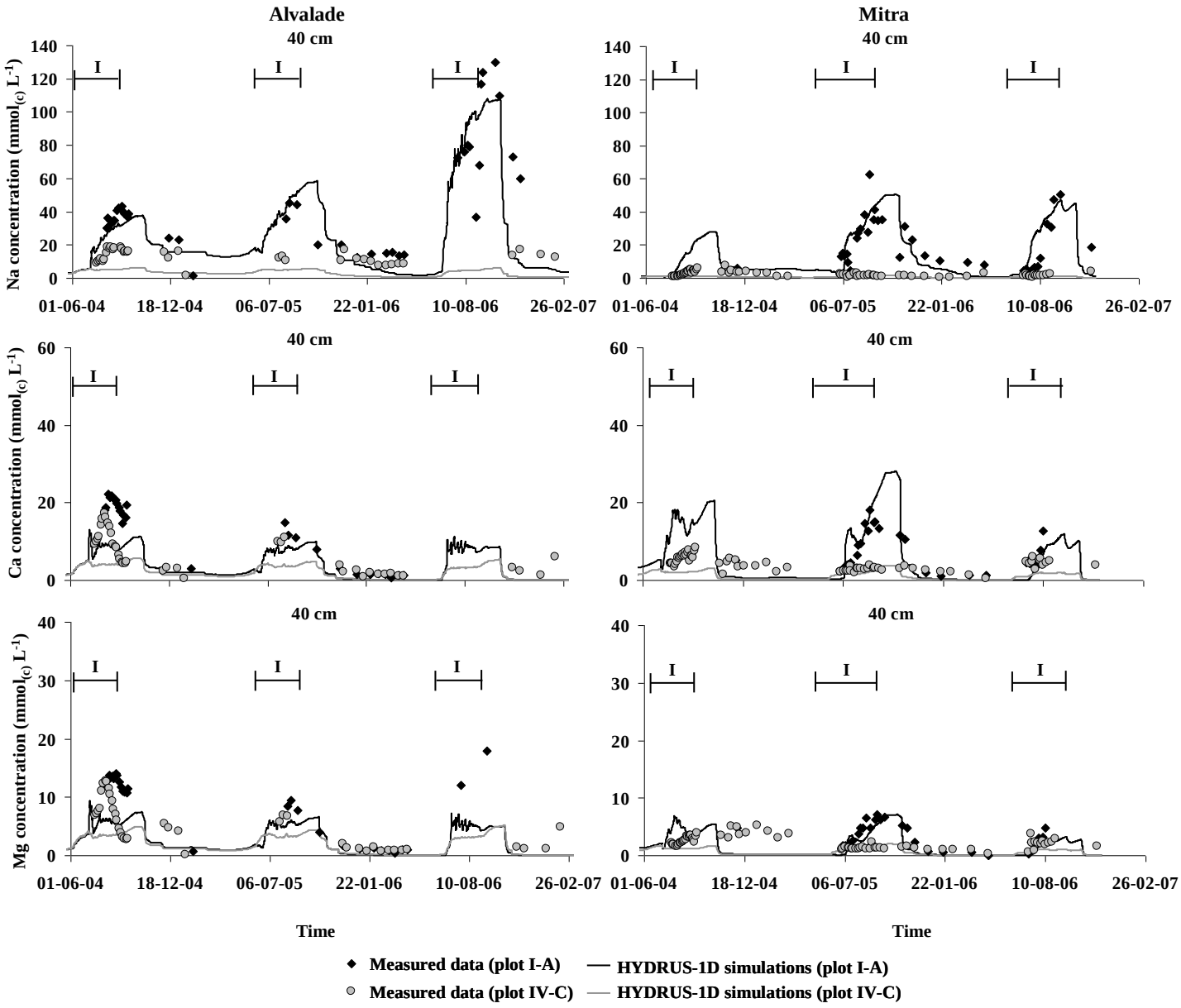

Fig. 6. Measured and simulated soluble sodium (top), calcium (middle), and magnesium (bottom) concentrations at a 40-cm depth in Alvalade (left) and Mitra (right). Symbol I denotes the irrigation periods.

The general dynamics of calcium and magnesium concentrations were similar to those of sodium and EC_{sw}. In both experimental fields, the highest measured Ca^{2+} and Mg^{2+} concentrations were about 20 and 10 $mmol_{(c)}\,L^{-1}$, respectively. During rainfall events, these values also decreased due to soil leaching. As Ca^{2+} and Mg^{2+} were not added to the synthetic saline irrigation waters applied

in plots I-A, concentrations of these cations in saline waters were the same as in fresh waters in plot IV-C (Table 5). Since Na^+ was applied in large concentrations to plot I-A, both Na^+ concentrations in the soil solution and in the solid phase (not shown) increased, leading to soil sodification. While the exchangeable Na^+ concentration in the solid phase increased, the other cations, namely Ca^{2+} and Mg^{2+}, were inevitably released to the soil solution. For this reason concentrations of Ca^{2+} and Mg^{2+} were higher in plots I-A than in plots IV-C where low concentrations of Na^+ were present in the irrigation waters. As the UNSATCHEM module is able to consider cation exchange, compared to simpler models based on the adsorption isotherms, this module is more adequate for representing reality than linear models with adsorption isotherms. RMSE obtained for Ca^{2+} and Mg^{2+} in Alvalade were 5.66 and 4.16 $mmol_{(c)}L^{-1}$, respectively. In Mitra, RMSE obtained for Ca^{2+} and Mg^{2+} were 3.54 and 1.75 $mmol_{(c)}\,L^{-1}$, respectively.

We believe that the inability of HYDRUS-1D to produce lower RMSE for Mitra, and to a lesser extent at Alvalade, was caused by multiple factors. In general, measurement errors, model input errors, and model structure errors could cause disagreement between simulated results and experimental data. First, while models usually report point values, measurements with suction cups are averaged over a sampling area of a certain volume, the size of which depends on soil hydraulic properties, the soil water content, and the applied suction in the ceramic cup (Weihermüller et al., 2005). Measured values thus do not represent point values. Second, while measured soil hydraulic and solute transport parameters were determined in the laboratory on soil samples of a certain size, the obtained parameters may not always be representative of simulated flow, transport and reaction processes at a much larger field scale. Third, while soil hydraulic and solute transport properties are spatially variable at the field scale, our HYDRUS-1D simulations assumed homogeneous soil environment and thus might not fully account for inherent spatial variability. Finally, as already discussed above, while only a one-dimensional model was used to evaluate experimental data, the drip irrigation used in the field experiments produces certain multidimensional phenomena that were not accounted for by the model.

4.5. Sodium adsorption ratio

Figure 7 presents the results for measured and simulated SAR values. SAR is an integral variable that characterizes salt-affected soils and provides information on comparative concentrations of

Na^+, Ca^{2+}, and Mg^{2+} in soil solutions. This variable takes into consideration that the adverse effects of sodium are moderated by the presence of calcium and magnesium ions. This makes SAR an important variable to consider when managing saline irrigation waters.

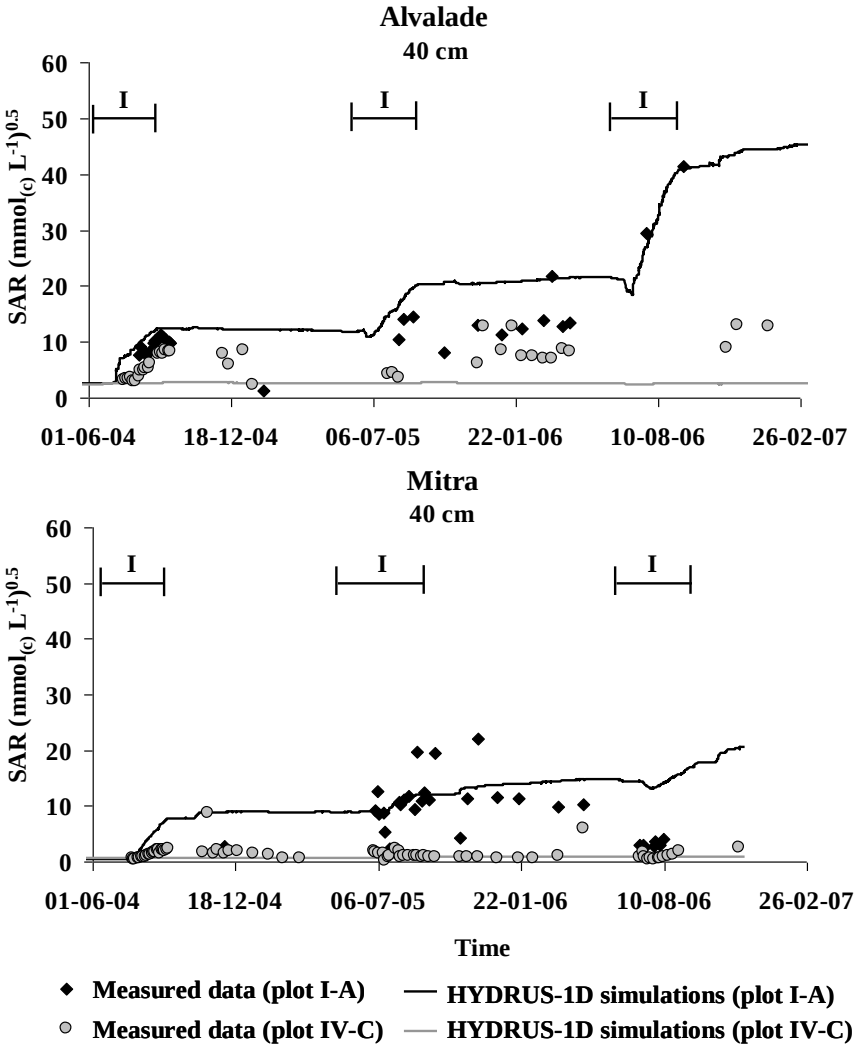

Fig. 7. Measured and simulated sodium adsorption ratios (SAR) at a 40-cm depth in Alvalade (top) and Mitra (bottom). Symbol I denotes the irrigation periods.

The standard HYDRUS solute transport module is unable to determine SAR. As a result, many studies found in the literature (e.g., Forkutsa et al., 2008; Hanson et al., 2008; Roberts et al., 2009) do not consider the effects of saline waters and management practices on soil sodification.

The major ion chemistry module is therefore a better tool for saline water management, as it is capable of evaluating interactions between individual ions, from which SAR can be determined. It is thus no surprise that the statistical indicators calculated for SAR showed the same trends as obtained for individual ions. RMSE obtained for Alvalade and Mitra were 6.27 and 3.91 $(mmol_{(c)} L^{-1})^{0.5}$, respectively.

The general behavior of SAR was very similar to that documented in Gonçalves et al. (2006). In plots I-A, SAR increased rapidly in the surface layers after irrigation events, and then gradually at deeper depths. The application of saline irrigation waters, in which SAR ranged from 38.8 to 80.2 $(mmol_{(c)} L^{-1})^{0.5}$ (Table 5), led to very high SAR values in the soil solution, reaching about 54 and 21 $(mmol_{(c)} L^{-1})^{0.5}$ at the end of the experiments in Alvalade and Mitra, respectively. In those plots irrigated with fresh waters (plots IV-C), SAR values did not vary significantly, having roughly the same values in the beginning as at the end of the experiments. While HYDRUS-1D simulations with the standard solute transport module revealed that overall salinity decreased as a result of soil leaching after rainfall, simulations using the UNSATCHEM module provided predictions of SAR, which is an important component in designing better management of irrigation practices with saline waters. Consequently, soil salinization and sodification could be considered simultaneously.

4.6. Nitrogen concentrations

Figures 8 and 9 present the measured and simulated concentrations of $N\text{-}NH_4^+$ and $N\text{-}NO_3^-$ in the soil solution at a depth of 40 cm. Since the amount of nitrogen applied in sub-groups A, B, and C was the same, $N\text{-}NH_4^+$ and $N\text{-}NO_3^-$ concentrations for sub-groups A and C are compared to determine the effect of salinity stress on nutrient uptake. Figure 8 compares $N\text{-}NH_4^+$ concentrations in plots I-A and I-C for both experimental fields. As the results obtained for experimental plots of the remaining three groups (II to IV) were very similar, results obtained in group I are used to exemplify $N\text{-}NH_4^+$ behavior. Figure 9 compares measured and simulated $N\text{-}NO_3^-$ concentrations in experimental plots of groups I (I-A and I-C) and IV (IV-A and IV-C). The results obtained for the remaining groups in the middle of the nitrogen gradient (groups II

and III) are not given, as the results in groups I and IV represent the maximum and minimum N-NO_3^- dynamics.

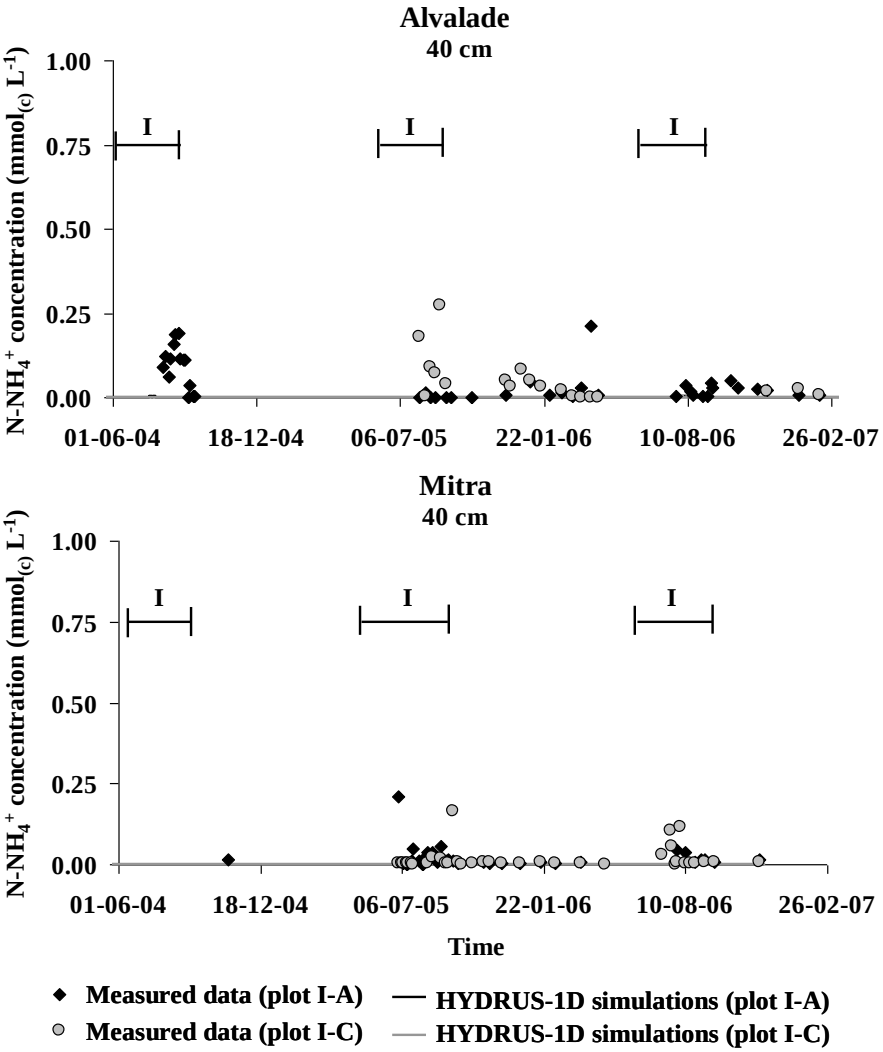

Fig. 8. Measured and simulated ammonium concentrations at a 40-cm depth in the experimental plots of group I in Alvalade (top) and Mitra (bottom). Symbol I denotes the irrigation periods.

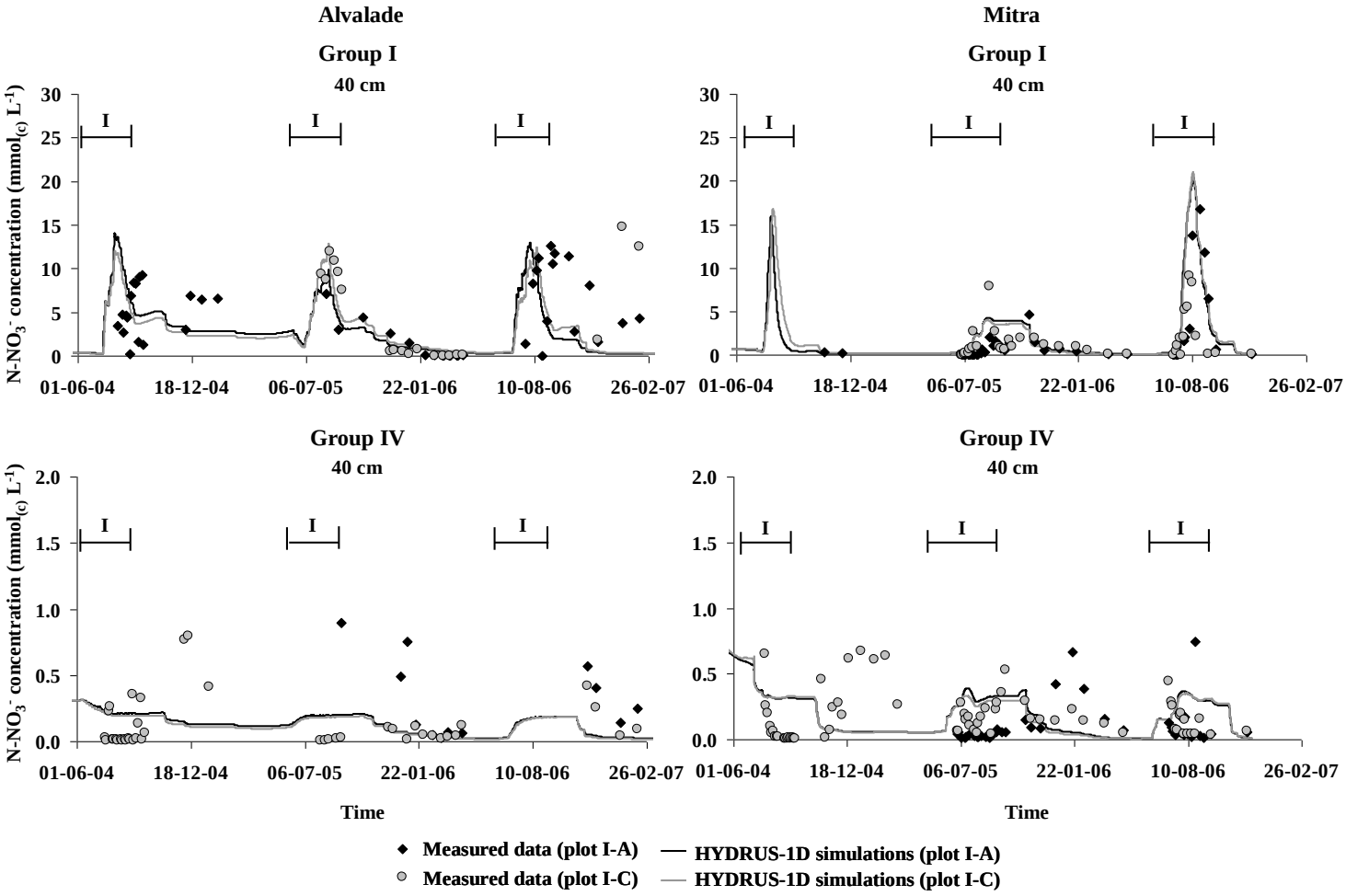

Fig. 9. Measured and simulated nitrate concentrations at a 40-cm depth in the experimental plots of groups I (top) and IV (bottom) in Alvalade (left) and Mitra (right). Symbol I denotes the irrigation periods.

Since nitrification in soils is usually a fast process, measured $N\text{-}NH_4^+$ concentrations in every experimental plot of both experimental fields were always lower than 0.30 $mmol_{(c)}\,L^{-1}$. While the highest residual values were observed during fertigation events, most values observed during remaining months were much lower and close to zero. Corresponding HYDRUS-1D simulations also predicted the highest $N\text{-}NH_4^+$ concentrations of about 0.13 $mmol_{(c)}\,L^{-1}$ during fertigation events, but only in the top layer of Alvalade (not shown graphically). Most simulated values were also close to zero, but even lower than the $N\text{-}NH_4^+$ concentrations measured in the soil solution.

Since most measured and calculated $N\text{-}NH_4^+$ concentrations were close to zero, RMSE resulted in values lower than 0.07 $mmol_{(c)}\ L^{-1}$ (Table 6), which may be quite significant since values measured in the field were practically residual.

There are a number of reasons that can explain low levels of agreement for $N\text{-}NH_4^+$ concentrations. The nitrification rate coefficient of 0.2 d^{-1} was an average value taken from Hanson et al. (2006). Since measured $N\text{-}NH_4^+$ values were higher than those simulated, nitrification in HYDRUS-1D was apparently faster than that occurring in the soil. This was more relevant for Alvalade where measured $N\text{-}NH_4^+$ concentrations were higher than in Mitra. When considering the lowest nitrification value (0.02 d^{-1}) found in Hanson et al. (2006) for the I-A plot in Alvalade, simulations showed higher $N\text{-}NH_4^+$ peaks, reaching values of 1.0 $mmol_{(c)}\ L^{-1}$ in the top 20 cm, and lower values with increasing depth. $N\text{-}NO_3^-$ concentration peaks decreased as ammonium was converted into nitrate at a rate 10 times slower than before (Fig. 10). However, this explanation can explain disagreement only during the days following fertigation events. A more likely explanation is related to the processes that were not considered in our simulations, but which are important for accurately describing $N\text{-}NH_4^+$ concentrations in the soil. Namely, mineralization of crop residues or other organic wastes, mineralization of the soil humus fraction, the release of $N\text{-}NH_4^+$ adsorbed to the solid phase into the liquid phase due to cation exchange, or other N processes that cannot be described with sequential first-order decay chains available in HYDRUS-1D. Since such processes were not considered in our simulations, here we are discussing only whether the model adequately simulated residual concentrations in the soil.

High nitrate concentrations were measured in both soil profiles during irrigation seasons due to fertigation and nitrification of the NH_4NO_3 fertilizer. In both experimental fields, the highest measured $N\text{-}NO_3^-$ concentrations were observed, as expected, in the plots located in group I, where the largest amount of fertilizer was applied. Measured $N\text{-}NO_3^-$ concentrations in group I reached a maximum value of about 15.0 and 16.5 $mmol_{(c)}\ L^{-1}$ in Alvalade and Mitra, respectively. Only a few isolated measurements produced values higher than these. In group IV, where no NH_4NO_3 fertilizer was added, the only source of nitrogen was the naturally occurring nitrogen in the fresh water. In both soils, the highest observed $N\text{-}NO_3^-$ concentrations were approximately

1.0 $mmol_{(c)}\ L^{-1}$. Similar values were also observed during rainy seasons. As discussed for N-NH_4^+, some of the observed N-NO_3^-, namely the values measured during the rainfall seasons, likely had origin in nitrogen processes that were not considered in our simulations. As a result, RMSE calculated for N-NO_3^- concentrations were 2.60 and 2.01 $mmol_{(c)}\ L^{-1}$ (Table 6).

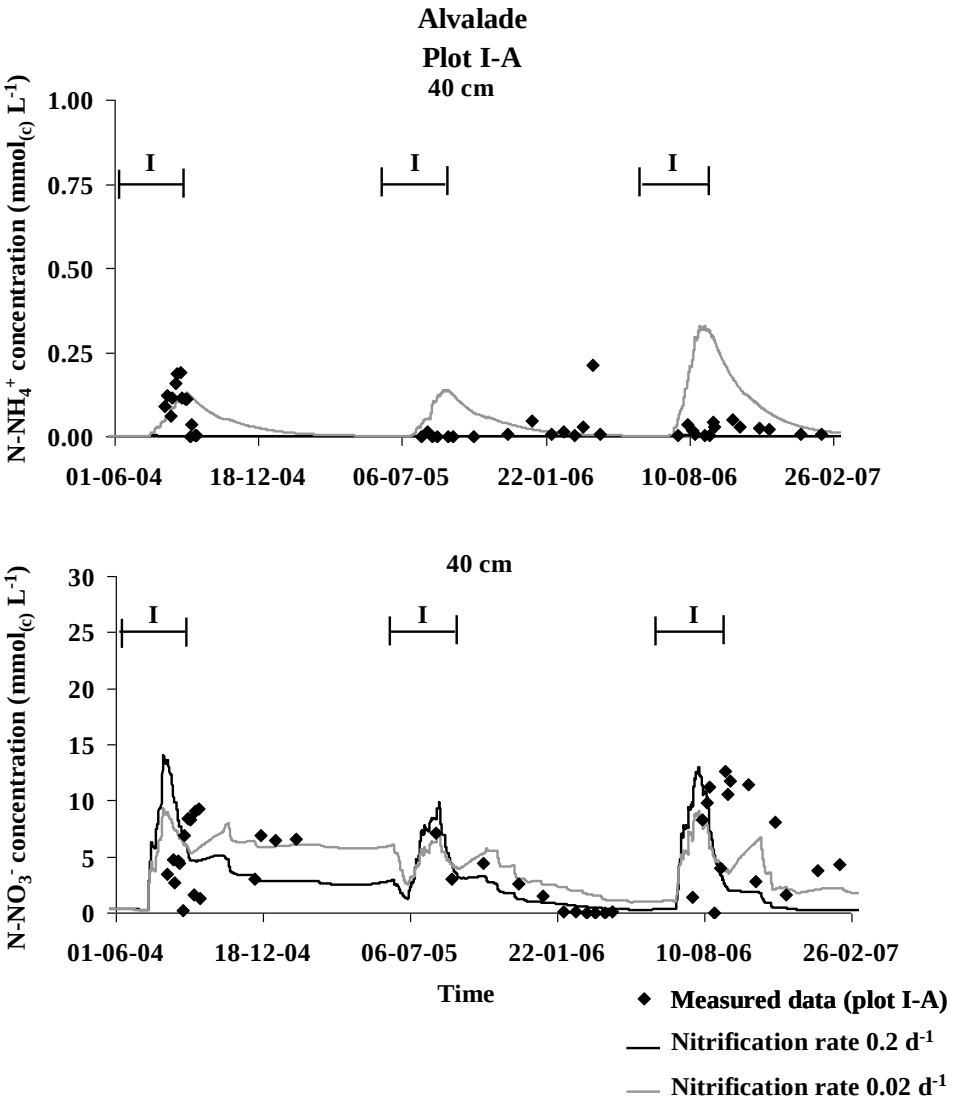

Fig. 10. Measured and simulated ammonium (top) and nitrate (bottom) concentrations at a 40-cm depth in the experimental plot I-A in Alvalade when considering nitrification rates of 0.2 and 0.02 d^{-1}. Symbol I denotes the irrigation periods.

The effect of the salinity stress on nutrient uptake is presented in Table 8. According to HYDRUS-1D simulations, cumulative nitrogen fluxes through the bottom of the plots located in sub-groups A were always higher than those predicted in the plots of sub-groups C. Such results were expected since only passive nutrient uptake was considered in our study. Irrigation of the experimental plots in sub-group A with saline waters led to the reduction of root water uptake due to osmotic stress, and consequently to the decreased mass flow of nutrients into roots. As a consequence of the salinity stress and reductions in nutrient uptake, the mass flow through the bottom of the soil profile increased.

Table 8. Cumulative nitrogen fluxes in the soil profiles of Alvalade and Mitra.

	Alvalade				Mitra			
	$N\text{-}NH_4^+$ ($g\ m^{-2}$)		$N\text{-}NO_3^-$ ($g\ m^{-2}$)		$N\text{-}NH_4^+$ ($g\ m^{-2}$)		$N\text{-}NO_3^-$ ($g\ m^{-2}$)	
Plots	A	C	A	C	A	C	A	C
Cumulative solute flux across the soil surface								
I	$1.24E^{+02}$	$1.29E^{+02}$	$1.30E^{+02}$	$1.33E^{+02}$	$6.37E^{+01}$	$6.37E^{+01}$	$7.07E^{+01}$	$6.98E^{+01}$
II	$6.18E^{+01}$	$6.17E^{+01}$	$6.70E^{+01}$	$6.66E^{+01}$	-	-	-	-
III	$3.12E^{+01}$	$3.20E^{+01}$	$3.65E^{+01}$	$3.70E^{+01}$	$1.27E^{+01}$	$1.17E^{+01}$	$1.99E^{+01}$	$1.81E^{+01}$
IV	$1.34E^{+00}$	$1.26E^{+00}$	$6.72E^{+00}$	$6.34E^{+00}$	$1.22E^{+00}$	$1.08E^{+00}$	$8.45E^{+00}$	$7.46E^{+00}$
Cumulative amount of solute removed from the flow region by root water uptake								
I	$5.95E^{-01}$	$1.03E^{+00}$	$4.97E^{+01}$	$8.00E^{+01}$	$3.59E^{-02}$	$1.45E^{-01}$	$7.12E^{+00}$	$1.34E^{+01}$
II	$3.31E^{-01}$	$5.26E^{-01}$	$2.88E^{+01}$	$4.24E^{+01}$	-	-	-	-
III	$1.81E^{-01}$	$2.87E^{-01}$	$1.57E^{+01}$	$2.37E^{+01}$	$8.76E^{-03}$	$2.99E^{-02}$	$2.88E^{+00}$	$4.52E^{+00}$
IV	$8.13E^{-03}$	$1.11E^{-02}$	$2.70E^{+00}$	$3.50E^{+00}$	$1.75E^{-03}$	$3.46E^{-03}$	$1.64E^{+00}$	$2.10E^{+00}$
Cumulative solute flux across the bottom of the soil profile								
I	$1.46\ E^{-05}$	$1.42\ E^{-05}$	$2.04\ E^{+02}$	$1.82\ E^{+02}$	$7.15\ E^{-05}$	$7.14\ E^{-05}$	$1.28\ E^{+02}$	$1.21\ E^{+02}$
II	$1.42\ E^{-05}$	$1.42\ E^{-05}$	$1.01\ E^{+02}$	$8.63\ E^{+01}$	-	-	-	-
III	$1.42\ E^{-05}$	$1.42\ E^{-05}$	$5.26\ E^{+01}$	$4.67\ E^{+01}$	$7.15\ E^{-05}$	$7.14\ E^{-05}$	$3.07\ E^{+01}$	$2.62\ E^{+01}$
IV	$1.42\ E^{-05}$	$1.41\ E^{-05}$	$6.36\ E^{+00}$	$5.12\ E^{-00}$	$7.15\ E^{-05}$	$7.16\ E^{-05}$	$9.04\ E^{+00}$	$7.47\ E^{+00}$

Although this simple approach was sufficient to describe our results, one could pose the obvious question whether active nutrient uptake should have been considered, and if it were, would we have obtained different results. Answers to these questions can be found in hypothetical examples discussed in Šimůnek and Hopmans (2009). First, nutrient concentrations measured in a soil do not provide sufficient evidence about the relative importance of active and passive nutrient uptake. Second, had active uptake been considered, root nutrient uptake would have been larger, which would have meant that $N\text{-}NH_4^+$ and $N\text{-}NO_3^-$ fluxes through the bottom of the soil profiles would have been smaller than those presented in Table 8. Nutrient uptake would have always

been reduced due to the effect of osmotic stress, which would likely reduce the nutrient demand. However, since our objective was to simulate our field experiments in a relatively simple way, considering only passive nutrient uptake seemed to be sufficient to describe nitrogen dynamics in the two studied soils. The values presented in Table 8 are merely indicative and serve only as a reference. The simulated cumulative $N\text{-}NO_3^-$ fluxes, fluxes, across the bottom of the soil profile for example, in plots I-A and I-C of Alvalade differed by only 22 g m^{-2} during the three years of the experiment. It is obvious that had we not simplified the LAI values used in our study, the LAI values that should have been used in I-C would have been higher than those measured in plot IV-C, which were simply extrapolated to the remaining plots in sub-group C. LAI values in plot I-C would then describe a crop well supplied with nitrogen, while plot IV-C was not, and with no salinity stress. In this scenario, higher LAI values would produce higher transpiration rates. Consequently, root water and nutrient uptakes would also increase, resulting in lower nitrogen fluxes to the groundwater. In this more realistic scenario the effect of the salinity stress on non-source pollution would have been much more considerable.

5. Summary and conclusions

The HYDRUS-1D numerical model successfully simulated water and solute transport in two multifactorial experiments, in which waters with different salinities and nitrogen concentrations were used. In these experiments, irrigation with waters blended using synthetic saline irrigation waters (EC_{iw}≤14.6 dS m^{-1}) and fresh irrigation waters (EC_{iw}≤1.2 dS m^{-1}) led to the salinization and sodification of the two studied soils.

The major ion chemistry module of HYDRUS-1D successfully simulated the water regime ($RMSE_{Alvalade}$ = 0.04 cm^3 cm^{-3}; $RMSE_{Mitra}$ = 0.04 cm^3 cm^{-3}), the overall salinity characterized by EC_{sw} ($RMSE_{Alvalade}$ = 2.04-2.35 dS m^{-1}; $RMSE_{Mitra}$ = 0.87-0.99 dS m^{-1}), the concentration of soluble Na^+ ($RMSE_{Alvalade}$ = 13.86 $mmol_{(c)}$ L^{-1}; $RMSE_{Mitra}$ = 6.44 $mmol_{(c)}$ L^{-1}), Ca^{2+} ($RMSE_{Alvalade}$ = 5.66 $mmol_{(c)}$ L^{-1}; $RMSE_{Mitra}$ = 3.54 $mmol_{(c)}$ L^{-1}), Mg^{2+} ($RMSE_{Alvalade}$ = 4.16 $mmol_{(c)}$ L^{-1}; $RMSE_{Mitra}$ = 1.75 $mmol_{(c)}$ L^{-1}), and SAR ($RMSE_{Alvalade}$ = 6.27 $(mmol_{(c)}L^{-1})^{0.5}$; $RMSE_{Mitra}$ = 3.91 $(mmol_{(c)}L^{-1})^{0.5}$) in different plots of each experimental field. RMSE were always lower in the soil with coarse texture of Mitra than in the soil with medium texture of Alvalade. Possible causes of disagreements between the modeling and experimental data were discussed in the Results section.

In addition, the less favorable hydraulic conditions of Alvalade, as compared to Mitra, namely the lower K_s values of the soil with medium texture, were decisive for not obtaining higher levels of performance in the goodness-of-fit tests for this soil. Note that in Alvalade, solute concentrations in the irrigation water were low (e.g., for Ca^{2+} and Mg^{2+}), resulting only from what was present in the available water in the region.

HYDRUS-1D further predicted root water uptake reductions due to water and osmotic stresses. Root water uptake was reduced by about 39% in the experimental plots at Alvalade and 77% at Mitra, due to water stress. These water stress reductions were a consequence of the soil physical and hydrodynamic characteristics and plant type, but mostly of the irrigation schedule. Potential transpiration was further reduced by about 59% at Alvalade and 83% at Mitra due to the effects of the osmotic stress in the experimental plots irrigated with saline waters.

Root water uptake reductions obtained with the major ion chemistry module were reproduced with the standard HYDRUS solute transport module in order to study the effect of salinity stress on nutrient uptake. HYDRUS-1D successfully modeled $N\text{-}NH_4^+$ ($RMSE_{Alvalade}$=0.07 $mmol_{(c)}\ L^{-1}$; $RMSE_{Mitra}$=0.05 $mmol_{(c)}\ L^{-1}$) and $N\text{-}NO_3^-$ ($RMSE_{Alvalade}$=2.60 $mmol_{(c)}\ L^{-1}$; $RMSE_{Mitra}$=2.01 $mmol_{(c)}\ L^{-1}$) concentrations while either assuming or neglecting the effect of the osmotic stress on nutrient uptake. HYDRUS-1D does not account for N processes that cannot be described with sequential first-order decay chains. As a result, RMSE obtained for $N\text{-}NH_4^+$ and for $N\text{-}NO_3^-$ reflect errors caused by not considering processes other than nitrification, which were apparently relevant for describing residual concentrations. According to HYDRUS-1D simulations, irrigation with saline waters led to root water and nutrient uptake reductions due to osmotic stress. Consequently, the fluxes of $N\text{-}NH_4^+$ and $N\text{-}NO_3^-$ through the bottom of the soil profiles increased.

In our study, most model inputs were independently measured in the laboratory and used in simulations without any further adjustments and/or calibration. The correspondence between measurements and model results would have obviously been better, had the input parameters been calibrated. However, only a model that can be successfully run with independently measured input parameters is sufficiently robust for practical applications.

In spite of the considerable demand on input data, HYDRUS-1D proved to be an effective and versatile tool that may become very useful for irrigation management in regions with scarce water resources where suitable waters are not always available for irrigation. HYDRUS-1D was able to analyze two of the most important soil processes (i.e., transport and reactions of salts and nitrogen species in the soil profile) resulting in degradation of groundwaters in these regions in an integrated way. HYDRUS-1D, after proper calibration and validation, should be considered to be a useful tool for establishing sound irrigation policies in order to mitigate soil salinization/sodification and non-point source pollution from agricultural applications of fertilizers in irrigated areas of countries located in regions with arid, semi-arid, and even sub-humid conditions.

Acknowledgment

This work was possible due to the funding provided by the Project PTDC/AGR-AAM/66004/2006 of the Fundação para a Ciência e a Tecnologia (FCT) and the Project AGRO 727 of the Portuguese Ministry of Agriculture, Fisheries, and Rural Development. T. B. Ramos was funded by the FCT grant (contract SFRH/BD/60363/2009).

References

Ahuja, L.R., Rojas, K. W., Hanson, J.D., Shaffer, M. J., Ma, L. (Eds.), 2000. The Root Zone Water Quality Model. Water Resources Publ., LLC, Highlands Ranch, CO, 372 pp.

Ajdary, K., Singh, D.K., Singh, A.K., Khanna, M., 2007. Modelling of nitrogen leaching from experimental onion field under drip irrigation. Agricultural Water Management 89, 15-28.

Allen, R.G., Pereira, L.S., Raes, D., Smith, M., 1998. Crop evapotranspiration – Guidelines for computing crop water requirements. Irrig. Drain. Pap. 56. FAO, Rome, Italy.

Ayers, R., Westcot. D., 1985. Water quality for agriculture. Irrig. Drain. Pap. 29. FAO, Rome, Italy.

Bascomb, C.L., 1964. Rapid method for the determination of cation-exchange capacity of calcareous and non-calcareous soils. J. Sci. Food Agric. 12, 821-823.

Beltrão, J., Jesus, S.B., Silva, V., Sousa, P.B., Carvalho, I., Trindade, D., Rodrigues, M.H., Machado, A., 2002. Efficiency of triple emitter source (TES) for irrigation experiments of horticultural crops. Acta Hortic. 573, 183-188.

Bresler, E., McNeal, B. L., Cárter, D.L., 1982. Saline and sodic soils. Principles-Dynamics-Modeling. Advanced Series in Agricultural Sciences 10. Springer-Verlag.

Cote, C.M., Bristow, K.L., Charlesworth, P.B., Cook, F.J., Thorburn, P.J., 2003. Analysis of soil wetting and solute transport in subsurface trickle irrigation. Irrig. Sci. 22, 143-156.

Crevoisier, D., Popova, Z., Mailhol, J.C., Ruelle, P., 2008. Assessment and simulation of water and nitrogen transfer under furrow irrigation. Agric. Water Manage. 95, 354-366.

Feddes, R.A., Kowalik, P.J., Zaradny, H., 1978. Simulation of field water use and crop yield. Simulation Monographs Pudoc, Wageningen, The Netherlands.

Feddes, R.A., Raats, P.A.C., 2004. Parameterizing the soil-water-plant-root system, in: Feddes, R. A., de Rooij, G.H., van Dam, J.C. (Eds.), Proceedings of the Unsaturated Zone Modelling: Progress, Challenges and Applications, pp. 95-141. Wageningen UR Frontis Series, vol. 6, Kluwer Academic Publishers, Dordrecht, The Netherlands.

Forkutsa, I., Sommer, R., Shirokova, Y.I., Lamers, J.P.A., Kienzler, K., Tischbein, B, Martius, C., Vlek, P.L.G., 2009. Modeling irrigated cotton with shallow groundwater in the Aral Sea Basin of Uzbekistan: II. Soil salinity dynamics. Irrig. Sci. 27, 319-330.

Gärdenäs, A., Hopmans, J.W., Hanson, B.R., Šimůnek, J., 2005. Two-dimensional modeling of nitrate leaching for various fertigation scenarios under micro-irrigation. Agric. Water Manage. 74, 219-242.

Gonçalves, J.M., Pereira, L.S., Fang, S.X., Dong. B., 2007. Modelling and multicriteria analysis of water saving scenarios for an irrigation district in the upper Yellow River Basin. Agric. Water Manage. 94, 93-108.

Gonçalves, M.C., Leij, F.J., Schaap, M.G., 2001. Pedotransfer functions for solute transport parameters of Portuguese soils. Euro. J. Soil Sci. 52, 563-574.

Gonçalves, M.C., Šimůnek, J., Ramos, T.B., Martins, J.C., Neves, M.J., Pires, F.P., 2006. Multicomponent solute transport in soil lysimeters with waters of different quality. Water Resour. Res. 42, W08401, doi:10.1029/2005WR004802.

Halbertsma, J.M., Veerman, G.J., 1994. A new calculation procedure and simple set-up for the evaporation method to determine soil hydraulic functions. DLO Winand Staring Centre, Report 88, Wageningen, The Netherlands.

Hanson, B.R., Šimůnek, J., Hopmans, J.W., 2006. Evaluation of urea-ammonium-nitrate fertigation with drip irrigation using numerical modeling. Agric. Water Manage. 86, 102-113.

Hanson, B.R., Šimůnek, J., Hopmans, J.W., 2008. Leaching with subsurface drip irrigation under saline, shallow ground water conditions. Vadose Zone J. 7, 810-818.

Hendrilsen, A., Selmer-Olsen, A.R., 1970. Automatic methods for determination of nitrate and nitrite in water and soil extracts. The Analyst 95, 514-518.

Jarvis, N.J., 1994. The MACRO model (Version 3.1). Technical description and sample simulations. Reports and Dissert. 19, Dept. Soil Sci., Swedish Univ. Agric. Sci., Uppsala, Sweden, 51 pp.

Legates, D.R., McCabe Jr, G.J., 1999. Evaluating the use of "goodness-of-fit" measures in hydrologic and hydroclimatic model validation. Water Resour. Res. 35, 233–241.

Machado, R., Oliveira, M.R., 2003. Comparison of tomato root distribution by minirhizotron and destructive sampling. Plant Soil 255, 375-385.

Mallants, D., Vanclooster, M., Meddahi, M., Feyen, J., 1994. Estimating solute transport in undisturbed soil columns using time domain reflectrometry. J. Contam. Hydrol. 17, 91-109.

Mass, E.V., 1990. Crop salt tolerance, in: Tanji, K. K (Ed.), Agricultural Salinity Assessment and Management. Manual Eng. Pract., vol. 71, pp. 262–304, Am. Soc. of Civ. Eng., Reston, Va.

McNeal, B.L., Oster, J.D., Hatcher, J.T., 1970. Calculation of electrical conductivity from solution composition data as an aid to in-situ estimation of soil salinity. Soil Sci. 110, 405-414.

Oster, J.D., Letey, J., Vaughan, P., Wu, L., Qadir, M., 2012. Comparison of transient state models that include salinity and matric stress effects on plant yield. Agric. Water Manage. 103, 167-175.

Pereira, L.S., Cordey, I., Iacovides, I., 2009. Coping with water scarcity. Addressing the challenges. Springer.

Pereira, L.S., Gonçalves, J.M., Dong, B., Mao, Z., Fang, S.X., 2007. Assessing basin irrigation and scheduling strategies for saving irrigation water and controling salinity in the upper Yellow River Basin, China. Agric. Water Manage. 93, 109-122.

Ramos, T.B.; Gonçalves, M.C.; Castanheira, N.L.; Martins, J.C.; Santos, F.L.; Prazeres, A., Fernandes, M. L., 2009. Effect of sodium and nitrogen on yield function of irrigated maize in southern Portugal. Agric. Water Manage. 96, 585-594.

Ritchie, J.T., 1972. Model for predicting evaporation from a row crop with incomplete cover. Water Resour. Res. 8, 1204-1213.

Roberts, T., Lazarovitch, N., Warrick, A.W., Thompson, T.L., 2009. Modeling salt accumulation with subsurface drip irrigation using HYDRUS-2D. Soil Sci. Soc. Am. J. 73, 233-240.

Roberts, T., White, S.A., Warrick, A.W., Thompson, T.L., 2008. Tape depth and germination method influence patterns of salt accumulation with subsurface drip irrigation. Agric. Water Manage. 95, 669-677.

Searle, P.L., 1984. The Berthlot or Indophenol reaction and its use in the analysis chemistry for nitrogen. The Analyst 109, 549-565.

Šimůnek, J., Hopmans, J.W., 2009. Modeling compensated root water and nutrient uptake. Ecol. Model. 220, 505-521.

Šimůnek, J., van Genuchten, M.Th., Šejna, M., 2006. The HYDRUS software package for simulating two- and three-dimensional movement of water, heat, and multiple solutes in variably-saturated media, Technical manual. Version 1.0, PC Progress, Prague, Czech Republic, 241 pp.

Šimůnek, J., Šejna, M., Saito, H., Sakai, M., van Genuchten, M.Th., 2008a. The HYDRUS-1D software package for simulating the movement of water, heat, and multiple solutes in

variably-saturated media. Version 4.0. HYDRUS Software Series 3, Department of Environmental Sciences, University of California Riverside, Riverside, CA, USA, 315 pp.

Šimůnek, J., Suarez, D.L., 1994. Two-dimensional transport model for variably saturated porous media with major ion chemistry. Water Resour. Res. 30, 1115-1133.

Šimůnek, J., Suarez, D.L., Šejna, M. 1996. The UNSATCHEM software package for simulating one-dimensional variably saturated water flow, heat transport, carbon dioxide production and transport, and multicomponent solute transport with major ion equilibrium and kinetic chemistry. Version 2.0, Res. Rep. 141, , U. S. Salinity Lab., Agric. Res. Serv., Riverside, Calif., 186 pp.

Šimůnek, J., Valocchi, A.J., 2002. Geochemical transport, in: Dane, J.H., Topp, G.C. (Eds.), Methods of Soil Analysis, part 1, Physical Methods, pp. 1511-1536. Soil Sci. Soc. of Am., Madison, Wisconsin, USA.

Šimůnek, J., van Genuchten, M.Th., Šejna, M., Toride, N., Leij, F.J., 1999. The STANMOD computer software for evaluating solute transport in porous media using analytical solutions of convection-dispersion equation. Versions 1.0 and 2.0, IGWMC - TPS - 71, International Ground Water Modeling Center, Colorado School of Mines, Golden, Colorado, 32 pp.

Šimůnek, J., van Genuchten, M.Th.., Šejna, M., 2008b. Development and applications of the HYDRUS and STANMOD software packages, and related codes. Vadose Zone J., Special Issue "Vadose Zone Modeling" 7, 587-600, doi:10.2136/VZJ2007.0077.

Skaggs, T.H., Shouse, P.J., Poss, J.A., 2006. Irrigating forage crops with saline waters: 2. Modeling root uptake and drainage. Vadose Zone J. 5, 824-837.

Soil Survey Staff, 2006. Keys to Soil Taxonomy. 10th Edition. Washington, DC, Natural Resources Conservation Service, United States Department of Agriculture.

Steppuhn, H., van Genuchten, M.Th., Grieve, C.M., 2005. Root-zone salinity: II. Indices for tolerance in agricultural crops. Crop Sci. 45, 221–232.

Stolte, J., 1997. Determination of the saturated hydraulic conductivity using the constant head method, in: Stolte, J. (Ed.), Manual for soil physical measurements. Technical document 37, DLO Winand Staring Centre, Wageningen, The Netherlands.

Toride, N., Leij, F.J., van Genuchten, M.Th., 1995. The CXTFIT code for estimating transport parameters from laboratory or field tracer experiments. Version 2.0. Research Report 137, US Salinity Laboratory, Riverside, California, USA.

Truesdell, A.H., Jones, B.F., 1974. Wateq, a computer program for calculating chemical equilibria of natural waters. J. Res. U.S. Geol. Surv. 2, 233– 248.

U.S. Salinity Laboratory Staff, 1954. Diagnosis and Improvement of Saline and Alcaly Soils. USDA Handbook 60. Washington, USA.

van Dam, J.C., Huygen, J., Wesseling, J.G., Feddes, R.A., Kabat, P., van Valsum, P.E.V., Groenendijk, P., van Diepen, C.A., 1997. Theory of SWAP, version 2.0. Simulation of water flow, solute transport and plant growth in the soil–water–atmosphere–plant environment. Dept. Water Resources, WAU, Report 71, DLO Winand Staring Centre, Wageningen, Technical Document 45.

van den Berg, M., Driessen, P.M., Rabbinge, R., 2002. Water uptake in crop growth models for land use systems analysis. II. Comparison of three simple approaches. Ecol. Model. 148, 233–250.

van Genuchten, M.Th., 1980. A closed form equation for predicting the hydraulic conductivity of unsaturated soils. Soil Sci. Soc. Am. J. 44, 892-898.

van Genuchen, M.Th., 1987. A numerical model for water and solute movement in and below the root zone. Res. Rep. 121, U.S. Salinity Laboratory, USDA, ARS, Riverside, California.

van Genuchten, M.Th., Leij, F. J., Yates, S.R., 1991. The RETC code for quantifying the hydraulic functions of unsaturated soils. Report No. EPA/600/2-91/065. R. S. Kerr Environmental Research Laboratory, U. S. Environmental Protection Agency, Ada, OK., 85 pp.

van Genuchen, M. Th., Šimůnek, J., 2004. Integrated modeling of vadose zone flow and transport processes, in: Feddes, R. A., de Rooij, G. H., van Dam, J. C. (Eds.), Proc. Unsaturated Zone Modelling: Progress, Challenges and Applications, pp. 37-69. Wageningen, The Netherlands, October 3-5.

Wagenet, R.J., Hutson, J.L., 1987. LEACHM: Leaching Estimation and Chemistry Model, a process-based model of water and solute movement, transformations, plant uptake and

chemical reactions in the unsaturated zone, continuum 2, report, Water Resour. Inst., Cornell Univ., Ithaca, N. Y.

Weihermüller, L., Kasteel, R., Vanderborght, J., Pütz, T., Vereecken, H., 2005. Soil Water Extraction with a Suction Cup: Results of Numerical Simulations. Vadose Zone J. 4, 899-907.

Wesseling, J.G., Elbers, J.A., Kabat, P., van den Broek, B.J., 1991. SWATRE: Instructions for input. Report, Winand Staring Cent., Wageningen, Netherlands.

Wind, G.P., 1968. Capillary conductivity data estimated by a simple method, in: Rijtema, P. E., Wassink, H. (Eds.), Water in the unsaturaded zone, pp. 181–191. Proceedings of a Symposium, June 1966, Wagningen, The Netherlands. IASH/AIHS – UNESCO, vol. I.

Chapter 3

Two-dimensional modeling of water and nitrogen fate from sweet sorghum irrigated with fresh and blended saline waters

(Published in: Agricultural Water Management 111, 87-104. 2012)

Two-dimensional modeling of water and nitrogen fate from sweet sorghum irrigated with fresh and blended saline waters

T. B. Ramos[1], J. Šimůnek[2], M. C. Gonçalves[1,3], J. C. Martins[3], A. Prazeres[3] and L. S. Pereira[1]

[1] CEER-Biosystems Engineering, Institute of Agronomy, Technical University of Lisbon, Tapada da Ajuda, 1349-017 Lisbon, Portugal

[2] Department of Environmental Sciences, University of California, Riverside, CA, 92521, USA.

[3] Estação Agronómica Nacional, L-INIA, Instituto Nacional de Recursos Biológicos, 2784-505 Oeiras, Portugal.

Abstract

The need for reducing irrigation water demand and non-point source pollution all across Europe has made sweet sorghum [*Sorghum bicolor* (L.) Moench], due to its lower water and nutrient requirements, an interesting alternative to other traditional summer crops in European Mediterranean regions. HYDRUS-2D was used to model the fate of nitrogen in a plot planted with sweet sorghum grown under Mediterranean conditions between 2007 and 2010, while considering drip irrigation scenarios with different levels of nitrogen and salty waters. HYDRUS-2D simulated water contents, EC_{sw}, and N-NH_4^+ and N-NO_3^- concentrations continuously for the entire duration of the field experiment, while producing RMSE between simulated and measured data of 0.030 cm^3 cm^{-3}, 1.764 dS m^{-1}, 0.042 $mmol_c$ L^{-1}, and 3.078 $mmol_c$ L^{-1}, respectively. Estimates for sweet sorghum water requirements varied between 360 and 457 mm depending upon the crop season and the irrigation treatment. Sweet sorghum proved to be tolerant to saline waters if applied only during one crop season. However, the continuous use of saline waters for more than one crop season led to soil salinization, and to root water uptake reductions due to the increasing salinity stress. The relation found between N-NO_3^- uptake and dry biomass yield (R^2=0.71) showed that nitrogen needs were smaller than the uptakes estimated for the scenario with the highest levels of nitrogen application. The movement of N out of the root zone was dependent on the amount of water flowing through the root zone, the amount of N applied, the

form of N in the fertilizer, and the timing and number of fertigation events. The simulations with HYDRUS-2D were useful to understand the best strategies toward increasing nutrient uptake and reducing nutrient leaching. In this sense, $N\text{-}NO_3^-$ uptakes were higher when fertigation events were more numerous and the amounts applied per event smaller.

Keywords: HYDRUS-2D, saline irrigation water, nitrates leaching, sorghum yields.

1. Introduction

Non-point source pollution is among the most important and widespread environmental problems in European Mediterranean agricultural regions. Farmers usually apply high rates of water and nitrogen fertilizer to insure that crop needs are fulfilled, while producing inefficient water and nitrogen use, and increasing leaching potential of nutrients into the groundwater.

The European Commission implemented the Council Directive 91/676/EEC in 1991, also referred to as the Nitrates Directive, which imposed upon EU-Member States the establishment of various action programs for reducing water contamination caused or induced by agricultural sources. However, twenty years later many European regions with higher agriculture intensity continue registering high nitrate concentrations in a significant number of groundwater monitoring stations. In particular, many monitoring stations in the European Mediterranean Member States showed relatively high values throughout 2004-2007. Nitrate vulnerable zones covered 3.7% of Portugal, 6.8% of Cyprus, 12.6% of Spain and Italy, 24.2% of Greece, and 100% of Malta's territories (European Commission, 2010a, 2010b).

In these water-scarce European Mediterranean regions, the use of crops with lower water and nutrient needs has recently been considered to be an adequate alternative to traditional crops such as corn, in order to reduce nutrient loads into the groundwater (Barbanti et al., 2006). Sweet sorghum (*Sorghum bicolor* (L.) Moench) was regarded among the most interesting annual crops to be grown in these environmentally stressed areas (Almodares and Hadi, 2009; Vasilakoglou et al., 2011). Sweet sorghum is a drought resistant crop with relatively low water requirements and high water-use efficiency (Mastrorilli et al, 1995, 1999; Steduto et al., 1997; Katerji et al., 2008), and is moderately tolerant to salinity (Maas, 1990; Hoffman and Shalhevet, 2007). Sweet

sorghum is furthermore an important alternative source for renewable energy because of its ability to store large quantities of non-structural carbohydrates (sucrose, glucose, and fructose) in its stems that can be converted into fuel ethanol (Prasad et al., 2005; Zhao et al., 2009; Almodares and Hadi, 2009).

A large number of analytical and numerical modeling tools are available to evaluate the effects of different agricultural practices on nitrogen leaching, nutrient uptake, and crop yield (e.g., Johnsson et al., 1987; Hutson and Wagenet, 1991; Ma et al., 2001; Šimůnek et al., 2008; Doltra and Muñoz, 2010). Simulation models can rapidly perform a long-term analysis of the effects of introducing new crops and/or new agricultural practices in nitrate vulnerable zones, and help develop action programs to minimize nutrient loads into groundwater as required by the Nitrates Directive.

Some of those physical-based models have been calibrated and/or validated to simulate water movement (Fernando, 2003; Cameira et al, 2005), nutrient transport (Cameira et al., 2003, 2007), soil salinity distribution (Gonçalves et al., 2006; Ramos et al., 2011), and runoff and soil erosion (Fontes et al., 2004) in different regions of Portugal. Semi-empirical water balance models have also been developed to improve irrigation scheduling and reduce water losses (Pereira et al., 1995; Rosa et al., 2012). However, these approaches have been only one-dimensional and neglected water and solute fluxes, and pressure head and concentration gradients in the horizontal direction. Additionally, one-dimensional models fail to adequately simulate micro-irrigation systems (such as drip emitters, drip tape, and micro-sprinklers), which can efficiently apply water and nutrients in the right amounts and precise locations throughout a field (Gärdenäs et al., 2005). Since drip irrigation is often used in Portugal it seems only adequate to find modeling approaches that are more suitable to represent complex physical and chemical processes that take place in the soil profile under this irrigation system.

The HYDRUS (2D/3D) software package (Šimůnek et al., 2006, 2008) is the state-of-the-art model for simulating water, heat, and solute movement in two- and three-dimensional variably-saturated porous media that can become a valuable tool for establishing sound agricultural practices in European Mediterranean agricultural regions. The model has been extensively used for simulating the fate of nutrients in soils by evaluating and comparing micro-irrigation and fertigation strategies for different crops (Cote et al., 2003; Gärdenäs et al., 2005; Hanson et al.,

2006; Ajdary et al., 2007; Crevoisier et al., 2008). It has also been used for a wide range of applications of interest for water scarce regions, such as improving irrigation management with poor quality waters (Gonçalves et al., 2006; Hanson et al., 2008; Roberts et al., 2008; 2009; Ramos et al., 2011). Furthermore, HYDRUS-2D (a two-dimensional module of HYDRUS (2D/3D)) results are often used as a reference for developing or validating new simulation models (Mmlowa and Or, 2003; Doltra and Muñoz, 2010; Mailhol el al., 2011).

The main objective of this study was to use the HYDRUS-2D software package to model nitrogen fate in a plot with sweet sorghum grown under Mediterranean conditions while considering different drip fertigation and water quality scenarios. From 2007 to 2010 (i.e., during three crop seasons), sweet sorghum was subjected to the application of different amounts of nitrogen, different fertigation events, and to irrigation with waters of different quality. Field data were used to calibrate and validate HYDRUS-2D for predicting (i) soil water contents and fluxes, (ii) the electrical conductivity of the soil solution (EC_{sw}), (iii) water uptake reductions due to the use of saline waters, and (iv) $N\text{-}NH_4^+$ and $N\text{-}NO_3^-$ concentrations in the soil and leaching. Water and nutrient balances were calculated based on HYDRUS-2D predictions for three crop seasons and for the entire simulation period. The modeling approach helped us understand the best irrigation and fertigation management practices to be adopted in future practical applications for increasing nutrient uptake and reducing nutrient leaching.

2. Material and methods

2.1. Experimental setup and measurements

The field experiment was conducted at the Alvalade Experimental Station (37º 56' 48'' N and 8º 23' 40'' W), southern Portugal, from May 2007 to April 2010. The climate in the region is dry, sub-humid, with hot dry summers and mild winters with irregular rainfall. Rainfall was 371, 299, and 676 mm in 2007/2008, 2008/2009, and 2009/2010, respectively, with 91, 63, and 35 mm of rain during the corresponding crop growth seasons. The soil was classified as a Eutric Fluvisol (FAO, 2006). The soil's main physical and chemical properties are presented in Table 1. Field and laboratory methodologies used for characterizing the soil profile were extensively described by Ramos et al. (2011).

Table 1. Main physical and chemical soil characteristics.

	Alvalade		
Depth (cm)	**0-30**	**30-75**	**75-100**
Coarse sand, 2000-200 µm (%)	8.3	6.5	5.8
Fine sand, 200-20 µm (%)	52.4	46.2	42.0
Silt, 20-2 µm (%)	26.3	29.3	27.6
Clay, <2 µm (%)	13.0	18.0	24.6
Texture	Loam	Silty Loam	Loam
Bulk density (g cm^{-3})	1.49	1.51	1.61
pH (H_2O)	7.27	7.23	7.21
Organic matter (%)	2.30	2.26	1.66
Soil initial conditions:			
Water content (cm^3 cm^{-3})	0.18	0.18	0.18
EC_{sw} (dS m^{-1})	2.17	2.99	4.68
N-NH_4^+ ($mmol_c$ L^{-1})	0.01	0.01	0.01
N-NO_3^- ($mmol_c$ L^{-1})	0.31	0.47	1.43
van Genuchten-Mualem parameters:			
θ_r (cm^3 cm^{-3})	0.050	0.108	0.000
θ_s (cm^3 cm^{-3})	0.380	0.380	0.375
α (cm^{-1})	0.027	0.115	0.045
η (-)	1.21	1.19	1.17
ℓ (-)	-4.41	-5.37	-6.48
K_s (cm d^{-1})	16.6	84.4	21.0
Solute transport parameters:			
ε_L (cm)	25.8	25.8	12.2

EC_{sw}, electrical conductivity of the soil solution; θ_r, residual water content; θ_s, saturated water content; α and η, are empirical shape parameters; ℓ, pore connectivity/tortuosity parameter; K_s, saturated hydraulic conductivity;. ε_L, longitudinal dispersivity.

The field experiment involved irrigation of sweet sorghum (*Sorghum bicolor* (L.) Moench var. *saccharatum* (L.) Mohlenbr) with synthetic saline waters blended with fresh irrigation waters and waters with nitrogen (NH_4NO_3) during three crop seasons. The crop hybrid selected for this experiment was the sweet sorghum "Madhura", developed in India. Sweet sorghum was sown on May 18, 2007, May 15, 2008, and May 15, 2009. The row spacing used was 0.75 m and the distance between plants was 0.15 m. Irrigation started on June 1, 2007 (15 days after sowing, or DAS), June 13, 2008 (30 DAS), and June 3, 2009 (20 DAS). The total amount of water applied was 425, 522, and 546 mm in 2007, 2008, and 2009, respectively.

The drip irrigation system was used to mix and deliver synthetic saline irrigation waters, fresh irrigation waters, and fertilizer (NH_4NO_3) to the experimental plots following the irrigation scheme documented in Ramos et al. (2009, 2011). This system consisted of three drip lines connected together in order to form a triple joint lateral placed along each sweet sorghum line

(Fig. 1). The first of the laterals was connected to the salt stock solution (NaCl), while the second one was connected to the nitrogen reservoir. The third lateral delivered fresh water and was used to obtain a constant water application rate for each dripping point along the triple joint lateral (the drip discharge of 18 L h^{-1} m^{-1}; which represents 24 mm h^{-1} considering an area for each dripping point of 100 cm x 75 cm). Gradients of applied salt (Na^{+}) and nitrogen (N) concentrations were then produced by placing different emitters in each dripping point along the corresponding laterals and varying their discharge rates to obtain various mixtures between the three lines. Table 2 lists the different discharge rates of the emitters applying salts, nitrogen, and fresh water to each experimental plot. Table 3 presents the amount of saline waters, fresh waters, and waters with nitrogen applied in each experimental plot. The blended amounts thus varied between experimental plots, while the total amount of water applied per irrigation event and per crop season, as well as the quality of the irrigation waters before blending (Table 4), remained identical in all experimental plots.

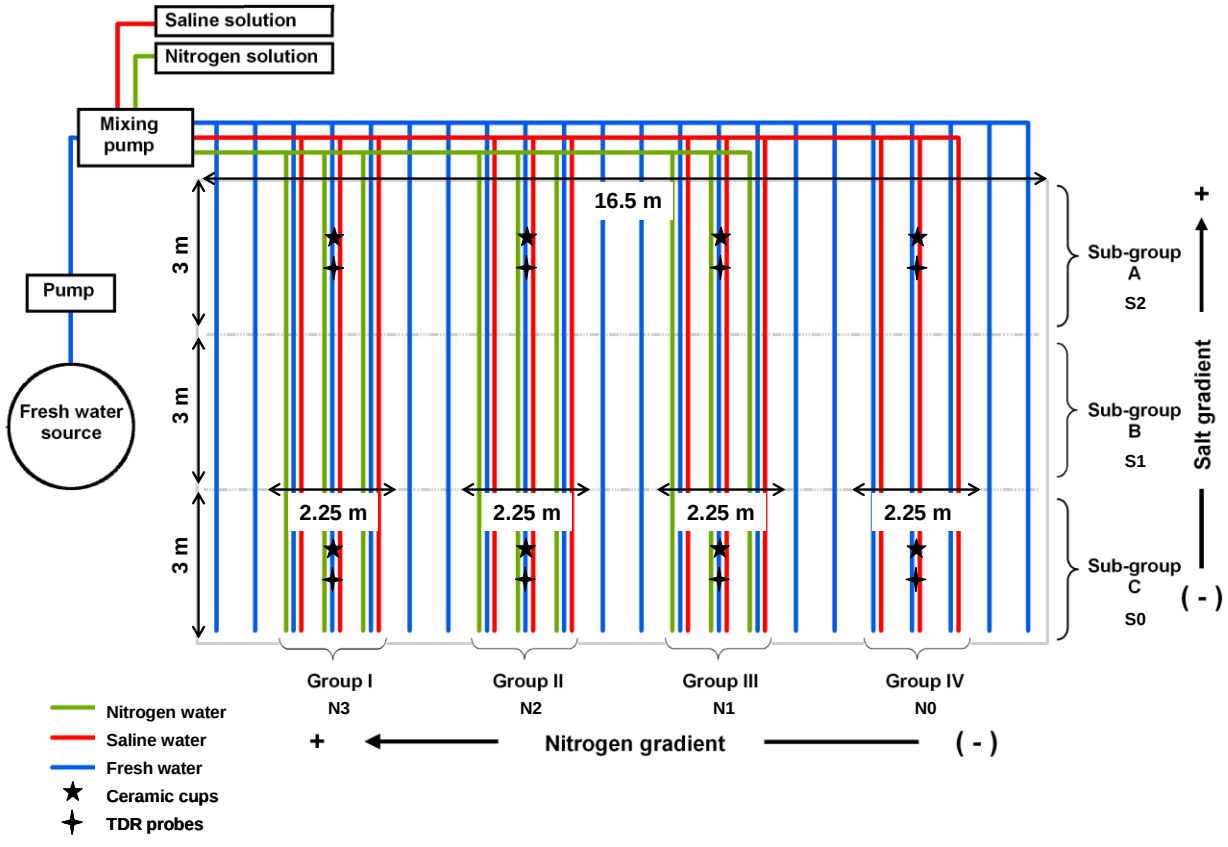

Fig. 1. Layout of the triple emitter source design (adapted from Ramos et al., 2009). The salt gradient decreases from sub-group A to C and the fertilizer gradient decreases from group I to IV.

Table 2. Discharge rates of the laterals applying salt (Na^+), nitrogen (N) and fresh water (W) in each experimental plot. There is an overall constant cumulative discharge at each dripping point of 18 L/h/m (Ramos et al., 2009).

Treatment	Application Rates (L/h/m)											
	Group I			Group II			Group III			Group IV		
	Na^+	N	W	Na^+	N	W	Na^+	N	W	Na^+	N	W
A	12	6	0	12	4	2	12	2	4	12	0	6
B	6	6	6	6	4	8	6	2	10	6	0	12
C	0	6	12	0	4	14	0	2	16	0	0	18

Table 3. Waters blended in each experimental plot during the three crop seasons.

Sub-group	Irrigation water	Water applied (mm)											
		Group I (N3)			Group II (N2)			Group III (N1)			Group IV (N0)		
		2007	2008	2009	2007	2008	2009	2007	2008	2009	2007	2008	2009
A (S2)	Saline water	228.0	184.0	316.0	228.0	184.0	316.0	228.0	184.0	316.0	228.0	184.0	316.0
	Water + NH_4NO_3	19.3	30.0	20.0	12.9	20.0	13.3	6.4	10.0	6.7	0.0	0.0	0.0
	Fresh water	177.7	308.0	210.0	184.1	318.0	216.7	190.6	328.0	223.3	197.0	338.0	230.0
B (S1)	Saline water	114.0	92.0	158.0	114.0	92.0	158.0	114.0	92.0	158.0	114.0	92.0	158.0
	Water + NH_4NO_3	19.3	30.0	20.0	12.9	20.0	13.3	6.4	10.0	6.7	0.0	0.0	0.0
	Fresh water	291.7	400.0	368.0	298.1	410.0	374.7	304.6	420.0	381.3	311.0	430.0	388.0
C (S0)	Saline water	0.0	0.0	0.0	0.0	0.0	0.0	0.0	0.0	0.0	0.0	0.0	0.0
	Water + NH_4NO_3	19.3	30.0	20.0	12.9	20.0	13.3	6.4	10.0	6.7	0.0	0.0	0.0
	Fresh water	405.7	492.0	526.0	412.1	502.0	532.7	418.6	512.0	539.3	425.0	522.0	546.0

N3, N2, N1, N0, nitrogen gradient; S2, S1, S0, salinity gradient.

Table 4. Characteristics of the irrigation waters blended in each experimental plot.

Irrigation waters	Year	EC_{iw} (dS m^{-1})	N-NH4+ ($mmol_c$ L^{-1})	N-NO3- ($mmol_c$ L^{-1})
Fresh waters	2007-2009	0.81	0.03	0.15
Saline waters	2007	7.60	0.03	0.15
	2008	9.60	0.03	0.15
	2009	10.60	0.03	0.15
Waters with nitrogen	2007	9.50	95.0	95.0
	2008	6.77	67.7	67.7
	2009	7.34	73.4	73.4

EC_{iw}, electrical conductivity of the irrigation water.

The experimental field (Fig. 1) was thus divided into four groups (I-IV), each with three triple joint laterals, establishing a N gradient decreasing from group I to group IV. Each group was then divided into 3 sub-groups, A, B and C, each with a surface area of 6.75 m^2 (2.25 m wide x 3 m long), and with the Na^+ gradient decreasing from A-C. The emitters were spaced 1 m apart, with a total of 9 dripping points in each of the 12 experimental plots. Two laterals of fresh water bordered the different groups (Fig. 1). Each sub-group area was bordered with earthen ridges, which prevented surface runoff from crossing over during rainfall and irrigation. The crop was irrigated three times per week from June to September with irrigation lasting 30 to 60 min per event. Figure 2 presents daily irrigation rates that were applied during three irrigation seasons. Application amounts averaged 15, 16, and 17 mm per irrigation event in 2007, 2008, and 2009, respectively. Nitrogen fertilization was applied in four (2007), six (2008), and three (2009) irrigation events during the vegetative stage (July).

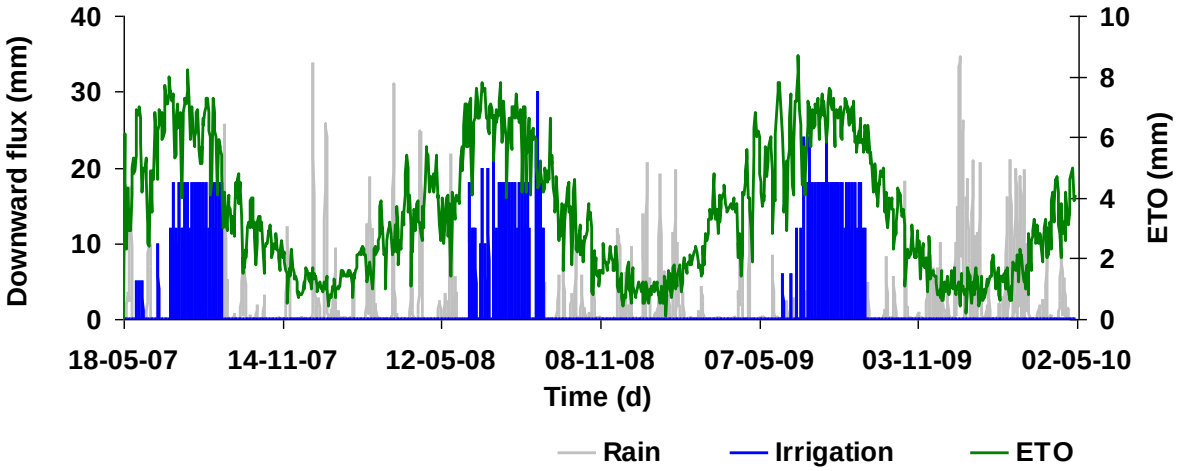

Fig. 2. Daily values of precipitation, irrigation, and reference evapotranspiration rates in Alvalade between 18th May 2007 and 2nd May 2010.

In the plots with the highest application of the synthetic saline waters (sub-group A), and those irrigated only with the locally available fresh water (sub-group C), TDR probes with waveguides from the Trase System (Soil Moisture Equipment Corp., Goleta, CA) and ceramic cups were installed at depths of 20, 40, and 60 cm to measure soil water contents and collect soil solutions, respectively. Only one TDR probe and one ceramic cup were installed in each depth. The soil solution was monitored for EC_{sw} and the concentrations of $N\text{-}NH_4^+$ and $N\text{-}NO_3^-$. Soil water content measurements and soil solutions were taken twice a week during irrigation seasons, generally 24 hours after an irrigation event, and twice a month during the rest of the year.

The crop was harvested manually on September 27, 2007 (132 DAS), on September 30, 2008 (138 DAS), and on September 29, 2009 (137 DAS). The dry biomass of sweet sorghum was determined by harvesting all sorghum plants in each experimental plot and oven drying at 70 ºC to a constant weight. Further details can be found in Ramos et al. (2012).

2.2. Modeling approach

Modeling of water flow and solute transport was carried out for all experimental plots included in sub-group A, irrigated with the highest application of synthetic saline waters, and in sub-group C, irrigated only with the water available in the region. The HYDRUS-2D software package (Šimůnek et al., 2006) was used to simulate the transient axisymmetrical (or radially symmetrical) three-dimensional movement of water and nutrients in the soil. In this approach, an individual emitter is represented as a point source located on the axis of rotation (Figs. 3 and 4). The axisymmetrical domain geometry representing the experimental conditions is shown in Fig. 4. The transport domain was set as a rectangle with a width of 37.5 cm (half the lateral spacing, i.e., the half-distance between triple joint laterals placed along the sorghum rows) and a depth of 100 cm. The transport domain was discretized into 2774 nodes, which corresponded to 5342 triangular elements (Fig. 4b). Observation nodes, corresponding to the locations where TDR probes and ceramic cups were installed, were placed at depths of 20, 40, and 60 cm, and at a radial distance of 20 cm away from the emitter source (Fig. 4a) and along the crop row (Fig. 3). A time-variable flux boundary condition was applied at the left part of the soil surface, approximately the first 20 cm to the right of the point emitter source, located at the top left corner of the soil domain (Fig. 4b). The flux boundary condition with the flux q was defined as:

$$q = \frac{volume\ \ of\ \ water\ \ applied}{surface\ \ wetted\ \ area \times duration} \tag{1}$$

where the volume of water applied (L^3) varied for different irrigation events, the surface wetted area (L^2) was approximately 1256 cm^2 (i.e., $3.14*20^2$), and the irrigation duration was adjusted to permit water to infiltrate into the soil without producing positive surface pressure heads. The application time was divided into multiple intervals to allow for the application of irrigation waters of different qualities within a particular irrigation event. While the dripper discharge was constant and the irrigation duration variable in the experiment, for numerical convenience (and to avoid positive surface pressures, which sometimes existed in reality), we adjusted irrigation flux to produce the applied irrigation volume for a particular irrigation event, i.e., discharge rates of the emitters given in Table 2 were adjusted to apply the same volume of water but during longer time periods. Possible positive pressure heads at the flux boundary, which would make the numerical code unstable, were avoided by distributing the surface flux over a relatively large surface area and by spreading irrigation over a sufficient time period to allow water to infiltrate (from 0.2 to the entire day, depending on the volume applied). The atmospheric boundary condition was assumed for the remainder of the soil surface during periods with irrigation and for the entire soil surface during periods without irrigation. A no flow boundary condition was set at the left and right sections of the soil profile, so that no water and solute movement from neighbouring emitters could be considered. A free drainage boundary condition was assumed at the bottom of the soil profile.

2.2.1. Water flow

The spatial distributions of transient soil water contents and volumetric fluxes were obtained using a numerical solution of the Richards equation for radially symmetric Darcian flow:

$$\frac{\partial \theta(h)}{\partial t} = \frac{1}{r}\frac{\partial}{\partial r}\left(r K(h)\frac{\partial}{\partial r}\right) + \frac{\partial}{\partial z}\left(K(h)\frac{\partial h}{\partial z} + K(h)\right) - S(r,z,t) \tag{2}$$

where θ is the volumetric soil water content ($L^3\ L^{-3}$), h is the soil water pressure head (L), t is time (T), r is the radial space coordinate (L), z is the vertical space coordinate (L), K is the hydraulic conductivity ($L\ T^{-1}$), and S is the sink term accounting for water uptake by plant roots

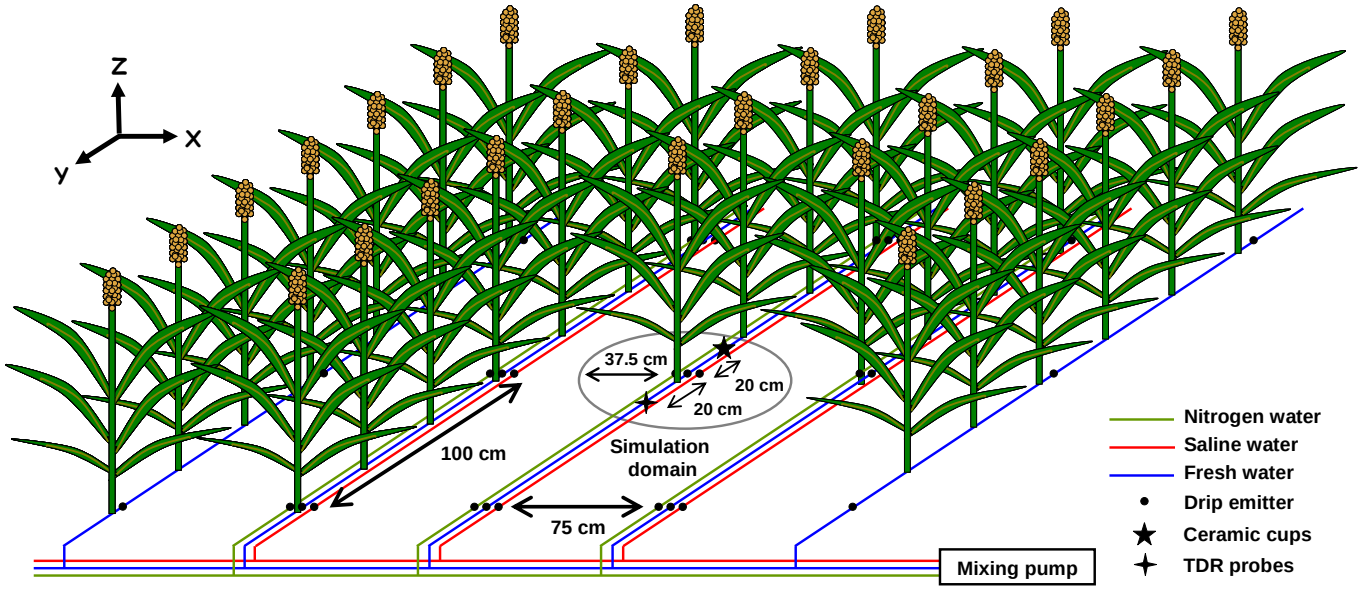

Fig. 3. Location of a point source emitter and monitoring sites in the experimental plot.

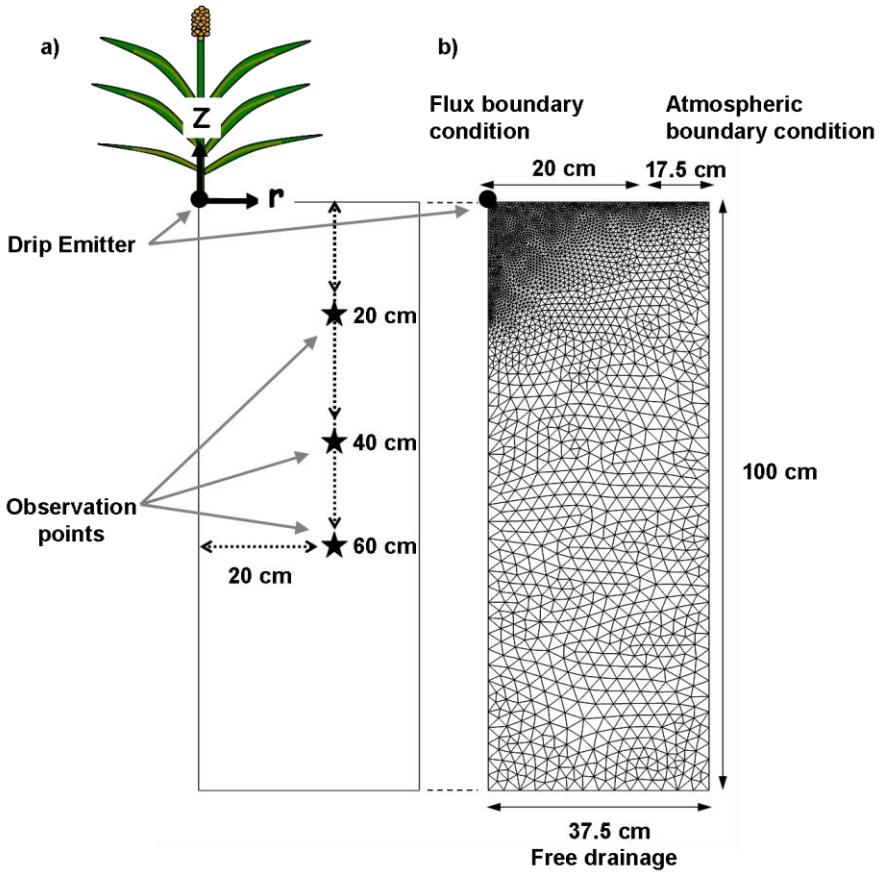

Fig. 4. Location of observation points within the soil profile (a) and an axisymmetrical domain geometry with the finite element discretization used in HYDRUS-2D simulations (b).

(L^3 L^{-3} T^{-1}). The unsaturated soil hydraulic properties were described using the van Genuchten-Mualem functional relationships (van Genuchten, 1980) as follows:

$$S_e(h)=\frac{\theta(h)-\theta_r}{\theta_s-\theta_r}=\frac{1}{\left(1+|\alpha h|^{\eta}\right)^m} \tag{3}$$

$$K(h)=K_s S_e^{\ell}\left[1-\left(1-S_e^{1/m}\right)^m\right]^2 \tag{4}$$

in which S_e is the effective saturation, θ_r and θ_s denote the residual and saturated water contents (L^3 L^{-3}), respectively, K_s is the saturated hydraulic conductivity (L T^{-1}), α (L^{-1}) and η (-) are empirical shape parameters, $m=1-1/\eta$, and ℓ is a pore connectivity/tortuosity parameter (-). The van Genuchten-Mualem parameters are presented in Table 1. They were obtained by fitting Eqs. (2) and (3) to laboratory data measured on undisturbed soil samples taken from a representative soil profile, as described in Ramos et al. (2011). The initial water content in the soil was set to a uniform value throughout the soil profile (Table 1). Since HYDRUS-2D simulations were started two weeks before the first irrigation event, the effects of the initial condition on long term simulations (2007-2010) of solute transport could be neglected.

2.2.2. Solute transport

Solute transport in a homogeneous porous medium and in a three-dimensional axisymmetrical domain was computed using the convection-dispersion equations (CDE) for each chemical species (EC_{sw}, N- NH_4^+, and N- NO_3^-) considered in our study, as follows:

$$\begin{aligned}\frac{\partial \theta c_k}{\partial t}+\rho\frac{\partial \bar{c}_k}{\partial t}&=\frac{\partial}{\partial r}\left(\theta D_{rr}\frac{\partial c_k}{\partial r}+\theta D_{rz}\frac{\partial c_k}{\partial z}\right)+\frac{1}{r}\left(\theta D_{rr}\frac{\partial c_k}{\partial r}+\theta D_{rz}\frac{\partial c_k}{\partial z}\right)+\\&+\frac{\partial}{\partial z}\left(\theta D_{zz}\frac{\partial c_k}{\partial z}+\theta D_{rz}\frac{\partial c_k}{\partial z}\right)-\left(\frac{\partial q_r c_k}{\partial r}+\frac{q_r c_k}{r}+\frac{\partial q_z c_k}{\partial z}\right)+\phi_k-S c_{root,k}\end{aligned} \tag{5}$$

where θ is the volumetric water content (L^3 L^{-3}), c, $\bar{c}$, and c_{root} are solute concentrations in the liquid phase (M L^{-3}), solid phase (M M^{-1}), and sink term (M L^{-3}), respectively, ρ is the soil bulk density (M L^{-3}), q_r and q_z are the components of the volumetric flux density (L T^{-1}), D_{rr}, D_{zz}, and D_{rz} are the components of the dispersion tensor (L^2 T^{-1}), ϕ represents chemical reactions of

solutes involved in a sequential first-order decay chain (M L^{-3} T^{-1}), S is again the sink term accounting for water uptake by plant roots (L^3 L^{-3} T^{-1}), and subscript k represents chemical species present in our study (EC_{sw}, N- NH_4^+, and N- NO_3^-).

The components of the dispersion tensor are given by (Bear, 1972):

$$\theta D_{rr} = \varepsilon_L \frac{q_r^2}{|q|} + \varepsilon_T \frac{q_z^2}{|q|} + \theta \tau D_0$$
$$\theta D_{zz} = \varepsilon_L \frac{q_z^2}{|q|} + \varepsilon_T \frac{q_r^2}{|q|} + \theta \tau D_0 \quad (6)$$
$$\theta D_{rz} = (\varepsilon_L - \varepsilon_T) \frac{q_r q_z}{|q|}$$

where $|q|$ is the absolute value of the volumetric flux density (L T^{-1}), ε_L and ε_T are the longitudinal and transversal dispersivities (L), D_0 is the molecular diffusion coefficient of the solute in free water (L^2 T^{-1}), and τ is the tortuosity factor. Table 1 gives the ε_L values used in our study. They were obtained by fitting analytical solutions of the CDE to observed breakthrough data measured on undisturbed soil samples taken from a representative soil profile of Alvalade as described in Gonçalves et al. (2001). The value of ε_T was simply set as one tenth of ε_L (e.g., Mallants et al., 2011).

The distribution of solutes between the soil liquid and solid phases was related in Eq. (5) with the following linear adsorption isotherm:

$$\overline{c_k} = K_{d,k}\, c_k \quad (7)$$

where $K_{d,k}$ (L^3 M^{-1}) is the distribution coefficient for the considered chemical species. Nitrate (N- NO_3^-) and EC_{sw} were assumed to be present only in the dissolved phase (K_d = 0 cm^3 g^{-1}), which simplified Eq. (5) for these two chemical species. Ammonium (N- NH_4^+) was assumed to adsorb to the solid phase according to Eq. (7) with the distribution coefficient K_d of 3.5 $cm^3 g^{-1}$ (Hanson et al., 2006).

Since the fertilizer used in our study was NH_4NO_3, nitrification of the N-NH_4^+ species to N-NO_3^- was assumed to be the main N process occurring in the soil. HYDRUS-2D incorporates this process in Eq. (5) by means of a sequential first-order decay chain as follows:

$$\phi_{N-NH_4^+} = -\phi_{N-NO_3^-} = -\mu_{w,N-NH_4^+}\theta c_{N-NH_4^+} - \mu_{s,N-NH_4^+}\rho \bar{c}_{N-NH_4^+} \quad (8)$$

where μ_w and μ_s are the first-order rate constants for solutes in the liquid and solid phases (T^{-1}), respectively. The first-order reaction terms, representing nitrification of N-NH_4^+ to N-NO_3^-, thus act as a sink for N-NH_4^+ and as a source for N-NO_3^-. The values for μ_w and μ_s were set to be 0.2 d^{-1}. The parameters K_d, μ_w, and μ_s were taken from a review of published data presented by Hanson et al. (2006), and represent the center of the range of reported values.

The last term of Eq. (5) represents a passive root nutrient uptake, i.e., the movement of nutrients into roots by convective mass flow of water, directly coupled with root water uptake (Šimůnek and Hopmans, 2009). This term was defined as:

$$c_{root}(r,z,t) = min\left[c(r,z,t), c_{max}\right] \quad (9)$$

where c_{max} is the *a priori* defined maximum concentration of the root solute uptake. Since we considered unlimited passive nutrient uptake for nitrogen species, c_{max} was set to a concentration value larger than the dissolved simulated concentrations, c, allowing all dissolved nutrients to be taken up by plant roots with root water uptake. Since for EC_{sw} a zero uptake was considered, c_{max} was set to zero.

2.2.3. Potential and actual evapotranspiration rates

The sink term (S) in Eqs. (2) and (5) was calculated using the macroscopic approach introduced by Feddes et al. (1978). In this approach, the actual local uncompensated root water uptake was obtained as follows (Feddes et al., 1978; van Genuchten, 1987; Skaggs et al., 2006a; Šimůnek and Hopmans, 2009):

$$S\left(h,h_\phi,r,z,t\right) = \alpha\left(h,h_\phi,r,z,t\right)S_p\left(r,z,t\right) = \alpha\left(h,h_\phi,r,z,t\right)\beta\left(r,z,t\right)T_p\left(t\right)A_t \quad (10)$$

where $S_p(r,z,t)$ and $S(h, h_\phi, r,z,t)$ are the potential and actual volumes of water removed from a unit volume of soil per a unit of time (L^3 L^{-3} T^{-1}), respectively, $\alpha(h, h_\phi, r,z,t)$ is a prescribed dimensionless stress response function of the soil water (h) and osmotic (h_ϕ) pressure heads ($0 \leq \alpha \leq 1$), $\beta(r,z,t)$ (L^{-3}) is a normalized root density distribution function, T_p is the potential transpiration rate (LT^{-1}), and A_t is the area of the soil surface associated with transpiration [L^2]. The actual transpiration rate, T_a (L T^{-1}), was then obtained by integrating Eq. (10) over the root domain, Ω (L^3), as follows:

$$T_a(t) = T_p(t) \int_{\Omega_r} \alpha(h, h_\phi, r, z, t)\, \beta(r, z, t)\, d\Omega \tag{11}$$

The root distribution is defined in HYDRUS-2D according to Vrugt et al. (2001):

$$\Omega(r,z) = \left(1 - \frac{r}{r_m}\right)\left(1 - \frac{z}{z_m}\right) e^{-\left(\frac{p_r}{r_m}\left|r^* - r\right| + \frac{p_z}{z_m}\left|z^* - z\right|\right)} \tag{12}$$

where r_m and z_m are the maximum radius and depth of the root zone (L), respectively, z^* and r^* are the locations of the maximum root water uptake in vertical and horizontal directions (L), respectively, and the p_r and p_z values are taken to be equal to one except for $r > r^*$ and $z > z^*$ when they become zero. The following parameters of the Vrugt et al. (2001) model were used in the simulations: r_m=37.5 cm, z_m=65 cm, r^*=10 cm, z^*=10 cm. We considered a simple root distribution model in which the roots of sweet sorghum expanded horizontally into all available space between sorghum lines (r_m=37.5 cm), were concentrated mainly around the drip emitter (r^*=10 cm, z^*=10 cm) where water and nutrients were applied, and extended to a depth of 65 cm (z_m=65 cm). We assumed that plants had no need of expanding their roots below this depth since water and nutrients were being applied at the soil surface and their life cycle lasted only five months. The parameters for defining the maximum root water uptake in vertical and horizontal directions (z and r^*) were also based on the scenarios developed by Gärdenäs et al. (2005) and Hanson et al. (2006, 2008). The selection of the maximum rooting depth was also based on the work carried out by Ramos et al. (2011) and the fact that root depths are relatively shallow under surface drip irrigation starting few days after sowing (Klepper, 1991; Allen et al., 1998; Zegada-Lizarazu et al., 2012). In addition, field observations carried out in November 2010 found no significant amounts of roots below this depth.

In this study we considered that during the growing seasons T_p rates were obtained by combining the daily values of reference evapotranspiration (ET_0), determined with the FAO Penman-Monteith method and the dual crop coefficient approach (Allen et al., 1998; 2005), as follows:

$$ET_c = \left(K_{cb} + K_e\right) ET_0 \tag{13}$$

where ET_c is the evapotranspiration (L T^{-1}), K_{cb} is the basal crop coefficient, which represents the plant transpiration component (-), and K_e is the soil evaporation coefficient (-).

Standard sweet sorghum K_{cb} values (Allen et al., 1998) were adjusted for the Alvalade climate, taking into consideration the crop height, wind speed, and minimum relative humidity averages for the period under consideration. The K_{cb} coefficient was further adjusted to account for the salinity and nitrogen stress, affecting sweet sorghum growth in each experimental plot, using the procedure for non-pristine agricultural vegetation (Allen et al., 1998):

$$K_{cb\ mid} = K_{c\ min} + \left(K_{cb\ full} - K_{c\ min}\right)\left(1 - e^{(-0.7\ LAI)}\right) \tag{14}$$

where $K_{cb\ mid}$ is the estimated basal K_{cb} during mid-season when the leaf area index (LAI) (L^2L^{-2}) is smaller than for full cover conditions, $K_{cb\ full}$ is the estimated basal K_{cb} during mid-season (at the peak plant size or height) for vegetation having LAI>3, and $K_{c\ min}$ is the minimum K_c for bare soil (0.15-0.20). For these estimations, LAI was monitored in each experimental plot during different stages of the sorghum cycle, using a non-destructive method to avoid removing plants from the experimental area. Length (L) and width (W) of crop leafs were measured on random plants grown in each experimental plot. These dimensions were then related to previously calibrated LAI values with the following equation:

$$LAI = 0.7586 \sum_{i=1}^{n} \left(L \times W\right) \tag{15}$$

where LAI are the values measured using a LI-COR area meter (Model LI-3100C, LI-COR Environmental and Biotechnology Research Systems, Lincoln, NE) and n is the number of green leafs on each measured sorghum plant. Cubic splines were then fitted to LAI data to obtain a continuous function throughout the crop seasons.

The evaporation coefficient K_e was calculated as (Allen et al., 1998, 2005):

$$K_e = K_r \left(K_{c\,max} - K_{cb}\right) \leq f_{ew}\, K_{c\,max} \tag{16}$$

where K_r is a dimensionless evaporation reduction coefficient dependent on the cumulative depth of water depleted (evaporated) from the topsoil, $K_{c\ max}$ is the maximum value of K_c (i.e., $K_{cb} + K_e$) after rain or irrigation, and f_{ew} is the fraction of the soil surface from which most evaporation occurs. Table 5 presents the crop coefficients and other crop related parameters estimated in each growing season.

Table 5. Crop and soil parameters used for estimating plant transpiration and soil evaporation in each sorghum growing season.

Parameter	2007	2008	2009
Planting date	May 18	May 15	May 15
Harvest date	September 27	September 27	September 27
Av. wind speed (m s^{-1})	2.2	2.4	2.3
Av. RH min (%)	26	32	24
Length stages (d):			
L_{ini}	63	64	64
L_{dev}	25	26	26
L_{mid}	24	25	25
L_{late}	21	24	23
f_w (irrigation)	0.3	0.3	0.3
REW (mm)	9	9	9
TEW (mm)	35.2	35.2	35.2
Z_e (cm)	15	15	15
LAI_{max} (m^2 m^{-2}):			
Highest value	5.1	4.7	5.4
Plot	I-C	III-A	II-B
Lowest value	3.3	2.8	2.6
Plot	IV-B	IV-A	IV-A
$K_{cb\ ini}$	0.15	0.15	0.15
$K_{cb\ mid}$	1.23	1.21	1.24
$K_{cb\ end}$	1.07	1.06	1.09
$K_{cb\ full}$	0.15-1.23	0.15-1.21	0.15-1.24
$K_{c\ max}$	1.16-1.35	1.14-1.38	1.01-1.29

RH, relative humidity; L_{ini}, L_{dev}, L_{mid}, and L_{late}, length of crop initial, development, mid-season, and end season stages, respectively; f_w, fraction of soil surface wetted by irrigation (0.3-0.4: an interval used in calibration; an optimal value is given in the table); REW, readily evaporable water; TEW, total evaporable water, Z_e, depth of the surface soil layer that is subject to drying by way of evaporation (10-15 cm); LAI_{max}, maximum leaf area index measured in the experimental plots; $K_{cb\ ini}$, $K_{cb\ mid}$, and $K_{cb\ end}$, basal crop coefficient during crop initial, mid-season, and end season stages, respectively; $K_{c\ full}$, estimated basal K_{cb} during mid-season (at peak plant size or height) for vegetation having LAI>3; $K_{c\ max}$, maximum value of K_c following rain or irrigation.

During non-growing seasons, the procedure to estimate ET_c was greatly simplified by using the single crop coefficient approach and a K_c of 0.15 to account for a bare soil with a small

percentage of weeds. Transpiration and evaporation were also separated as a function of leaf area index (Ritchie; 1972) using a fictitious LAI value of 1.0.

In all experimental plots, it was assumed that the potential root water uptake was reduced due to water stress as a result of the adopted irrigation schedule, which could lead to insufficient or excessive supply of water to the crop. It was also assumed that the potential root water uptake was further reduced by osmotic stress, resulting from the use of blended saline water. The effects of water and salinity stresses were considered to be multiplicative as described by van Genuchten (1987) (i.e., $\alpha(h,h_\phi)=\alpha_1(h)\alpha_2(h_\phi)$ in Eq. 10), so that different stress response functions could be used for the water and salinity stresses. Root water uptake reductions due to water stress, $\alpha_1(h)$, were described using the piecewise linear model proposed by Feddes et al. (1978). The water uptake is at the potential rate when the pressure head is between h_2 and h_3, drops off linearly when $h > h_2$ or $h < h_3$, and becomes zero when $h < h_4$ or $h > h_1$. The following parameters of the Feddes et al. (1978) model were used: h_1=-15, h_2=-30, h_3=-325 to -600, h_4=-8000 cm.

Root water uptake reductions due to salinity stress, $\alpha_2(h_\phi)$, were described by adopting the Maas (1990) salinity threshold and slope function. The salinity threshold (EC_T) for sweet sorghum corresponds to a value for the electrical conductivity of the saturation extract (EC_e) of 6.8 dS m^{-1}, and a slope (s) of 16 % per dS m^{-1}. As required by HYDRUS-2D, these values were converted into EC_{sw} assuming that the EC_{sw}/EC_e ratio (k_{EC}) was 2, which is a common approximation used for soil water contents near field capacity in medium-textured soils (U.S. Salinity Laboratory Staff, 1954; Skaggs et al., 2006b).

2.3. Statistical analysis

Model validation was carried out by comparing field measured values with HYDRUS-2D simulations using various quantitative measures of the uncertainty, such as, the mean error (ME), mean absolute error (MAE) and the root mean square error (RMSE), given by:

$$ME = \frac{1}{N}\sum_{i=1}^{N}\left(O_i - P_i\right) \tag{17}$$

$$MAE = \frac{1}{N}\sum_{i=1}^{N}\left|O_i - P_i\right| \tag{18}$$

$$RMSE = \sqrt{\frac{\sum_{i=1}^{N}(O_i - P_i)^2}{N-1}} \tag{19}$$

where O_i and P_i are observation values and model predictions in the units of a particular variable, and N is the number of observations.

The dual crop coefficient approach used here to estimate atmospheric demands requires various crop and soil parameters that need to be adjusted to particular experimental conditions. Therefore, these parameters, i.e., lengths of various growth stages, the basal crop coefficients during initial ($K_{cb\ ini}$), mid-season ($K_{cb\ mid}$) and end season ($K_{cb\ end}$) growth stages, the total evaporable water (TEW), the readily evaporable water (REW), the thickness of evaporation soil layer (Z_e), and the fraction of soil surface wetted by irrigation (f_w) were first calibrated by trial and error using HYDRUS-2D and the experimental data from the first crop season (2007), and then used to define the atmospheric demands for the second (2008) and third crop seasons (2009). The optimized parameters were considered to be calibrated when the RMSEs found for the soil water content, EC_{sw}, and N species were lower than those reported in Ramos et al. (2011), i.e., $RMSE_\theta$<0.04 $cm^3\ cm^{-3}$; $RMSE_{ECsw}$<2.04 $dS\ m^{-1}$; $RMSE_{N\text{-}NH4+}$<0.07 $mmol_c\ L^{-1}$; and $RMSE_{N\text{-}NO3-}$ <2.60 $mmol_c\ L^{-1}$. Ramos et al. (2011) used the one-dimensional version of HYDRUS (i.e., HYDRUS-1D, Šimůnek et al., 2008) and the single crop coefficient approach to simulate the same solutes for similar experimental conditions, albeit with a different crop. Therefore, when RMSEs obtained here with a more complex approach, i.e., using a dual crop coefficient procedure and a more appropriate geometrical description, were lower than those obtained previously with a simpler methodology, optimized parameters were considered to be calibrated. All other necessary HYDRUS-2D input material parameters, such as soil hydraulic and solute transport parameters, were determined in the laboratory. Note that since our modeling approach is processed-based, rather than conceptual, our input parameters can be obtained/measured independently. In general, we find that it is superior to measure input material parameters independently rather than fitting them. The correspondence between measurements and model predictions would have obviously been better, had the input parameters been fitted using numerical modeling. However, the model that can be successfully run with independently measured input material parameters is more robust for practical applications than calibrated

models. Moreover, with this approach we not only validate the used modeling approach but also applied laboratory methodologies and various involved experimental procedures.

3. Results and Discussion

3.1. Soil water balance

The HYDRUS-2D simulations began on May 18, 2007 and were carried out for the first crop and subsequent rainfall seasons (i.e., for 362 days) in order to calibrate the crop and soil parameters that were needed for estimating atmospheric demands using the dual crop coefficient approach. Table 6 presents the statistical indicators used to evaluate the level of agreement between water contents measured using TDRs and those simulated using the calibrated HYDRUS-2D model for three depths of plots I-A and I-C. The subsequent simulations with calibrated HYDRUS-2D began again on May 18, 2007 and were carried out continuously for the following 1078 days.

Table 6. Results of the statistical analysis between measured and simulated soil water contents, electrical conductivities of the soil solution (EC_{sw}), and N- NH_4^+, and N- NO_3^- concentrations.

Statistic	Water content ($cm^3\ cm^{-3}$)	EC_{sw} ($dS\ m^{-1}$)	$N\text{-}NH_4^+$ ($mmol_c\ L^{-1}$)	$N\text{-}NO_3^-$ ($mmol_c\ L^{-1}$)
Data from 2007/2008 (calibration data):				
N	82	36	93	75
ME	-0.007	-0.216	0.029	-0.218
MAE	0.024	0.602	0.029	0.617
RMSE	0.033	0.854	0.042	1.253
Data from 2008/2010:				
N	276	211	241	263
ME	-0.007	-0.668	0.019	-1.668
MAE	0.023	1.255	0.026	2.244
RMSE	0.028	1.877	0.043	3.427
Data from 2007/2010 (all data):				
N	358	247	334	338
ME	-0.007	-0.602	0.022	-1.346
MAE	0.023	1.160	0.027	1.883
RMSE	0.030	1.764	0.042	3.078

N, number of observations; ME, mean error; MAE, mean absolute error; RMSE, root mean square error.

Figure 5 shows the water contents measured at depths of 20, 40, and 60 cm in plots I-A and I-C, and compares these values with HYDRUS-2D simulations. Water contents increased to full saturation near the emitter after an irrigation or rain event, and then decreased gradually during the following hours and days, until the next irrigation or rain event took place. Deeper depths

showed smaller water content variations since root water uptake and soil evaporation were more pronounced at shallower depths. Similar results were also obtained for the remaining plots (not shown). A ME of -0.007 cm^3 cm^{-3} and a RMSE of 0.030 cm^3 cm^{-3} were found between measured and simulated water contents during the entire simulation period. Deviations between measured and simulated water contents can be attributed to different causes, including errors related to field measurements and to model input and model structure errors. They will be discussed below in detail.

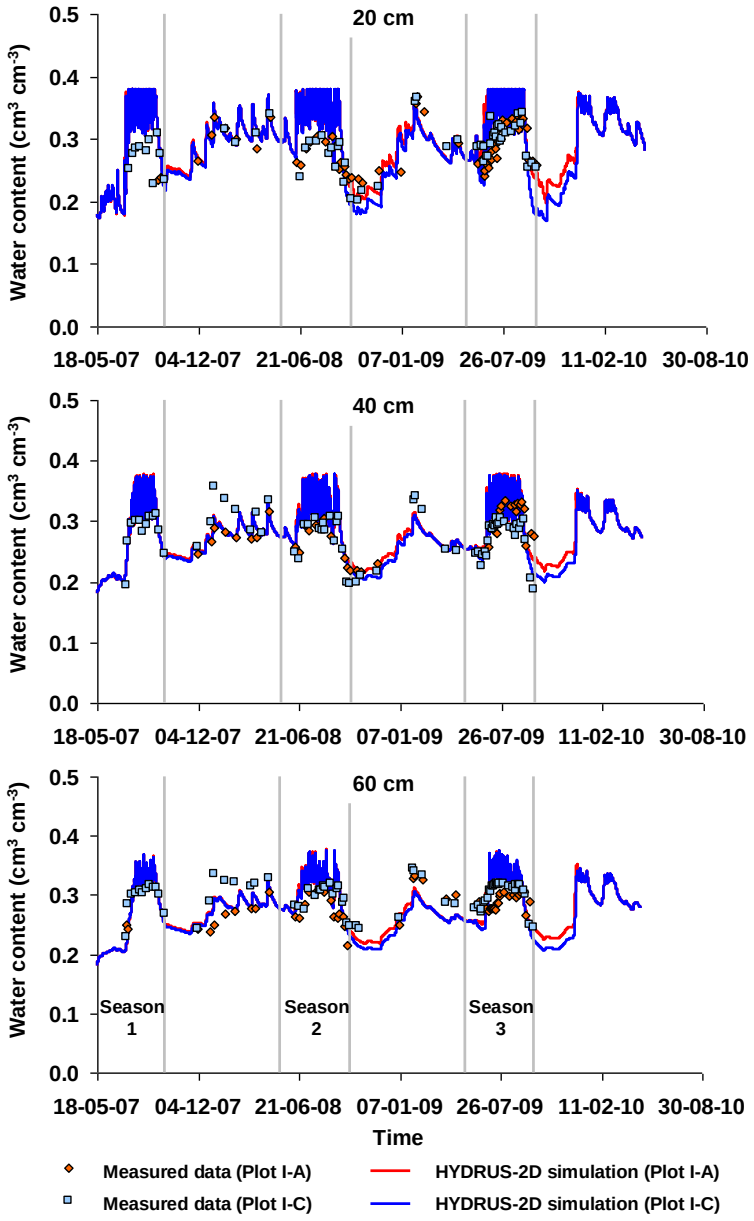

Fig. 5. Measured and simulated water contents at depths of 20 (top), 40 (middle), and 60 cm (bottom) depth in plots I-A and I-C.

Table 7 presents the output components of the soil water balance (i.e., potential transpiration, actual transpiration, soil evaporation, and percolation) in all experimental plots located in sub-groups A and C. The input components, i.e., irrigation and rainfall amounts, were already given in Section 2 and in Table 3. Since HYDRUS-2D does not have a crop growth module, the potential root water uptake (PRWU), i.e., potential transpiration (T_p) obtained in each experimental plot, was given as input for defining the atmospheric boundary conditions. T_p varied between 360 (plot IV-A, 2008) and 457 mm (plots I-C and II-A, 2009). Plots located in group IV, where no nitrogen was applied, generally had lower T_p values. In groups I-III, T_p averaged 394, 397, and 450 mm in 2007, 2008, and 2009, respectively. In group IV, T_p was lower, averaging 382, 379, and 413 mm during the same time periods. Considering that nitrogen requirements of sweet sorghum are relatively low (Barbanti et al., 2006), the amount of nitrogen applied in plot III (N1=130 to 190 kg/ha y^{-1} of N) was apparently sufficient to maximize T_p. Plots located in group I and II may thus have experienced some 'luxury' uptake, i.e., a continued uptake of nitrogen beyond what was required for immediate growth.

T_p values obtained in plots irrigated with saline waters (sub-group A) were generally lower that those obtained in plots irrigated with fresh waters (sub-group C). However, the differences were found to be very small since sweet sorghum is moderately to highly tolerant to salinity, depending on the variety (Maas, 1990; Vasilakoglou et al., 2011). The largest T_p differences were found in 2009, in plots IV-A and IV-C (58 mm). Thus, in plot IV-A, the plant development was particularly affected by the continuous application of synthetic saline waters.

Apart from minor T_p variations found in the experimental plots, which resulted mainly from the differences in the spline functions fitted to the LAI measurements taken in each plot and in each crop season, T_p values estimated for sweet sorghum can be considered low. Ramos et al. (2011) estimated T_p for maize to vary between 600 and 800 mm. Water requirements estimated in this study for sweet sorghum are much lower than those for traditionally grown, irrigated crops in Portugal. Sweet sorghum thus seems to be a reasonable alternative crop to be grown in water scarce European Mediterranean regions.

Actual root water uptake, i.e., actual transpiration (T_a), as simulated by HYDRUS-2D, varied between 264 (plot IV-A, 2009) and 334 mm (plot I-C, 2009). T_p reductions due to water stress

Table 7. Output components of the soil water balance in each experimental plot.

Sub-plot	Group I				Group II				Group III				Group IV			
	T_p (mm)	T_a (mm)	E (mm)	P (mm)	T_p (mm)	T_a (mm)	E (mm)	P (mm)	T_p (mm)	T_a (mm)	E (mm)	P (mm)	T_p (mm)	T_a (mm)	E (mm)	P (mm)
Season 1 (2007)																
A	386	280	173	162	391	294	170	167	394	296	168	168	384	290	174	168
C	399	298	163	170	396	297	164	172	395	295	169	173	380	284	177	174
Season 2 (2008)																
A	398	291	191	292	383	283	200	295	402	296	190	294	360	273	207	296
C	406	316	192	293	390	301	197	299	404	312	192	298	398	311	192	299
Season 3 (2009)																
A	456	307	172	292	457	305	170	294	434	291	183	299	384	264	206	302
C	457	334	174	298	449	331	177	302	449	328	176	309	442	324	181	309
Cumulative fluxes (2007-2010)																
A	1382	982	-	1101	1374	981	-	1107	1373	983	-	1111	1270	930	-	1119
C	1401	1065	-	1083	1377	1045	-	1097	1390	1051	-	1102	1363	1036	-	1105

T_p, potential transpiration; T_a, actual transpiration; E, evaporation; P, percolation.

were a function of the adopted irrigation schedule. Within the same crop season, transpiration reductions were very similar since the irrigation schedule was the same in all experimental plots. In the plots located in sub-group C, irrigated only with fresh waters, T_p was reduced due to water stress by 25.3-27.4, 21.9-22.8, and 26.3-26.9% in 2007, 2008, and 2009, respectively. Water stress was thus a function of the adopted irrigation schedule during each season and did not vary among experimental plots.

In plots located in sub-group A (irrigated with saline waters), T_p was further reduced due to salinity stress. During 2007, T_a estimated for the different plots included in sub-group A was generically the same as in sub-group C (irrigated with fresh waters), i.e., sweet sorghum showed to be tolerant to the levels of salinity reached in the soil solution of all experimental plots irrigated with fresh or synthetic saline waters. However, in 2008 and 2009, T_p suffered reductions (in sub-group A) of 24.2-26.9, and 31.3-33.3%, respectively, due to the combined effects of water and salinity stresses, i.e., 2.3-4.7% (in 2008) and 4.6-7.0% (in 2009) higher than T_p reductions found in the plots irrigated only with fresh waters (sub-group C). In the following years, the salinity stress thus became increasingly higher (in sub-group A). Hence, soil salinization and the increase of the salinity stress was related to the continuous and increasing amount of synthetic saline waters being applied in each experimental plot.

Figure 6 relates actual transpiration T_a calculated using HYDRUS-2D with the experimentally determined sorghum yield (Y), given in terms of dry biomass, by means of the empirical relationship, $Y = f\left(T_a\right)$. This relationship, generally thought to be approximately linear, is valid for a particular plant (canopy) at a particular site subject to standard tillage and nutrition conditions (Novák and van Genuchten, 2008). The relation found in our study was somewhat poor, with the agreement between T_a and dry biomass reaching R^2 of only 0.51. Since HYDRUS-2D does not account for a crop growth module, this result was not particularly surprising. Nevertheless, had water been the only limiting factor in our experiment, the relation would likely have been better. However, this could not be easily observed in our study since the amount of water applied per year was the same, while the total water depths applied during each crop season were apparently not different enough to establish a closer relation. The relation in Figure 6 essentially resulted from the effects that water quality had on T_a and crop yield. While plots irrigated with fresh water (sub-group C) had higher sorghum yields and T_a values, plots irrigated

with saline waters (sub-group A) had lower sorghum yields and T_a values (Fig. 6). Nitrogen also did not influence the $Y(T_a)$ relation since N stress at a given period can mainly affect sorghum yield, while LAI, and consequently T_a, remain high.

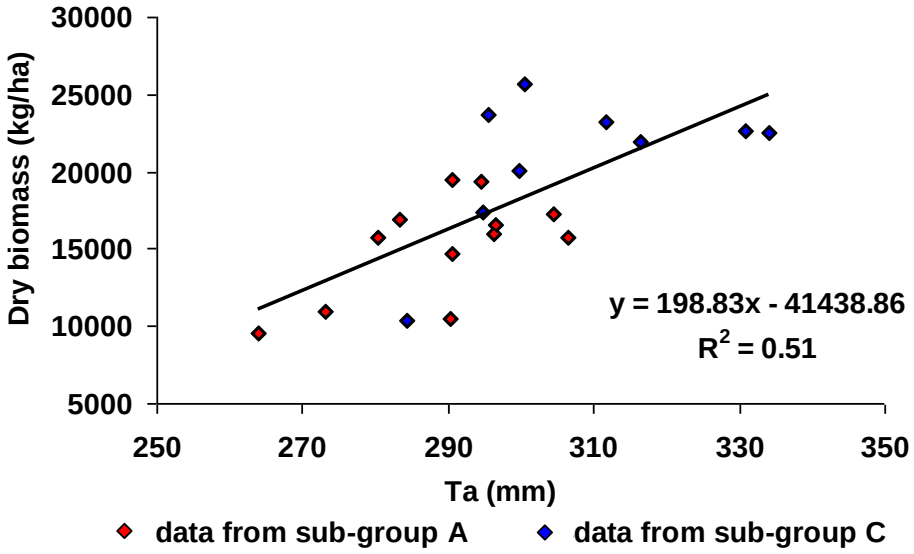

Fig. 6. Relationship between actual transpiration (T_a), as simulated by HYDRUS-2D, and dry biomass yield (Y).

Finally, the soil water balance (Table 7) in each experimental plot shows relatively high percolation. Percolation reached 162-174, 292-299, and 292-309 mm in 2007, 2008, and 2009, respectively. These values correspond to 31-34, 50-51, and 51-54% of the water applied during crop seasons, i.e., from sowing to harvest. While percolation was expected to be large, since application rates during irrigation seasons were high, the values estimated for crop seasons of 2008 and 2009 may be somewhat deceiving. They result from running HYDRUS-2D continuously for the entire simulation period. Since cumulative percolation obtained during the entire simulation period (2007-2010) only reached 36-37% of the applied water, and considering that root water uptake was much higher during crop seasons, percolation in 2008 and 2009 also accounted for the water stored below the root zone. Therefore, we ended up not being able to actually quantify percolation due to the adopted irrigation schedule, since the water balance evaluated for each crop season also accounted for the water that was no longer accessible to

plants. Nevertheless, the effects of nitrogen applications and water quality on drainage were small. Plots with higher root water uptake showed generally lower percolation.

3.2. Salinity build-up and distribution

Figure 7 shows EC_{sw} measured at the 20, 40, and 60 cm depth in plots I-A and I-C, and compares these values with HYDRUS-2D simulations. Similar results were also found for the remaining plots of sub-groups A and C. Within the same sub-group (Fig. 1), EC_{sw} varied due to the effect of nitrogen fertigation on root water uptake. Between sub-groups (but within the same group), EC_{sw} varied due to the effect of water quality on root water uptake.

The statistical indicators (Table 6) obtained while comparing measured and simulated EC_{sw} for three depths of all plots in sub-groups A and C resulted in a ME of -0.602 dS m^{-1} and a RMSE of 1.764 dS m^{-1}.

Figures 8 and 9 show the simulated distributions of EC_{sw} in plots I-A and I-C, respectively, at the beginning and at the end of each crop season. Based on model simulations, the continuous use of synthetic saline irrigation waters led to soil salinization in plot I-A over the years (Fig. 8). At harvest, simulations showed that EC_{sw} increased considerably to values above 24 dS m^{-1} in the region around the drip emitter. At the beginning of each crop season that essentially correspond to the end of the rainfall leaching periods, simulated EC_{sw} values were also increasingly higher throughout the years, especially at deeper depths.

Considering that the Maas (1990) salinity threshold parameter for sweet sorghum corresponds to EC_{sw} of 13.2 dS m^{-1} (EC_e=6.8 dS m^{-1}; k_{EC}=2), the part of the soil domain with EC_{sw} above this threshold was already considerable during harvest in 2007. However, EC_{sw} only increased above the threshold EC_{sw} near the end of the crop season when irrigation ceased and the soil dried out (Fig. 7). Therefore, transpiration was not significantly reduced due to the salinity stress during that year (Table 7). In 2008 and 2009, the threshold value was reached earlier, with the region around the drip emitter with EC_{sw} values above 13.2 dS m^{-1} being much larger than in 2007. Hence, transpiration was increasingly reduced due to the salinity stress as a result of the accumulation of salts in the soil domain.

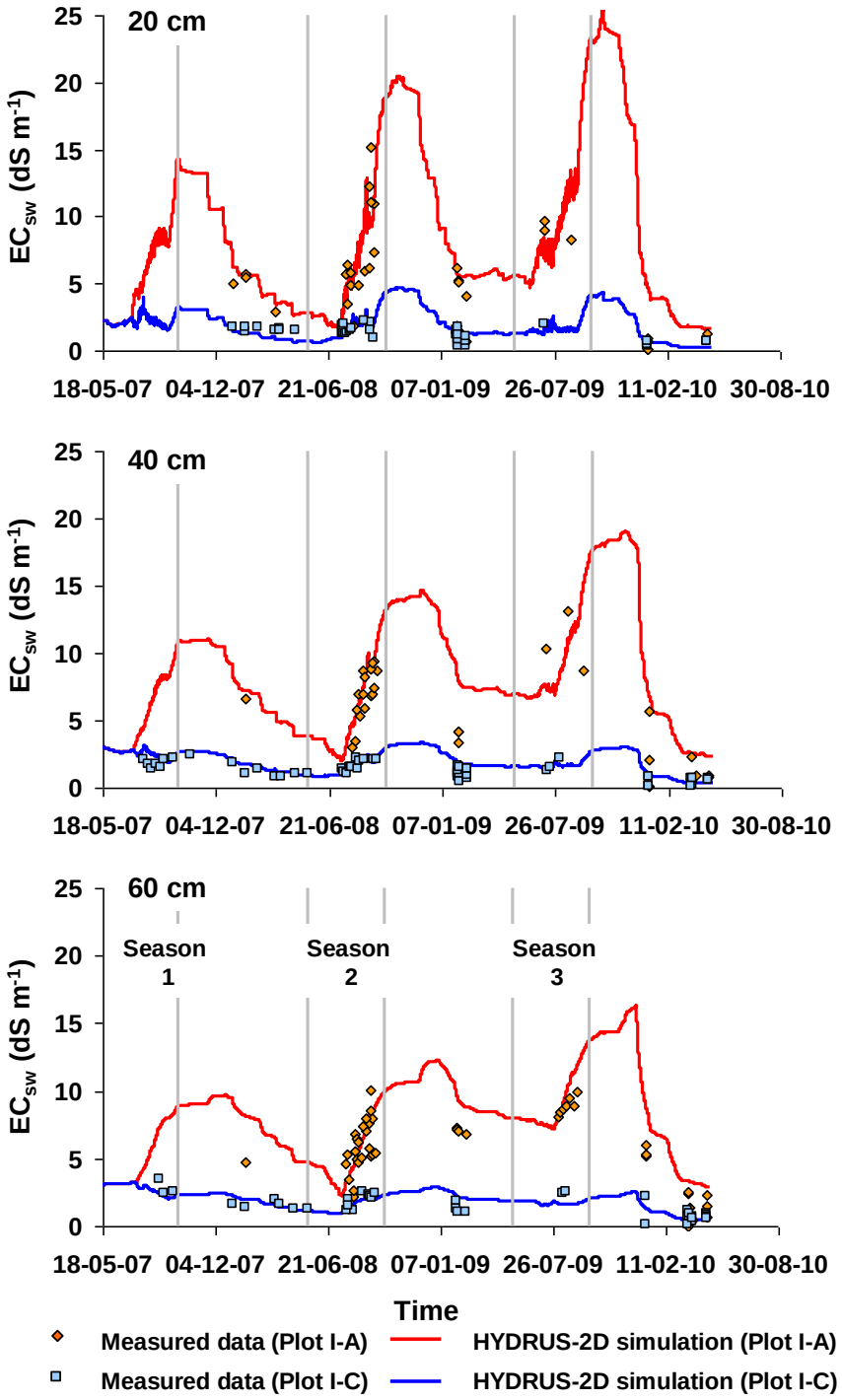

Fig. 7. Measured and simulated electrical conductivities of the soil solution at 20 (top), 40 (middle), and 60 cm (bottom) depth in plots I-A (irrigated with the highest application of synthetic saline waters) and I-C (irrigated with fresh waters only).

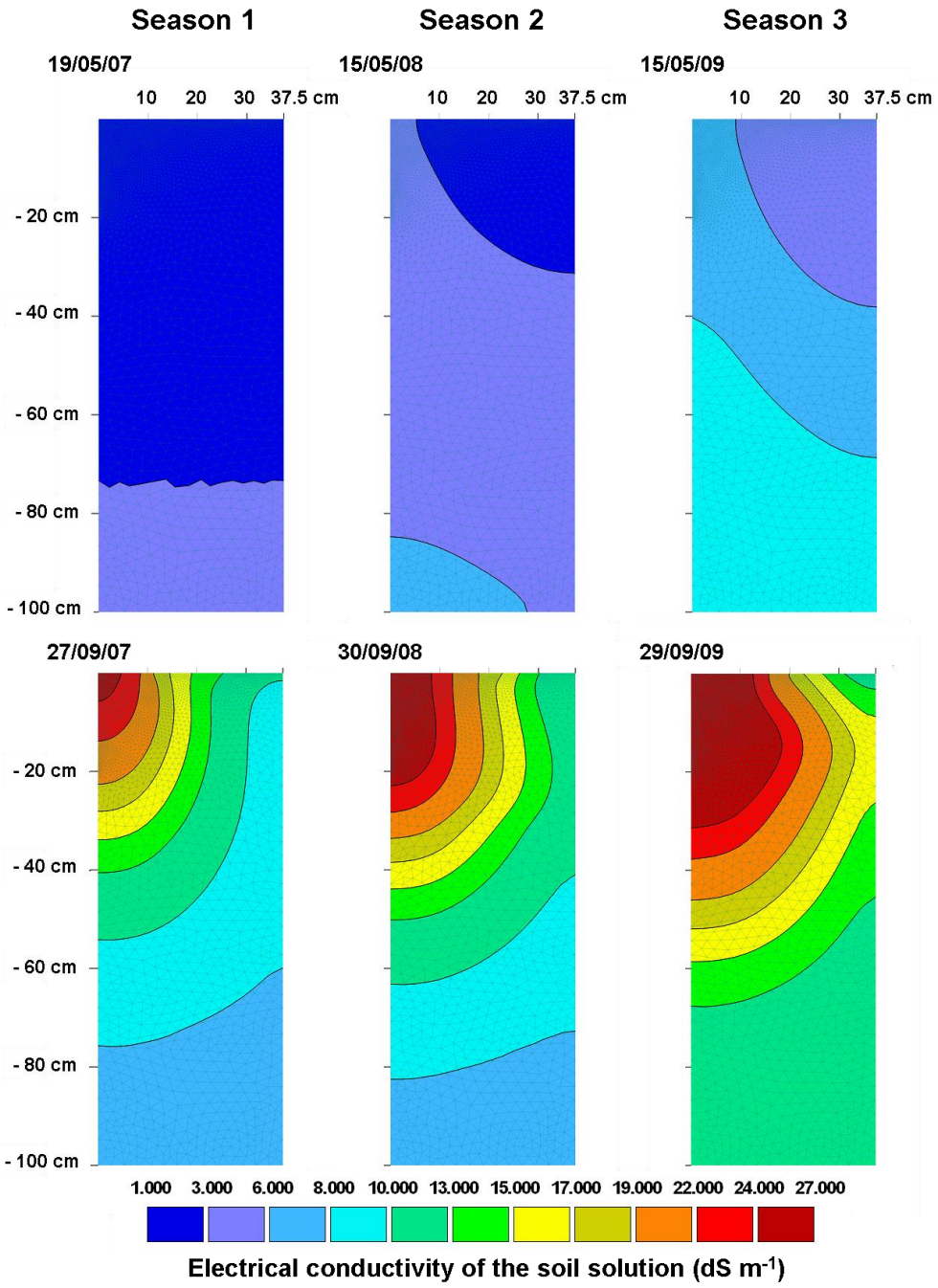

Fig. 8. Simulated distributions of the electrical conductivity of the soil solution in plot I-A (irrigated with synthetic saline waters) during sowing (top) and harvest (bottom) of each crop season. The drip emitter was located in the top left corner of each contour plot.

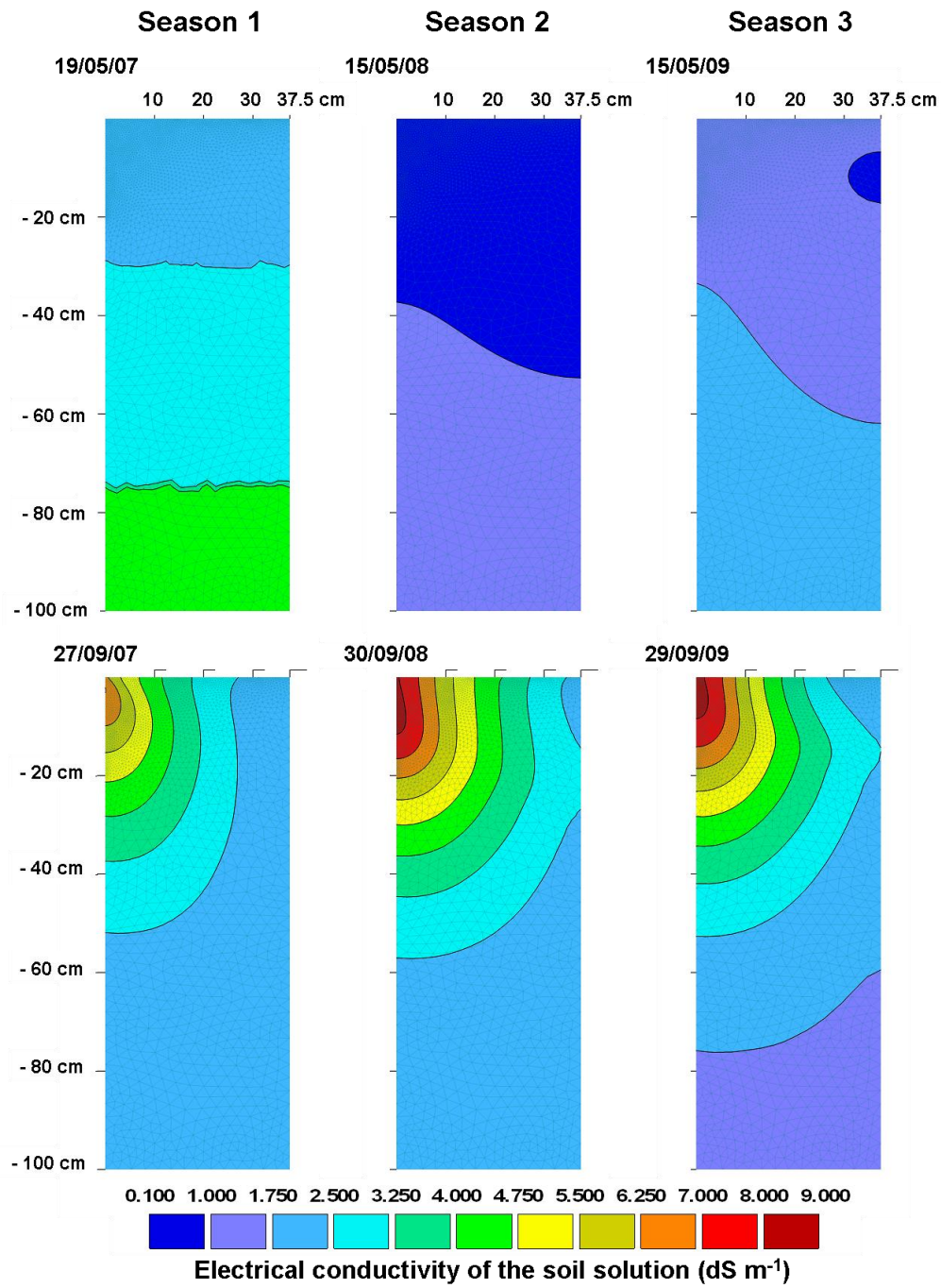

Fig. 9. Simulated distributions of the electrical conductivity of the soil solution in plot I-C (irrigated with fresh waters only) during sowing (top) and harvest (bottom) of each crop season. The drip emitter was located in the top left corner of each contour plot.

On the other hand, irrigation with fresh waters, having a relatively low salinity (EC_{iw}>0.8; Table 4), also led to larger EC_{sw} at the end of each crop season, but the levels reached were always lower than 9 dS m^{-1} and decreased significantly due to rainfall leaching (Fig. 9). Therefore, in sub-group C, root water uptake was not affected by the salinity stress.

3.3. Nitrogen balance

Figure 10 shows N-NH_4^+ and N-NO_3^- concentrations measured at a depth of 20, 40, and 60 cm in plots I-C and IV-C, and compares these values with HYDRUS-2D simulations. Figures 11 and 12 show the simulated distributions of N-NH_4^+ and N-NO_3^- concentrations in plot I-A during the second crop season. In groups I through IV, N-NH_4^+ and N-NO_3^- concentrations varied according to the amounts of nitrogen applied in each experimental plot. In sub-group A-C (but within the same group), N-NH_4^+ and N-NO_3^- concentrations varied due to the effects of water quality on root water uptake.

The statistical indicators (Table 6) obtained while comparing measured and simulated N-NH_4^+ concentrations for three depths, and for all experimental plots located in sub-groups A and C, showed a ME of 0.022 $mmol_c$ L^{-1} and a RMSE of 0.042 $mmol_c$ L^{-1}. Corresponding statistical indicators for N-NO_3^- concentrations resulted in a ME of -1.346 $mmol_c$ L^{-1} and a RMSE of 3.078 $mmol_c$ L^{-1}.

Table 8 shows the nitrogen balances evaluated for each experimental plot during the three crop seasons included in the simulation period. While most components of the nitrogen balance were restricted to the duration of a crop season, leaching was calculated to also include the solute mass lost during the subsequent rainfall period. Nitrogen leaching was directly related to water flow through the bottom boundary of the soil domain. Therefore, since the percolation component of the water balance was high, so was the nitrogen leaching component here. The movement of N out of the root zone also depended on the amount of applied N, the form of N in the fertilizer, and the time and number of fertigation events.

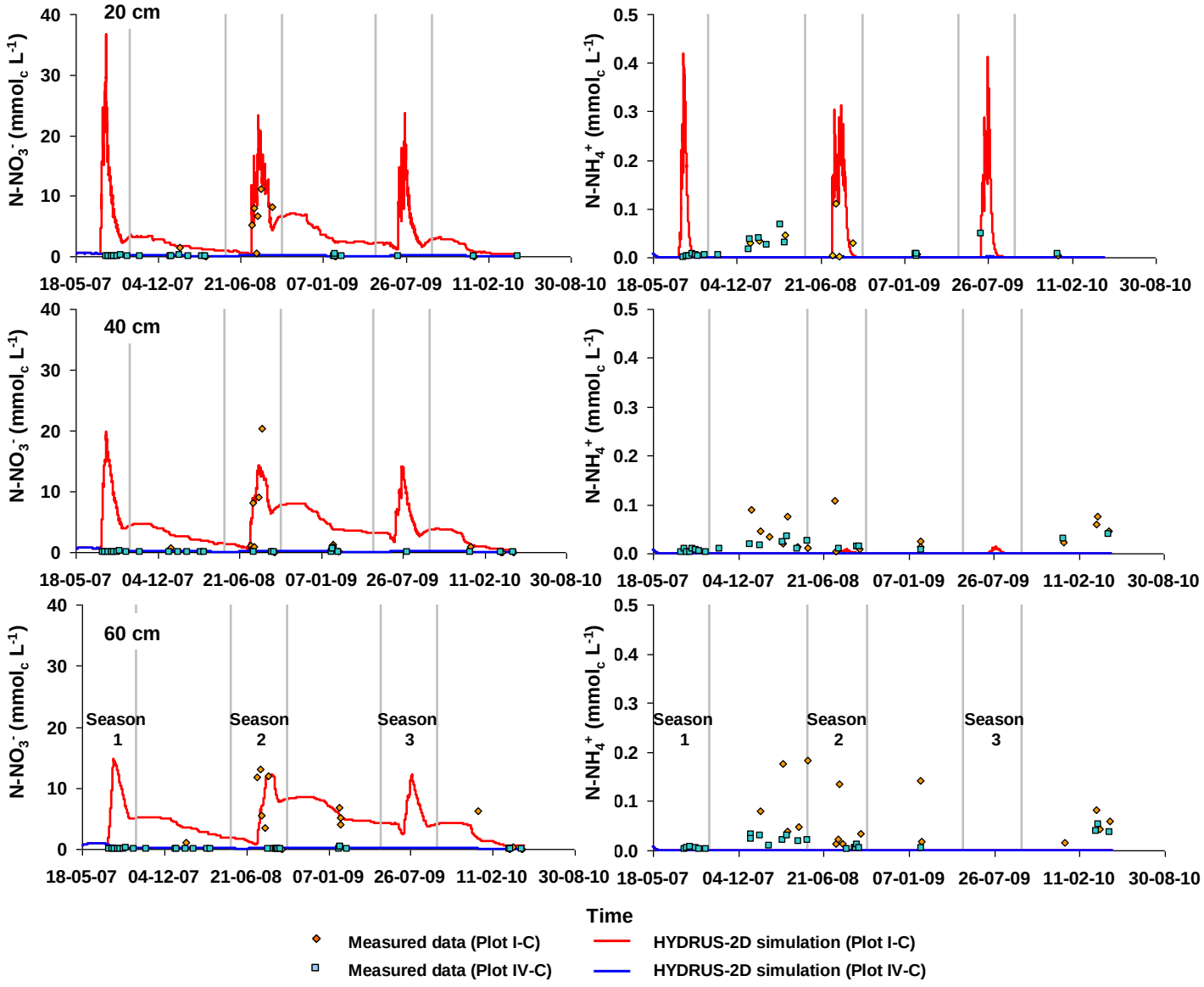

Fig. 10. Measured and simulated $N\text{-}NO_3^-$ (left) and $N\text{-}NH_4^+$ (right) concentrations at 20 (top), 40 (middle), and 60 cm (bottom) depth in plots I-C (highest application of N) and I-C (no fertigation events).

Table 8. Nitrogen balance in each experimental plot during the three crop growth seasons.

Plot	$N\text{-}NH_4^+$ $soil_{Initial}$ (kg/ha)	$N\text{-}NH_4^+$ applied (kg/ha)	$N\text{-}NH_4^+$ leached (kg/ha)	$N\text{-}NH_4^+$ adsorbed (kg/ha)	$N\text{-}NH_4^+$ sorghum uptake (kg/ha)	$N\text{-}NH_4^+$ weeds uptake (kg/ha)	$N\text{-}NH_4^+$ decay (kg/ha)	$N\text{-}NH_4^+$ $soil_{end}$ (kg/ha)	$N\text{-}NO_3^-$ $soil_{Initial}$ (kg/ha)	$N\text{-}NO_3^-$ applied (kg/ha)	$N\text{-}NO_3^-$ leached (kg/ha)	$N\text{-}NO_3^-$ sorghum uptake (kg/ha)	$N\text{-}NO_3^-$ weeds uptake (kg/ha)	$N\text{-}NO_3^-$ $soil_{end}$ (kg/ha)	Mass balance error[a] (kg/ha)
Group I															
Season 1 (2007)															
A	5	259	0	1	3	0	259	0	10	266	271	198	6	104	4.03
C	5	259	0	1	3	0	259	0	10	266	272	200	6	101	3.77
Season 2 (2008)															
A	0	286	0	1	5	0	280	0	38	295	249	245	13	152	4.05
C	0	286	0	1	5	0	280	0	37	295	248	250	17	144	2.74
Season 3 (2009)															
A	0	208	0	1	2	0	205	0	81	217	350	118	3	76	4.20
C	0	208	0	0	2	0	206	0	81	217	350	123	6	69	2.84
Cumulative masses (2007-2010)															
A	5	753	0	4	10	0	744	0	10	777	870	583		11	4.36
C	5	753	0	2	10	0	746	0	10	777	870	600		11	3.37
Group II															
Season 1 (2007)															
A	5	174	0	1	2	0	175	0	10	180	185	135	4	71	4.10
C	5	174	0	1	2	0	175	0	10	181	186	135	4	69	3.73
Season 2 (2008)															
A	0	192	0	1	3	0	187	0	26	200	171	161	9	106	3.86
C	0	192	0	1	3	0	188	0	26	200	169	166	12	100	2.61
Season 3 (2009)															
A	0	139	0	1	1	0	136	0	56	148	231	80	2	51	6.01
C	0	139	0	1	1	0	137	0	56	148	231	82	4	47	4.71
Cumulative masses (2007-2010)															
A	5	504	0	3	7	0	499	0	10	528	586	392		7	4.99
C	5	504	0	2	7	0	500	0	10	529	586	403		7	3.99

[a] $Mass\ balance\ error = \left(\sum N_{input} - \sum N_{output}\right) / \sum N_{input} \times 100$

Table 8. Nitrogen balance in each experimental plot during the three crop growth seasons (continuation).

Plot	$N\text{-}NH_4^+$ $soil_{Initial}$ (kg/ha)	$N\text{-}NH_4^+$ applied (kg/ha)	$N\text{-}NH_4^+$ leached (kg/ha)	$N\text{-}NH_4^+$ adsorbed (kg/ha)	$N\text{-}NH_4^+$ sorghum uptake (kg/ha)	$N\text{-}NH_4^+$ weeds uptake (kg/ha)	$N\text{-}NH_4^+$ decay (kg/ha)	$N\text{-}NH_4^+$ $soil_{end}$ (kg/ha)	$N\text{-}NO_3^-$ $soil_{Initial}$ (kg/ha)	$N\text{-}NO_3^-$ applied (kg/ha)	$N\text{-}NO_3^-$ leached (kg/ha)	$N\text{-}NO_3^-$ sorghum uptake (kg/ha)	$N\text{-}NO_3^-$ weeds uptake (kg/ha)	$N\text{-}NO_3^-$ $soil_{end}$ (kg/ha)	Mass balance error (kg/ha)
Group III															
Season 1 (2007)															
A	5	87	0	0	1	0	90	0	10	94	100	73	2	38	2.44
C	5	87	0	0	1	0	90	0	10	94	102	72	2	38	1.84
Season 2 (2008)															
A	0	97	0	0	2	0	95	0	14	106	87	88	5	54	2.34
C	0	97	0	0	2	0	95	0	14	106	88	90	6	52	1.07
Season 3 (2009)															
A	0	71	0	0	1	0	70	0	29	80	125	42	1	29	3.59
C	0	71	0	0	1	0	70	0	29	80	124	45	2	26	2.18
Cumulative masses (2007-2010)															
A	5	254	0	1	3	0	255	0	10	279	312	211		4	2.87
C	5	254	0	1	3	0	255	0	10	279	314	217		4	1.62
Group IV															
Season 1 (2007)															
A	5	2	0	0	0	0	6	0	10	9	16	7	0	5	1.94
C	5	2	0	0	0	0	6	0	10	9	16	7	0	5	1.70
Season 2 (2008)															
A	0	2	0	0	0	0	2	0	2	11	8	4	0	4	3.19
C	0	2	0	0	0	0	2	0	2	11	7	5	0	3	2.00
Season 3 (2009)															
A	0	2	0	0	0	0	2	0	2	12	10	4	0	4	3.27
C	0	2	0	0	0	0	2	0	2	12	9	5	0	3	1.52
Cumulative masses (2007-2010)															
A	5	6	0	0	0	0	11	0	10	32	33	16		1	3.33
C	5	6	0	0	0	0	11	0	10	32	32	18		1	2.24

Based on model simulations, most of the applied $N\text{-}NH_4^+$ was rapidly nitrified into $N\text{-}NO_3^-$, not reaching depths deeper than 20 cm and not being significantly taken up by plant roots. On the one hand, $N\text{-}NH_4^+$ adsorbs to the solid phase and thus its movement is significantly retarded compared to $N\text{-}NO_3^-$, and on the other hand, due to rapid nitrification, it does not stay long enough in the root zone to be taken up by plant roots. Figure 11 exemplifies how, based on model simulations, $N\text{-}NH_4^+$ concentrations never increased at depths below 20 cm during the crop season of 2008. Also, at the end of the irrigation season (September 6, 2008), $N\text{-}NH_4^+$ concentrations in the soil profile were already very low. Leaching of nitrogen occurred mainly in the $N\text{-}NO_3^-$ form.

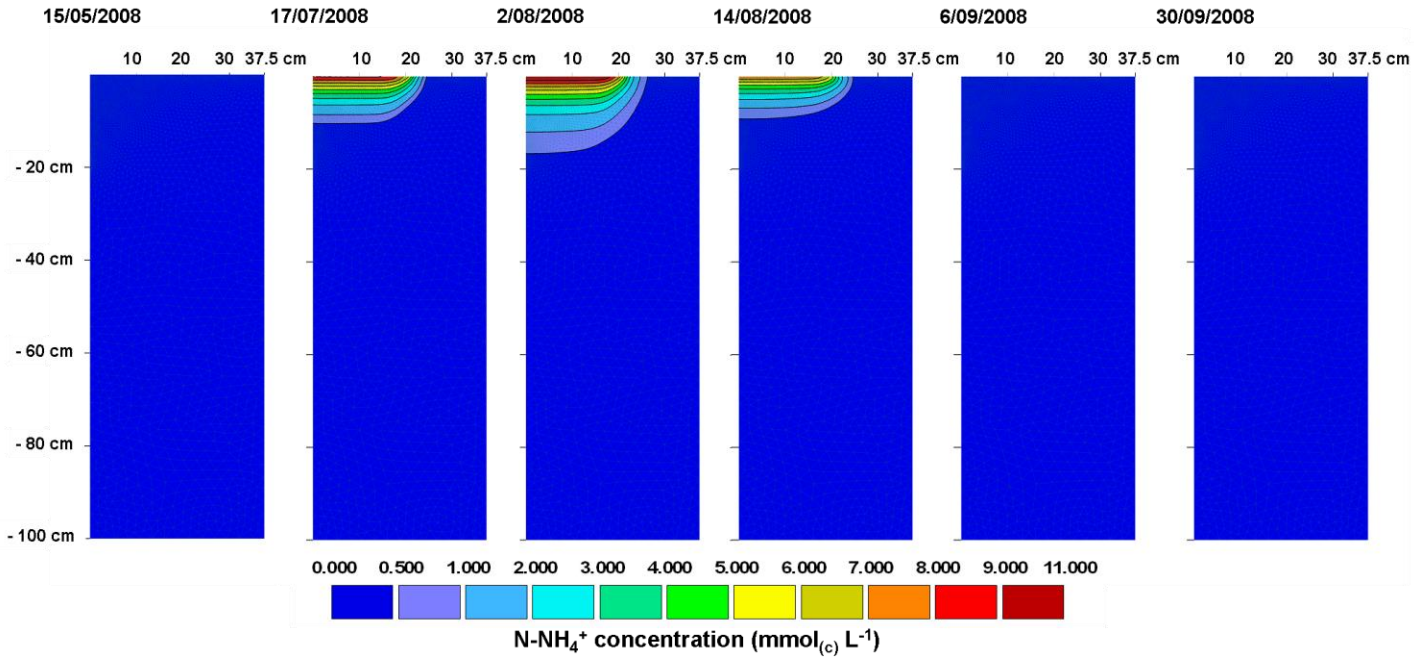

Fig. 11. Simulated distributions of $N\text{-}NH_4^+$ concentration in plot I-A during crop season 2, after sowing (May 15, 2008), after the first fertigation event (July 17, 2008), after the forth fertigation event (August 2, 2008), after the sixth and last fertigation event (August 14, 2008), at the end of the irrigation period (September 9, 2008), and at harvest (September 30, 2008). The drip emitter was located in the top left corner of each contour plot.

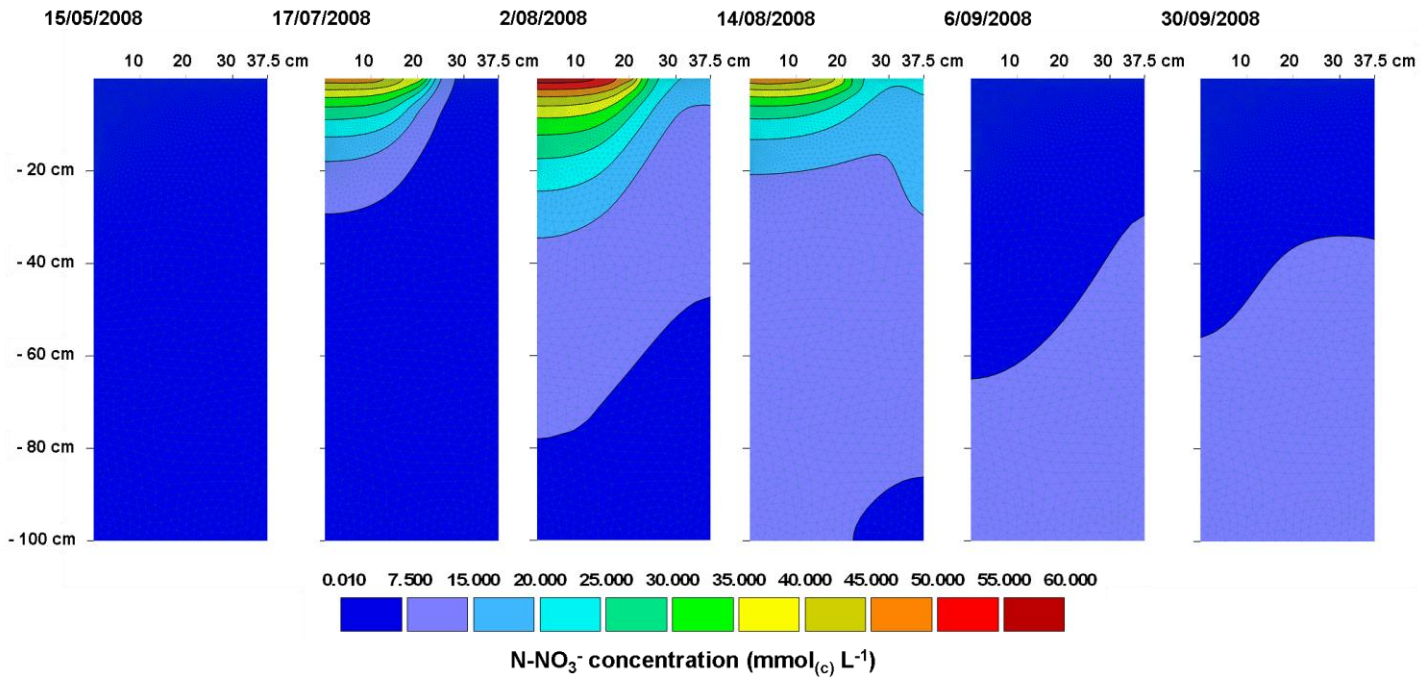

Fig. 12. Simulated distributions of $N\text{-}NO_3^-$ concentration in plot I-A during crop season 2, after sowing (May 15, 2008), after the first fertigation event (July 17, 2008), after the forth fertigation event (August 2, 2008), after the sixth and last fertigation event (August 14, 2008), at the end of the irrigation period (September 9, 2008), and at harvest (September 30, 2008). The drip emitter was located in the top left corner of each contour plot.

Figure 12 shows relatively high $N\text{-}NO_3^-$ concentrations below the root zone (> 65 cm) during the entire crop season of 2008. $N\text{-}NO_3^-$ leaching reached 41 to 70% of the total amount of $N\text{-}NO_3^-$ available in the soil system, whether it came from direct application or from $N\text{-}NH_4^+$ nitrification. The higher the number of fertigation events, the lower the amount of N applied per event, and thus the lower the amount of leached $N\text{-}NO_3^-$. In 2007, when nitrogen was applied in only 4 fertigation events, $N\text{-}NO_3^-$ leaching varied between 51 and 53% of the total amount of $N\text{-}NO_3^-$ available in the soil system. In 2008, when nitrogen was applied in 6 fertigation events, only 41% of the total amount of available $N\text{-}NO_3^-$ leached. Finally, in 2009, when only 3 fertigation events took place, 68 to 70% of the total amount of available $N\text{-}NO_3^-$ was leached.

Since $N\text{-}NH_4^+$ was rapidly nitrified and $N\text{-}NO_3^-$ easily leached, model simulations produced relatively low concentrations of both solutes in the soil profile at harvest and at the beginning of the following year's crop season. Simulations were thus in agreement with $N\text{-}NH_4^+$ and $N\text{-}NO_3^-$ concentrations measured in the saturation extract of samples collected at 20, 40, and 60 cm depth of every experimental plot. Experimental $N\text{-}NH_4^+$ concentrations were always lower than 0.17 $mmol_c\ L^{-1}$, while $N\text{-}NO_3^-$ concentrations reached a maximum value of 10.28 $mmol_c\ L^{-1}$ in deeper soil layers.

Nutrient uptake by plant roots occurred mainly in the $N\text{-}NO_3^-$ form as well. The number of fertigation events also significantly influenced the amount of $N\text{-}NO_3^-$ taken up by plant roots. Nutrient uptake varied between 23 and 42% of the total amount of $N\text{-}NO_3^-$ available in the soil system. In 2007, $N\text{-}NO_3^-$ uptake reached 37% of the applied $N\text{-}NO_3^-$. In 2008, with two additional fertigation events, nutrient uptake increased to 39 to 42% of the applied $N\text{-}NO_3^-$. Finally, in 2009, with only 3 fertigation events, $N\text{-}NO_3^-$ uptake decreased to values between 23 and 25% of the total amount of available $N\text{-}NO_3^-$. The higher number of fertigation events also led to higher yields. The average dry biomass yield measured in all plots with the N supply (groups I-III) was 19.3, 20.4, and 18.3 ton/ha in 2007, 2008, and 2009, respectively. However, in this last analysis we have to also take into consideration the increase in the salinity stress from one crop season to the next in plots irrigated with saline waters, which negatively influenced the crop yield.

The effects of the salinity stress on nutrient uptake (and inversely on nutrient leaching) was relatively small since sweet sorghum has a medium to high tolerance to salinity, and consequently there were only small reductions in transpiration due to the increase of the osmotic stress. Although nutrient uptake was somewhat lower in the plots irrigated with saline waters, only in group I, which had the highest applications of nitrogen, were the differences in N uptake between plots larger. However, even here, the difference in the cumulative N uptake between plots I-A and I-C was only 17.9 kg/ha. This was not significant enough to conclude that one could save on nitrogen applications by considering the quality of the irrigation water when defining an optimum fertigation schedule.

Figure 13 shows the relationship between the $N\text{-}NO_3^-$ plant uptake calculated using HYDRUS-2D and the experimentally determined dry biomass yield expressed using a logarithmic function with a R^2 of 0.71. This logarithmic function fitted to experimental data shows that an additional incremental increase of $N\text{-}NO_3^-$ uptake produces diminishing returns in the total dry biomass response. Each additional unit of $N\text{-}NO_3^-$ taken up by plant roots added less to the total biomass output than the previous unit did. After a certain level of $N\text{-}NO_3^-$ uptake was reached (estimated here to be between those registered for groups II-III, i.e., 130-180 kg/ha), further increases in nutrient uptake did not contribute directly to the increase of the dry biomass yield. Group I thus involved some 'luxury' uptake, since the amount of $N\text{-}NO_3^-$ taken up by plant roots did not contribute significantly to the dry biomass yield. More detailed results of the effect of brackish waters on nitrogen needs and dry biomass yield of sweet sorghum can be found in Ramos et al. (2012).

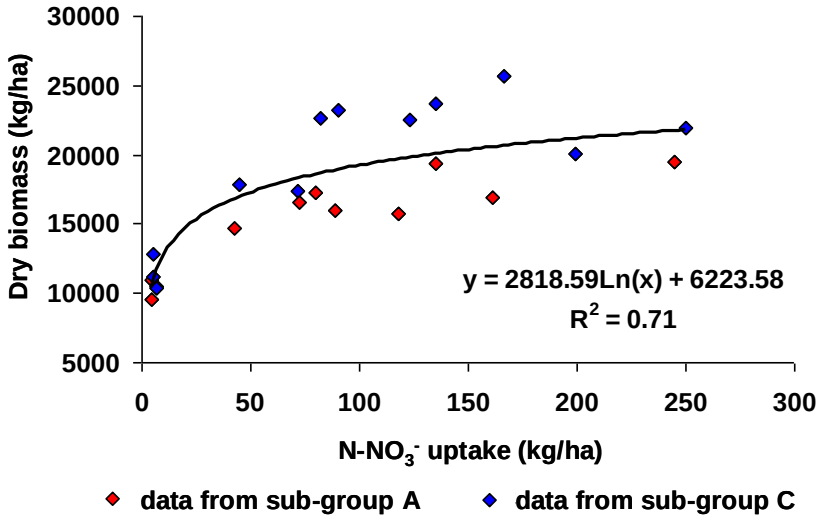

Fig. 13. Relationship between $N\text{-}NO_3^-$ uptake, as simulated by HYDRUS-2D, and dry biomass yield (Y).

3.4. About model validation

Deviations between measured data and simulated variables (Table 6) can be attributed to different causes, including errors related to field measurements, and to model input and model structure errors.

Field measurements: The most relevant source of errors related to field measurements refers to the representativeness of TDR measurements and ceramic cup samplings at different depths. TDR probes measure spatially averaged water contents over a certain soil volume, the size of which depends on the size and orientation of TDR probes (Ferré et al., 2002). However, the distribution of water under drip irrigation is highly spatially non-uniform (Gärdenäs et al., 2005; Hanson et al., 2006). Water contents were highest near the drip emitter after an irrigation event and then redistributed throughout the soil profile. Therefore, TDR probes averaged water contents over soil regions with different moisture status, while HYDRUS-2D reports water contents for a precise soil location (Fig. 4). Note that due to the dimensionality (axisymmetrical) of our calculations, by averaging water content over a certain area around the observation node, we would obtain an average value for a circular pipe, rather than for a straight cylinder over which TDR averages its measurements. Likewise, measurements taken with suction cups were averaged over a sampling area of a certain volume, the size of which depends on soil hydraulic properties, the soil water content, and the applied suction in the ceramic cup (Weihermüller et al., 2005, 2011). Measured values thus did not represent point values as the simulations did. Spatial soil variability can also affect concentrations measured by suction cups, an issue extensively studied by Weihermüller et al. (2011).

Model input errors: The accuracy of the soil hydraulic properties, which were measured on undisturbed soil samples taken not in each experimental plot, but from a representative soil profile, and their representativeness in describing water infiltration and redistribution in different experimental plots seem to be important sources of error to consider. Soil hydraulic properties were determined in the laboratory on soil samples of a certain size (from 100 to 630 cm^3) and may not be representative of the much larger simulated flow domain under field conditions. For example, soil samples are normally saturated in the laboratory by capillarity, with water entering the sample through the bottom, decreasing the possibility of the air being trapped inside. For this reason, saturation values are usually much higher in the laboratory than under field conditions

(Šimůnek et al., 1998), where this obviously cannot be accomplished. This may explain some of the deviations found in simulated water contents at a depth of 20 cm (Fig. 5) where HYDRUS-2D tended to simulate higher values during irrigation seasons than what field data showed. Additionally, the soil was considered homogeneous in HYDRUS-2D simulations, and more complex physical phenomena, such as spatial and temporal variability of the soil hydraulic properties and the probable existence of preferential flow paths in the different experimental plots, were neglected. Considering these additional phenomena in HYDRUS simulations would likely have helped improve the agreement between measured and simulated data.

It is also important for water flow simulations to accurately estimate plant transpiration and soil evaporation. The dual crop coefficient approach used is generally considered accurate (Tolk and Howell, 2001; Howell et al., 2004; Liu and Luo, 2010), but is complex and requires various crop and soil parameters that need to be adjusted to experimental conditions. Finally, the crop parameters, such as those used in the Feddes et al. (1978) model, were taken from the literature and do not take differences among crop varieties into account. The Maas (1990) threshold and slope parameters, which were mainly intended to serve as a guideline to relative tolerances among crops, may vary with cultivars, climate, soil conditions, and cultural practices. Thus, estimates of uptake reductions must be regarded with some uncertainty (Skaggs et al., 2006b). The same can be said about the empirical relationship between EC_e and EC_{sw}.

Model structure (or modeling approach) errors: Limitations involved in considering an axisymmetrical domain to represent the three-dimensional movement of water and nutrients have to be considered. This approach has been widely used for analyzing surface and buried drip irrigation experiments (Cote et al., 2003; Skaggs et al., 2004; Gärdenäs et al., 2005; Lazarovitch et al., 2005; Hanson et al., 2006; Ajdary et al., 2007; Kandelous and Šimůnek, 2010ab; Ravikumar et al., 2011). Nevertheless, Kandelous et al. (2011) pointed out some of the limitations of this approach to be considered. Namely, the fact that flow from each emitter only remains axisymmetrical until the wetting patterns from neighboring emitters begin overlapping each other. Kandelous et al. (2011) state that the axisymmetrical representation is only an approximation of the fully three-dimensional problem and that the numerical results should increasingly depart from reality as time and irrigation volumes increase. Using a fully three-dimensional model, which is also available in HYDRUS (2D/3D), could improve water content simulations. In Ramos et al. (2011), a 1D version of HYDRUS, used for simulating a similar

experiment, produced a *RMSE* (0.04 cm^3 cm^{-3}) larger than the 2D approach (0.03 cm^3 cm^{-3}) adapted in this study. Thus, adopting the 2D version of HYDRUS proved to be beneficial in lowering the simulation errors. However, numerical modeling is not that straightforward, and the notion that using a fully three-dimensional model would immediately bring better correspondence between measured and simulated data is unrealistic. The agreement between measured and simulated $N\text{-}NO_3^-$ obtained here can serve as an example, since these results were worse than those obtained by Ramos et al. (2011). Considering a cylindrically shaped (0.375 m wide) simulation domain (Fig. 3) could be another possible model structure error, since the drip emitters' grid was in fact rectangular (0.75 m wide x 1 m long). This means that, in reality, water and solutes could redistribute in a larger soil domain than that considered in simulations.

Modeling of the N species: There are some additional considerations that need to be taken into account with regards to modeling the nitrogen fate and transport. The approach to model the transport of the nitrogen species using the sequential first-order decay chain reactions is relatively simple and has produced satisfactory results in many different studies (Ajdary et al., 2007; Mailhol et al., 2007; Crevoisier et al., 2008). However, this approach can only consider nitrogen processes that are involved in a sequential-first order decay chain, such as nitrification ($N\text{-}NH_4^+$ transformation into $N\text{-}NO_2^-$, and then further into $N\text{-}NO_3^-$), denitrification ($N\text{-}NO_3^-$ transformation into N_2 and $N\text{-}N_2O$), and volatilization ($N\text{-}NH_4^+$ transformation into $N\text{-}NH_3$). Other nitrogen reactions, with probable relevance for long-term applications such as ours, simply cannot be accounted for using this approach. Examples of such reactions are nitrogen fixation from the atmosphere, mineralization of crop residues and other organic wastes, mineralization of the soil humus fraction, and so on. The relevance of these processes on N dynamics can be documented in Figure 10, which shows that $N\text{-}NH_4^+$ and $N\text{-}NO_3^-$ concentrations in the soil increased after fertigation events during crop seasons, and then decreased due to plant uptake and leaching. During fertigation events, simulations matched the measured data well since nitrification was the main process occurring in the soil. However, the deviation between measured and simulated N data was visually more pronounced during non-crop seasons, due to the limitations discussed above. For example, sweet sorghum was harvested at the end of the growing season so that its biomass production could be estimated. This involved cutting the

entire plant above the ground while leaving roots in the soil. Residual $N\text{-}NH_4^+$ and $N\text{-}NO_3^-$ concentrations measured during non-crop seasons could, to some extent, be attributed to the mineralization of the root system, and thus were not considered in model simulations.

Additionally, only the passive nutrient uptake mechanism was considered in our approach. Since root nitrogen uptake likely involves both passive and active mechanisms (e.g., Šimůnek and Hopmans, 2009), considering only passive uptake likely underestimated the total N uptake and overestimated downward N leaching, providing thus the most conservative assessment of N leaching. However, the extent of this underestimation is currently unknown. Finally, deviations between measured and simulated N data could also be attributed to other model limitations and relevant physical phenomena that were not considered in our modeling approach, such as root growth.

4. Conclusions

The irrigation scheme used in this study allowed investigation of the response of sweet sorghum to irrigation scenarios with different levels of nitrogen and different water qualities between 2007 and 2010. The water contents, EC_{sw}, $N\text{-}NH_4^+$ and $N\text{-}NO_3^-$ concentrations simulated continuously during the entire field experiment, compared well with collected experimental data, having a RMSE of 0.030 $cm^3\ cm^{-3}$, 1.764 dS m^{-1}, 0.042 $mmol_c\ L^{-1}$, and 3.078 $mmol_c\ L^{-1}$, respectively. Possible causes of deviations between measured data and simulations were likely related to field measurements, model input data, and model structure errors, and were extensively discussed, showing HYDRUS-2D advantages and limitations for this application. However, model simulations helped to understand the best irrigation and fertigation management practices to be adopted in order to increase nutrient uptake and reduce nutrient leaching.

Sweet sorghum transpiration was estimated to vary between 360 and 457 mm depending on the crop season and the irrigation scenario considered. The lower water needs of sweet sorghum, compared to other traditional crops grown in water-scarce European Mediterranean regions, makes it a good alternative to other crops for these environmentally stressed regions.

Sweet sorghum appears to be tolerant to the use of saline waters. Only during the second crop season, but mainly during the third year, started the sweet sorghum transpiration be reduced due

to the increase in the salinity stress and salt accumulation over time. Thus, in water-scarce regions where even saline waters can be viewed as an important source of irrigation water during drought seasons, the use of marginal waters showed viability for irrigating sweet sorghum during a limited time period.

HYDRUS-2D successfully estimated the fate of nitrogen in field plots grown with sweet sorghum under European Mediterranean conditions. The logarithmic function describing the relation between estimates of $N\text{-}NO_3^-$ uptake and the dry biomass yield (R^2=0.71) showed that sweet sorghum N requirements were lower than estimated N uptakes for the scenario with the highest levels of applied nitrogen, revealing some luxury uptake in these plots. The leaching of N out of the root zone depended closely on drainage, the amount of N applied, the form of N in the fertilizer, and the time and number of fertigation events. Based on model simulations, leaching of nitrogen occurred mainly in the $N\text{-}NO_3^-$ form, reaching 41 to 70% of the total amount of NO_3^- available in the soil system. According to HYDRUS-2D, higher $N\text{-}NO_3^-$ uptakes were obtained when the number of fertigation events was larger.

Acknowledgments

This work was funded by the Project PTDC/AGR-AAM/66004/2006 of the Fundação para a Ciência e a Tecnologia (FCT). T. B. Ramos was funded by the FCT grant SFRH/BD/60363/2009.

References

Ajdary, K., Singh, D.K., Singh, A.K., Khanna, M., 2007. Modelling of nitrogen leaching from experimental onion field under drip irrigation. Agric. Water Manage. 89, 15-28.

Allen, R.G., Pereira, L.S., Raes, D., Smith, M., 1998. Crop Evapotranspiration – Guidelines for Computing Crop Water Requirements. Irrig. Drain. Pap. 56. FAO, Rome, Italy.

Allen, R.G., Pereira, L.S., Smith, M., Raes, D., Wright, J.L., 2005. FAO-56 dual crop coefficient method for estimating evaporation from soil and application extensions. J. Irrig. Drain. Eng. 131, 2-13.

Almodares, A., Hadi, M.R., 2009. Production of bioethanol from sweet sorghum: A review. Afr. J. Agric. Res. 4, 772-780.

Barbanti, L., Grandi, S., Vecchi, A., Venturi, G., 2006. Sweet and fibre sorghum (*Sorghum bicolor* (L.) Moench), energy crops in the frame of environmental protection from excessive nitrogen loads. Eur. J. Agron. 25, 30-39.

Bear, J., 1972. Dynamics of fluids in porous media. Elsevier, New York.

Cameira M.R., Fernando R.M., Pereira, L.S., 2003. Monitoring water and NO_3-N in irrigated maize fields in the Sorraia Watershed, Portugal. Agric. Water Manage. 60, 199-216.

Cameira M.R., Fernando R.M., Ahuja, L.R., Pereira, L.S., 2005. Simulating the fate of water in field soil-crop environment. J. Hydrol. 315, 1-24.

Cameira M.R., Fernando R.M., Ahuja L.R., Ma L., 2007. Using RZWQM to simulate the fate of nitrogen in field soil–crop environment in the Mediterranean region. Agric. Water Manage. 90, 121-136.

Cote, C. M., Bristow, K.L., Charlesworth, P.B., Cook, F.J., Thorburn, P.J., 2003. Analysis of soil wetting and solute transport in subsurface trickle irrigation. Irrig. Sci. 22, 143-156.

Crevoisier, D., Popova, Z., Mailhol, J.C., Ruelle, P., 2008. Assessment and simulation of water and nitrogen transfer under furrow irrigation. Agric. Water Manage. 95, 354-366.

Doltra, J., Muñoz, P., 2010. Simulation of nitrogen leaching from a fertigated crop rotation in a Mediterranean climate using the EU-Rotate_N and Hydrus-2D models. Agric. Water Manage. 97, 277-285.

European Commission, 2010a. On implementation of Council Directive 91/676/EEC concerning the protection of waters against pollution caused by nitrates from agricultural sources based on Member State reports for the period 2004-2007. Report from the Commission to the Council and the European Parliament 47, Brussels.

European Commission, 2010b. On implementation of Council Directive 91/676/EEC concerning the protection of waters against pollution caused by nitrates from agricultural sources based on Member State reports for the period 2004-2007. Accompanying document to the Report

from the Commission to the Council and the European Parliament. Commission Staff Working Document 118, Brussels.

FAO, 2006. World reference base for soil resources. A framework for international classification, correlation and communication. World Soil Resources Reports 103. Food and Agriculture Organization of the United Nations, Rome.

Feddes, R.A., Kowalik, P.J., Zaradny, H., 1978. Simulation of field water use and crop yield. Simulation Monographs Pudoc, Wageningen, The Netherlands.

Fernando, R.M., 1993. Quantificação do balanço hídrico de um solo regado na presença de uma toalha freática. Simulação com o modelo SWATRER. PhD thesis, Institute of Agronomy, Technical University of Lisbon, Lisbon, Portugal.

Ferré, T.P.A., Nissen, H.H., Šimůnek, J., 2002. The effect of the spatial sensitivity of TDR on inferring soil hydraulic properties from water content measurements made during the advance of a wetting front. Vadose Zone J. 1, 281-288.

Fontes, J.C., Pereira, L.S., Smith, R.E., 1992. Runoff and erosion in volcanic soils of Azores: simulation with OPUS. Catena 56, 199-212.

Gärdenäs, A., Hopmans, J.W., Hanson, B.R., Šimůnek, J., 2005. Two-dimensional modeling of nitrate leaching for various fertigation scenarios under micro-irrigation. Agric. Water Manage. 74, 219-242.

Gonçalves, M.C., Leij, F.J., Schaap, M.G., 2001. Pedotransfer functions for solute transport parameters of Portuguese soils. Euro. J. Soil Sci. 52, 563-574.

Gonçalves, M.C., Šimůnek, J., Ramos, T.B., Martins, J.C., Neves, M.J., Pires, F.P., 2006. Multicomponent solute transport in soil lysimeters with waters of different quality. Water Resour. Res. 42, W08401, doi:10.1029/2005WR004802.

Hanson, B.R., Šimůnek, J., Hopmans, J.W., 2006. Evaluation of urea-ammonium-nitrate fertigation with drip irrigation using numerical modeling. Agric. Water Manage. 86, 102-113.

Hanson, B.R., Šimůnek, J., Hopmans, J.W., 2008. Leaching with subsurface drip irrigation under saline, shallow ground water conditions. Vadose Zone J. 7, 810-818.

Hoffman, G.J., Shalhevet, J., 2007. Controlling salinity. In: Hoffman, G.J., et al. (eds.), Design and operation of farm irrigation systems. 2nd ed, pp. 160-207. American Society of Agricultural and Biological Engineers, St. Joseph, Michigan, USA.

Howell, T.A., Evett, R., Tolk, J.A., Schneider, A.D., 2004. Evapotranspiration of full-, deficit-irrigated, and dryland cotton on the Northern Texas High Plains. J. Irrig. Drain. Eng. 130, 277-285.

Hutson, J.L., Wagenet, R.J., 1991. Simulating nitrogen dynamics in soils using a deterministic model, Soil Use Manage. 7, 74–78.

Johnsson, H., Bergström, L., Jansson, P.-E., Paustian, K., 1987. Simulated nitrogen dynamics and losses in a layered agricultural soil. Agric. Ecosyst. Environ. 18, 333–356.

Kandelous, M.M., Šimůnek, J., 2010a. Comparison of numerical, analytical and empirical models to estimate wetting pattern for surface and subsurface drip irrigation. Irrig. Sci. 28, 435–444.

Kandelous, M.M., Šimůnek, J. 2010b. Numerical simulations of water movement in a subsurface drip irrigation system under field and laboratory conditions using HYDRUS-2D. Agric. Water Manage. 97, 1070–1076.

Kandelous, M.M., Šimůnek, J., van Genuchten, M.Th., Malek, K., 2011. Soil water content distributions between two emitters of a subsurface drip irrigation system. Soil Sci. Soc. Am. J. 75, 488–497.

Katerji, N., Mastrorilli, M., Rana G., 2008. Water use efficiency of crops cultivated in the Mediterranean region: Review and analysis. Eur. J. Agron. 28, 493-507.

Klepper, B., 1991. Crop root system response to irrigation. Irrig. Sci. 12: 105-108.

Lazarovitch, N., Šimůnek, J., Shani, U., 2005. System-dependent boundary condition for water flow from subsurface source. Soil Sci. Soc. Am. J. 69, 46–50.

Liu, Y.J., Luo, Y., 2010. A consolidated evaluation of the FAO-56 dual crop coefficient approach using the lysimeter data in the North China Plain. Agric.Water Manage. 97, 31-40.

Ma, L., Ahuja, L.R., Ascough II, J.C., Shaffer, M.J., Rojas, K.W., Malone, R.W., Cameira, M.R., 2001. Integrating system modeling with field research in agriculture: applications of the root zone water quality model (RZWQM). Adv. Agron. 71, 233-292.

Mailhol, J.C., Crevoisier, D., Triki, K., 2007. Impact of water application conditions on nitrogen leaching under furrow irrigation: Experimental and modelling approaches. Agric. Water Manage. 87, 275–284.

Mailhol, J.C., Ruelle, P., Walser, S., Schütze, N., Dejean, C., 2011. Analysis of AET and yield predictions under surface and buried drip irrigation systems using the Crop Model PILOTE and Hydrus-2D. Agric. Water Manage. 98, 1033–1044.

Mallants, D., van Genuchten, M.Th., Šimůnek, J., Jacques, D., Seetharam, S., 2011. Leaching of contaminants to groundwater. In: Swartjes, F.A. (Ed.), Dealing with Contaminated Sites. From Theory to Practical Applications, pp. 787-850. Springer, The Netherlands.

Maas, E.V., 1990. Crop salt tolerance. In: Tanji, K.K (Ed.), Agricultural Salinity Assessment and Management. Manual Eng. Pract., vol. 71, ., pp. 262–304. Am. Soc. of Civ. Eng., Reston, Va.

Mastrorilli, M., Katerji, N., Rana, G., Steduto, P., 1995. Sweet sorghum in Mediterranean climate: radiation use and biomass water use efficiencies. Ind. Crop Prod. 3, 253-260.

Mastrorilli, M., Katerji, N., Rana, G., 1999. Productivity and water use efficiency of sweet sorghum as affected by soil water deficit occurring at different vegetative growth stages. Eur. J. Agron. 11, 207-215.

Mmolawa, K., Or, D., 2003. Experimental and numerical evaluation of analytical volume balance model for soil water dynamics under drip irrigation. Soil Sci. Soc. Am. J. 67, 1657–1671.

Novák, V., van Genuchten, M.Th., 2008. Using the transpiration regime to estimate biomass production. Soil Sci. 173, 401-407.

Pereira L.S., van den Broek, B., Kabat, P., Allen, R.G., 1995. Crop-Water Simulation Models in Practice. Wageningen Pers, Wageningen, The Netherlands.

Prasad, S., Singh, A., Jain, N., Joshi, H.C., 2007. Ethanol production from sweet sorghum syrup for utilization as automotive fuel in India. Energ. Fuel. 21, 2415–2420.

Ramos, T.B., Gonçalves, M.C., Castanheira, N.L., Martins, J.C., Santos, F.L., Prazeres, A., Fernandes, M.L., 2009. Effect of sodium and nitrogen on yield function of irrigated maize in southern Portugal. Agric. Water Manage. 96, 585-594.

Ramos, T.B., Šimůnek, J., Gonçalves, M.C., Martins, J.C., Prazeres, A., Castanheira, N.L., Pereira, L.S., 2011. Field evaluation of a multicomponent solute transport model in soils irrigated with saline waters. J. Hydrol. 407, 129-144, doi:10.1016/j.jhydrol.2011.07.016.

Ramos, T.B., Castanheira, N.L., Gonçalves, M.C., Fernandes, M.L., Januário, M.I., Lourenço, M.E., Pires, F.P., Martins, J.C., 2012. Effect of combined use of brackish water and nitrogen fertilizer on biomass and sugar yield of sweet sorghum. Pedosphere 22, 785-794.

Ravikumar, V., Vijayakumar, G., Šimůnek, J., Chellamuthu, S., Santhi, R., Appavu, K., 2011. Evaluation of fertigation scheduling for sugarcane using a vadose zone flow and transport model. Agric. Water Manage. 98, 1431-1440.

Ritchie, J.T., 1972. Model for predicting evaporation from a row crop with incomplete cover. Water Resour. Res. 8, 1204-1213.

Roberts, T., Lazarovitch, N., Warrick, A.W., Thompson, T.L., 2009. Modeling salt accumulation with subsurface drip irrigation using HYDRUS-2D. Soil Sci. Soc. Am. J. 73, 233-240.

Roberts, T., White, S.A., Warrick, A.W., Thompson, T.L., 2008. Tape depth and germination method influence patterns of salt accumulation with subsurface drip irrigation. Agric. Water Manage. 95, 669-677.

Rosa, R.D., Paredes, P., Rodrigues, G.C., Alves, I., Fernando, R.M., Pereira, L.S., Allen, R.G., 2012. Implementing the dual crop coefficient approach in interactive software: 1. Background and computational strategy. Agric. Water Manage. 103, 62-77.

Šimůnek, J., Wang, D., Shouse, P.J., van Genuchten, M. Th., 1998. Analysis of a field tension disc infiltrometer experiment by parameter estimation. Intern. Agrophysics 12, 167-180.

Šimůnek, J., van Genuchten, M. Th., Šejna, M., 2006. The HYDRUS software package for simulating two- and three-dimensional movement of water, heat, and multiple solutes in variably-saturated media, Technical manual. Version 1.0, PC Progress, Prague, Czech Republic, 241 pp.

Šimůnek, J., van Genuchten, M.Th., Šejna, M., 2008. Development and applications of the HYDRUS and STANMOD software packages, and related codes, Vadose Zone J. 7, 587-600.

Šimůnek, J., Hopmans, J.W., 2009. Modeling compensated root water and nutrient uptake. Ecol. Model. 220, 505-521.

Skaggs, T.H., Trout, T.J., Šimůnek, J., Shouse, P.J., 2004. Comparison of HYDRUS-2D simulations of drip irrigation with experimental observations. J. Irrig. Drain. Eng. 130, 304–310.

Skaggs, T.H., van Genuchten, M.Th., Shouse, P.J., Poss, J.A., 2006a. Macroscopic approaches to root water uptake as a function of water and salinity stress. Agric. Water Manage. 86, 140-149.

Skaggs, T.H., Shouse, P.J., Poss, J.A., 2006b. Irrigating forage crops with saline waters: 2. Modeling root uptake and drainage. Vadose Zone J. 5, 824-837.

Steduto, P., Katerji, N., Puertos-Molina, H., Unlü, M., Mastrorilli, M., Rana, G., 1997. Water-use efficiency of sweet sorghum under water stress conditions. Gas-exchange investigations at leaf and canopy scales. Field Crops Res. 54, 221-234.

Tolk, J.A., Howell, T.A., 2001. Measured and simulated evapotranspiration of grain sorghum grown with full and limited irrigation in three High Plains soils. T. ASABE 44, 1553–1558.

U.S. Salinity Laboratory Staff, 1954. Diagnosis and Improvement of Saline and Alcaly Soils. USDA Handbook 60. Washington, USA.

van Genuchten, M.Th., 1980. A closed form equation for predicting the hydraulic conductivity of unsaturated soils. Soil Sci. Soc. Am. J. 44, 892-898.

van Genuchten, M.Th., 1987. A numerical model for water and solute movement in and below the root zone. Res. Rep. 121, U.S. Salinity Laboratory, USDA, ARS, Riverside, California.

Vasilakoglou, I., Dhima, K., Karagiannidis, N., Gatsis, T., 2011. Sweet sorghum productivity for biofuels under increased soil salinity and reduced irrigation. Field Crops Res. 120, 38-46.

Vrugt, J.A., Hopmans, J.W., Šimůnek, J., 2001. Calibration of a two dimensional root water uptake model. Soil Sci. Soc. Am. J. 65, 1027–1037.

Weihermüller, L., Kasteel, R., Vanderborght, J., Pütz, T., Vereecken, H., 2005. Soil water extraction with a suction cup: Results of numerical simulations. Vadose Zone J. 4, 899-907.

Weihermüller, L., Kasteel, R., Vanderborght, J., Šimůnek, J., Vereecken, H., 2011. Uncertainty in pesticide monitoring using suction cups: Evidence from numerical simulations. Vadose Zone J. 10, 1287-1298.

Zegada-Lizarazu, W., Zatta, A., Monti, A., 2012. Water uptake efficiency and above- and belowground biomass development of sweet sorghum and maize under different water regimes. Plant Soil 351, 47-60.

Zhao, Y.L., Dolat, A., Steinberger, Y., Wang, X., Osman, A., Xie, G.H., 2009. Biomass yield and changes in chemical composition of sweet sorghum cultivars grown for biofuel. Field Crops Res. 111, 55-64.

Chapter 4

Effect of combined use of brackish water and nitrogen fertilizer on biomass and sugar yield of sweet sorghum

(Published in: Pedosphere 22, 785-794. 2012)

Effect of combined use of brackish water and nitrogen fertilizer on biomass and sugar yield of sweet sorghum

T. B. Ramos[1], N. L. Castanheira[2], M. C. Gonçalves[1,2], M. L. Fernandes[2], M. I. Januário[1], M. E. Lourenço[3], F. P. Pires[2] and J. C. Martins[2]

[1] CEER-Biosystems Engineering, Institute of Agronomy, Technical University of Lisbon, Tapada da Ajuda, 1349-017 Lisbon (Portugal)

[2] Estação Agronómica Nacional, L-INIA, Instituto Nacional de Recursos Biológicos, Quinta do Marquês, Av. República, 2784-505 Oeiras (Portugal)

[3] Departamento de Fitotecnia, Instituto de Ciências Agrárias e Ambientais Mediterrânicas, Universidade de Évora, Apartado 94, 7002-554 Évora (Portugal)

Abstract

Soil salinization and non-point source pollution are among the most important and widespread environmental problems in European Mediterranean regions. Sweet sorghum (*Sorghum bicolor* (L.) Moench var. *saccharatum*) is a moderate to high salinity tolerant crop with low water and nutrient needs, seen as an alternative to grow in the water scarce regions. A three-year multifactorial study was conducted in southern Portugal to evaluate the combined effects of saline water and nitrogen application on the dry biomass (total, stems, and leaves yield), sugar content (total reducing sugars and sucrose contents), and sugar yield (here defined as the product of total reducing sugars and stems dry biomass) functions of sweet sorghum. Sorghum dry biomass and sugar yield showed diminishing returns for each incremental change of nitrogen. The use of saline irrigation waters also led to yield reduction. Exception was sucrose content which increased with increasing levels of sodium in the soil. Nitrogen need decreased as the amount of sodium applied increased. Stem dry biomass, sucrose content, and sugar yield progressively increased with progress in the experiment. The effect could be attributed to the increase of the amount of irrigation applied throughout the years, thus increasing the leaching

fraction which promoted salt leaching from the root zone, reduced the salinity stress, increased plant transpiration, nitrogen uptake and biomass yield.

Keywords: Mediterranean conditions, non-point source pollution, salinity, sweet sorghum, yield functions.

1. Introduction

Human-induced soil salinization, sodification and non-point source pollution are among the most important and widespread environmental problems in agricultural regions with arid, semi-arid, and even dry sub-humid conditions. Improving crop productivity by use of water and nutrients more efficiently has been a leading research approach for these water scarce regions (Pereira et al., 2009). Crop yield-water consumption relationships are among the most common techniques used to measure the effects and interactions of water and nutrients on crop yield (Igbadun et al., 2007; Mandal et al., 2010). However, in water scarce regions even saline waters are seen as an important resource to meet food demands (Rhoades et al., 1992; Qadir and Oster, 2004; Pereira et al., 2009). Thus, the quality of the irrigation water and the understanding of the combined effects of saline water and nitrogen application on the yield function are of fundamental importance since it could give answers on how to overcome the soil salinization/sodification process and how to reduce nitrate leaching in those regions (Dinar et al., 1991; Datta et al., 1998).

Besides improving water and nutrients efficiency, the use of crops with less water and nutrient needs and higher salt tolerance has been considered by the scientific community as an alternative to traditional crops in the water scarce regions (Zhao et al., 2009; Vasilakoglou et al., 2011). Sweet sorghum (Sorghum bicolor (L.) Moench) is seen as one of the most interesting annual crops to grow in these stressed areas (Lourenço et al., 2007; Vasilakoglou et al., 2011). Sweet sorghum has a high drought resistance due to its relatively low water requirements (Mastrorilli et al., 1999) and high water-use efficiency (Mastrorilli et al., 1995; Steduto et al., 1997), and possesses a moderate to high tolerance to salinity (Maas, 1990). Sweet sorghum is furthermore an important alternative source for renewable energy by storing large quantities of non-structural carbohydrates (sucrose, glucose, and fructose) in the stems which can be converted into fuel ethanol (Almodares and Hadi, 2009).

The effects of N fertilizer on sweet sorghum growth and yield have been evaluated for several times in various regions of the world (Wiedenfeld, 1984; Barbanti et al., 2006). The effect of the salinity stress on sweet sorghum have been also presented in literature (Begdullayeva et al., 2007; Almodares et al., 2008a, 2008b; Vasilakoglou et al., 2011). However, studies focusing on the combined effects of saline water and nitrogen application on sweet sorghum have been very limited despite the growing interest for this annual crop throughout vast regions of the world. Thus, the objective of this study was to evaluate the combined effects of saline water and nitrogen application on sweet sorghum (Sorghum bicolor (L.) Moench) dry biomass and sugar yield (here defined as the product of total reducing sugars and stems dry biomass) functions under Mediterranean conditions.

2. Materials and methods

2.1. Site description

Field plot experiment was conducted at the Alvalade Experimental Station (37º 56' 48" N and 8º 23' 40" W) located in the Alentejo region of southern Portugal. The experiment was carried out from 2007 to 2009, always at the same location, on a field with an Eutric Fluvisol. The soil is a clay loam with coarse sand 8.3%, fine sand 52.4%, silt 26.3%, and clay 13.0% by weight; dry bulk density 1.49 g cm^{-3}; the field capacity 31.0%; the wilting point 9.8%; the saturated hydraulic conductivity 14.2 cm d^{-1}; pH(H_2O) 7.2; the average organic matter 20.0 g kg^{-1}; cation exchange capacity 11.67 $cmol_c$ kg^{-1}; electrical conductivity (*EC*) of the saturation extract 3.04 dS m^{-1}; and at the beginning of the three growing seasons of 2007, 2008 and 2009, exchangeable Na^+ 1.94, 1.53, and 1.84 $cmol_c$ kg^{-1}; NO_3^--N 2.90, 4.60, and 4.85 mg kg^{-1}; and NH_4^+-N 2.17, 0.46, and 0.55 mg kg^{-1}, respectively.

The climate in the Alentejo region is mostly dry sub-humid to semi-arid, with hot dry summers, and mild winters with irregular rainfall. Sweet sorghum potential transpiration (T_p) rates in each field plot were obtained from the daily values of reference evapotranspiration (ET_0), determined with the FAO Penman-Monteith method (Allen et al., 1998; 2005), as follows:

$$ET_c = \left(K_{cb} + K_e\right) ET_0 \quad (1)$$

where ET_c is the crop evapotranspiration (L T^{-1}), K_{cb} is the basal crop coefficient, which represents the plant transpiration component (-), and K_e is the soil evaporation coefficient (-). Standard sweet sorghum K_{cb} values (Allen et al., 1998) were adjusted for the Alvalade climate, taking into consideration the crop height, wind speed, minimum relative humidity averages for the period under consideration, as well as the effect of the salinity and nitrogen stress on the leaf area index (LAI), using the procedure for non-pristine agricultural vegetation described in Allen et al. (1998).

2.2. Crop management

Sweet sorghum (*Sorghum bicolor* (L.) Moench var. *saccharatum*) was sown on May 18, 2007, May 15, 2008, and May 15, 2009. The hybrid selected for this experiment was sweet sorghum "Madhura" developed in India. The row spacing used was 0.75 m and the distance between plants was 0.15 m. Soil surface was prepared for seeding using a minimum tillage system. The crop was irrigated with a trickle irrigation system. Irrigation started 15 days after sowing (DAS) in 2007, 30 DAS in 2008, and 20 DAS in 2009. The total amount of water applied was 425, 522, and 546 mm in 2007, 2008, and 2009, respectively. Experimental plots were irrigated three times per week between June and September. Application amounts averaged 15, 16, and 17 mm per irrigation event occurred in 2007, 2008, and 2009, respectively. Nitrogen fertilization (NH_4NO_3) was applied in 4 (2007), 6 (2008), and 3 (2009) irrigation events during the vegetative stage (July). The crop was harvested manually at 132 DAS in 2007, 138 DAS in 2008, and 137 DAS in 2009. From harvest to the following growing season, soil was left with no crop and subjected to atmospheric conditions, namely rainfall leaching.

2.3. Experimental design and treatments

The trickle irrigation system was used to mix and deliver synthetic saline irrigation waters, fresh irrigation waters, and fertilizer (NH_4NO_3) to the experimental plots following the irrigation scheme documented in Ramos et al. (2009, 2011, 2012). This system consisted of three trickle laterals connected together in order to form a triple joint lateral placed along each crop line. The first of the laterals was connected to the salt stock solution (NaCl), while the second one was connected to the N reservoir. The third lateral delivered fresh water and was used to obtain a

constant water application rate for each dripping point along the triple joint lateral (24 mm h^{-1}). Gradients of applied salt (Na^+) and nitrogen (N) concentrations were then produced by placing different emitters in each dripping point along the corresponding laterals and varying their discharge rates to obtain various mixtures between the three lines. Table 1 presents the amounts of saline waters, fresh waters, and waters with nitrogen applied in each experimental plot. The blended amounts thus varied between experimental plots, while the total amount of water applied per irrigation event and per crop season, as well as the quality of the irrigation waters before blending (Table 2), remained identical in all experimental plots.

Table 1. Irrigation waters blended in each experimental plot during the three crop seasons of 2007, 2008, 2009

Sub-group		Group I			II			III			IV		
		2007	2008	2009	2007	2008	2009	2007	2008	2009	2007	2008	2009
		——————————————————————— mm ———————————————————————											
A	Saline water	228.0	184.0	316.0	228.0	184.0	316.0	228.0	184.0	316.0	228.0	184.0	316.0
	Water + NH_4NO_3	19.3	30.0	20.0	12.9	20.0	13.3	6.4	10.0	6.7	0.0	0.0	0.0
	Fresh water	177.7	308.0	210.0	184.1	318.0	216.7	190.6	328.0	223.3	197.0	338.0	230.0
B	Saline water	114.0	92.0	158.0	114.0	92.0	158.0	114.0	92.0	158.0	114.0	92.0	158.0
	Water + NH_4NO_3	19.3	30.0	20.0	12.9	20.0	13.3	6.4	10.0	6.7	0.0	0.0	0.0
	Fresh water	291.7	400.0	368.0	298.1	410.0	374.7	304.6	420.0	381.3	311.0	430.0	388.0
C	Saline water	0.0	0.0	0.0	0.0	0.0	0.0	0.0	0.0	0.0	0.0	0.0	0.0
	Water + NH_4NO_3	19.3	30.0	20.0	12.9	20.0	13.3	6.4	10.0	6.7	0.0	0.0	0.0
	Fresh water	405.7	492.0	526.0	412.1	502.0	532.7	418.6	512.0	539.3	425.0	522.0	546.0

Table 2. Characteristics of the irrigation waters blended in each experimental plot

Irrigation water	Year	EC_{iw} [a)]	NH_4^+-N	NO_3-N
		dS m^{-1}	——— $mmol_c$ L^{-1} ———	
Fresh water	2007--2009	0.81	0.03	0.15
Saline water	2007	7.60	0.03	0.15
	2008	9.60	0.03	0.15
	2009	10.60	0.03	0.15
Water with nitrogen	2007	9.50	95.0	95.0
	2008	6.77	67.7	67.7
	2009	7.34	73.4	73.4

[a)]Electrical conductivity of the irrigation water.

The experimental field was thus divided into four groups (I--IV), each with three triple joint laterals, establishing a N gradient decreasing from group I to group IV. Each group was then divided into 3 sub-groups, A, B and C, each with a surface area of 6.75 m^2 (2.25 m × 3 m), and

with the Na^+ gradient decreasing from A to C. The amount of N applied in each group (I--IV) is presented in Table 3. The amount of Na^+ applied in the different sub-groups (A--C) is presented in Table 4. The dripping points were spaced 1 m apart, with a total of 9 dripping points in each of the 12 experimental plots. Two laterals of fresh water bordered the different groups. Each sub-group area was bordered with earthen ridges, which prevented surface runoff from crossing over during rainfall and irrigation.

Table 3. Total amount of nitrogen (N) applied in each group plot during the three irrigation seasons of 2007, 2008, 2009.

Group	2007	2008	2009
	——————————g m^{-2}——————————		
I	51.4	56.8	41.1
II	34.2	37.9	27.4
III	17.2	19.0	13.7
IV	0.0	0.0	0.0

Table 4. Total amount of Na^+ applied in each sub-group during the three irrigation seasons of 2007, 2008, 2009.

Sub-group	2007	2008	2009
	——————————g m^{-2}——————————		
A	1096	1133	2166
B	576	599	1162
C	60	66	158

2.4. Biomass and sugar yield determination

Sugar content was determined at milk stage 95 DAS (in 2007), 112 DAS (in 2008), and 110 DAS (in 2009) when the maximum sugar yield was achieved (Almodares and Hadi, 2009). In each experimental plot, four plants were randomly selected, and harvested manually for biomass and sugar content determination. The stems were cut in 0.3 m long pieces. The total and free reducing sugars (TRS and FRS) were determined on sorghum juice extracted from each piece, after sucrose acid hydrolysis, by the 3,5-dinitrosalicylic acid (DNS) method (Miller, 1959). The sucrose content was calculated by the difference between TRS and FRS multiplied by a conversion factor of 0.95 (ratio between molecular mass of sucrose and the sum of glucose plus fructose produced by the sucrose acid hydrolysis). The sugar yield (g m^{-2}) was defined as the

product of total reducing sugars (g $100g^{-1}$) and stems dry biomass (g m^{-2}) of the four plants harvested in each experimental plot for sugar content estimation.

The dry biomass of sweet sorghum was also determined at harvest when the maximum value was achieved. The fresh sorghum biomass yield was determined by harvesting manually all sorghum plants in each separate line of each experimental plot. Stems and leaves were separated and then oven-dried at 70 ºC to constant weight in order to gravimetrically estimate plant dry biomass. Total dry biomass was determined as the sum of stems and leaves dry biomasses. The dry weights of the four plants that had already been removed during the determination of the sugar yield were not considered in this analysis.

2.5. Relationships between applied factors and yield functions analysis

Sweet sorghum yield functions were determined in terms of biomass (total, stems, and leaves dry biomass), sugar content (reducing and non-reducing), and total sugar yields. Relationship of sweet sorghum yield with applied factors (nitrogen and sodium) during irrigation cycles was evaluated by stepwise multiple regression analysis as follows:

$$y = a_0 + a_1 x_1 + a_2 x_2 + ... + a_n x_n \quad (2)$$

where y is the sorghum yield to be predicted (biomass, sugar content, and sugar yield), a_0, a_1, a_2, …, a_n are the regression coefficients; and x_1, x_2, …, x_n are the applied factors, *i.e.*, nitrogen and sodium. In the process, two dummy variables (Y_1 and Y_2) were introduced as orthogonal polynomial coefficients to take into account the effect of each experimental year on crop yield. These two dummy variables considered the variations in ET_0 and in the total amount of the irrigation water applied (425, 522, and 546 mm in 2007, 2008, and 2009, respectively) along the crop seasons, and the existence of plagues, diseases, weeds, and all other external factors that might have influenced crop production during the three seasons. The orthogonal polynomial coefficients Y_1 assumed the values of -1, 0, and 1, while Y_2 assumed the values of 1, -2, and 1, when describing 2007, 2008, and 2009, respectively.

Means and coefficients of variation were calculated for the replicates from each treatment (three replicates for the biomass yield estimation corresponding to the three sorghum lines harvested in each experimental plot, and nine replicates for sugar yield estimation corresponding to the triplicates determined from the three samples composed of stems top, middle, and bottom

sections from the plants harvested for sugar content estimation). For determining significant effects, mean values were compared using the least significant difference (LSD) test at $P = 0.05$ (Fisher, 1941).

3. Results and discussion

Mean total, stems and leaves dry biomass yield, mean total reducing sugars, sucrose content, and sugar yield of the individual plots and the coefficients of variation of the repetitions are presented in Table 5. Table 6 presents the yield functions obtained by stepwise multiple regression analysis for total dry biomass (Y_{total}), stems dry biomass (Y_{stems}), leaves dry biomass (Y_{leaves}), total reducing sugars content (Y_{TRS}), sucrose content ($Y_{sucrose}$) and sugar yield (Y_{sugar}).

Table 5. Mean values of dry biomass (total, stems and leaves), total reducing sugars (TRS) content, sucrose content and sugar yield in sweet sorghum determined during the three seasons.

Group	Sub-group	Dry biomass			TRS	Sucrose	Sugar yield
		Total	Leaves	Stems			
		——————g m^{-2}——————			————g $100g^{-1}$————		g m^{-2}
I	A	1697.2bc[a)]	643.5abc	1053.7cde	27.38a	17.54bc	228.05bc
		(0.22)[b)]	(0.24)	(0.34)	(0.09)	(0.20)	(0.20)
	B	2102.5ab	738.8ab	1363.7abc	26.51a	17.70bc	288.65ab
		(0.12)	(0.31)	(0.14)	(0.13)	(0.29)	(0.18)
	C	2151.3ab	810.8ab	1340.5abc	25.61a	16.04c	293.18ab
		(0.12)	(0.20)	(0.18)	(0.18)	(0.28)	(0.29)
II	A	1782.4bc	670.1abc	1112.3f	27.10a	19.70abc	242.36bc
		(0.20)	(0.34)	(0.17)	(0.13)	(0.19)	(0.16)
	B	2159.8ab	704.2abc	1455.6ab	26.28a	16.58c	287.02ab
		(0.15)	(0.31)	(0.11)	(0.23)	(0.39)	(0.27)
	C	2399.3a	836.1a	1563.1a	29.35a	20.54abc	340.44a
		(0.13)	(0.29)	(0.12)	(0.09)	(0.16)	(0.18)
III	A	1572.8cd	575.9bc	996.9cdc	27.62a	19.38abc	213.60bc
		(0.09)	(0.23)	(0.14)	(0.11)	(0.20)	(0.15)
	B	1585.6cd	476.8cd	1108.8bcd	28.76a	19.92abc	248.58abc
		(0.10)	(0.31)	(0.11)	(0.06)	(0.10)	(0.15)
	C	1949.4abc	602.6abc	1346.7abc	29.13a	20.08abc	299.62ab
		(0.16)	(0.26)	(0.22)	(0.16)	(0.24)	(0.28)
IV	A	1035.3e	329.1d	706.2e	31.74a	24.06a	166.91c
		(0.17)	(0.30)	(0.24)	(0.09)	(0.14)	(0.17)
	B	1136.1de	320.6d	815.5de	31.18a	22.57ab	180.69c
		(0.29)	(0.54)	(0.22)	(0.05)	(0.09)	(0.15)
	C	1146.2de	302.4d	843.7de	28.61a	19.30abc	166.90c
		(0.16)	(0.31)	(0.18)	(0.14)	(0.22)	(0.19)
LSD (0.05)		470.0	237.8	373.9	6.14	5.75	93.35

[a)]Values within a column followed by the same letter(s) are not significantly different at $P < 0.05$ among sub-groups.
[b)]The values in brackets are the coefficients of variation obtained from the repetitions in each experimental plot.

Table 6. Yield functions and statistical indicators obtained for total dry biomass (Y_{total}), stems dry biomass (Y_{stems}), leaves dry biomass (Y_{leaves}), total reducing sugars content (Y_{TRS}), sucrose content ($Y_{sucrose}$) and sugar yield (Y_{sugar}).

Item[a)]	Y_{total}		Y_{stems}		Y_{leaves}		Y_{TRS}		$Y_{sucrose}$		Y_{sugar}	
	g m^{-2}											
Independent variable												
Constant	1213.33	***	844.47	***	332.00	***	30.22	***	18.94	***	189.48	***
	-	ns[b)]	-	ns	-	ns	1.96	***	-	ns	34.64	**
Y_2	-86.95	**	-53.84	*	-	ns	-7.40×10^{-1}	**	-1.34	***	-	ns
N	53.84	***	32.86	***	21.50	***	-7.83×10^{-2}	***	-	ns	6.65	***
Na^+	-1.66×10^{-1}	*	-	ns	-1.72×10^{-1}	**	-	ns	3.14×10^{-3}	***	-	***
N^2	-6.27×10^{-1}	***	-3.84×10^{-1}	***	-1.95×10^{-1}	***	-	ns	-	ns	-7.65×10^{-2}	*
$(Na^+)^2$	-	ns	-5.24×10^{-5}	*	1.26×10^{-4}	***	-	ns	-	ns	-1.40×10^{-5}	ns
N Na^+	-5.27×10^{-3}	*	-4.48×10^{-3}	*	-3.72×10^{-3}	***	-	ns	-9.66×10^{-5}	***	-9.53×10^{-4}	*
Y_1 N	-	ns	3.57	**	-	**	-	ns	8.28×10^{-2}	***	1.22	**
Y_1 Na^+	-	ns	-	ns	-7.38×10^{-2}	**	-	ns	-	ns	-	ns
Y_2 N	-	ns	-	ns	9.30×10^{-1}	ns	-	ns	-	ns	-	ns
Y_2 Na^+	8.12×10^{-2}	*	-	ns	-	ns	-	ns	-	ns	-	ns
Statistical analysis												
n	36		36		36		36		36		36	
SSR	6.68×10^{6}		2.74×10^{6}		1.33×10^{6}		215.77		393.8		1.59×10^{5}	
SSE	7.19×10^{5}		4.84×10^{5}		1.19×10^{5}		148.81		145.7		3.11×10^{4}	
R^2	0.903		0.850		0.917		0.592		0.730		0.836	
F-ratio	44.91		27.35		44.44		15.47		20.94		24.73	

*, **, ***Significant at $P \leq 0.05$, $P \leq 0.01$, and $P \leq 0.001$, respectively.

[a)] Y_1 and Y_2 = orthogonal polynomial coefficients; N = nitrogen; Na^+ = sodium; N^2 = square of the nitrogen application; $(Na^+)^2$ = square of sodium application; N Na^+, Y_1 N, Y_1 Na^+, Y_2 N, and Y_2 Na^+ = product of one input factor (ex: nitrogen) by the other (ex: sodium); *n* = observations fitted; SSR = sum of squares due to regression; SSE = sum of squares due to error; R^2 = coefficient of determination.

[b)] Not significant.

3.1. Analysis of total dry biomass response curves

The models obtained for total (Y_{total}), stems (Y_{stems}), and leaves dry biomass (Y_{leaves}) explained 85.0% to 90.3% of the observed variations, with a total of 36 observations analysed (Table 6). Dry biomass responded significantly to the application of N and Na^+. Also, a significant interaction was found between these two input factors which affected yield response negatively. The response to one of the input factors was thus inversely dependent on the other factor. This inverse relation has been reported, for example, for maize (Pang and Letey, 1998; Shenker et al., 2003) since the use of saline waters, without proper irrigation management, may lead to the accumulation of salts in the root zone which will increase the osmotic stress and reduce plant transpiration, N uptake, and eventually crop yield. In this experiment, sweet sorghum potential transpiration (T_p) varied between 360 and 457 mm in the different experimental plots and along the years. T_p values obtained in plots irrigated with saline waters (sub-group A) were generally lower than those obtained in plots irrigated with fresh waters (sub-group C) despite sweet sorghum, depending on the variety, is a moderately to highly tolerant crop to salinity (Maas, 1990). Nutrient uptake was also reduced due to the use of saline waters and the salinity build up in the soil profile as shown in Ramos et al. (2012). These authors quantified nitrogen uptake reductions of 18 kg ha^{-1} between plots in sub-groups A and C using a state-of-the-art transient water dynamics and solute transport model.

Fig. 1 shows the response curves of total, stems, and leaves dry biomass yield to different levels of N and Na^+. Response curves are presented for the mean annual yield. Regression analysis showed that total dry biomass response curves to N were quadratic with diminishing response for each incremental change of N. Each additional unit of N added less to the total output than the previous unit did. The partial derivates of the multiple regression equations obtained for Y_{total}, Y_{stems}, and Y_{leaves} (Table 6) with respect to N show the decrease in yield per unit increase in N levels. Increasing N application indefinitely would not result in a direct increase of dry biomass. Also, as a result of the interaction found between N and Na^+, the optimum level of applied N decreased for each unit increase in Na^+ levels. The higher the amount of Na^+ applied the lower the level of N necessary to achieve maximum yield. For example, by equating the partial derivate to zero and solving for N, the maximum total dry biomass was determined to be obtained for 42.7, 39.8, 36.8, and 33.9 g m^{-2} of N when considering increasing levels of 60, 760, 1460, and 2160 g m^{-2} of Na^+, respectively. The optimum levels of N obtained here were comparable with

those obtained for maize grown in the same soil (Ramos et al., 2009), even though sweet sorghum is considered to be more environmentally friendly than maize because of its relatively low N needs (Barbanti et al., 2006; Almodares and Hadi, 2009). A similar decrease in N needs with increasing Na^+ levels was found while analyzing stems and leaves dry biomass separately.

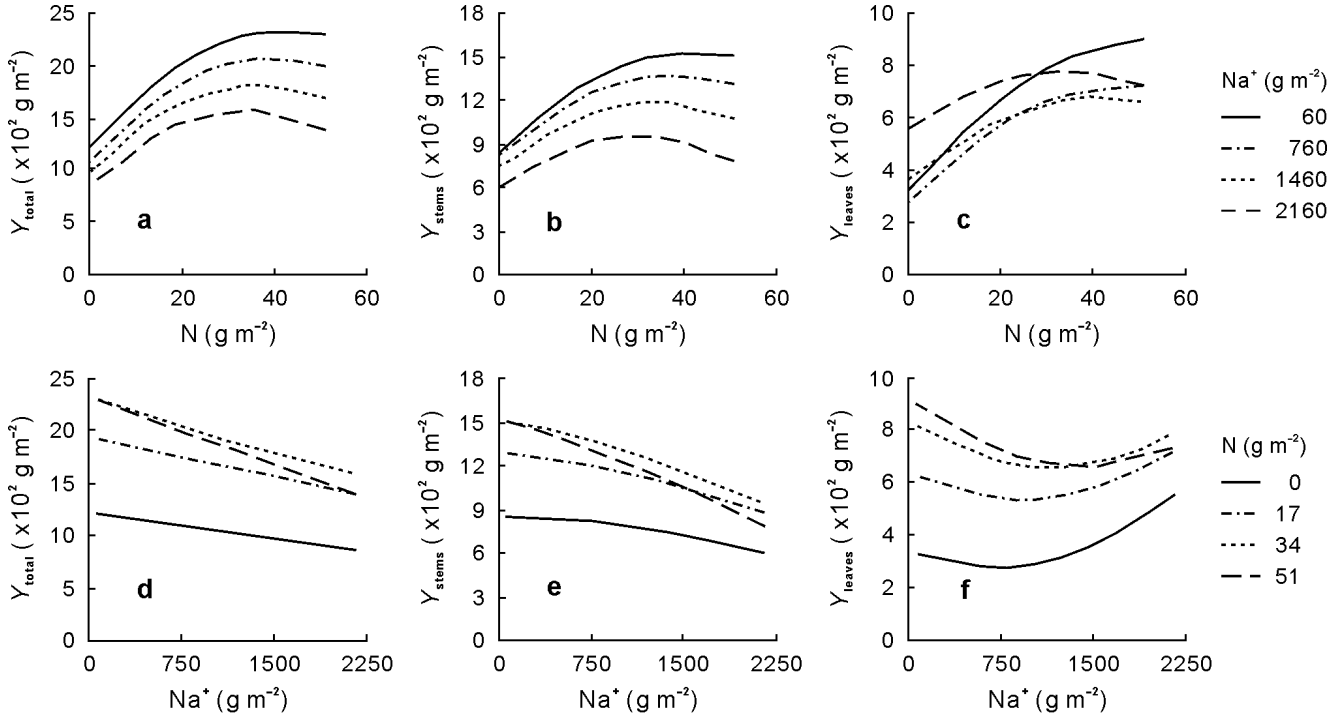

Fig. 1. Sweet sorghum total (Y_{total}; a, d), stems (Y_{stems}; b, e) and leaves (Y_{leaves}; c, f) dry biomass curves with decreasing returns to nitrogen (top), and to sodium (bottom). Response to the mean annual yield measured while maintaining all other input factors constant.

If the experimental years are analysed individually, it is possible to observe that the optimum level of applied N for stems dry biomass, despite decreasing with increasing Na^+ levels as shown above, increased through the years (Y_1). Taking the level of 760 g m^{-2} of Na^+ as an example, maximum yield was achieved at optimum levels of 36.7, 38.3, and 42.9 g m^{-2} of N during the years of 2007, 2008, and 2009, respectively. This could most likely be explained with the total amount of irrigation water applied in each crop season. Higher amounts of water applied to the crop during 2008 (522 mm), and even higher in 2009 (546 mm), promoted salt leaching from the root zone, thus reducing the osmotic stress, increasing plant transpiration and allowing higher N

uptake. The use of additional irrigation water to account for a leaching fraction and to counteract soil salinization/sodification is, in fact, one of the most common techniques presented in literature (US Salinity Laboratory Staff, 1954; Pang and Letey, 1998). Leaves dry biomass response to N application also varied along the years (Y_2).

Total dry biomass response to Na^+ was linear while stems and leaves dry biomass responses to Na^+ were quadratic (Fig. 1). The partial derivates of the multiple regression equations obtained for Y_{total}, Y_{stems}, and Y_{leaves} (Table 6) with respect to Na^+ showed the decrease in yield per unit increase in Na^+ levels. Higher levels of Na^+ applied to the soil with the irrigation water led to total and stems dry biomass reduction. Identical results were reported in a vast number of experiments conducted for sweet sorghum under field or laboratory conditions (Netondo et al., 2004; Begdullayeva et al., 2007; Hassanein et al., 2010; Vasilakoglou et al., 2011). These authors found that dry biomass reductions with increasing soil salinity conditions may be attributed to reductions in the plant physiological parameters usually related to photosynthesis, namely reductions in the chlorophyll content, chlorophyll fluorescence and photosystem II quantum yield, and stomatal conductance. In Alvalade, as a result of the interaction obtained between N and Na^+, the decrease in yield per unit increase in Na^+ levels showed to be greater at higher levels of N. For the mean annual yield, sweet sorghum total dry biomass (Y_{total}) decreased by -0.17, -0.26, -0.35 and -0.43 g m^{-2} per unit increase of Na^+ applied to the soil, when the levels of N applied were considered to be 0, 17, 34, and 51 g m^{-2}, respectively. If the experimental years were analysed individually, similar tendencies were observed.

For stems dry biomass the rate of yield decrease per unit increase of Na^+ was only dependent of the N level applied (no interaction was found). Stems dry biomass response to Na^+ was more negative with higher N levels. Considering the level of 17 g m^{-2} of N as a first example, stems dry biomass decreased by 7%, 17%, and 32% when the levels of Na^+ applied were 760, 1 460, and 2 160 g m^{-2}, respectively. Considering now the level of 34 g m^{-2} of N, yield losses reached 10%, 22%, and 38% for the same levels of Na^+ applied.

Leaves dry biomass response to Na^+ was also dependent on the level of N applied to the crop. Leaves dry biomass decreased to each incremental change of Na^+, but only when considering the lower levels of this input factor. Higher levels of Na^+ apparently promoted leaves development. For the mean annual yield, the minimum of the quadratic function was found at Na^+ levels of

682, 933, 1 185, and 1 436 g m^{-2}, when assuming N levels of 0, 17, 34 and 51 g m^{-2}, respectively. Above those levels, leaves dry biomass increased at increasing levels of Na^+ due to the quadratic nature of the response curve to Na^+. However, as shown in Table V the effect of Na^+ was negative for both stems and leaves dry biomass. Therefore, the effect of Na^+ application was apparently more pronounced for stems dry biomass than for leaves.

3.2. Analysis of sugar yield response curves

The models obtained for TRS content (Y_{TRS}), sucrose content ($Y_{sucrose}$), and sugar yield (Y_{sugar}) explained 59.2% to 83.6% of the observed variations (Table 6). TRS content responded significantly to the application of N, but not to Na^+. Sucrose responded significantly to N and also to Na^+. However, N only affected significantly sucrose content while interacting with Na^+ and Y_1. Sugar yield response to the input factors was mostly in agreement with stems dry biomass responses since it was determined in part from this yield component. Sugar yield responded significantly to the application of N and Na^+. These two input factors also interacted negatively to affect sugar yield, in accordance with what was already described for stems dry biomass. The effect of N varied also in the response to each individual year and in the variability of mean annual yield. Fig. 2 shows the response curves of TRS content, sucrose content, and sugar yield to different levels of N and Na^+. Response curves are presented for the mean annual yield.

Regression analysis results showed that TRS response curves to N was linear. TRS content decreased at a constant rate of -0.0783 g $100g^{-1}$ per unit increase of N. A similar trend was reported by Wiedenfeld (1984) where stems carbohydrates content were reduced with increasing N application and uptake, despite increasing biomass yield. However, Smith and Buxton (1993) found little discernible effect on increasing fermentable sugar production with increasing N fertilization.

Sucrose content responded linearly to the application of N and Na^+. The partial derivate of the stepwise multiple regression equation obtained for $Y_{sucrose}$ with respect to N showed that the effect of N on sucrose content depended on the level of Na^+ applied and the year in question. For the mean annual yield, sucrose content decreased at rates of -0.01, -0.07, -0.14, and -0.22 g $100g^{-1}$ per unit increase of N, when considering the levels of 60, 760, 1 460, and 2 160 g m^{-2} of Na^+,

respectively. In 2007, these rates were even higher with sucrose content responding more

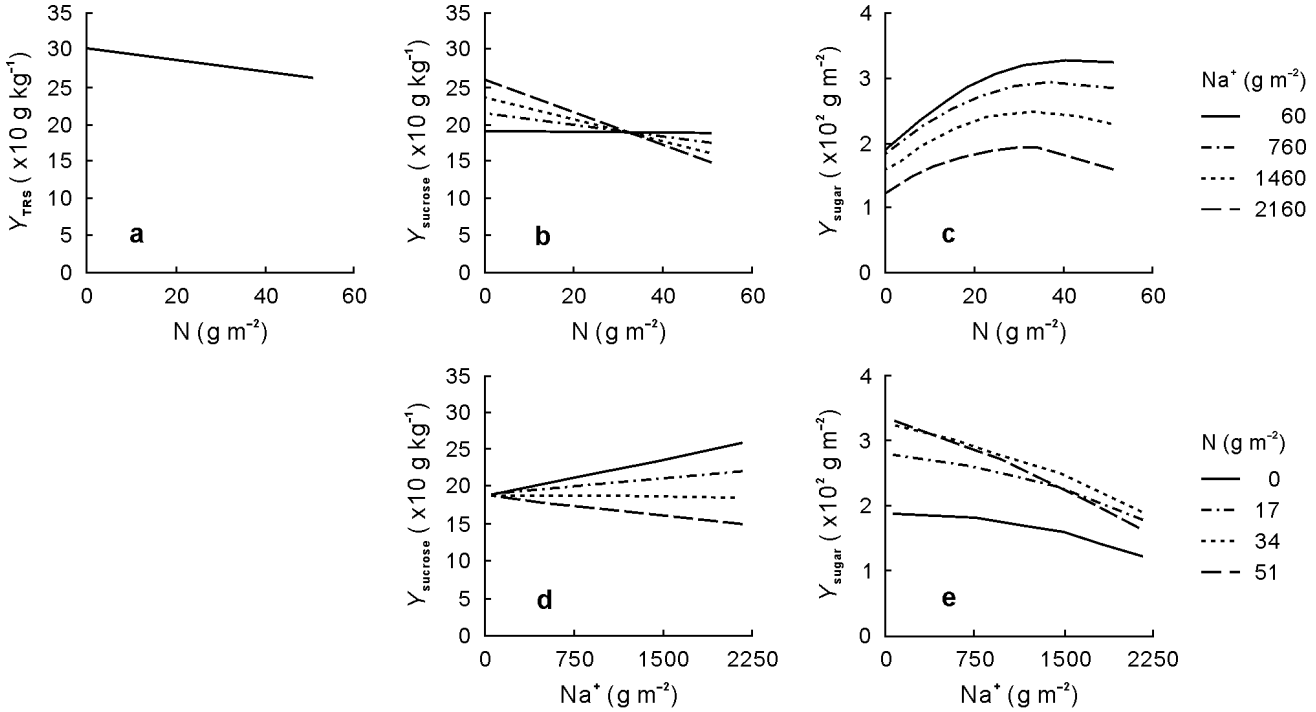

Fig. 2. Total reducing sugars content (Y_{TRS}; a), sucrose content ($Y_{sucrose}$; b, d), and sugar yield (Y_{sugar}; c, e) curves with decreasing returns to nitrogen (top), and to sodium (bottom). Response to the mean annual yield measured while maintaining all other input factors constant.

negatively to each incremental change of N. However, in 2009, some mixed tendencies were observed with sucrose content responding positively to N for levels of Na^+ up to 857 g m^{-2}, and negatively to N for levels of Na^+ above that quantity. This contrasting response is a result of the positive effect of Na^+ on sucrose content, as shown by the partial derivate of the same multiple regression equation with respect to Na^+. Sucrose content responded positively to Na^+ application but only for small levels of N, *i.e.*, for levels of N up to 32.5 g m^{-2}. For larger applications sucrose content response to each incremental change of Na^+ became negative. Thus, for levels of 0 and 17 g m^{-2} of N, the rate of sucrose increase per unit increase in Na^+ level was +0.0031 and +0.0015 g $100g^{-1}$, respectively. For levels of 34 and 51 g m^{-2} of N, sucrose content decreased at rates -0.0001 and -0.0018 g $100g^{-1}$ per unit increase of the Na^+ level, respectively. This means that, in Alvalade sorghum plants affected by salinity and nitrogen stresses, *i.e.*, plants harvested

from plots in groups III and IV, ended up having higher sucrose contents. Not many studies exist where the quality of sugar content has been related to soil salinity and to N fertilization. Therefore, comparing the results obtained here with others is not straightforward. Nevertheless, Almodares et al. (2007) found no effect of N fertilization on sucrose content. Also, Almodares et al. (2008a; 2008b) found different responses for sucrose content in saline environments. As salinity increased, the sucrose content decreased in some varieties while for others sucrose content increased.

Sugar yield response curves to N and Na^+ were quadratic. The partial derivate of the multiple regression obtained for Y_{sugar} with respect to N yielded the same decrease in yield per unit increase in N levels reported in the dry biomass analysis. Increasing N application indefinitely would once more not result in a direct increase in sugar yield. The optimum level of applied N also decreased per unit increase of applied Na^+. For the mean annual yield, the maximum sugar yield was determined to be obtained for decreasing amounts of 43.1, 38.8, 34.4, and 30.0 g m^{-2} of N when considering increasing levels of 60, 760, 1 460, and 2 160 g m^{-2} of Na^+, respectively. The N needs were once more dependent on the year in question. Like for stems dry biomass and sucrose content, sugar yield and N needs progressively increased throughout the years. This is again likely explained by the increasing amounts of irrigation water applied per year and the increase of the leaching fraction available to remove Na^+ from the root zone, reducing the salinity stress and increasing plant transpiration.

The partial derivate of Y_{sugar} with respect to Na^+ showed that, for the same N level, the higher the amount of Na^+ applied, the greater would be the decrease in sugar yield. Taking the level of 60 g m^{-2} of N as a first example, sugar yield decreased by 4%, 16%, and 34% when the levels of Na^+ applied were 760, 1 460, and 2 160 g m^{-2}, respectively. If the level of 51 g m^{-2} of N is now considered, sugar yield losses would reach 13%, 30%, and 51% when applying the same levels of Na^+ as mentioned above. These results are in accordance with Almodares et al. (2008a; 2008b). These authors reported while studying five sweet sorghum varieties that as salinity increased from 2 to 12 dS m^{-1}, total soluble carbohydrates decreased by 21%. Vasilakoglou et al. (2011) also reported that higher levels of soil salinity (6.9 dS m^{-1}) led to biomass reductions, which led to juice and total sugar yield reductions. They attributed these reductions to changes in sweet sorghum physiological parameters.

4. Conclusions

Sweet sorghum dry biomass yield showed to be dependent of the amount of N and Na^+ applied to each experimental plot. Sorghum dry biomass presented diminishing returns for each incremental change of N. Therefore, increasing N application above the optimum level did not result in an increase in total, stems or leaves dry biomass.

The use of saline irrigation waters also led to yield reduction. The higher the amount of Na^+ applied to the soil with the irrigation water the lower the level of N necessary to achieve maximum yield. This effect was explained by an accumulation of salts in the root zone, which increased the osmotic stress and reduced plant transpiration, N uptake, and crop yield.

As for sugar content, total reducing sugars content and sucrose content were dependent on the amount of N applied to the crop. N had a negative effect on sugar content though. Sucrose content was also dependent on the amount of Na^+ applied, but in this case the salinity stress ended up promoting sucrose content.

Sugar yield embodied some of the trends observed mostly in sorghum dry biomass. Sugar yield presented similar diminishing returns for each incremental change of N. Higher levels of Na^+ applied to the soil also led to sugar yield reductions and minor N needs to achieve maximum sugar yield.

Stems dry biomass, sucrose content, and sugar yield progressively increased along the years of the experiment. This complementary effect between yield and years was attributed to the increasing amounts of irrigation applied throughout the years, and the increase of the leaching fraction which promoted salt leaching from the root zone, thus reducing the salinity stress and increasing plant transpiration, nitrogen uptake and sorghum yield.

Acknowledgments

Supported by the Portuguese Foundation for Science and Technology (FCT), Project PTDC/AGR-AAM/66004/2006. T. B. Ramos and N. L. Castanheira acknowledge funding by FCT (contracts SFRH/BD/60363/2009 and SFRH/BD/69185/2010, respectively).

References

Allen, R.G., Pereira, L.S., Raes, D., Smith, M., 1998. Crop Evapotranspiration---Guidelines for Computing Crop Water Requirements. FAO Irrig. Drain. Paper. n^{o} 56. FAO, Rome.

Allen, R.G., Pereira, L.S., Smith, M., Raes, D., Wright, J.L., 2005. FAO-56 dual crop coefficient method for estimating evaporation from soil and application extensions. J. Irrig. Drain. Eng. 131, 2-13.

Almodares, A., Hadi, M.R., 2009. Production of bioethanol from sweet sorghum: A review. Afr. J. Agr. Res. 4, 772-780.

Almodares, A., Hadi, M.R., Ahmadpour, H., 2008a. Sorghum stem yield and soluble carbohydrates under different salinity levels. Afr. J. Biotechnol. 7, 4051-4055.

Almodares, A., Hadi, M.R., Dosti, B., 2008b. The effects of salt stress on growth parameters and carbohydrates contents in sweet sorghum. Afr. J. Agr. Res. 2, 298-304.

Almodares, A., Hadi, M.R., Ranjbar, M., Taheri, R., 2007. The effects of nitrogen treatments, cultivars and harvest stages on stalk yield and sugar content in sweet sorghum. Asian. J. Plant Sci. 6, 423-426.

Barbanti, L., Grandi, S., Vecchi, A., Venturi, G., 2006. Sweet and fibre sorghum (Sorghum bicolor (L.) Moench), energy crops in the frame of environmental protection from excessive nitrogen loads. Eur. J. Agron. 25, 30-39.

Begdullayeva, T., Kienzler, K.M., Kan, E., Ibragimov, N., Lamers, J.P.A., 2007. Response of Sorghum bicolor varieties to soil salinity for feed and food production in Karakalpakstan, Uzbekistan. Irrig. Drain Syst. 21, 237-250.

Datta, K.K., Sharma, V.P., Sharma, D.P., 1998. Estimation of a production function for wheat under saline conditions. Agric. Water Manage. 36, 85-94.

Dinar, A., Rhoades, J.D., Nash, P., Waggoner, B.L., 1991. Production functions relating crop yield, water quality and quantity, soil salinity and drainage volume. Agric. Water Manage. 19, 51-66.

Fisher, R.A., 1941. Statistical Methods for Research Workers. 8th Edition. Oliver and Boyd, Edinburgh.

Hassanein, M.S., Ahmed, A.G., Zaki N.M., 2010. Growth and productivity of some sorghum cultivars under saline soil conditions. J. Appl Sci. Res. 6, 1603-1611.

Igbadun, H.E., Tarimo, A.K.P.R., Salim, B.A., Mahoo, H.F., 2007. Evaluation of selected crop water production functions for an irrigated maize crop. Agric. Water Manage. 94, 1-10.

Lourenço, M.E.V., Massa, V.M.L., Palma, P.M.M., Rato, A.E.M., 2007. The potential of sweet sorghum [Sorghum bicolor (L.) Moench] for sustainable bioethanol production in Alentejo (in Portuguese). Rev. Ciências Agrárias 30, 103-110.

Mandal, K.G., Hati, K.M., Misra, A.K., Bandyopadhyay, K.K., 2010. Root biomass, crop response and water-yield relationship of mustard (Brassica juncea L.) grown under combinations of irrigation and nutrient application. Irrig. Sci. 28, 271-280.

Maas, E.V., 1990. Crop salt tolerance. In: Tanji, K.K. (ed.) Agricultural Salinity Assessment and Management Manual, pp. 262—304. American Society of Civil Engineers, Reston.

Mastrorilli, M., Katerji, N., Rana, G., 1999. Productivity and water use efficiency of sweet sorghum as affected by soil water deficit occurring at different vegetative growth stages. Eur. J. Agron. 11, 207-215.

Mastrorilli, M., Katerji, N., Rana, G., Steduto, P., 1995. Sweet sorghum in Mediterranean climate: radiation use and biomass water use efficiencies. Ind. Crop. Prod. 3, 253-260.

Miller, G.L., 1959. Use of dinitrosalicyclic acid reagent for determination of reducing sugar. Anal. Chem. 31, 426-428.

Netondo, G.W., Onyango, J.C., Beck, E., 2004. Sorghum and salinity: I. Response of growth, water relations, and ion accumulation to NaCl salinity. Crop Sci. 44, 797-805.

Pang, X.P., Letey, J., 1998. Development and evaluation of ENVIRO-GRO, an integrated water, salinity, and nitrogen model. Soil Sci. Soc. Am. J. 62, 1418-1427.

Pereira, L.S., Cordey, I., Iacovides, I., 2009. Coping with Water Scarcity: Addressing the Challenges. Springer, Dordrecht, The Netherlands.

Qadir, M., Oster, J.D., 2004. Crop and irrigation management strategies for saline-sodic soils and waters aimed at environmentally sustainable agriculture. Sci. Total Environ. 323, 1-19.

Ramos, T.B., Gonçalves, M.C., Castanheira, N.L., Martins, J.C., Santos, F.L., Prazeres, A., Fernandes, M.L., 2009. Effect of sodium and nitrogen on yield function of irrigated maize in southern Portugal. Agric. Water Manage. 96, 585-594.

Ramos, T.B., Šimůnek, J., Gonçalves, M.C., Martins, J.C., Prazeres, A., Castanheira, N.L., Pereira, L.S., 2011. Field evaluation of a multicomponent solute transport model in soils irrigated with saline waters. J. Hydrol. 407, 129-144.

Ramos, T.B., Šimůnek, J., Gonçalves, M.C., Martins, J.C., Prazeres, A., Pereira, L. S., 2012. Two-dimensional modeling of water and nitrogen fate from sweet sorghum irrigated with fresh and blended saline waters. Agric. Water Manage. 111, 87-104.

Rhoades, J.D., Kandiah, A., Mashali, A.M., 1992. The Use of Saline Waters for Crop Production. FAO Irrig. Drain. Paper. N^{O} 48. FAO, Rome.

Shenker, M., Ben-Gal, A., Shani, U., 2003. Sweet corn response to combined nitrogen and salinity environmental stresses. Plant Soil. 256, 139-147.

Smith, G.A., Buxton, D.R. 1993. Temperate zone sweet sorghum ethanol production potential. Bioresource. Technol. 43, 71-75.

Steduto, P., Katerji, N., Puertos-Molina, H., Unlü, M., Mastrorilli, M., Rana, G., 1997. Water-use efficiency of sweet sorghum under water stress conditions. gas-exchange investigations at leaf and canopy scales. Field Crops Res. 54, 221-234.

US Salinity Laboratory Staff., 1954. Diagnosis and Improvement of Saline and Alcaly Soils. USDA Handbook 60. Washington, USA.

Vasilakoglou, I., Dhima, K., Karagiannidis, N., Gatsis, T., 2011. Sweet sorghum productivity for biofuels under increased soil salinity and reduced irrigation. Field Crops Res. 120, 38-46.

Wiedenfeld, R.P., 1984. Nutrient requirements and use efficiency by sweet sorghum. Energ Agr. 3, 49-59.

Zhao, Y.L., Dolat, A., Steinberger, Y., Wang, X., Osman, A., Xie, G.H., 2009. Biomass yield and changes in chemical composition of sweet sorghum cultivars grown for biofuel. Field Crops Res. 111, 55-64.

Chapter 5

Propriedades hidráulicas do solo para as diferentes classes texturais

(Based on the paper published in: Revista de Ciências Agrárias 34(2), 252-264. 2011)

Propriedades hidráulicas do solo para as diferentes classes texturais

Soil hydraulic properties in different soil texture classes

T. B. Ramos[1], M. C. Gonçalves[1,2], J. C. Martins[2], F. P. Pires[2] and L. S. Pereira[1]

[1] CEER-Biosystems Engineering, Institute of Agronomy, Technical University of Lisbon, Tapada da Ajuda, 1349-017 Lisbon, Portugal

[3] Estação Agronómica Nacional, Unidade de Ambiente e Recursos Naturais, L-INIA, Instituto Nacional de Recursos Biológicos, Quinta do Marquês, 2784-505 Oeiras.

Resumo

As propriedades hidráulicas apresentam uma grande variabilidade espacial devido à heterogeneidade do solo, sendo a textura um dos factores determinantes dessa heterogeneidade. Neste trabalho estudou-se a variabilidade da curva de retenção de água, $\theta(h)$, e da curva da condutividade hidráulica, $K(h)$, determinadas em solos de texturas diferentes e correspondentes a 11 das 12 classes texturais do diagrama triangular de Gomes & Silva (1962). Com base em 558 curvas $\theta(h)$ e em 245 curvas $K(h)$, obtidas a partir de amostras não perturbadas e incluídas na base de dados PROPSOLO da Estação Agronómica Nacional, indicam-se, para cada classe, os valores médios, o desvio padrão, os valores máximos e mínimos de cada parâmetro do modelo de Mualem-van Genuchten. Indica-se ainda uma função $\theta(h)$ e $K(h)$ média para cada classe textural.

Palavras chave: condutividade hidráulica; PROPSOLO; retenção de água no solo.

Abstract

Soil texture influences significantly soil hydraulic properties, which due to soil heterogeneity normally present large spatial variability. The variability of soil retention $\theta(h)$, and hydraulic

conductivity $K(h)$ curves, in 11 of the 12 texture classes of the diagram of Gomes & Silva (1962) was studied. For each textural class, average, maximum, minimum, and the standard deviation values for the Mualem van Genuchten parameters are presented based on 558 $\theta(h)$ and 245 $K(h)$ curves determined in undisturbed soil samples which are included in the PROPSOLO database of Estação Agronómica Nacional. An average function describing $\theta(h)$ and $K(h)$ in each textural class is also presented.

Keywords: hydraulic conductivity; PROPSOLO; soil water retention.

1. Introdução

As propriedades hidráulicas do solo, nomeadamente as curvas de retenção da água no solo e da condutividade hidráulica, constituem a base de muitos estudos agronómicos e ambientais. A curva de retenção de água no solo, $\theta(h)$, relaciona teor de água volúmico da fase líquida do solo (θ) com o potencial matricial ou pressão efectiva da água no solo (h). A condutividade hidráulica, $K(h)$, é o factor de proporcionalidade entre o fluxo e o gradiente da carga hidráulica na equação de Darcy. As propriedades hidráulicas do solo são geralmente descritas através de modelos paramétricos, cujos parâmetros constituem os dados de entrada da maior parte dos modelos de simulação do movimento de água e de transporte de solutos na região vadosa do solo. De entre os vários modelos paramétricos existentes, o mais utilizado é o modelo de Mualem-van Genuchten (van Genuchten, 1980), que relaciona θ e h, através de:

$$S_e(h) = \frac{\theta(h) - \theta_r}{\theta_s - \theta_r} = \frac{1}{\left(1 + |\alpha h|^{\eta}\right)^m} \tag{1}$$

e a condutividade hidráulica, K, e h, através de:

$$K(h) = K_s S_e^{\ell} \left[1 - \left(1 - S_e^{1/m}\right)^m\right]^2 \tag{2}$$

em que S_e é o teor de água efectivo [L^3L^{-3}], θ_r e θ_s correspondem aos teores de água residual e na saturação [L^3L^{-3}], respectivamente, K_s é a condutividade hidráulica saturada [LT^{-1}], α [L^{-1}] e η [-]

são parâmetros de ajustamento empíricos, $m = 1 - 1/n$, e ℓ é um parâmetro que descreve a conectividade/tortuosidade dos poros [-].

Embora de uso relativamente simples, muitos dos métodos laboratoriais e de campo utilizados para determinação das propriedades hidráulicas (Dane & Topp, 2002) são morosos, dispendiosos, bastante trabalhosos e limitados ao tamanho das amostras colhidas para o efeito, restringindo a sua utilização devido à heterogeneidade do meio. De facto, estas propriedades são afectadas pela textura e estrutura do solo, teor de matéria orgânica, fenómenos de expansão de argilas, dispersão de partículas, formação de crosta, concentração e composição iónica da solução de solo e ainda pelas práticas culturais, originando grande variabilidade espacial.

Para melhor compreender essa variabilidade espacial têm sido criadas internacionalmente, bases de dados que procuram reunir os estudos existentes, relacionando as propriedades hidráulicas dos solos com outras características do solo, nomeadamente, as suas propriedades básicas. Os exemplos mais relevantes são a HYPRES (*HYdraulic PRoperties of European Soils*) (Wösten et al., 1999), que reúne a informação existente na Europa, e a UNSODA (*UNsaturated SOil hydraulic DAtabase*) (Nemes et al., 2001), que reúne a informação existente produzida a nível mundial.

A partir da informação existente na base de dados UNSODA, Carsel & Parish (1988) e Schaap et al. (1998) publicaram os parâmetros médios do modelo de Mualem-van Genuchten para cada classe textural, segundo a classificação USDA. Para os limites da escala de Atterberg, recomendada pela Sociedade Internacional de Ciência do Solo e seguida pela Sociedade Portuguesa da Ciência do Solo, essa informação não existe.

Este trabalho tem como objectivo estudar a variabilidade das propriedades hidráulicas dos solos portugueses em cada classe textural do diagrama triangular de Gomes & Silva (1962), a partir da informação reunida na base de dados PROPSOLO (Ramos et al., 2007) existente na Estação Agronómica Nacional (EAN).

2. Material e métodos

2.1. Esquema relacional da base de dados PROPSOLO

A base de dados PROPSOLO (PROPriedades do SOLO) foi criada em 1997 com o objectivo de reunir a informação relativa às propriedades físicas, químicas e hidrodinâmicas dos perfis dos solos estudados no Departamento de Ciência do Solo (DCS) da EAN e que anteriormente se encontrava dispersa por diversas teses de doutoramento, trabalhos de fim de curso, artigos científicos e relatórios.

A primeira versão da base de dados PROPSOLO, constituída apenas por uma tabela relacional criada numa folha de cálculo, teve como finalidade desenvolver funções de pedo-transferência para a obtenção dos parâmetros do modelo de van Genuchten (van Genuchten, 1980) e de Gardner (Gardner, 1958) para as curvas $\theta(h)$ e $K(h)$, respectivamente, a partir das propriedades básicas do solo (Gonçalves et al., 1997). Agregava informação relativa a 230 curvas $\theta(h)$ e 120 curvas $K(h)$, incluindo medições do teor de água a 11 pressões efectivas, entre -2.5 e -15848.9 cm de água, medições da condutividade hidráulica saturada e insaturada, granulometria, massa volúmica aparente, pH e matéria orgânica. Os perfis de solo eram classificados de acordo com Cardoso (1974) e segundo a classificação da FAO então em vigor. O primeiro perfil incluído na base de dados datava de 1977. Uma segunda versão da base de dados foi desenvolvida pouco tempo depois, em que apenas se adicionaram os parâmetros de Mualem-van Genuchten (Gonçalves et al., 1999).

A terceira versão (Ramos et al., 2007) teve como principal objectivo a georreferenciação de todos os perfis de solo existentes na base de dados. A informação contida na base de dados foi ainda alargada a outras propriedades físicas e químicas do solo. A PROPSOLO, para além das propriedades presentes na primeira versão, passou também a incluir: a porosidade total; os teores de carbonatos; os teores de azoto total, nítrico e amoniacal; os teores de fósforo e potássio; os teores de Na^+, Ca^{2+}, Mg^{2+}, K^+ extraíveis, solúveis e de troca; a condutividade eléctrica (*CE*); a razão de adsorção de sódio (SAR); a percentagem de sódio de troca (*ESP*); a capacidade de troca catiónica (*CTC*) e os teores de cloretos (Cl^-) no solo. De modo a melhor organizar a informação nela contida, a PROPSOLO foi dividida em 8 tabelas relacionais (DISTRITO, CONCELHO, FREGUESIA, SOLO, HORIZONTE, FISICA, QUIMICA e HIDRODINAMICA). Dado o número significativo de perfis de solo que a base de dados já dispunha, foi também desenvolvido

um *script* em SQL (*Structured Query Language*) de modo a permitir mais facilmente a consulta da informação pretendida através do sistema gestor de base de dados MySQL (versão 5.0). A PROPSOLO passou assim a utilizar um sistema gestor de distribuição gratuita e uma linguagem vulgarmente usada em grande parte das bases de dados (Henley, 2006). Apesar de usar um sistema gestor diferente, a PROPSOLO seguia os modelos das bases de dados internacionais dedicadas ao estudo das propriedades hidráulicas dos solos, nomeadamente a HYPRES (Wösten et al., 1999) que foi desenvolvida no sistema gestor ORACLE, e a UNSODA (Nemes et al., 2001), esta implementada em Microsoft Access. A PROPSOLO tornava-se ainda compatível com um Sistema de Informação Geográfica (SIG), devido à obrigatoriedade dos perfis nela incluídos estarem georreferenciados.

Em 2009 e 2011 procedeu-se a nova reestruturação da informação disponível na base de dados, de modo a incluir, também, as metodologias utilizadas na determinação de cada propriedade do solo e que anteriormente vinham descritas em Ramos *et al.* (2007). Na prática, esta reestruturação do esquema relacional implicou a possibilidade de a PROPSOLO poder acolher, também, a informação de perfis dos solos estudados noutros laboratórios e onde as metodologias utilizadas poderão diferir das utilizadas regularmente no DCS. Foi ainda incluída a informação existente sobre os parâmetros de transporte de solutos no solo com a introdução da tabela SOLUTOS e todas as determinações laboratoriais (não tratadas) relativas às curvas $\theta(h)$, $K(h)$ e curvas de breakthrough (tabelas THETA_RAW, KUNSAT_RAW e SOLUTOS_RAW). O novo esquema relacional da base de dados PROPSOLO é apresentado na Figura 1.

O corpo principal da base de dados é composto pelas tabelas SOLO e HORIZONTE. A tabela SOLO contém as referências de cada perfil de solo estudado, nomeadamente, a sua identificação, localização geográfica, data de amostragem, classificação do solo, referência bibliográfica onde os dados foram publicados e identificação do laboratório responsável por esses dados. A tabela HORIZONTE contém os limites, profundidade média e espessura de cada camada/horizonte. As duas tabelas estão interligadas entre si por uma multiplicidade de 1:n, ou seja, um perfil de solo pode conter um ou mais horizontes, mas um determinado horizonte faz apenas parte de um perfil de solo. A tabela HORIZONTE tem por isso, como chave estrangeira, a chave primária da tabela SOLO.

A tabela HORIZONTE está por sua vez associada às tabelas FISICA, QUIMICA e HIDRODINAMICA que agrupam as propriedades físicas, químicas do solo e os parâmetros hidráulicos do modelo de Mualem-van Genuchten de cada horizonte/camada, respectivamente. A tabela FISICA contém, assim, a granulometria, massa volúmica aparente, porosidade total, teores de água a diversas sucções e a condutividade hidráulica saturada de cada horizonte/camada. A tabela QUIMICA agrupa por sua vez os teores de carbonatos; os teores de azoto total, nítrico e

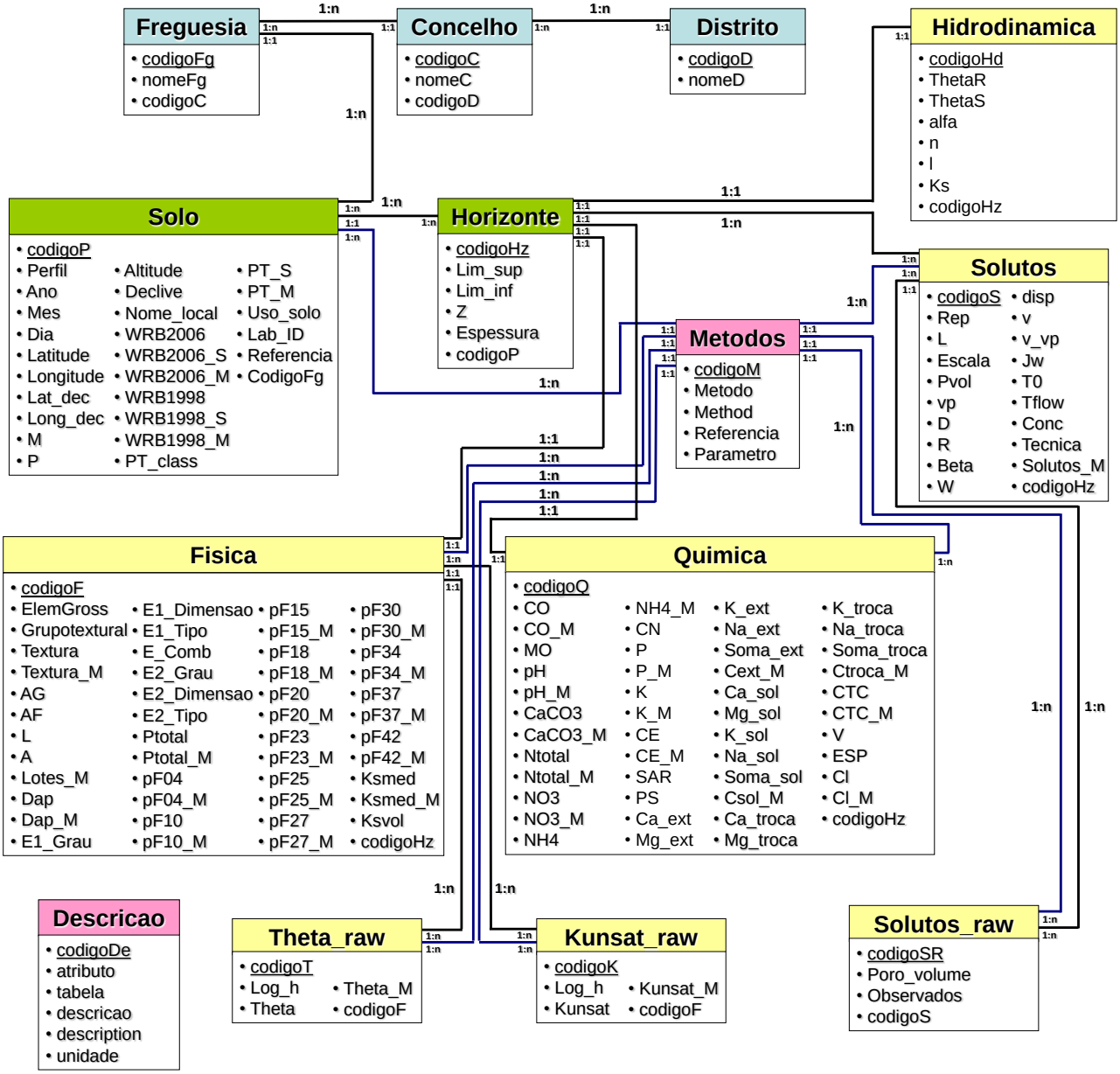

Fig. 1. Esquema relacional da base de dados PROPSOLO.

amoniacal; os teores de fósforo e potássio; os teores de Na^+, Ca^{2+}, Mg^{2+}, K^+ extraíveis, solúveis e de troca; a *CE*; o SAR; o ESP; a CTC e os teores de Cl^- de cada horizonte/camada. A tabela HIDRODINAMICA reúne os parâmetros do modelo de Mualem-van Genuchten (θ_r, θ_s, α, η, ℓ e K_s) que descrevem as curvas de retenção de água e da condutividade hidráulica de cada horizonte/camada. O tipo de ligação entre estas três tabelas e a tabela HORIZONTE é do tipo 1:1, isto é, cada camada/horizonte de solo é caracterizado apenas por um valor de uma determinada propriedade do solo (ex: massa volúmica aparente), assim como cada valor de uma determinada propriedade do solo diz respeito apenas a um determinado horizonte. São as tabelas FISICA, QUIMICA e HIDRODINAMICA que possuem como chave estrangeira, a chave primária da tabela HORIZONTE, para assim facilitar a remoção e actualização destas tabelas, alterações de campos e adição de novos atributos que venham a ser considerados de interesse.

Nesta nova versão, a base de dados tem ainda associada à tabela HORIZONTE, a tabela SOLUTOS que integra os parâmetros de transportes de solutos determinados em cada horizonte/camada de solo, nomeadamente, os coeficientes de dispersão (*D*) e de retardação (*R*) e a dispersividade (*disp*). Os parâmetros de transporte de solutos incluídos na base de dados foram obtidos de acordo com os procedimentos experimentais descritos em Gonçalves et al. (2001). Contudo, esta tabela permite a inclusão de todas as metodologias utilizadas na determinação daqueles parâmetros tendo-se seguido para isso o modelo proposto por Vanderborght & Vereecken (2007). O tipo de ligação da tabela SOLUTOS à tabela HORIZONTE é do tipo 1:n permitindo também a inclusão dos valores de todas as repetições analisadas para cada horizonte/camada.

As tabelas SOLO, FISICA e QUIMICA estão ligadas à tabela METODOS permitindo a identificação das metodologias utilizadas na classificação dos solos ou na determinação das suas propriedades físicas e químicas. O tipo de ligação entre estas tabelas é do tipo 1:n uma vez que o mesmo método pode ser utilizado para mais do que uma propriedade do solo. Essas ligações fazem-se através das chaves estrangeiras identificadas na Figura 1 pelos atributos terminados na letra M.

Acessoriamente, a tabela SOLO está também associada à tabela FREGUESIA, que por sua vez está associada à tabela CONCELHOS, a qual está também relacionada com a tabela DISTRITOS.

Estas tabelas com a divisão administrativa do país servem apenas para melhor localizar cada perfil de solo estudado, seguindo uma multiplicidade de 1:n. As tabelas THETA_RAW, KUNSAT_RAW e SOLUTOS_RAW contêm os dados não tratados, permitindo assim o ajustamento de qualquer outro modelo paramétrico aos dados laboratoriais. Finalmente, a tabela DESCRICAO contém a descrição, em português e inglês, de todos os atributos e tabelas incluídas na base de dados, não estando por isso associada a qualquer outra tabela relacional.

Todos os campos não preenchidos na base de dados PROPSOLO são representados pelo valor NULL. Esta situação é comum nas bases de dados de solos (Henley, 2006) e resulta de nem sempre ser possível realizar a amostragem de solo e/ou a respectiva análise laboratorial, ou ainda por o parâmetro correspondente a esse campo não ter sido avaliado nos estudos de solos em cujos objectivos não se incluía a obtenção desse parâmetro.

2.2. Propriedades hidráulicas do solo

As curvas $\theta(h)$ e $K(h)$ existentes na tabela HIDRODINAMICA da base de dados PROPSOLO foram analisadas por classes texturais, segundo o diagrama triangular de Gomes & Silva (1962). Em cada classe textural foram considerados todos os tipos de horizontes que fazem parte da base de dados não se fazendo qualquer distinção entre camadas. Desta análise foram apenas retiradas as curvas $\theta(h)$ e $K(h)$ obtidas para os solos do Arquipélago dos Açores que, devido à presença de minerais de argila do tipo alofanas, apresentam características muito diferentes dos solos existentes em Portugal Continental, nomeadamente, a massa volúmica aparente que é muito baixa e a porosidade total e capacidade de retenção de água que são muito elevadas (Fontes et al., 2004).

Para Portugal Continental, a PROPSOLO contém 558 curvas $\theta(h)$ e 245 curvas $K(h)$, cuja distribuição por classes texturais é apresentada na Figura 2. É importante referir que todas as curvas aqui analisadas foram determinadas em amostras no estado natural (não perturbadas). Também importa referir que a base de dados não contém solos de textura Limosa, uma vez que, até à data, tal classe textural nunca foi encontrada nos estudos conduzidos pelo DCS.

Para cada classe textural, determinaram-se os valores médios (x_m), desvio padrão (σ), valores máximos (max) e mínimos (min) de cada um dos parâmetros do modelo de Mualem-van Genuchten disponíveis na base de dados.

Os valores de θ e de K para as pressões efectivas de 0, -2.5, -10, -20, -50, -100, -200, -250, -500, -1000, -2000, -5000, -10000, -15000 e -16000 cm de água foram gerados a partir de cada curva parametrizada existente na base de dados. Calcularam-se os valores médios de θ e de K em função de h, e respectivo desvio padrão, garantindo-se assim que todos os horizontes/camadas tinham o mesmo número de observações nos cálculos realizados. Com base nos valores médios de θ e de K obtidos, utilizou-se o *software* RETC (van Genuchten, 1991) para estimar funções médias representativas de cada classe textural ($\theta_{r\ \text{classe}}$, $\theta_{s\ \text{classe}}$, α_{classe}, η_{classe}, $\ell_{\ \text{classe}}$ e $K_{s\ \text{classe}}$).

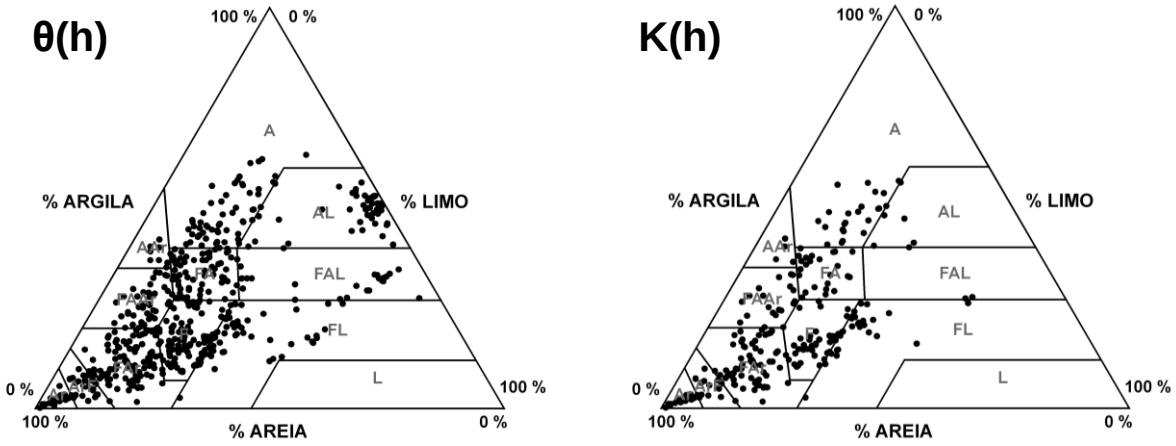

Curva	Ar	ArF	FAr	F	FL	FAAr	FA	FAL	AAr	AL	A
θ(h)	17	27	106	97	58	47	71	24	8	46	57
K(h)	13	17	65	43	29	19	24	3	4	5	23

Fig. 2. Distribuição das curvas de retenção de água $\theta(h)$ e da condutividade hidráulica $K(h)$ no diagrama triangular de Gomes & Silva (1962). (Ar, Arenosa; ArF, Areno-Franca; FAr, Franco-Arenosa; F, Franca; FL, Franco-Limosa; FAAr, Franco-Argilo-Arenosa; FA, Franco-Argilosa; FAL, Franco-Argilo-Limosa; AAr, Areno-Argilosa; AL, Argilo-Limosa; A, Argilosa).

3. Resultados e discussão

No Quadro 1 apresentam-se os valores médios, desvio padrão, valores máximos e mínimos dos parâmetros de Mualem van Genuchten (θ_r, θ_s, α, η, ℓ e K_s) para cada classe textural, de acordo com o diagrama triangular de Gomes & Silva (1962). No mesmo quadro apresentam-se, também,

os valores médios dos parâmetros de Mualem-van Genuchten por classe de textura estimados a partir das pressões efectivas impostas ($\theta_{r\ \text{classe}}$, $\theta_{s\ \text{classe}}$, α_{classe}, η_{classe}, $\ell_{\ \text{classe}}$ e $K_{s\ \text{classe}}$). Estes parâmetros permitem obter uma função $\theta(h)$ e $K(h)$ média para cada classe de textura.

Quadro 1. Valores médios (x_m), desvio padrão (σ), valores máximos (max) e mínimos (min) e valores médios estimados ($\theta_{r\ \text{classe}}$, $\theta_{s\ \text{classe}}$, α_{classe}, η_{classe}, $\ell_{\ \text{classe}}$ e $K_{s\ \text{classe}}$) dos parâmetros de Mualem van Genuchten para as classe texturais do diagrama de Gomes & Silva (1962).

M-vG	**Ar**	**ArF**	**FAr**	**F**	**FL**	**FAAr**	**FA**	**FAL**	**AAr**	**AL**	**A**
θ_r ($cm^3\ cm^{-3}$)											
x_m	0.021	0.013	0.010	0.023	0.004	0.057	0.049	0.016	0.073	0.034	0.087
σ	0.014	0.024	0.026	0.046	0.017	0.075	0.080	0.036	0.090	0.069	0.111
max	0.047	0.080	0.112	0.169	0.114	0.238	0.278	0.137	0.228	0.202	0.352
min	0.002	0.000	0.000	0.000	0.000	0.000	0.000	0.000	0.000	0.000	0.000
$\theta_{r\ \text{classe}}$	0.021	0.000	0.000	0.000	0.000	0.000	0.000	0.000	0.151	0.000	0.000
θ_s ($cm^3\ cm^{-3}$)											
x_m	0.396	0.406	0.408	0.417	0.441	0.383	0.420	0.500	0.414	0.563	0.482
σ	0.060	0.076	0.072	0.059	0.067	0.049	0.065	0.077	0.139	0.046	0.067
max	0.485	0.568	0.612	0.573	0.568	0.495	0.647	0.636	0.639	0.637	0.653
min	0.290	0.221	0.279	0.306	0.332	0.294	0.313	0.377	0.275	0.444	0.344
$\theta_{s\ \text{classe}}$	0.400	0.412	0.406	0.414	0.448	0.386	0.421	0.538	0.399	0.582	0.474
α (cm^{-1})											
x_m	0.049	0.064	0.173	0.227	0.153	0.147	0.247	0.097	0.184	0.063	0.482
σ	0.125	0.056	0.256	0.453	0.547	0.313	0.721	0.178	0.213	0.091	0.292
max	0.508	0.263	1.504	3.043	3.831	1.857	5.333	0.719	0.574	0.339	1.679
min	0.022	0.008	0.012	0.007	0.001	0.001	0.002	0.003	0.006	0.002	0.005
α_{classe}	0.080	0.069	0.107	0.083	0.053	0.132	0.116	0.298	0.043	0.116	0.085
η (-)											
x_m	2.05	1.38	1.20	1.20	1.21	1.18	1.14	1.16	1.30	1.13	1.15
σ	0.81	0.16	0.13	0.12	0.10	0.14	0.09	0.06	0.23	0.05	0.12
max	4.59	1.92	1.73	1.90	1.48	1.80	1.53	1.29	1.62	1.29	1.72
min	1.35	1.19	1.10	1.01	1.07	1.05	1.06	1.06	1.05	1.05	1.05
η_{classe}	1.62	1.29	1.17	1.15	1.15	1.09	1.08	1.08	1.36	1.08	1.08
ℓ (-)											
x_m	-0.48	-1.43	-4.42	-5.07	-6.75	-5.64	-8.21	-9.84	-1.25	-8.18	-6.45
σ	1.15	1.71	2.47	2.43	2.37	4.73	2.77	3.01	1.39	3.46	3.66
max	2.02	1.21	0.15	0.00	-3.30	0.00	-1.90	-7.86	-0.05	-4.45	0.00
min	-2.36	-4.23	-8.74	-11.32	-11.98	-14.48	-14.36	-13.30	-2.61	-13.19	-11.86
$\ell_{\ \text{classe}}$	-1.19	-2.19	-5.07	-6.17	-6.59	-10.58	-10.77	-11.97	-1.14	-9.61	-9.29
K_s ($cm\ d^{-1}$)											
x_m	499.6	164.9	152.0	84.1	71.8	94.9	158.1	548.4	199.5	267.1	171.5
σ	438.6	142.2	173.6	127.1	85.1	139.1	504.2	775.8	232.1	204.5	195.2
max	1405.6	527.2	939.7	526.7	325.6	427.1	2494.0	1436.8	545.2	588.7	796.6
min	84.5	19.4	1.1	1.4	1.7	3.7	1.0	4.9	64.8	102.3	1.2
$K_{s\ \text{classe}}$	315.1	179.9	146.2	84.4	53.4	88.9	153.4	390.5	184.9	255.7	222.1

Ar, Arenosa; ArF, Areno-Franca; FAr, Franco-Arenosa; F, Franca; FL, Franco-Limosa; FAAr, Franco-Argilo-Arenosa; FA, Franco-Argilosa; FAL, Franco-Argilo-Limosa; AAr, Areno-Argilosa; AL, Argilo-Limosa; A, Argilosa.

Os valores médios disponíveis na PROPSOLO para o parâmetro θ_r variam entre 0.004 (FL – textura Franco-Limosa) e 0.087 (A) cm^3 cm^{-3}. Estes valores são contudo inferiores aos indicados por Carsel & Parish (1988) cujos valores se situavam entre 0.045 (Ar) e os 0.100 (AAr) cm^3 cm^{-3}, e também em relação a Schaap et al. (1998), cujos valores variam entre 0.049 (ArF) e 0.117 (AAr) cm^3 cm^{-3}. Tal deve-se ao facto de 66% dos horizontes presentes na base de dados PROPSOLO terem sido ajustados a um θ_r de 0.000 cm^3 cm^{-3}. Pela mesma razão, o parâmetro $\theta_{r\ classe}$ foi também de 0.000 cm^3 cm^{-3}, para a maior parte das classes texturais.

Os valores médios para o parâmetro θ_s variam entre 0.383 (FAAr) e 0.563 (A) cm^3 cm^{-3}, verificando-se uma tendência para o aumento de θ_s das texturas ligeiras para as finas. O mesmo pode ser observado em Schaap *et al*. (1998), onde θ_s aumenta de 0.375 (Ar) para 0.489 (L) e 0.457 (A) cm^3 cm^{-3}. No entanto, Carsel & Parish (1988) apresentam uma diminuição do parâmetro θ_s das texturas mais finas (θ_s =0.38 cm^3 cm^{-3}, na classe Argilosa) para as grosseiras (θ_s =0.43 cm^3 cm^{-3}, na classe Arenosa). Os valores de θ_s disponíveis na PROPSOLO são da mesma ordem de grandeza dos disponíveis nas bases de dados internacionais.

O parâmetro α (valor médio) varia entre 0.049 (Ar) e 0.482 (A) cm^{-1}, não se observando, tal como em Schaap et al. (1998), qualquer tendência de aumento ou diminuição deste parâmetro em função do tipo de classe textural. Contudo, em Carsel & Parish (1988) essa tendência é clara, onde α diminui das classes ligeiras (α =0.145 cm^{-1} na classe arenosa) para as classes mais finas (α =0.008 cm^{-1} na classe argilosa). O parâmetro α_{classe} apresenta valores diferentes dos observados para os valores médios (x_m), confirmando a dificuldade de representar uma classe textural com base naquele parâmetro.

O parâmetro η diminui das classes de textura grosseira (η=2.05 na classe Arenosa) para as classes de textura mais fina (η=1.15 na classe Argilosa), tal como reportado por Carsel & Parish (1988) e por Schaap et al. (1998).

O parâmetro ℓ varia entre -0.48 (Ar) e -11.97 (FAL), o que revela o aumento da tortuosidade, como seria de esperar, das texturas grosseiras para as texturas mais finas. Apenas Schaap et al. (1998) apresenta dados sobre este parâmetro, seguindo as mesmas tendências observadas na PROPSOLO, embora os valores médios observados variem entre 0.365 (FL) e -3.665 (AL).

A condutividade hidráulica saturada (K_s) apresenta grandes variações dentro de cada classe textural, sendo o desvio padrão, em todos os casos, da mesma ordem de grandeza, ou mesmo superior aos valores médios de cada classe. Assim, apesar da PROPSOLO contar já com 245 curvas $K(h)$, é um número ainda não suficiente de modo a caracterizar este parâmetro para cada classe textural, devido à sua grande heterogeneidade espacial.

Nas Figuras 3, 4 e 5 apresentam-se as curvas $\theta(h)$ e $K(h)$ médias obtidas para cada uma das classes texturais em função dos parâmetros de Mualem-van Genuchten ajustados ($\theta_{r\ \text{classe}}$, $\theta_{s\ \text{classe}}$, α_{classe}, η_{classe}, $\ell_{\ \text{classe}}$ e $K_{s\ \text{classe}}$) e obtidos a partir dos teores médios de água no solo obtido às sucções e -0, -2.5, -10, -20, -50, -100, -200, -250, -500, -1000, -2000, -5000, -10000, -15000 e -16000 cm de água. Nas mesmas figuras pode-se também observar o desvio padrão dos teores de água em cada uma das sucções definidas.

Como exemplo, passa-se a discutir alguns aspectos das classes texturais Arenosa e Argilosa. A curva $\theta(h)$ obtida para a classe Arenosa apresenta uma porosidade total média de 0.396 $cm^3\ cm^{-3}$ (σ=0.060 $cm^3\ cm^{-3}$) e teores médios de água às sucções de 100 e 16000 cm de 0.119 (σ=0.072 $cm^3\ cm^{-3}$) e 0.027 $cm^3\ cm^{-3}$ (σ=0.017 $cm^3\ cm^{-3}$), respectivamente. Por sua vez, a curva $\theta(h)$ para a classe Argilosa apresenta uma porosidade total média de 0.482 $cm^3\ cm^{-3}$ (σ=0.067 $cm^3\ cm^{-3}$) e teores médios de água às sucções de 100 e 16000 cm de água de 0.391 (σ=0.044 $cm^3\ cm^{-3}$) e 0.271 $cm^3\ cm^{-3}$ (σ=0.053 $cm^3\ cm^{-3}$), respectivamente.

Em relação às curvas $K(h)$, as curvas médias obtidas para aquelas duas texturas (Arenosa e Argilosa) descrevem os dois principais tipos de curvas existentes. Para os solos arenosos, os valores de $K(h)$ permanecem constantes até ao valor da pressão de entrada de ar nestes solos. A partir deste ponto, $K(h)$ apresenta um decréscimo muito acentuado. Para os solos argilosos, a curva $K(h)$ obtida é típica de solos com macroporos, uma vez que os valores de K_s são de uma ordem de magnitude superior aos valores de condutividade hidráulica correspondentes a apenas alguns centímetros de pressão efectiva, mas suficientes para drenar os macroporos. Na maior parte das classes texturais, as curvas $K(h)$ apresentam características intermédias às duas curvas aqui descritas.

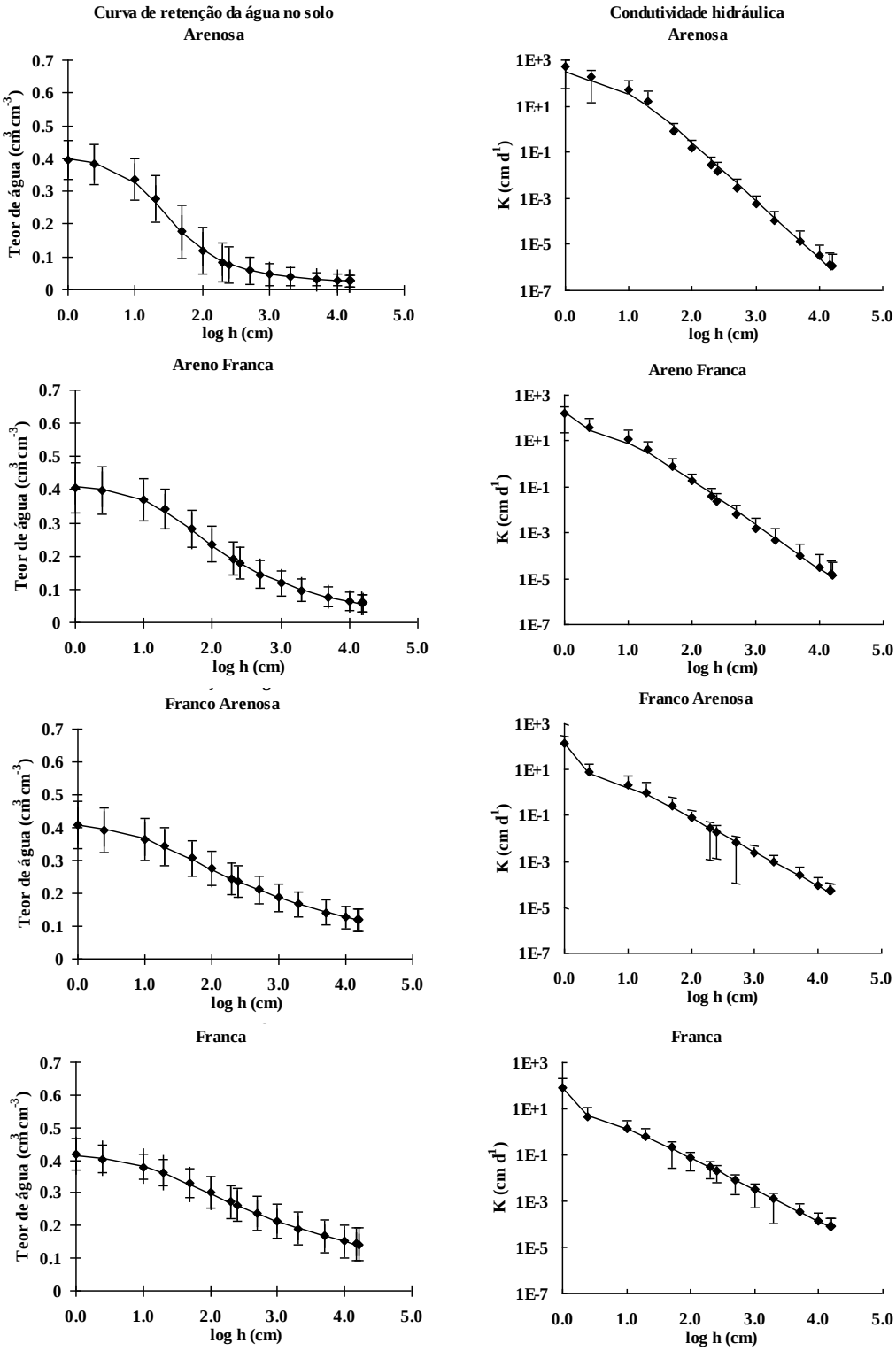

Fig. 3. Curvas de retenção de água e da condutividade hidráulica para as texturas Arenosa, Areno-franca, Franco-Arenosa e Franca.

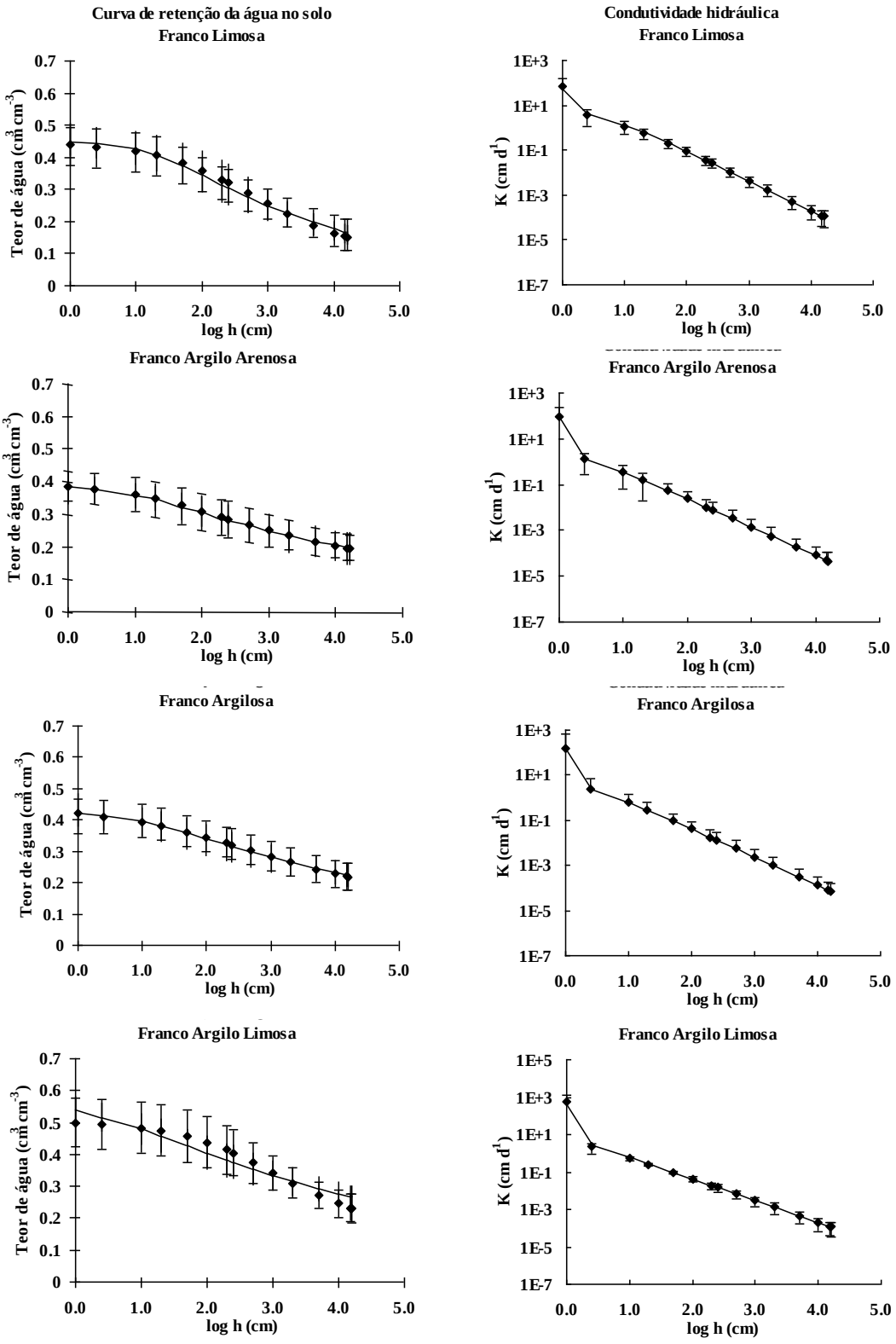

Fig. 4. Curvas de retenção de água e da condutividade hidráulica para as texturas Franco-Limosa, Franco-Argilo-Arenosa, Franco-Argilosa e Franco-Argilo-Limosa.

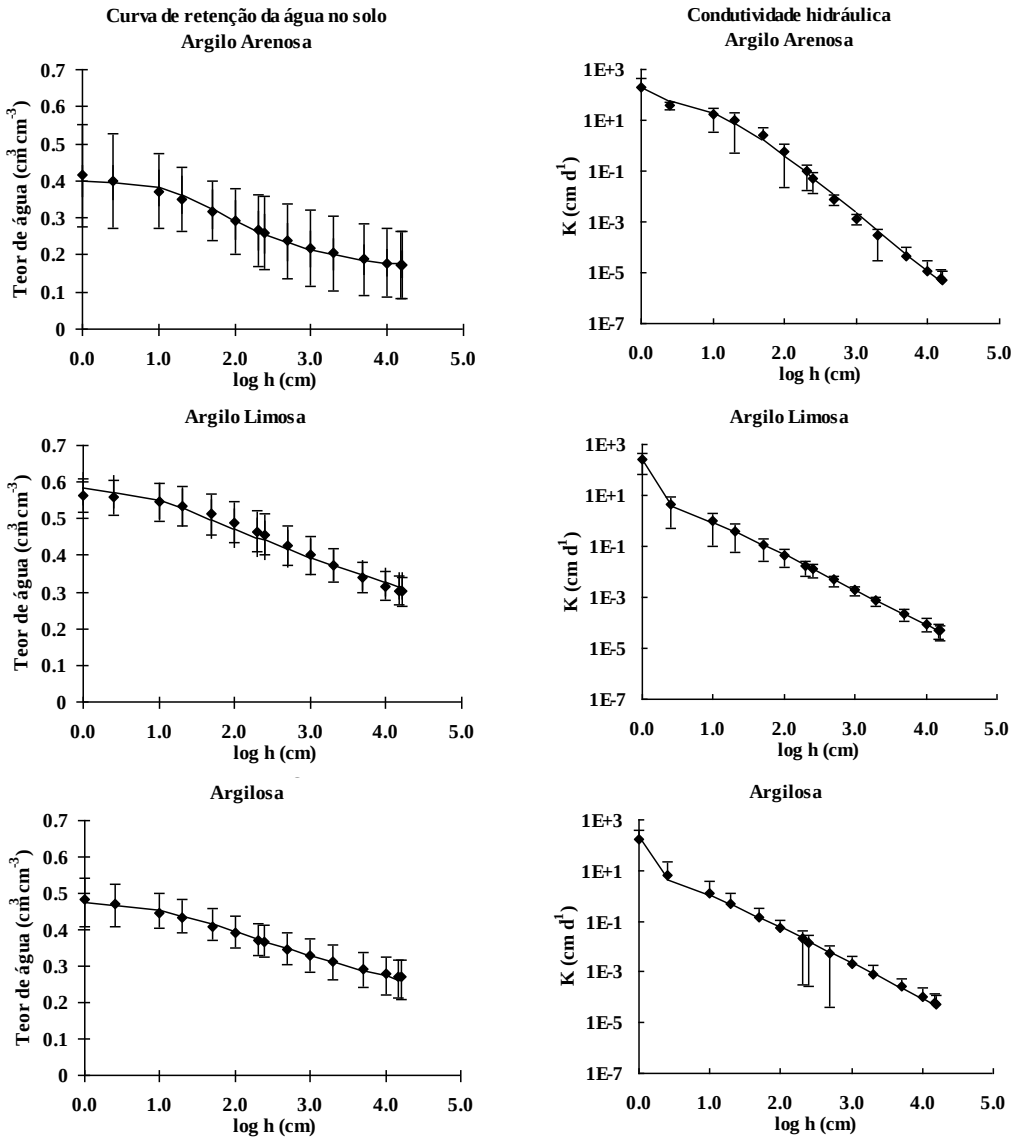

Fig. 5. Curvas de retenção de água e da condutividade hidráulica para as texturas Argilo-Arenosa, Argilo-Limosa e Argilosa.

4. Conclusões

Os parâmetros do modelo de Mualem-van Genuchten (θ_r, θ_s, α, η, ℓ e K_s) disponíveis na base de dados PROPSOLO apresentam grande variabilidade, mesmo dentro de cada classe textural, nomeadamente, os parâmetros α e K_s. A quantificação da variabilidade das propriedades hidráulicas do solo requererá, no entanto, um trabalho contínuo e mais profundo, de modo a aumentar o número de curvas $\theta(h)$ e $K(h)$ disponíveis para este tipo de estudos. Existem lacunas

de informação relativas às propriedades hidráulicas que deverão ser colmatadas no futuro, nomeadamente, para as classes texturais Limosa e Argilo-Arenosa e da condutividade hidráulica insaturada para a totalidade das classes texturais.

Agradecimentos

Este trabalho foi realizado no âmbito dos Projectos NITROSAL (PTDC/AGR-AAM/66004/2006) e EUTROPHOS (PTDC/AGR-AAM/098100/2008) da Fundação para a Ciência e a Tecnologia (FCT). T. B. Ramos é financiado por uma bolsa FCT (contrato SFRH/BD/60363/2009).

Bibliografia

Cardoso, J.C., 1974. A classificação de solos de Portugal. Boletim de Solos do S.R.O.A. 17, 14-46.

Dane, J.J., Topp, G.C., 2002. Methods of Soil Analysis, Part 4. Physical Methods. Soil Sci. Soc. Am., Inc., Madison, WI.

Fontes, J.C., Gonçalves, M.C., Pereira, L.S., 2004. Andosols of Terceira, Azores: measurement and significance of soil hydraulic properties. Catena 56, 145-154.

Gardner, W.R., 1958. Some steady-state solutions of unsaturated moisture flow equations with application to evaporation from a water table. Soil Sci. 85, 228–232.

Gomes, M.P., Silva, A.A., 1962. Um novo diagrama triangular para a classificação básica da textura do solo. Garcia da Orta 10, 171-179.

Gonçalves, M.C., Pereira, L.S., Leij, J.F., 1997. Pedo-Transfer Functions for Estimating Unsaturated Hydraulic Properties of Portuguese Soils. Euro. J. Soil Sci. 48, 387-400.

Gonçalves, M.C., Almeida, V.V., Pereira, L.S., 1999. Estimation of Hydraulic parameters for portuguese soils. In: van Genuchten, M.Th., Leij, F., Wu, L. (Eds). Characterization and Measurement of the Hydraulic Properties of Unsaturated Porous Media. Part 2, pp 1199-1210. University of California Riverside, CA, USA.

Gonçalves, M.C., Leij, F.J., Schaap, M.G., 2001. Pedotransfer functions for solute transport parameters of Portuguese soils. Euro. J. Soil Sci. 52, 563-574.

Henley, S., 2006. The problem of missing data in geoscience databases. Comp. & Geosci. 32, 1368-1377.

Nemes, A., Schaap, M.G., Leij, F.J., Wösten, J.H.M., 2001. Description of the unsaturated soil hydraulic database UNSODA version 2.0. J. Hydrol. 251, 151-162.

Ramos, T.B., Gonçalves, M.C., Martins, J.C., Pires, F.P., 2007. PROPSOLO – Base de dados georreferenciada de propriedades do solo. II Congresso Nacional de Rega e Drenagem, CD-ROM, 26 a 28 de Junho, Fundão.

Schaap, M.G., Leij, F.L., van Genuchten, M.Th., 1998. Neural network analysis for hierarchical prediction of soil hydraulic properties. Soil Sci. Soc. Am. J. 62, 847-855.

van Genuchten, M.Th., 1980. A closed form equation for predicting the hydraulic conductivity of unsaturated soils. Soil Sci. Soc. Am. J. 44, 892-898.

van Genuchten, M. Th., Leij, F.J., Yates, S.R., 1991. The RETC code for quantifying the hydraulic functions of unsaturated soils. Report No. EPA/600/2-91/065. R. S. Kerr Environmental Research Laboratory, U. S. Environmental Protection Agency, Ada, OK. 85 pp.

Vanderborght, J., Vereecken, H., 2007. Review of dispersivities for transport modeling in soils. Vadose Zone J. 6, 29-52.

Wösten, J.H.M., Lilly, A., Nemes, A., Le Bas, C., 1999. Development and use of a database of hydraulic properties of European soils. Geoderma 90, 169-185.

Chapter 6

Development of class pedotransfer functions for integrating water retention properties into Portuguese soil maps

(Published in: Soil Research 51, 262-277. 2013)

Development of class pedotransfer functions for integrating water retention properties into Portuguese soil maps

T. B. Ramos[1], M. C. Gonçalves[1,2], Brito, D.[3], J. C. Martins[3] and L. S. Pereira[1]

[1] CEER, Institute of Agronomy, Technical University of Lisbon, Tapada da Ajuda, 1349-017 Lisbon, Portugal

[2] INIAV, National Institute of Agronomic and Veterinarian Research, Av. República, 2784-505 Oeiras, Portugal.

[3] MARETEC, Technical Superior Institute, Technical University of Lisbon, Av. Rovisco Pais 1, 1049-001 Lisbon, Portugal.

Abstract

Hydrological modellers have recently been challenged to improve watershed models by better integrating soil information into model applications. Reliable soil hydraulic information is thus necessary for better describing the water balance components at the catchment scale. Frequently, that information does not exist. This study presents a set of class-pedotransfer functions (PTFs) for estimating the water retention properties of Portuguese soils. The class-PTFs were established from a dataset containing 697 soil horizons/layers, by averaging values of total porosity and volumetric water contents at –0.25, –1, –3.2, –6.3, –10, –33, –100, –250, and –1500 kPa matric potentials after grouping data by soil texture class, soil horizon, and bulk density. Fitted retention curves using the van Genuchten model were also obtained for every class-PTF. The root mean square error varied between 0.039 and 0.057 cm^3 cm^{-3}, with smaller values found when using the 12 texture classes of the International Soil Science Society (ISSS) system rather than the five texture classes of FAO, and when bulk density was also considered. The class-PTFs were then integrated into Portuguese soil maps and its usage was demonstrated by deriving maps of available water capacity to be used for modelling the water balance in a small catchment area with the SWAT model. The model successfully simulated the reservoir inflow when using the derived maps, but the results did not vary much whether using coarser or finer description of the catchment soils. Nonetheless, the class-PTFs contributed to a better soil characterisation than when using coarse-scaled information. The approach followed here was simple, inexpensive, and

feasible for modellers with few resources but interested in considering the spatial variability of soil retention properties at large scales and in advancing hydrologic modelling in Portugal.

Keywords: bulk density, soil grouping, soil horizons, soil mapping units, texture classes.

1. Introduction

Recently, watershed modeling has emerged as one of the most important assessment tools in watershed planning and management. Nonetheless, hydrological modelers have been challenged to improve watershed models by better integrating soil information into model applications (Lin et al., 2006; Bouma et al., 2011). Soil type is a major factor influencing soil evaporation, crop evapotranspiration, crop nutrition, recharge to groundwater, and soil erosion. In addition, soil physical and chemical properties present inherent spatial and temporal variability within the catchment scale. However, in many model applications, soils have been considered simplistically, frequently as homogeneous and isotropic, simplifying important hydrologic processes occurring at the catchment level (Bouma et al., 2011). As a result, the classic calibration of watershed models, in which a few discharge gauges near the outlet of a catchment are used to compare measured and simulated discharges, has been criticized because it does not assure that other processes such as evapotranspiration, crop growth, and groundwater recharge are correctly represented in the catchment area (Lin et al., 2006; Bouma et al., 2011).

Hydrological modelers generally have no alternative to these simplistic representations of field soils, because detailed and reliable soil information is rare in most regions of the world. Hydropedology, an emerging interdisciplinary field merging soil science and hydrology, intends to overcome such limitations in watershed modeling by better addressing the intimate relationships linking soil, landscape, and hydrology (Lin, 2003, 2010; Bouma, 2006; Lin et al., 2006; Pachepsky et al., 2006; Bouma et al., 2011). Of particular interest to this study is the bridging of data gaps between soil survey databases and soil hydraulic information needed in simulation models. Classical methods for direct measurement of soil hydraulic properties (Dane and Topp, 2002) are known to be costly, time-consuming, and impractical for large-scale applications in which many samples are required to quantify the spatial and temporal variability of those properties. Remote-sensing techniques may eventually overcome those limitations and

then be used to derive effective soil hydraulic properties at a much larger scale (Weihermüller et al., 2007; Steenpass et al., 2010; Jana and Mohanty, 2012). However, further advancement in the research on these techniques is needed, as remote-sensing signals are usually sensitive only to a very limited surface depth and are unable to characterize the soil profile at the greater depths required in hydrological modeling. Hence, pedotransfer functions (PTFs), which relate soil hydraulic properties to basic soil physical and chemical properties usually available from soil survey studies (Bouma, 1989; Vereecken et al., 1989; McBratney et al., 2002; Pachepsky and Rawls, 2004), may still be the best approach when characterizing soil hydraulic properties at large scales.

Soil survey studies can provide important information to improve hydrological modeling, especially soil maps, which are a common way to portray soil heterogeneity and to describe structural patterns across the landscape (Lin, 2003, 2010). However, that information alone may not be sufficient, as soil hydraulic properties show spatial variability even within the same mapping unit (Wösten et al., 2001). Therefore, information obtained from soil survey studies should most likely be first used to derive a set of pedotransfer rules for each soil profile, which then could be used to integrate estimates of hydrological data and the associated uncertainty

That strategy was the primary motivation in this study in which class-PTFs were developed as tools for assimilating soil hydraulic information into Portuguese soil maps. Class-PTFs provide class-average water contents at specific pressure heads or one average water-retention curve for every textural class. They are usually obtained from the arithmetic mean (e.g. Bruand et al., 2003; Al Majou et al., 2008a, 2008b), geometric mean (Wösten et al., 1995, 1999), and the statistical distribution of the dataset (Baker 2008). Hence, class-PTFs are considered the simplest approach for presenting reliable soil hydraulic information to hydrological modellers, as the models require only very basic soil data and are well suited for predicting water retention properties at regional or national scales (Wösten et al., 1995, 1999; Nemes et al., 2003; Al Majou et al., 2008b).

The simplicity of the data inputs of class-PTFs when compared with other more sophisticated PTFs (Gonçalves et al., 1997; Wösten et al., 1999; Schaap et al., 2001) also makes them ideal tools to overcome some of the constraints in the Portuguese soil survey database (Madeira et al., 2004; Gonçalves et al., 2005) if that information is to be used in modern hydrological modeling studies. Some of these constraints are: (i) different soil classification systems were used in the

available soil maps, thus making basic soil properties such as soil texture classes the easiest link available among the different maps; (ii) soil maps within a single catchment area may show different levels of detail as a result of the scales used for mapping soils in different regions of the country; (iii) the coordinates of the representative soil profiles were never released, with only a broad location being given; and (iv) the information on soil hydraulic properties is limited to a few specific retention points (normally, the wilting point and field capacity), with most of the data being obsolete because they were determined on disturbed soil samples.

Consequently, most watershed modeling studies performed in Portugal have struggled to find reliable soil information for characterizing field soils in their model applications (e.g. Nunes et al., 2006; Duarte et al., 2008; Yevenes and Mannaerts, 2011). Some of these studies were able to proceed with a simplistic characterization of soil hydraulic properties by analyzing a few soil profiles in the studied areas. However, many others used data from Cardoso (1965), which are far from adequate in modern hydrological studies, or applied 'external' PTFs that have not been validated for Portuguese soils, sometimes not even accounting for the differences in the particle limits between the existing data and the requirements of the PTFs.

This study presents a set of class-PTFs developed from a currently underused database of Portuguese soil hydraulic properties (Gonçalves et al., 2011). The main purpose is thus to make the data available for watershed modelers, irrigation managers, and others, because data are more valuable when used by technicians, policy makers and scientists, including those interested in advancing hydrological modeling (Lin et al., 2006). The specific objectives of the study were to develop class-PTFs for integrating soil-water retention properties into Portuguese soil maps. Class-PTFs were derived for estimating water retention at 10 different values of matric potential, with soil texture classes, soil horizon, and bulk density being used as ancillary variables. Then, the effectiveness of the class-PTFs in simulations of a catchment water balance was assessed with the Soil and Water Assessment Tool (SWAT; Neitsch et al., 2011).

2. Material and methods

2.1. The dataset

The class-PTFs were developed from data available in the PROPSOLO soil database (Gonçalves et al., 2011), which gathers all information on soil hydraulic and pedological properties from soil

profiles obtained from research projects and academic studies performed at the Portuguese National Institute of Agronomic and Veterinarian Research (former Estação Agronómica Nacional). This database contains practically all of the existing knowledge on the soil hydraulic properties of Portuguese soils (with the exception of a few specific retention points found in soil survey studies).

The data extracted for this study included a set of 697 horizons/layers studied in 330 soil profiles in Portugal (Fig. 1) between 1977 and 2011. This dataset comprised 315 topsoil (0–30 cm depth) and 382 subsoil (>30 cm depth) horizons. The soil reference groups (FAO, 1998) represented were Fluvisols (36.4%), Luvisols (29.4%), Vertisols (10.3%), Cambisols (8.5%), Calcisols (6.1%), Anthrosols (4.2%), Arenosols (1.5%), Podzols (0.9%), Regosols (0.9%), Ferralsols (0.6%), Leptosols (0.6%), and Planosols (0.6%). Table 1 presents the main physical and chemical properties of the 697 soil horizons/layers selected for the study. The particle size distribution was obtained using the pipette method for particles of diameter <2 mm (clay) and 20–2 mm (silt), and by sieving for particles 200–20 mm (fine sand) and 200–2000 mm (coarse sand). These textural classes follow the Portuguese classification system (Gomes and Silva, 1962) and they are based on the International Soil Science Society (ISSS) particle limits (Atterberg scale). The organic carbon (*OC*) content was determined by the Walkley–Black method (Nelson and Sommers, 1982). Dry bulk density (ρ_b) was obtained by drying volumetric soil samples (100 cm^3) at 105ºC for 48 h. Total porosity (φ) was determined from the maximum holding capacity of 100 cm^3 undisturbed soil cores on a volumetric basis. Gravimetric water content was determined on undisturbed soil samples (100 cm^3) using suction tables at –0.25, –1, –3.2, –6.3, –10, and –33 kPa matric potentials (Romano et al., 2002) and the pressure plate apparatus at –33, –100, –250, and –1500 kPa matric potentials (Dane and Hopmans, 2002). Then, the volumetric water content for each horizon/layer and each matric potential was computed from the gravimetric water contents and the bulk density of the corresponding horizon/layer. The volumetric water content at –33 kPa was obtained from only one method at the time (using suction tables with sand and kaolin until 2005 and using the pressure plate apparatus after 2006).

Table 1. Main physical and chemical characteristics of the 697 soil horizons.

Statistics	Particle size distribution				Organic carbon	Bulk density	Total porosity	Volumetric water content [a]								
	2000-200 µm	200-20 µm	20-2 µm	<2 µm				$\theta_{0.25}$	θ_{1}	$\theta_{3.2}$	$\theta_{6.3}$	θ_{10}	θ_{33}	θ_{100}	θ_{250}	θ_{1500}
	(%)				(g kg^{-1})	(g cm^{-3})	(cm^3 cm^{-3})	(cm^3/cm^3)								
N	-	-	-	-	-	-	697	690	691	692	552	696	661	301	331	697
Mean	20.7	34.2	21.5	23.6	8.24	1.50	0.441	0.424	0.399	0.370	0.348	0.332	0.286	0.239	0.210	0.162
SD	17.6	15.4	12.2	14.8	5.02	0.18	0.074	0.075	0.076	0.080	0.085	0.088	0.090	0.086	0.083	0.080
Min.	0.1	0.7	0.9	0.1	0.01	0.91	0.250	0.231	0.192	0.114	0.049	0.036	0.029	0.008	0.009	0.006
Max.	94.6	73.6	68.1	63.3	25.10	1.90	0.659	0.635	0.624	0.607	0.590	0.574	0.536	0.474	0.449	0.407

[a] θ_i, volumetric water contents measured at -*i* kPa matric potentials.

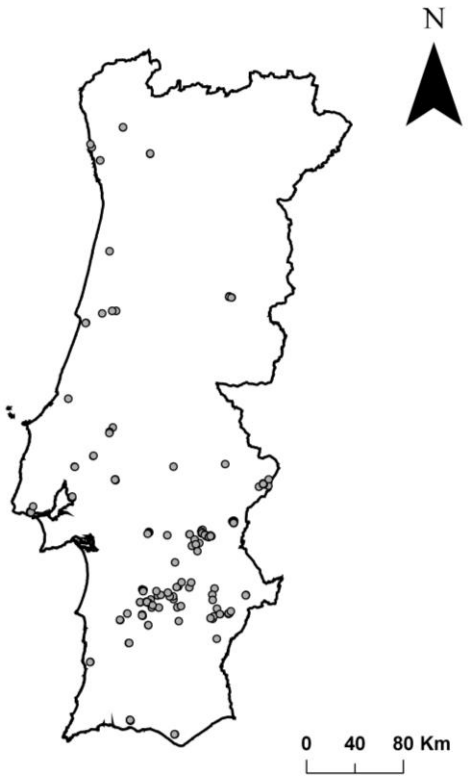

Fig. 1. Location of the 330 soil profiles in Portugal.

The missing values in the volumetric water content dataset were estimated by introducing values derived from the fitted van Genuchten model (1980):

$$S_e(h)=\frac{\theta(h)-\theta_r}{\theta_s-\theta_r}=\frac{1}{\left(1+|\alpha h|^{\eta}\right)^{1-1/\eta}} \quad (1)$$

where *Se* is the effective saturation; θ_r and θ_s are the residual and saturated water contents (L^3 L^{-3}), respectively; α (L^{-1}) and η (–) are empirical shape parameters; and *h* is the pressure head (L). This procedure introduced an error to the subsequent calculations and model evaluations resulting from the non-perfect fit of the fitted model to the experimental data (root mean square error (RMSE) = 0.014 cm^3 cm^{-3}), in line with published results (e.g. Nemes and Rawls, 2006). The errors were thus relatively small compared with the errors usually obtained using PTFs, and therefore, the fitted values were assumed as if they were measured. Table 1 presents the number of determinations of the water content at each matric potential in the original dataset. The number of missing values can be found by subtracting those numbers from the full set of data used in this

study (697, where 23.2% of the retention curves were complete while 1.9% missed four or five values).

2.2. Development of class-PTFs

The class-PTFs were developed by averaging the values of total porosity (φ) and volumetric water contents (θ) at –0.25, –1, –3.2, –6.3, –10, –33, –100, –250, and –1500 kPa matric potentials after grouping the data using the following criteria: (i) the five textural classes of the FAO triangle adapted to the ISSS particle limits (Gomes and Silva, 1980) and the 12 textural classes of the ISSS triangle (Fig. 2); (ii) the FAO and ISSS texture classes and the type of horizon (topsoil and subsoil horizons), to account for differences in pore structure, pore size, and OC content between the two horizons; (iii) the FAO and ISSS texture classes and bulk density, to account for the effect of soil structure on water retention; and (iv) the FAO texture classes, soil horizon, and bulk density in conjunction — this option was not available for the ISSS texture class-PTFs due to data limitations.

The class-PTFs were complemented by fitting the van Genuchten model (van Genuchten, 1980) (Eqn. 1) to the arithmetic mean value of θ at different water potentials using the RETC (retention curve) program (van Genuchten et al., 1991). The average water retention curves were obtained for the texture classes represented in the FAO and ISSS triangles after stratification by texture class, soil horizon (topsoil and subsoil), and bulk density as described above.

2.3. Uncertainty analyses

For each class-PTF type, the data were divided into two subsets: a calibration set composed of two-thirds of the data, and a validation set with the remaining one-third of the data. The random division and subsequent model development and validation were performed 10 times. Each time, the data that were used in the development of the class-PTFs were not used in validation, and *vice versa*. The class-PTFs were then established by averaging the arithmetic means of the water contents at each matric potential and the van Genuchten model parameters obtained in the 10 random development datasets. The standard deviations and the 95% confidence intervals for the

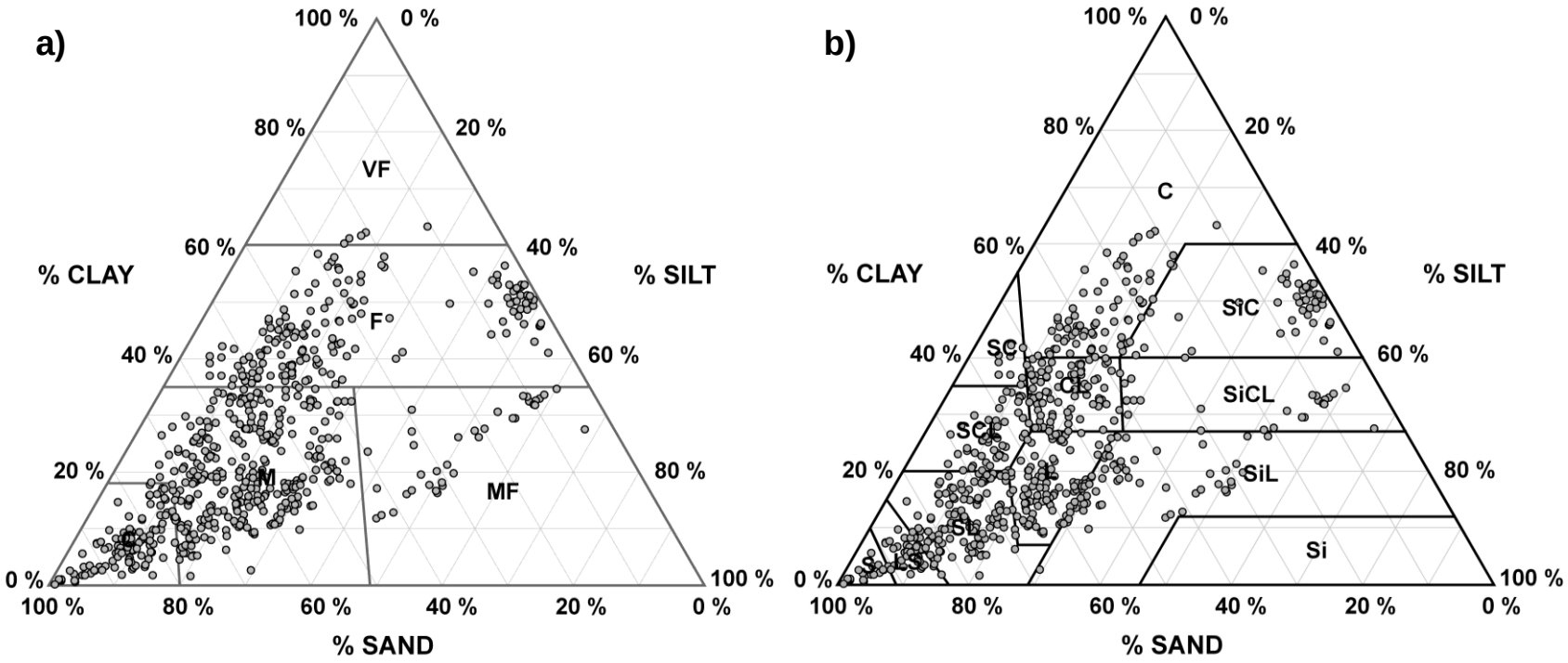

Fig. 2. Textural distribution of the 697 soil horizons classified in accordance with the FAO (a) and ISSS (b) textural classification systems. FAO triangle: C, coarse; M, medium; MF, medium fine; F, fine; VF, very fine texture classes. ISSS triangle: S, sand; LS, loamy sand; SL, sandy loam; L, loam; SCL, sandy clay loam; CL, clay loam; SC, sandy clay; C, clay; SiC, silty clay; SiCL, silty clay loam; SiL, silty loam; Si, silt.

means and standard deviations were also determined from the 10 random estimates. Class-PTFs having data from fewer than five horizons/layers were thus not considered due to the approach used here for analyzing class-PTF uncertainty. In addition, it was assumed that estimates with fewer than five horizons would not produce a consistent estimate.

The precision bias and the average accuracy of the estimations were expressed by the mean error of predictions (MEP) and the RMSE, respectively, as follows:

$$MEP = \frac{1}{H\,l}\sum_{j=1}^{H}\sum_{i=1}^{l}\left(\theta_{p,j,i} - \theta_{m,j,i}\right) \tag{2}$$

$$RMSE = \left\{\frac{1}{H\,l}\sum_{j=1}^{H}\sum_{i=1}^{l}\left(\theta_{p,j,i} - \theta_{m,j,i}\right)^2\right\}^{1/2} \tag{3}$$

where $\theta_{p,j,i}$ is the predicted water content at potential i for horizon j; $\theta_{m,j,i}$ is the measured water content at potential i for horizon j; l is the number of water potentials for each horizon (l = 10 in this study); and H is the number of horizons (H = 697 in this study). The MEP and RMSE values were thus obtained for the estimates of volumetric water contents at each matric potential and not for the fitted van Genuchten model parameters, because the latter derived from the former. Positive and negative MEP values indicated overestimation and underestimation of the water contents, respectively. MEP and RMSE were determined for each of the 10 random validation datasets. The mean MEP and RMSE values, standard deviations, and 95% confidence intervals for the mean and standard deviation were also determined from the 10 estimates.

The accuracy of the class-PTFs was also compared with water content estimates from published PTFs that used part of our dataset (Gonçalves et al., 1997, 1999; Wösten et al., 1999; Paz et al., 2009). For the class and continuous PTFs of Wösten et al. (1999), it was necessary to interpolate the silt content, defined as the fraction between 2 and 50 mm, from the cumulative particle size distribution of each horizon/layer included in our dataset. Smoothing splines (Nemes et al. 1999) were thus fitted to the cumulative particle size limits of 0, 2, 20, 200, and 2000 mm to obtain the cumulative percentage of particles at 50 mm. Smoothing splines were adjusted to the data with the Curve Fitting Toolbox 2.0 available in MATLAB R2009a version 7.8.0 (MathWorks Inc., Natick, MA, USA), resulting in an RMSE of 4.631%. However, because the most significant deviations were found for the fraction between 0 and 2 mm, the interpolation results for the

fractions between 20 and 2000 mm and thus for the cumulative fraction at 50 mm were considered acceptable.

2.4. Assessment of the influence of the class-PTFs on the catchment water balance

A sensitivity analysis was performed using the river basin model SWAT (Soil and Water Assessment Tool; Neitsch et al., 2011) to assess the effect of different available water capacity (AWC) estimates on the catchment water balance. SWAT is a semidistributed, process-oriented model for simulating water, nutrient, and pesticide transport. The hydrologic simulation is based on describing the water balance, which accounts for rainfall interception, evapotranspiration, surface runoff, infiltration, soil percolation, lateral flow, groundwater flow, and channel routing processes.

In SWAT, surface runoff is computed using a modification of the SCS (Soil Conservation Services) curve number method (Neitsch et al., 2011). Reference evapotranspiration (*ETo*) is calculated with the FAO Penman–Monteith method (Allen et al., 1998) and partitioned into soil evaporation and plant transpiration as described by Ritchie (1972). Soil percolation occurs when the field capacity of a soil layer is exceeded, and the percolation rate is governed by the *Ks* of the soil layer. Finally, lateral flow accounts for horizontal transport due to variations in the *Ks*, slope, and soil water content in the different sub-basins (Neitsch et al., 2011).

The sensitivity analysis was performed in the Enxoé catchment (60.8 km2), in the Alentejo region of southern Portugal. The Enxoé is a tributary of the Guadiana River, one of the main rivers in the southern Iberian Peninsula. The dominant soils are Luvisols (covering 47% of the area), Cambisols (31%), Calcisols (14%), and Vertisols (6%) (FAO, 1998). The main land uses are olive groves (18.3 km^2), agroforestry of holm oak 'montado' (17.6 km^2), and annual winter crops (17.0 km^2). The agro-forestry of holm oak montado is mostly in areas with Cambisols, whereas olive groves and annual winter crops are mainly found in areas with Luvisols and Calcisols. The slopes are relatively gentle, and the average altitude of the catchment is 200 m.

Brito et al. (2012) studied the long-term dynamics of sediment and nutrients in that catchment using the SWAT model. Soil data were obtained from the European Soil Database version 2.0 (Daroussin et al., 2006), which comprises several specific databases, including the Soil Geographical Database of Eurasia (1 : 1 000 000) and the Soil Profile Analytical Database of

Europa. The former is a simplified representation of the diversity and spatial variability of the soil coverage, whereas the latter incorporates quantitatively measured or estimated analytical data (e.g. texture, root depth, organic matter, and soil water retention) from representative soil profiles into soil mapping units. Although the soil data inputs were very generic, several parameters related to the travel time of water between the soil and the aquifer and between the aquifer and the river were calibrated and adjusted so that the SWAT estimates of the simulated flow regime were in good agreement with the field data. Further details can be found in Brito et al. (2012). The performance of the model was evaluated using the coefficient of efficiency (NSE) (Nash and Sutcliffe, 1970):

$$NSE = 1.0 - \frac{\sum_{i=1}^{N}(O_i - P_i)^2}{\sum_{i=1}^{N}\left(O_i - \bar{O}\right)^2} \quad (4)$$

where N is the number of observations, O_i are the observations at time i, P_i is the model predictions at time i, and O is the average of observations; NSE = 1.0 represents a perfect fit, whereas negative NSE values indicate poor modeling performance.

The sensitivity analysis was performed by introducing different AWC estimates as inputs into the simulations of Brito et al. (2012). The AWC was here defined as the difference between the volumetric water contents at –33 and –1500 kPa matric potentials multiplied by the depth of the porous media. All other input parameters included in the simulations of Brito et al. (2012) were kept constant. The soil maps from Cardoso (1965), at a scale of 1 : 25.000, were used instead of the previous coarse-scale maps. The AWC was obtained by integrating each of the seven class-PTFs developed in this study into the regional soil maps. For each alternative estimate of AWC, the model performance was also evaluated using Eqn. 4, and the different components of the catchment water balance determined using SWAT were compared.

3. Results and discussion

3.1. Performance analyses of the class-PTFs based on the FAO texture classification

The class-PTFs that were developed after grouping the data according to the different criteria are reported as follows. The class-PTFs following the five textural classes of the FAO triangle are presented in Table 2; and those following the FAO texture classes and bulk density are presented in Table 3. The resulting MEP and RMSE values obtained for each of these class-PTFs are presented in Table 4. Because of the amount of information obtained in the development of the class- PTFs, the standard deviations and the 95% confidence intervals for the means and standard deviations cannot be presented here in detail.

The class-PTFs established for the FAO texture classes (Table 2) produced an acceptable estimation of φ and soil water retention when considering all texture classes combined (MEP = –0.001 cm^3 cm^{-3} with a 95% confidence interval of ±0.002 cm^3 cm^{-3}). However, the water retention values in the medium fine texture classes were slightly overestimated, whereas they were slightly underestimated in the fine texture classes. Nevertheless, the RMSE values were relatively high, varying between 0.041 (±0.009) and 0.069 (±0.008) cm^3 cm^{-3} for the very fine and fine texture classes, respectively. Hence, the RMSE values obtained when combining all textures classes were also high (RMSE = 0.057±0.001 cm^3 cm^{-3}). The low accuracy of these class-PTFs was expected, because they resulted from an attempt to explain soil variability using only five average retention curves. The uncertainty related to these five average retention curves was mostly associated with volumetric water contents approaching to saturation, i.e. where the effect of pore size (macroporosity in particular) on water retention was more significant.

The class-PTFs established after the stratification by FAO texture classes and bulk density (Table 3) produced a significant improvement of the estimates of φ and soil water retention at different matric potentials. Table 3 shows that the effect of soil structure on the water retention curve was significant between φ and the –100 kPa matric potential, with soils with lower bulk density presenting higher water retention values and soils with higher bulk density values showing lower values for the water retention properties. The MEP for all texture classes combined was again good (MEP = 0.000±0.001 cm^3 cm^{-3}), and the estimates were more acceptable for each texture class individually, varying between –0.002±0.004 and 0.002±0.005 cm^3 cm^{-3} for the medium fine

Table 2. Class pedotransfer functions established after stratification by FAO texture classes.

class-PTF [a]	*N*	φ	Volumetric water content									van Genuchten's parameters			
			$\theta_{0.25}$	θ_1	$\theta_{3.2}$	$\theta_{6.3}$	θ_{10}	θ_{33}	θ_{100}	θ_{250}	θ_{1500}	θ_r	θ_s	α	η
			(cm^3 cm^{-3})									(cm^3 cm^{-3})		(cm^{-1})	(-)
Very fine	5	0.541	0.528	0.504	0.479	0.465	0.457	0.428	0.391	0.364	0.318	0.052	0.535	0.103	1.082
Fine	162	0.496	0.484	0.463	0.440	0.422	0.410	0.373	0.333	0.306	0.260	0.039	0.488	0.059	1.103
Medium fine	36	0.529	0.516	0.495	0.474	0.461	0.451	0.407	0.331	0.281	0.197	0.032	0.508	0.009	1.213
Medium	386	0.421	0.401	0.376	0.348	0.328	0.314	0.269	0.222	0.192	0.142	0.039	0.406	0.041	1.197
Coarse	108	0.396	0.376	0.345	0.303	0.260	0.231	0.167	0.125	0.103	0.067	0.021	0.388	0.061	1.301

[a] N, number of soil horizons; φ, total porosity; θ_i, volumetric water contents measured at -*i* kPa matric potentials.

Table 3. Class pedotransfer functions established after stratification by FAO texture classes and dry bulk density (ρ_b).

class-PTF [a]	*N*	φ	Volumetric water content									van Genuchten's parameters			
			$\theta_{0.25}$	θ_1	$\theta_{3.2}$	$\theta_{6.3}$	θ_{10}	θ_{33}	θ_{100}	θ_{250}	θ_{1500}	θ_r	θ_s	α	η
			(cm^3 cm^{-3})									(cm^3 cm^{-3})		(cm^{-1})	(-)
Very fine	-	-	-	-	-	-	-	-	-	-	-	-	-	-	-
Fine	162														
ρ_b<1.20	21	0.589	0.580	0.562	0.535	0.507	0.487	0.435	0.380	0.345	0.281	0.045	0.585	0.071	1.129
1.20≤ρ_b<1.40	57	0.539	0.527	0.502	0.474	0.454	0.440	0.398	0.353	0.323	0.273	0.059	0.534	0.067	1.115
1.40≤ρ_b<1.60	52	0.471	0.459	0.442	0.421	0.408	0.398	0.366	0.330	0.305	0.262	0.041	0.465	0.060	1.095
1.60≤ρ_b	32	0.412	0.399	0.379	0.361	0.347	0.339	0.310	0.280	0.259	0.226	0.054	0.407	0.100	1.100
Medium fine	36														
ρ_b<1.20	11	0.583	0.570	0.547	0.516	0.496	0.484	0.422	0.331	0.276	0.184	0.031	0.562	0.012	1.242
1.20≤ρ_b<1.40	19	0.537	0.523	0.503	0.483	0.470	0.461	0.419	0.347	0.301	0.218	0.072	0.515	0.009	1.237
1.40≤ρ_b	6	0.394	0.388	0.367	0.354	0.347	0.343	0.314	0.250	0.200	0.138	0.039	0.376	0.006	1.276
Medium	386														
ρ_b<1.20	8	0.540	0.522	0.493	0.445	0.416	0.384	0.305	0.232	0.190	0.120	0.026	0.524	0.030	1.275
1.20≤ρ_b<1.40	59	0.495	0.464	0.435	0.397	0.371	0.352	0.290	0.230	0.192	0.133	0.033	0.474	0.039	1.231
1.40≤ρ_b<1.60	181	0.430	0.410	0.386	0.359	0.339	0.324	0.277	0.226	0.194	0.141	0.054	0.413	0.030	1.230
1.60≤ρ_b<1.80	119	0.373	0.357	0.335	0.311	0.296	0.284	0.250	0.214	0.189	0.150	0.064	0.362	0.049	1.188
1.80≤ρ_b	19	0.342	0.329	0.305	0.282	0.267	0.257	0.228	0.198	0.180	0.148	0.065	0.336	0.090	1.169
Coarse	108														
ρ_b<1.40	15	0.492	0.471	0.436	0.379	0.321	0.282	0.180	0.129	0.104	0.064	0.030	0.480	0.042	1.402
1.40≤ρ_b<1.60	41	0.409	0.383	0.349	0.299	0.256	0.228	0.161	0.119	0.099	0.062	0.019	0.398	0.067	1.315
1.60≤ρ_b<1.80	44	0.372	0.355	0.326	0.289	0.245	0.217	0.163	0.123	0.102	0.070	0.032	0.365	0.058	1.318
1.80≤ρ_b	8	0.302	0.289	0.271	0.249	0.232	0.220	0.180	0.141	0.118	0.083	0.028	0.291	0.032	1.252

[a] N, number of soil horizons; φ, total porosity; θ_i, volumetric water contents measured at -*i* kPa matric potentials.

Table 4. Performance analyses of the class pedotransfer functions based on the FAO texture triangle, established after stratification by texture classes, soil horizon, and bulk density.

class-PTF	N [a]	Mean Error of Predictions, MEP (cm^3/cm^3)	Root Mean Square Error, RMSE (cm^3/cm^3)
FAO texture classes			
Very fine	2	0.000	0.041
Fine	54	-0.004	0.069
Medium fine	12	0.006	0.062
Medium	129	-0.001	0.049
Coarse	36	0.002	0.059
All textures together	233	**-0.001**	**0.057**
FAO texture classes + soil horizon			
Very fine	-	-	-
Fine	55	0.000	0.067
Medium fine	13	0.001	0.061
Medium	129	0.003	0.049
Coarse	37	-0.004	0.056
All textures together	234	**0.001**	**0.056**
FAO texture classes + bulk density			
Very fine	-	-	-
Fine	54	0.002	0.052
Medium fine	13	-0.002	0.038
Medium	131	-0.001	0.038
Coarse	37	0.002	0.053
All textures together	235	**0.000**	**0.044**
FAO texture classes + soil horizon + bulk density			
Very fine	-	-	-
Fine	56	0.002	0.051
Medium fine	12	0.003	0.038
Medium	137	0.000	0.037
Coarse	38	0.001	0.051
All textures together	243	**0.001**	**0.043**

[a] N, number of soil horizons used in validation.

and coarse texture classes, respectively. The RMSE was 0.013 cm^3 cm^{-3} smaller for this class-PTF compared with that derived from texture class only. The performance of the class-PTF derived from the FAO texture classes and bulk density was better for the estimates produced for the medium fine and medium texture classes than for the fine texture class.

Inclusion of the type of horizon did not significantly improve the performance of the previous class-PTFs and thus they are not presented in detail. The RMSE values were only 0.001 cm^3 cm^{-3} smaller for these class-PTFs compared with those derived solely from texture class or when also considering bulk density (Table 4). Similar results were obtained by Al Majou et al. (2008b). A

possible explanation is related to the size of the cores (100 cm^3) used to develop the class-PTFs. This small sample volume may have led to overestimations of the bulk density in tilled horizons/layers, with consequent underestimations of volumetric soil-water retention values. Thus, the possible effect of including the type of horizon was not reached, as soil macroporosity was mostly not taken into account (Bruand et al., 2003). However, the constant sample volume used in all determinations (and generally standardized in many studies related to soil-water retention properties) allowed the comparison of different soils, land uses and managements, and laboratory methodologies. Other techniques, such as the clod bulk density, may be superior in those cases with tilled horizons because they may further include the structural (macroporosity) and textural porosity in tilled soils and their variability with time and management (Bruand et al., 2003).

The class-PTFs established according to the FAO texture classification and after stratification by texture classes, soil horizon, and bulk density produced RMSE values that varied between 0.043 and 0.057 cm^3 cm^{-3}. These were comparable to most results available in the literature for evaluating the performance of different class-PTFs (e.g. Wösten et al., 2001; Schaap et al., 2001; Bruand et al., 2003; Al Majou et al., 2008a). Of particular note, only Al Majou et al. (2008b) were able to obtain smaller RMSE (0.013–0.050 cm^3 cm^{-3}) than those of this study. Nevertheless, as the prediction accuracies depend on the extent of the area studied, on the spatial variability of soils within the area or database, and on the methods used for sampling and measurement (Wösten et al., 2001), the prediction accuracies found in the literature served here only as benchmarks.

3.2. Performance analyses of the class-PTFs based on ISSS texture classification

The class-PTFs based on the ISSS texture classification referred to (i) the 12 textural classes of the ISSS triangle, which are presented in Table 5; (ii) the ISSS texture classes and soil horizon, presented in Table 6; and (iii) the ISSS texture classes and bulk density, shown in Table 7. The resulting MEP and RMSE obtained for each of these class-PTFs are presented in Table 8. However, it was not possible to provide any estimate for the silt texture class, as the dataset contains no information for this texture (Fig. 2), and estimates for the sandy clay class were limited by the number of samples available.

The class-PTFs established for the ISSS texture classes (Table 5) produced an acceptable precision bias of the water retention estimates when considering all texture classes combined (MEP = 0.001±0.002 cm^3 cm^{-3}). However, the precision bias varied again slightly within each textural class, with water retention values in the clay loam texture class being underestimated and in the sandy clay texture class being overestimated. This latter relatively higher MEP value was obtained from only five soil horizons where the standard deviations (s.d.) of the water retention values in the different matric potentials were also high ($0.023 \leq$ s.d. ≤ 0.042). The clay loam and silty clay texture classes showed the highest uncertainty for the mean values of the water retention curve, with the 'true' values being associated with relatively large confidence intervals. The class-PTFs established for the ISSS texture classes also produced a large RMSE (0.052±0.001 cm^3 cm^{-3}) when considering all texture classes together, which may be comparable to the ones obtained for the class-PTFs based on FAO texture classification. Assuming 12 texture classes instead of five resulted in a decrease of the RMSE by 0.005 cm^3 cm^{-3}. Thus, moving from the five texture classes of the FAO triangle to the 12 texture classes of the ISSS system did not result in a significant increase of the class-PTFs prediction accuracy. This was likely explained by the fact that the class-PTFs presented in this study also accounted for the variability in bulk density values, thus inducing part of the variability in the volumetric water contents. For this reason, Bruand et al. (2003) first estimated the water content on a mass basis, and only then multiplied it by the horizon bulk density. Those authors showed that the variability was much smaller when the gravimetric water contents were first predicted.

In contrast to the results obtained with the class-PTFs based on the FAO texture classification, the inclusion of soil horizon information in the class-PTFs based on the ISSS texture classes (Table 6) slightly improved the performance of these latter class-PTFs, with RMSE being 0.003 cm^3 cm^{-3} smaller.

Finally, the class-PTFs established after the stratification of the ISSS texture classes and bulk density (Table 7) produced the best estimates of φ and soil water retention at different matric potentials. Again, the inclusion of soil structure information through the bulk density had a significant effect on the performance of the class-PTFs. The precision bias of the water retention estimates when considering all texture classes combined was good (MEP = 0.000 ± 0.002 cm^3 cm^{-3}; Table 8), although the water retention values were slightly underestimated in soils with silty

Table 5. Class pedotransfer functions established after stratification by ISSS texture classes.

class-PTF [a]	*N*	φ	Volumetric water content									van Genuchten's parameters			
			$\theta_{0.25}$	θ_{1}	$\theta_{3.2}$	$\theta_{6.3}$	θ_{10}	θ_{33}	θ_{100}	θ_{250}	θ_{1500}	θ_r	θ_s	α	η
			(cm^3 cm^{-3})									(cm^3 cm^{-3})		(cm^{-1})	(-)
Sand	18	0.398	0.370	0.329	0.243	0.165	0.127	0.065	0.042	0.040	0.021	0.018	0.386	0.060	1.661
Loamy sand	38	0.404	0.386	0.356	0.323	0.272	0.236	0.159	0.115	0.091	0.055	0.022	0.394	0.039	1.378
Sandy loam	121	0.404	0.384	0.356	0.323	0.297	0.278	0.224	0.174	0.147	0.104	0.031	0.392	0.047	1.243
Sandy clay loam	51	0.398	0.384	0.363	0.338	0.321	0.309	0.279	0.245	0.224	0.187	0.063	0.393	0.086	1.137
Sandy clay	8	0.416	0.399	0.370	0.338	0.309	0.293	0.256	0.223	0.202	0.170	0.069	0.413	0.129	1.169
Clay	74	0.491	0.478	0.454	0.429	0.413	0.402	0.368	0.332	0.308	0.268	0.040	0.488	0.117	1.090
Clay loam	83	0.429	0.416	0.395	0.373	0.357	0.346	0.314	0.279	0.257	0.219	0.044	0.425	0.097	1.107
Loam	171	0.429	0.404	0.379	0.351	0.331	0.317	0.269	0.218	0.184	0.128	0.028	0.410	0.033	1.214
Silty loam	62	0.456	0.441	0.417	0.392	0.376	0.361	0.313	0.247	0.206	0.142	0.053	0.436	0.015	1.269
Silt	-	-	-	-	-	-	-	-	-	-	-	-	-	-	-
Silty clay loam	25	0.517	0.507	0.486	0.461	0.446	0.434	0.392	0.327	0.290	0.218	0.059	0.502	0.017	1.183
Silty clay	46	0.568	0.559	0.545	0.525	0.507	0.490	0.443	0.390	0.353	0.290	0.050	0.561	0.040	1.129

[a] N, number of soil horizons; φ, total porosity; θ_i, volumetric water contents measured at -*i* kPa matric potentials.

Table 6. Class pedotransfer functions established after stratification by ISSS texture classes and soil horizon (topsoil and subsoil).

class-PTF [a]	*N*	*φ*	Volumetric water content									van Genuchten's parameters			
			$\theta_{0.25}$	θ_{1}	$\theta_{3.2}$	$\theta_{6.3}$	θ_{10}	θ_{33}	θ_{100}	θ_{250}	θ_{1500}	θ_r	θ_s	α	η
			(cm^3 cm^{-3})									(cm^3 cm^{-3})		(cm^{-1})	(-)
Topsoils	312														
Sand	6	0.439	0.415	0.371	0.275	0.204	0.164	0.076	0.052	0.049	0.026	0.023	0.427	0.053	1.673
Loamy sand	19	0.446	0.429	0.391	0.348	0.297	0.260	0.175	0.127	0.099	0.065	0.030	0.435	0.044	1.376
Sandy loam	65	0.402	0.383	0.352	0.321	0.295	0.277	0.223	0.177	0.152	0.109	0.044	0.389	0.047	1.255
Sandy clay loam	22	0.410	0.397	0.369	0.337	0.318	0.306	0.272	0.235	0.211	0.174	0.051	0.407	0.119	1.133
Sandy clay	-	-	-	-	-	-	-	-	-	-	-	-	-	-	-
Clay	37	0.505	0.492	0.463	0.431	0.411	0.398	0.360	0.323	0.300	0.258	0.056	0.504	0.145	1.104
Clay loam	33	0.461	0.448	0.420	0.389	0.369	0.355	0.315	0.277	0.253	0.215	0.043	0.459	0.127	1.118
Loam	85	0.444	0.413	0.384	0.352	0.330	0.315	0.266	0.215	0.179	0.120	0.014	0.422	0.040	1.209
Silty loam	24	0.452	0.437	0.413	0.386	0.366	0.349	0.300	0.231	0.192	0.130	0.031	0.435	0.020	1.247
Silt	-	-	-	-	-	-	-	-	-	-	-	-	-	-	-
Silty clay loam	7	0.507	0.495	0.476	0.450	0.432	0.419	0.373	0.312	0.274	0.205	0.055	0.493	0.028	1.188
Silty clay	14	0.574	0.564	0.547	0.524	0.498	0.479	0.422	0.364	0.328	0.265	0.056	0.570	0.036	1.143
Subsoils	377														
Sand	12	0.377	0.351	0.313	0.230	0.139	0.102	0.056	0.035	0.032	0.017	0.016	0.364	0.055	1.778
Loamy sand	19	0.370	0.351	0.329	0.300	0.251	0.213	0.140	0.098	0.077	0.044	0.018	0.359	0.034	1.415
Sandy loam	56	0.406	0.387	0.362	0.329	0.304	0.286	0.230	0.175	0.144	0.099	0.024	0.392	0.037	1.250
Sandy clay loam	29	0.387	0.372	0.356	0.337	0.323	0.311	0.283	0.250	0.232	0.194	0.068	0.379	0.063	1.131
Sandy clay	-	-	-	-	-	-	-	-	-	-	-	-	-	-	-
Clay	37	0.476	0.464	0.444	0.424	0.411	0.402	0.373	0.338	0.314	0.275	0.045	0.471	0.084	1.086
Clay loam	50	0.412	0.399	0.381	0.364	0.352	0.343	0.315	0.281	0.259	0.221	0.064	0.404	0.055	1.115
Loam	86	0.408	0.390	0.368	0.344	0.325	0.312	0.266	0.217	0.185	0.133	0.053	0.356	0.024	1.247
Silty loam	38	0.456	0.441	0.417	0.394	0.380	0.368	0.320	0.255	0.212	0.146	0.055	0.434	0.013	1.270
Silt	-	-	-	-	-	-	-	-	-	-	-	-	-	-	-
Silty clay loam	18	0.508	0.498	0.478	0.455	0.441	0.431	0.394	0.334	0.298	0.229	0.053	0.494	0.017	1.166
Silty clay	32	0.565	0.556	0.544	0.525	0.511	0.496	0.454	0.402	0.367	0.304	0.054	0.558	0.020	1.123

[a] N, number of soil horizons; φ, total porosity; θ_i, volumetric water contents measured at -*i* kPa matric potentials.

Table 7. Class pedotransfer functions established after stratification by ISSS texture classes and dry bulk density (ρ_b).

class-PTF [a]	N	φ	Volumetric water content									van Genuchten's parameters			
			$\theta_{0.25}$	θ_{1}	$\theta_{3.2}$	$\theta_{6.3}$	θ_{10}	θ_{33}	θ_{100}	θ_{250}	θ_{1500}	θ_r	θ_s	α	η
			(cm^3/cm^3)									(cm^3/cm^3)		(1/cm)	(-)
Sand	18														
ρ_b<1.60	10	0.421	0.392	0.352	0.258	0.198	0.162	0.076	0.052	0.049	0.026	0.018	0.409	0.065	1.586
1.60≤ρ_b	8	0.374	0.350	0.309	0.226	0.121	0.082	0.050	0.029	0.026	0.015	0.014	0.360	0.050	1.906
Loamy sand	38														
ρ_b<1.40	10	0.494	0.474	0.437	0.381	0.321	0.280	0.186	0.127	0.097	0.059	0.052	0.482	0.042	1.404
1.40≤ρ_b<1.60	12	0.411	0.390	0.361	0.327	0.263	0.224	0.144	0.107	0.085	0.051	0.028	0.399	0.039	1.437
1.60≤ρ_b	16	0.352	0.337	0.312	0.292	0.253	0.219	0.154	0.110	0.091	0.057	0.025	0.342	0.030	1.372
Sandy loam	121														
ρ_b<1.40	21	0.502	0.480	0.448	0.403	0.368	0.343	0.272	0.207	0.171	0.112	0.018	0.488	0.043	1.247
1.40≤ρ_b<1.60	43	0.421	0.399	0.369	0.338	0.312	0.295	0.235	0.177	0.148	0.101	0.026	0.405	0.038	1.254
1.60≤ρ_b<1.80	45	0.365	0.348	0.322	0.292	0.270	0.253	0.208	0.167	0.141	0.104	0.023	0.356	0.061	1.208
1.80≤ρ_b	12	0.322	0.309	0.281	0.256	0.240	0.230	0.192	0.154	0.132	0.099	0.035	0.313	0.054	1.219
Sandy clay loam	51														
ρ_b<1.60	21	0.432	0.416	0.389	0.360	0.341	0.329	0.293	0.256	0.233	0.195	0.059	0.427	0.111	1.135
1.60≤ρ_b<1.80	25	0.373	0.359	0.344	0.322	0.308	0.296	0.269	0.237	0.219	0.183	0.060	0.367	0.072	1.130
1.80≤ρ_b	5	0.350	0.342	0.325	0.304	0.289	0.276	0.249	0.223	0.202	0.166	0.055	0.346	0.075	1.144
Sandy clay	-	-	-	-	-	-	-	-	-	-	-	-	-	-	-
Clay	74														
ρ_b<1.20	5	0.564	0.548	0.507	0.451	0.420	0.406	0.371	0.328	0.309	0.266	0.104	0.567	0.262	1.129
1.20≤ρ_b<1.40	27	0.523	0.508	0.477	0.447	0.425	0.412	0.376	0.338	0.313	0.273	0.063	0.521	0.164	1.100
1.40≤ρ_b<1.60	32	0.469	0.459	0.439	0.419	0.405	0.395	0.362	0.327	0.302	0.260	0.030	0.464	0.070	1.091
1.60≤ρ_b	10	0.436	0.427	0.408	0.392	0.382	0.375	0.346	0.314	0.294	0.258	0.055	0.431	0.068	1.090
Clay loam	83														
ρ_b<1.40	13	0.521	0.508	0.468	0.432	0.408	0.390	0.339	0.296	0.267	0.223	0.041	0.520	0.132	1.128
1.40≤ρ_b<1.60	34	0.441	0.428	0.408	0.384	0.370	0.358	0.324	0.285	0.262	0.220	0.039	0.434	0.065	1.114
1.60≤ρ_b<1.80	31	0.392	0.380	0.364	0.347	0.334	0.326	0.301	0.273	0.252	0.220	0.064	0.386	0.076	1.103
1.80≤ρ_b	5	0.382	0.369	0.353	0.337	0.326	0.319	0.295	0.268	0.252	0.220	0.053	0.374	0.078	1.095

[a] N, number of soil horizons; φ, total porosity; θ_i, volumetric water contents measured at -*i* kPa matric potentials.

Table 7 (continuation). Class pedotransfer functions established after stratification by ISSS texture classes and dry bulk density (ρ_b).

class-PTF [a]	N	φ	Volumetric water content									van Genuchten's parameters			
			$\theta_{0.25}$	θ_{1}	$\theta_{3.2}$	$\theta_{6.3}$	θ_{10}	θ_{33}	θ_{100}	θ_{250}	θ_{1500}	θ_r	θ_s	α	η
			(cm^3/cm^3)									(cm^3/cm^3)		(1/cm)	(-)
Loam	171														
ρ_b<1.40	29	0.494	0.455	0.423	0.382	0.357	0.342	0.283	0.226	0.186	0.124	0.021	0.468	0.045	1.225
1.40≤ρ_b<1.60	95	0.434	0.409	0.386	0.359	0.339	0.324	0.274	0.220	0.185	0.124	0.024	0.413	0.027	1.224
1.60≤ρ_b	47	0.370	0.355	0.330	0.308	0.292	0.280	0.244	0.206	0.177	0.134	0.057	0.356	0.035	1.220
Silty loam	62														
ρ_b<1.20	6	0.552	0.538	0.519	0.490	0.480	0.456	0.390	0.301	0.243	0.154	0.030	0.531	0.010	1.282
1.20≤ρ_b<1.40	19	0.520	0.501	0.478	0.452	0.434	0.417	0.362	0.286	0.239	0.163	0.030	0.498	0.026	1.231
1.40≤ρ_b<1.60	21	0.432	0.419	0.392	0.364	0.344	0.329	0.282	0.225	0.191	0.134	0.035	0.418	0.027	1.224
1.60≤ρ_b	16	0.382	0.369	0.348	0.330	0.318	0.310	0.277	0.224	0.188	0.137	0.048	0.364	0.015	1.235
Silt	-	-	-	-	-	-	-	-	-	-	-	-	-	-	-
Silty clay loam	25														
ρ_b<1.20	7	0.600	0.588	0.564	0.530	0.507	0.493	0.428	0.330	0.278	0.182	0.021	0.580	0.013	1.238
1.20≤ρ_b<1.40	10	0.534	0.523	0.502	0.480	0.466	0.457	0.420	0.361	0.323	0.248	0.047	0.518	0.017	1.155
1.40≤ρ_b	8	0.403	0.392	0.375	0.354	0.343	0.331	0.304	0.272	0.250	0.212	0.070	0.397	0.061	1.122
Silty clay	46														
ρ_b<1.20	17	0.597	0.591	0.577	0.557	0.529	0.507	0.450	0.391	0.352	0.282	0.049	0.597	0.028	1.141
1.20≤ρ_b<1.40	23	0.565	0.555	0.542	0.523	0.510	0.496	0.452	0.399	0.362	0.299	0.051	0.556	0.020	1.125
1.40≤ρ_b	6	0.495	0.481	0.461	0.432	0.418	0.411	0.383	0.347	0.330	0.289	0.055	0.491	0.120	1.085

[a] N, number of soil horizons; φ, total porosity; θ_i, volumetric water contents measured at -*i* kPa matric potentials.

Table 8. Performance analyses of the class pedotransfer functions based on the ISSS texture triangle, established after stratification by texture classes, soil horizon, and bulk density.

class-PTF	N [a]	Mean Error of Predictions, MEP (cm^3/cm^3)	Root Mean Square Error, RMSE (cm^3/cm^3)
ISSS texture classes			
Sand	6	0.003	0.054
Loamy sand	13	-0.001	0.055
Sandy loam	41	-0.003	0.053
Sandy clay loam	17	0.005	0.045
Sandy clay	3	0.009	0.103
Clay	25	0.001	0.049
Clay loam	28	-0.004	0.048
Loam	57	0.005	0.042
Silty loam	21	-0.002	0.064
Silt	-	-	-
Silty clay loam	9	0.011	0.068
Silty clay	16	0.000	0.047
All texture together	236	**0.001**	**0.052**
ISSS texture classes + soil horizon			
Sand	6	0.000	0.050
Loamy sand	14	0.001	0.046
Sandy loam	41	0.001	0.051
Sandy clay loam	18	0.002	0.043
Sandy clay	-	-	-
Clay	26	-0.002	0.049
Clay loam	28	-0.001	0.047
Loam	58	-0.003	0.040
Silty loam	21	-0.006	0.066
Silt	-	-	-
Silty clay loam	9	-0.002	0.067
Silty clay	16	0.002	0.049
All texture together	237	**-0.001**	**0.049**
ISSS texture classes + bulk density			
Sand	7	0.004	0.053
Loamy sand	14	0.004	0.043
Sandy loam	41	0.001	0.036
Sandy clay loam	18	0.001	0.040
Sandy clay	-	-	-
Clay	26	-0.004	0.046
Clay loam	30	0.002	0.039
Loam	58	0.000	0.032
Silty loam	22	0.005	0.044
Silt	-	-	-
Silty clay loam	10	-0.005	0.033
Silty clay	16	-0.001	0.042
All texture together	242	**0.000**	**0.039**

[a] N, number of soil horizons used in validation.

clay loam texture and overestimated in soils with silty loam texture. The precision bias was thus worst for soils with medium textures. Gonçalves et al. (1997) had already faced similar difficulties in deriving continuous-PTFs for medium texture soils when using an early version of this dataset (230 soil horizons). The RMSE relative to all texture classes combined was the lowest obtained for all of the class-PTFs developed in this study (RMSE = 0.039 ± 0.001 cm^3 cm^{-3}). The estimations for the loam soils were again the most accurate, whereas the results for sandy soils were worst.

3.3. Do we need new PTFs?

Table 9 presents the accuracy of published PTFs (Gonçalves et al., 1997, 1999; Wösten et al., 1999; Paz et al., 2009) that used a portion of our data. These PTFs were now tested on the entire dataset to evaluate their performance in predicting the hydraulic behavior of the Portuguese soils. Most of them refer to parametric PTFs that describe the water retention properties as continuous curves using the van Genuchten model (Eqn. 1), thus allowing the computation and comparison of water retention values at the corresponding matric potentials developed for the class-PTFs. The only exceptions were the point PTFs developed by Paz et al. (2009) for specific pressure heads, namely, for soil water retention at –0.25, –10, and –1500 kPa matric potentials.

Gonçalves et al. (1997) and Wösten et al. (1999) developed continuous PTFs for *all soils* (i.e. without grouping data) that resulted in similar RMSE values (0.044 and 0.045 cm^3 cm^{-3}) when using various predictors instead of texture classes (Table 9). The errors found were thus comparable to the ones obtained for the class-PTFs based on the FAO texture classes (Table 4) and for most of the class-PTFs based on the ISSS texture classes (Table 8). The exception was the class-PTFs established after the stratification by ISSS texture classes and bulk density (Table 7), which resulted in a lower RMSE (0.039 cm^3 cm^{-3}). Hence, these results show that estimates similar to, or even better than, those obtained by much more sophisticated functions could be achieved with the simpler PTFs presented. Nonetheless, the main advantage of the class-PTFs is the reduced number of basic predictors necessary to estimate the water retention properties of Portuguese soils. For a country where soil cartography shows so many constraints, as previously discussed, the number of predictors in a PTF is significant for those interested in mapping the water retention properties of soils.

Table 9. Accuracy of published pedotransfer functions in the estimation of water retention properties of soil horizons included in the dataset.

Published PTFs					**Accuracy of PTFs**[d]			
Study	**Method**[a]	**Model**	**Dataset**[b]	**Predictors**[c]	**Texture class**	**N**	**ME**	**RMSE**
1. Gonçalves *et al*. (1997)	RA, continuous PTFs	VG, m=1	230	CS, FS, $Si_{20\ \mu m}$, C, ρ_b, Z, OM, pH	-	440	**-0.002**	**0.045**
2. Gonçalves *et al*. (1997)	RA, continuous PTFs	VG, m=1	230	CS, FS, $Si_{20\ \mu m}$, C, ρ_b, Z, OM, pH	Fine	152	-0.008	0.050
					Medium	206	-0.002	0.048
					Coarse	82	-0.000	0.047
					All textures together	440	**-0.004**	**0.049**
3. Gonçalves *et al*. (1999)	RA, continuous PTFs	VG, m=1-1/η	70	CS, FS, $Si_{20\ \mu m}$, C, ρ_b, OM, pH	-	440	**0.019**	**0.067**
4. Paz *et al*. (2009)	RA, point PTFs	-	304	CS, FS, $Si_{20\ \mu m}$, C, ρ_b, Z	-	697	**-0.018**	**0.128**
5. Wösten *et al*. (1999)	GM, class PTFs	VG, m=1-1/η	54	FAO texture classes, depth	Very fine	5	0.043	0.062
					Fine	162	0.026	0.075
					Medium fine	17	-0.104	0.113
					Medium	421	0.014	0.057
					Coarse	92	-0.009	0.061
					All textures together	697	**0.011**	**0.064**
6. Wösten *et al*. (1999)	RA, continuous PTFs	VG, m=1-1/η	54	$Si_{50\ \mu m}$, C, ρ_b, OM, depth	-	626	**-0.019**	**0.044**

[a] RA, regression analysis; GM, geometric means.
[b] Data used in the development of the PTFs.
[c] CS, coarse sand; FS, fine sand; $Si_{20\ \mu m}$, Silt fraction at 20 μm; $Si_{50\ \mu m}$, Silt fraction at 50 μm; C, clay; ρ_b, bulk density; Z, mean depth; OM, Organic matter; depth, qualitative variable having the values 1 (topsoils) and 0 (subsoils).
[d] N, number of samples where the PTF could be applied; MEP, Mean Error of Predictions; RMSE, Root Mean Square Error.

Wösten et al. (1999) also provided class-PTFs for European soils by grouping data by FAO texture classes and soil horizon. These resulted in RMSE= 0.064 cm^3 cm^{-3} when applied to our dataset (Table 9). Thus, the class-PTFs developed in this study, which used exactly the same inputs (Table 4), resulted in better estimates than the previous study. Curiously, the performance of the PTFs developed using the HYPRES database (Wösten et al., 1999) in predicting the hydraulic behavior of the Portuguese soils had not been previously assessed. Although the contribution from Portugal was only minor (54 soil horizons/ layers; 104 samples with repetitions), the estimates of water retention properties can be considered adequate.

The literature on PTFs is abundant, and hydrological modelers may well find alternatives to the class-PTFs presented here (e.g. Schaap et al., 2001). However, the use of such 'external' PTFs causes two basic problems extensively discussed in the literature that should be first taken into account: (i) most 'external' or 'international' PTFs were never tested with Portuguese soil data, which means that the hydraulic characteristics of the Portuguese soils may fall outside the range of the original databases used to develop those PTFs (Wösten et al., 2001); and (ii) most PTFs were developed using different texture systems (normally the USDA texture system) from the one used in the Portuguese soil survey database (the ISSS system). Interpolation techniques are thus necessary to convert the ISSS texture limits into those required by 'international' PTFs (Nemes et al., 1999; Shirazi et al., 2001; Nemes and Rawls 2006). Users cannot simply start using PTFs regardless of their textural and regional validity.

3.4. Integrating soil hydraulic properties into soil mapping units

Figure 3 presents four different maps of the AWC for the Enxoé catchment. The maps were derived after integrating the class-PTFs into local soil maps (1 : 25 000) using the class-PTFs established according to the FAO texture classes (Fig. 3*a*), the FAO texture classes and bulk density (Fig. 3*b*), the ISSS texture classes (Fig. 3*c*), and the ISSS texture classes and bulk density (Fig. 3*d*).

The maps derived solely from soil texture classes (Fig. 3*a*, *c*) showed greater differences in AWC than the maps developed with both texture classes and bulk density (Fig. 3*b*, *d*). Differences among the four AWC maps were quite meaningful, namely in the eastern region of the catchment area where they approach 50mm in some locations (Fig. 4).

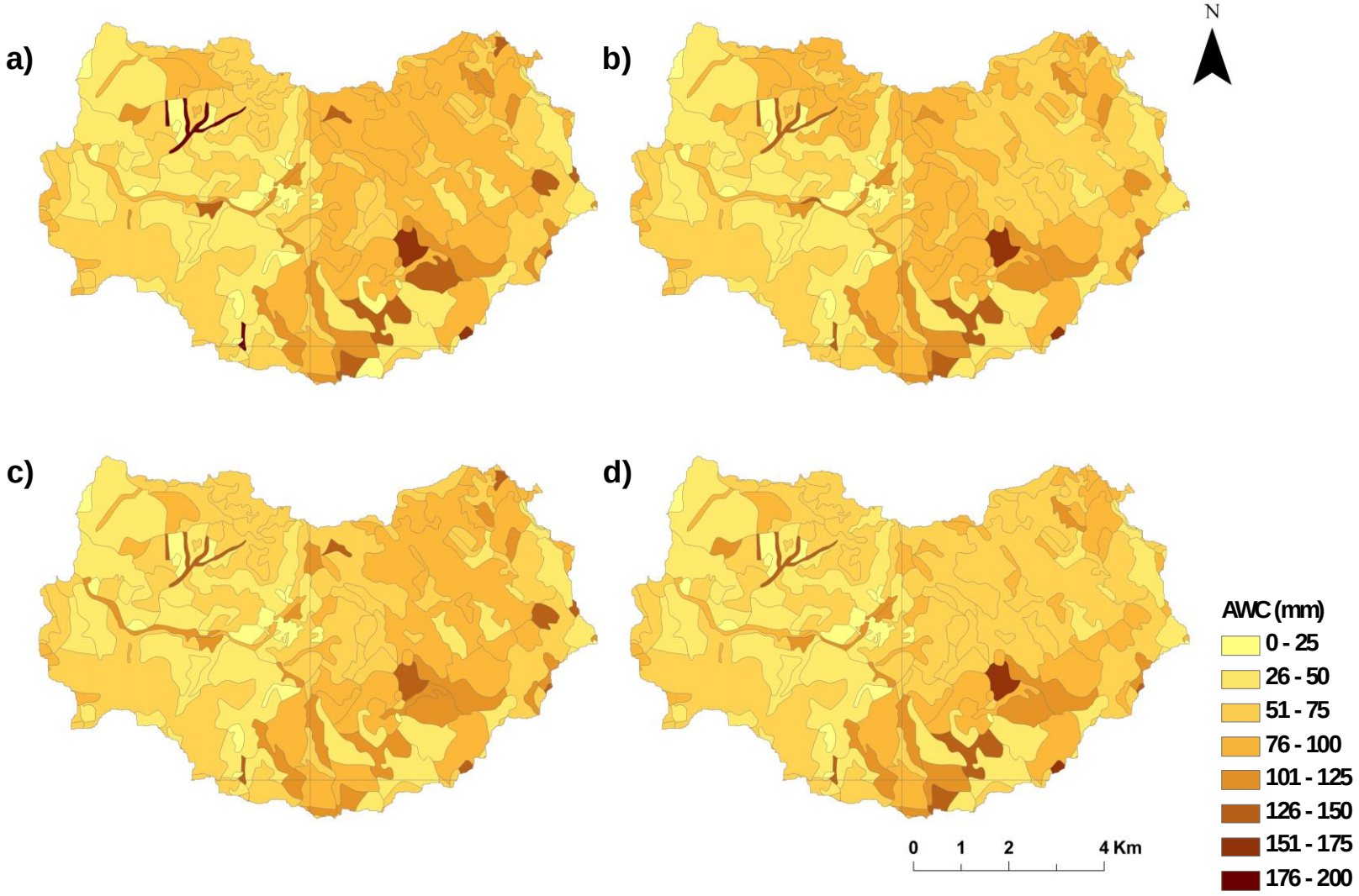

Fig. 3. Available water capacity (AWC) maps derived for the Enxoé catchment area by integrating the class-PTFs, established after grouping data by (*a*) FAO texture classes, (*b*) FAO textural classes and bulk density, (*c*) ISSS texture classes, (*d*) and ISSS texture classes and bulk density, into Portuguese soil maps at a scale of 1 : 25 000.

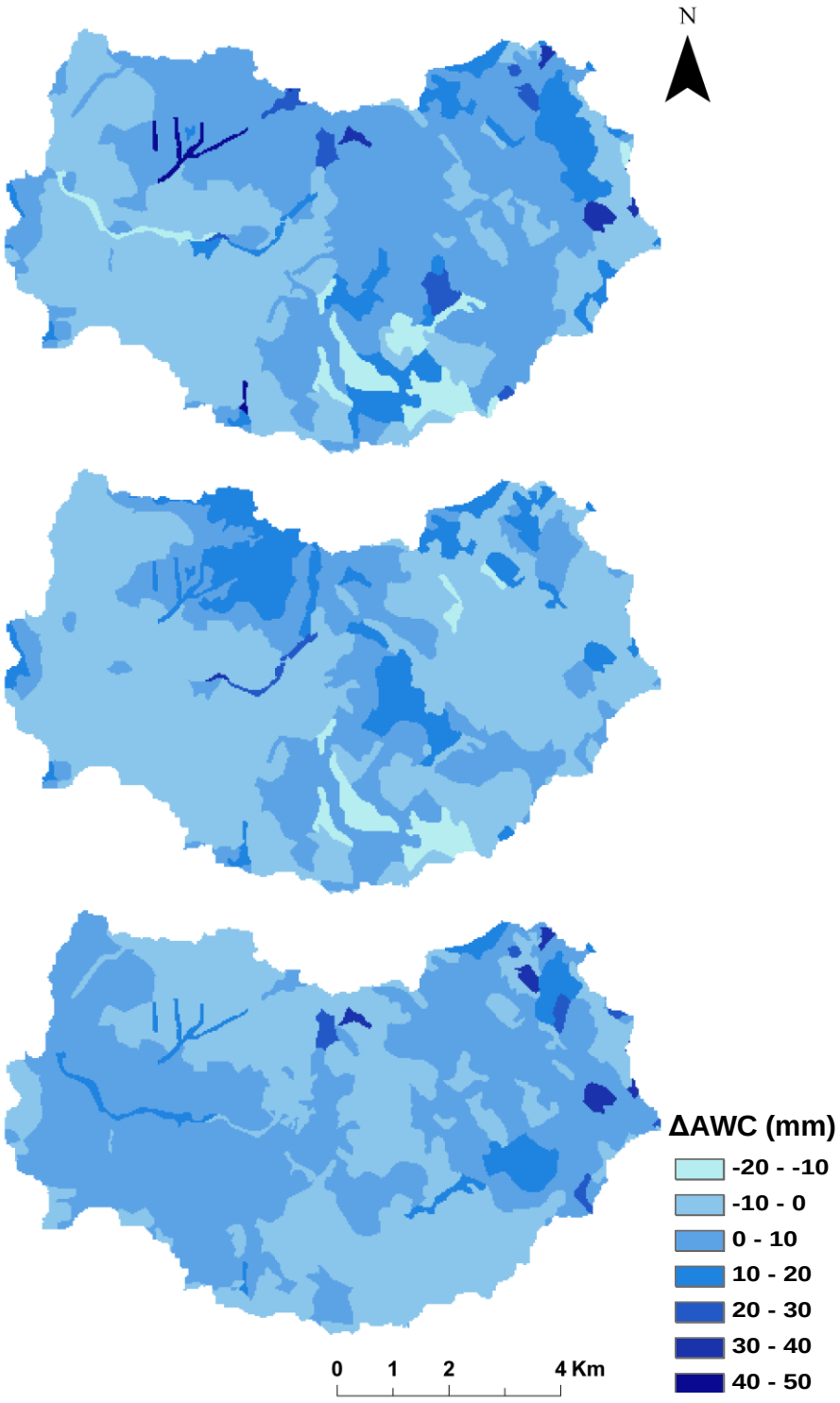

Fig. 4. Differences between the available water capacity (AWC) maps derived from the class-PTFs established after grouping data by FAO texture classes (top); FAO textural classes and bulk density (middle); ISSS texture classes (bottom) and the map derived from the class-PTFs established after the stratification of the ISSS texture classes and bulk density (reference map).

The approach presented here is the simplest, most inexpensive, and most feasible technique available today to modelers for characterizing soil hydraulic properties at large scales (Al Majou et al., 2008b), especially considering constraints such as those discussed above that are relevant to the Portuguese soil survey database. This approach was performed simply by grouping all of the available information on water retention properties of Portuguese soils in such a way that the derived maps were not validated *per se*. However, this information should facilitate soil characterization for many of the applications being performed presently. No unique approach exists for upscaling soil hydraulic properties from soil cores to large catchment areas (Vogel and Roth, 2003; Lin et al., 2006; Vereecken et al., 2007; Lin, 2010). Most of these techniques are certainly more complex than the one presented here. Most of them also require more information on soil hydraulic properties than currently available for characterizing catchment areas in Portugal, in particular those using geostatistical methods. One advantage of the approach followed here is that modelers can optimize the water retention values of the catchment soils during parameter calibration, a common procedure in hydrological modeling for fitting measured and simulated discharges in the catchment area. However, modelers should be aware that going outside the confidence intervals of the considered class-PTFs would be ill advised.

Integration of class-PTFs into soil mapping units would ideally require minimal surveyed soil data (texture classes and bulk density) from the catchment area to better characterize soil hydraulic properties locally. Skilled pedologists can even determine soil texture classes manually. Hydrological modelers who do not possess such skills and cannot afford minimal soil survey studies should alternatively look for the required information in the representative soil profiles published in soil survey or PROPSOLO databases (Gonçalves et al., 2011). For bulk density, the latter database is the only option available. Particular attention should be given to soil complexes, i.e. soil mapping units that include two or more soil units that cannot be represented separately at a specific scale on the soil map. For these complexes, Portuguese soil maps generally have the weighted distribution of each soil within the mapping unit. The quantification of map unit purity for different scales of soil maps is of fundamental importance for improving modern hydrological applications (Lin et al., 2006; Lin, 2010). Therefore, that information should not be ignored. In Fig. 3, the AWC of soil complexes was in fact computed based on the weight of each soil unit within the soil-mapping unit. If information is available, the PTF with the smaller error should be

used (Wösten et al., 2001; McBratney et al., 2002), this being the class-PTFs based on the ISSS texture classes and bulk density (Fig. 3*d*; Table 8).

3.5. Sensitivity analysis of a catchment model to different estimates of AWC

The SWAT model simulations of the catchment water balance using different AWC inputs are presented in Table 10. The information available in the European Soil Database and used in Brito et al. (2012) was estimated over large areas by expert judgment rather than measured on local soil samples. These estimations resulted from synthesis and generalization of national or regional maps published at more detailed scales (Daroussin et al., 2006). Nevertheless, despite the use of generic, coarse-scale soil data, SWAT predicted reasonably well the monthly inflows of the catchment reservoir (NSE = 0.75), as shown by Brito et al. (2012).

Table 10. Water balance components of the Enxoé catchment estimated using the SWAT model based on different Available Water Capacity inputs.

Available water capacity inputs	Water balance components (%)				
	Runoff	Lateral flow	Evapotranspiration	Groundwater recharge	Deep aquifer loss
1. European Soil Database					
Representative soil profiles	6.7	0.5	77.6	13.7	0.7
2. Class-PTFs					
FAO texture classes	5.6	2.1	73.2	17.6	0.9
FAO texture classes + soil horizon	5.6	1.8	73.3	17.9	0.9
FAO texture classes + bulk density	5.8	1.7	72.5	18.5	1.0
FAO texture classes + soil horizon+ bulk density	5.8	1.7	72.9	18.0	1.0
ISSS texture classes	5.9	1.6	73.2	17.4	0.9
ISSS texture classes + soil horizon	5.9	1.6	72.8	17.7	0.9
ISSS texture classes + bulk density	6.0	1.6	72.8	17.9	0.9

The use of AWC soil maps at 1 : 25 000 derived from the class-PTFs as model inputs resulted in small differences compared with the results reported in Brito et al. (2012). The largest differences were found for the actual evapotranspiration, which decreased up to 4.6% when using the more detailed soil maps, whereas groundwater recharge increased up to 4.2% (Table 10). The small differences found were not particularly surprising, because the long-term results represent

average annual behavior (30-year simulation) and the difference in the level of detail of inputs is filtered in such a time scale. The fact that two datasets of distinct origins yield similar outputs confirms the results obtained in Enxoé.

A successful simulation of the reservoir inflow was obtained using all class-PTFs (Fig. 5; NSE >0.73). For long-term assessment (30-year water balance), the AWC soil maps at 1 : 25 000 derived from each of the class-PTFs successful estimated the water balance components of the Enxoé watershed. Moreover, these maps described soil spatial and vertical heterogeneity in more detail than the coarse-scaled maps and are suited to implementations where the heterogeneity may be crucial for describing small-scale (space or time) processes (e.g. heavy rain concentrated in small areas producing localized runoff). Thus, although the use of AWC estimates based on different origins and levels of detail led to the equifinality problem (Ebel and Loague, 2006; Bouma et al., 2011) in SWAT, i.e. different conditions led to the same effects, the use of more detailed soil maps complemented with the information provided by the class-PTFs contributed meaningfully to a better soil characterization than that resulting from using coarse-scaled information.

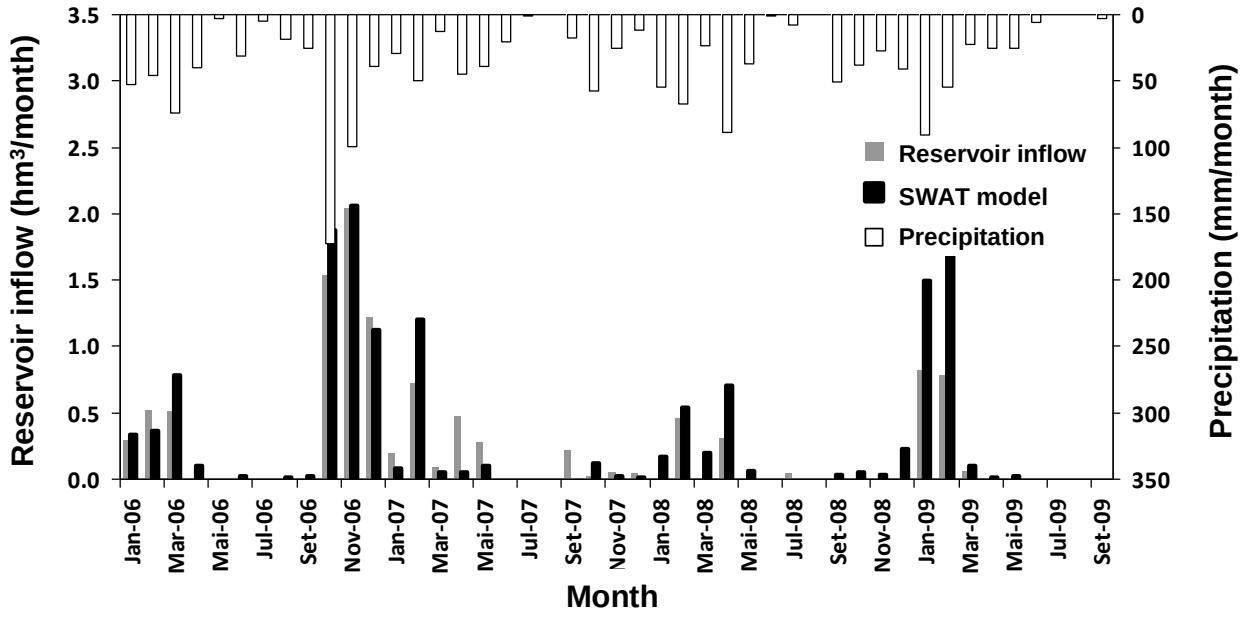

Fig. 5. Measured and simulated monthly inflows at the Enxoé reservoir.

The integration of the different class-PTFs into soil maps at 1 : 25 000 (Fig. 3) and their use as inputs to the SWAT model resulted in only small variations in the water balance components (Table 10). The largest variations were found for the actual evapotranspiration and groundwater recharge fractions, which varied only 0.8 and 1.1%, respectively. These small variations were somewhat expected because those maps also showed small variations in the AWC for most of the area (Fig. 4). Nonetheless, the class-PTF estimates may eventually be used as an inexpensive alternative to account for soil spatial variability in catchment areas.

4. Conclusions

The class-PTFs developed for Portuguese soils were established after stratifying data by texture classes, soil horizon, and bulk density. The accuracy of the predictions varied between 0.039 and 0.057 cm^3 cm^{-3}. The best performances were obtained for the class-PTFs established after grouping the data by the 12 texture classes based on the ISSS particle limits and bulk density. The inclusion of the horizon type only slightly improved the prediction performance of the class-PTFs. The confidence intervals of the estimates were relatively narrow for most classes, with the exception of clay loam and silty clay texture classes.

Portuguese soil maps currently have many constraints to their use in modern hydrological studies. The class-PTFs developed here may partially overcome those constraints as they may be easily integrated into soil maps because only very basic soil data are required. For incorporating such information, minimal soil survey studies (texture classes and bulk density) need to be performed. For modelers without the necessary resources, the analysis of representative soil profiles included in soil survey or PROPSOLO databases would serve as an alternative. However, the use of those soil maps with different AWC estimates according to the integrated class-PTFs may only result in minimal differences when modeling the catchment water balance or other applications with a process-based, distributed hydrological model such as SWAT, which is less sensitive to the soil hydraulic properties. Nonetheless, those inputs may contribute to a better soil characterization than when using coarse-scaled information.

The approach presented here gathered all of the currently available knowledge on soil hydraulic properties of Portuguese soils. This approach is the simplest, cheapest, and most feasible

technique available today to modelers without many resources for characterizing water retention properties at large scales.

Acknowledgments

This research was performed within the framework of the Project PTDC/AGR-AAM/098100/2008 of the Fundação para a Ciência e a Tecnologia (FCT). T. B. Ramos was funded by the FCT grant SFRH/BD/60363/2009.

References

Al Majou, H., Bruand, A., Duval, O., Le Bas, C., 2008a. The use of in situ volumetric water content at field capacity to improve the predictions of soil water retention properties. Can. J. Soil Sci. 88, 533-541, doi:10.4141/CJSS07065.

Al Majou, H., Bruand, A., Duval, O., Le Bas, C., Vautier, A., 2008b. Prediction of soil water retention properties after stratification by combining texture, bulk density and the type of horizon. Soil Use Manage. 24, 383-391, doi:10.1111/j.1475-2743.2008.00180.x.

Allen, R.G., Pereira, L.S., Raes, D., Smith, M., 1998. Crop evapotranspiration – Guidelines for computing crop water requirements. Irrig. Drain. Paper 56, FAO, Rome, Italy.

Baker, L., 2008. Development of class pedotransfer functions of soil water retention – A refinement. Geoderma 144, 225-230, doi:10.1016/j.geoderma.2007.11.017.

Bouma, J., 1989. Using soil survey data for quantitative land evaluation. Adv. Soil Sci. 9, 177-213.

Bouma, J., 2006. Hydropedology as a powerful tool for environmental policy research. Geoderma 131, 275-286, doi:10.1016/j.geoderma.2005.03.009.

Bouma, J., Droogers, P., Sonneveld, M.P.W., Ritsema, C.J., Hunink, J.E., Immerzeel, W.W., Kauffman, S., 2011. Hydropedological insights when considering catchment classification. Hydrol. Earth Syst. Sci. 15, 1909-1919, doi:10.5194/hess-15-1909-2011.

Bruand, A., Pérez Fernandez, P., Duval, O., 2003. Use of class pedotransfer functions based on texture and bulk density of clods to generate water retention curves. Soil Use Manage. 19, 232-242, doi: 10.1111/j.1475-2743.2003.tb00309.x.

Brito, D., Neves, R., Branco, M.A., Prazeres, Â., Rodrigues, S., Gonçalves, M.C., Ramos, T.B., 2012. Assessing the long-term dynamics and nutrient loads to an eutrophic reservoir in a temporary river in southeast Portugal (Enxoé). J. Hydrol. (under review).

Cardoso, J.C., 1965. Os Solos de Portugal. Sua classificação, caracterização e génese. I – A sul do Rio Tejo. Direcção Geral dos Serviços Agrícolas, Lisboa.

Dane, J.H., Hopmans, J.W., 2002. Pressure plate extractor. In: Dane, J.H., Topp, G.C. (Eds.), Methods of Soil Analysis, Part 4. Physical Methods, pp. 688-690. Soil Science Society of America book Series, Madison, Wisconsin.

Dane, J.H., Topp, G.C., 2002. Methods of soil analysis. Part 4. Physical methods. Soil Science Society of America book Series, Madison, Wisconsin.

Daroussin, J., King, D., Le Bas, C., Vrščaj, B., Dobos, E., Montanarella, L., 2006. The Soil Geographical Database of Eurasia at Scale 1:1.000.000: history and perspective in digital soil mapping. Dev. Soil Sci. 31, 55–65, doi:10.1016/S0166-2481(06)31004-5.

Duarte, P., Azevedo, B., Guerreiro, M., Ribeiro, C., Bandeira, R., Pereira, A., Falcão, M., Serpa, D., Reia, J., 2008. Biochemical modelling of Ria Formosa (South Portugal). Hydrobiologia 611, 115-132, doi:10.1007/s10750-008-9464-3.

Ebel, B.A., Loague, K., 2006. Physics-based hydrologic-response simulation: Seeing through the fog of equifinality. Hydrol. Proc. 20, 2887-2900, doi:10.1002/hyp.6388.

FAO, 1998. World Reference Base for Soil Resources. 84 World Soil Resources Reports, FAO: Rome.

Gomes, M.P., Silva, A.A., 1962. Um novo diagrama triangular para a classificação básica da textura do solo. Garcia da Orta 10, 171–179.

Gomes, M.P., Silva, A.A., 1980. Inserção das grandes divisões e subdivisões da textura do solo adoptadas pela FAO (1970) no diagrama de classificação de Gomes & Silva (1962). Congresso 80 da Ordem dos Engenheiros, Coimbra.

Gonçalves, M.C., Pereira, L.S., Leij, F.J., 1997. Pedo-transfer functions for estimating unsaturated hydraulic properties of Portuguese soils. Eur. J. Soil Sci. 48, 387-400, doi:10.1111/j.1365-2389.1997.tb00205.x.

Gonçalves, M.C., Almeida, V.V., Pereira, L.S., 1999. Estimation of hydraulic parameters for Portuguese soils. In: van Genuchten, M.Th., Leij, F., Wu, L. (Eds.), Characterization and measurement of the hydraulic properties of unsaturated porous media. Part 2, pp. 1199-1210, University of California Riverside, CA, USA.

Gonçalves, M.C., Reis, L.C.L., Pereira, M.V., 2005. Progress of soil survey in Portugal. In: Jones, R.J.A., Houšková, B., Bullock, P., Montanarella, L. (Eds.), European Soil Bureau Research Report No.9, pp. 275-279, Office for Official Publications of the European Communities, Luxembourg.

Gonçalves, M.C., Ramos, T.B., Pires, F.P., 2011. Base de dados georreferenciada das propriedades do solo. In: Coelho, P.S., Reis, P. (Eds.), Agrorrural. Contributos Científicos, pp. 564-574. Instituto Nacional dos Recursos Biológicos, Oeiras.

Jana, R.B., Mohanty, B.P., 2012. A comparative study of multiple approaches to soil hydraulic parameter scaling applied at the hillslope scale. Water Resour. Res. 48, W02520, doi:10.1029/2010WR010185.

Lin, H., 2003. Hydropedology: bridging disciplines, scales, and data. Vadose Zone J. 2, 1-11, doi:10.2113/2.1.1.

Lin, H., 2010. Earth's Critical Zone and hydropedology: concepts, characteristics, and advances. Hydrol. Earth Syst. Sci 14, 25-45, doi:10.5194/hess-14-25-2010.

Lin, H., Bouma, J., Pachepsky, Y., Western, A., Thompson, J., van Genuchten, M.Th., Vogel, H-J., Lilly, A., 2006. Hydropedology: Synergistic integration of pedology and hydrology. Water Resour. Res. 42, W05301, doi:10.1029/2005WR004085.

Madeira, M., Constantino, A.T., Réffega, A.G., Martins, A.A., Alexandre, C.J., Sousa, E., Monteiro, F.G., Pinheiro, J.F., Cardoso, J.C., Silva, J.V., Ricardo, R.P., 2004. Bases para a revisão e actualização da classificação dos solos de Portugal. Sociedade Portuguesa de Ciência do Solo, Lisbon.

McBratney, A.B., Minasny, B., Cattle, S.R., Vervoort, R.W., 2002. From pedotransfer functions to soil inference systems. Geoderma 109, 41–73, doi:10.1016/S0016-7061(02)00139-8.

Nash, J.E., Sutcliffe, J.V., 1970. River flow forecasting through conceptual models. I. A discussion of principles. J. Hydrol. 10, 282–290, doi:10.1016/0022-1694(70)90255-6.

Neitsch, S.L., Arnold, J.G., Kiniry, J.R., Williams, J.R., 2011. Soil and Water Assessment Tool, Theoretical documentation, version 2009. Texas Water Resources Institute Technical Report nº 406, Texas A&M University System, College Station, TX.

Nelson, D.W., Sommers, L.E., 1982. Total carbon, organic carbon, and organic matter. In: Page, A.L. et al. (Eds.), Methods of soil analysis. Part 2. Chemical and microbiological properties, pp. 539–579, ASA and SSSA, Madison, WI.

Nemes, A., Wösten, J.H.M., Lilly, A., Oude Voshaar, J.H., 1999. Evaluation of different procedures to interpolate particle-size distribution to achieve compatibility within soil databases. Geoderma 90, 187-202, doi:10.1016/S0016-7061(99)00014-2.

Nemes, A., Schaap, M.G., Wösten, J.H.M., 2003. Functional evaluation of pedotransfer functions derived from different scales of data collection. Soil Sci. Soc. Am. J. 67, 1093-1102, doi:10.2136/sssaj2003.1093.

Nemes, A., Rawls, W.J., 2006. Evaluation of different representations of the particle-size distribution to predict soil water retention. Geoderma 132, 47-58, doi:10.1016/j.geoderma.2005.04.018.

Nunes, J.P., Lima, J.L.M.P., Singh, V.P., Lima, M.I.P., Vieira, G.N., 2006. Numerical modeling of surface runoff and erosion due to moving rainstorms at the drainage basin scale. J. Hydrol. 330, 709-720, doi:10.1016/j.jhydrol.2006.04.037.

Pachepsky, Y.A., Rawls, W.J., 2004. Development of pedotransfer functions in soil hydrology. Elsevier, Amesterdam.

Pachepsky, Y.A., Rawls, W.J., Lin, H.S., 2006. Hydropedology and pedotransfer functions. Geoderma 131, 308-316, doi:10.1016/j.geoderma.2005.03.012.

Paz, A.M., Cipriano, D., Gonçalves, M.C., Pereira, L.S., 2009. Funções de pedo-transferência para a curva de retenção da água no solo. Rev. Ciências Agrárias 32, 337-343.

Ritchie, J.T., 1972. Model for predicting evaporation from a row crop with incomplete cover. Water Resour. Res. 8, 1204-1213, doi:10.1029/WR008i005p01204.

Romano, N., Hopmans, J.W., Dane, J.H., 2002. Suction table. In: Dane, J.H., Topp, G.C. (Eds.), Methods of Soil Analysis, Part 4. Physical Methods, pp. 692-698, Soil Science Society of America Book Series, Madison, Wisconsin.

Schaap, M.G., Leij, F.J., van Genuchten, M.Th., 2001. ROSETTA: a computer program for estimating soil hydraulic parameters with hierarchical pedotransfer functions. J. Hydrol. 251, 163-176, doi:10.1016/S0022-1694(01)00466-8.

Shirazi, M.A., Boersma, L., Johnson, C.B., 2001. Particle-size distributions: comparing texture systems, adding rock and predicting soil properties. Soil Sci. Soc. Am. J. 65, 300-310, doi:10.2136/sssaj2001.652300x.

Steenpass, C., Vanderborght, J., Herbst, M., Šimůnek, J., Vereecken, H., 2010. Estimating soil hydraulic properties from infrared measurements of soil surface temperatures and TDR data. Vadose Zone J. 9, 910-924, doi:10.2136/vzj2009.0176.

van Genuchten, M.Th., 1980. A closed form equation for predicting the hydraulic conductivity of unsaturated soils. Soil Sci. Soc. Am. J. 44, 892-898, doi:10.2136/sssaj1980.03615995004400050002x

van Genuchten, M.Th., Leij, F.J., Yates, S.R., 1991. The RETC code for quantifying the hydraulic functions of unsaturated soils. U. S. Environmental Protection Agency, Ada, OK.

Vereecken, H., Maes, J., Feyen, J., Darius, P., 1989. Estimating the soil moisture retention characteristics from texture, bulk density, and carbon content. Soil Sci. 148, 389-403.

Vereecken, H., Kasteel, R., Vanderborght, J., Harter, T., 2007. Upscaling hydraulic properties and soil water flow processes in heterogeneous soils: a review. Vadose Zone J. 6, 1-28, doi:10.2136/vzj2006.0055

Vogel, H.J., Roth, K., 2003. Moving through scales of flow and transport in soil. J. Hydrol. 272, 95-106, doi:10.1016/S0022-1694(02)00257-3.

Weihermüller, L., Huisman, J.A., Lambot, S., Herbst, M., Vereecken, H., 2007. Mapping the spatial variation of soil water content at the field scale with different ground penetrating radar techniques. J. Hydrol. 340, 205–216, doi:10.1016/j.jhydrol.2007.04.013.

Wösten, J.H.M., Finke, P.A., Jansen, M.J.W., 1995. Comparison of class and continuous pedotransfer functions to generate soil hydraulic characteristics. Geoderma 66, 227-237, doi:10.1016/0016-7061(94)00079-P.

Wösten, J.H.M., Pachepsky, Y.A., Rawls, W.J., 2001. Pedotransfer functions: bridging the gap between available basic soil data and missing soil hydraulic characteristics. J. Hydrol. 251, 123-150, doi:10.1016/S0022-1694(01)00464-4.

Wösten, J.H.M., Lilly, A., Nemes, A., Le Bas, C., 1999. Development and use of a database of hydraulic properties of European soils. Geoderma 90, 169-185, doi:10.1016/S0016-7061(98)00132-3

Yevenes, M.A., Mannaerts, C.M., 2011. Seasonal and land use impacts on the nitrate budget and export of a mesoscale catchment in Southern Portugal. Agric. Water Manage. 102, 54-65, doi:10.1016/j.agwat.2011.10.006.

Chapter 7

Development of ternary diagrams for estimating water retention properties using a geostatistical approach

(Submitted to: Geoderma. 2013)

Development of ternary diagrams for estimating water retention properties using a geostatistical approach

T. B. Ramos[1], M. C. Gonçalves[1,2], A. M. Horta[3], J. C. Martins[2] and L. S. Pereira[1]

[1] CEER-Biosystems Engineering, Institute of Agronomy, Technical University of Lisbon, Tapada da Ajuda, 1349-017 Lisbon, Portugal

[2] INIAV, National Institute of Agronomic and Veterinarian Research, Av. República, 2784-505 Oeiras, Portugal.

[3] Department of Environmental Sciences, Faculty of Agriculture and Environment, The University of Sidney, Eveleigh NSW 2015, Australia.

Abstract

Most pedotransfer functions (PTFs) have adopted soil texture information as the main predictor to estimate soil hydraulic properties, whether inputs are defined in terms of the relative proportion of different grain size particles or texture-based classifications. The objective of this study was to develop ternary diagrams for estimating soil water retention at -33 and -1500 kPa matric potentials, corresponding to the field capacity and wilting point, respectively, from particle size distribution using a geostatistical approach. The texture triangle was divided into a 1% grid of soil texture composition resulting in 4332 different soil textures. Measured soil water retention values determined in 742 soil horizons/layers located in Portugal were then used to develop and validate the ternary diagrams. The development subset included two-thirds of the data, and the validation subset the remaining samples. The soil water content values were displayed in the ternary diagram according to the coordinates given by the particles size distribution determined in the same soil samples. The measured volumetric water content values were then interpolated to the remaining areas of the ternary diagrams using ordinary kriging. Uncertainty analysis resulted in a root mean square error of 0.040 and 0.033 cm^3 cm^{-3} obtained when comparing the interpolated water contents at -33 and -1500 kPa matric potentials values, respectively, with the measured ones included in the validation dataset. The estimation variance was also considered to access the uncertainty of the estimations. The available water content of Portuguese soils was

then derived from both ternary diagrams. The ternary diagrams may thus serve as simplified tools for estimating water retention properties from particle size distribution and eventually serve as an alternative to the traditional statistical regression and data mining techniques used to derive PTFs.

Keywords: Field capacity; Ordinary kriging; Soil Texture; Uncertainty; Wilting point.

1. Introduction

Modern hydrologic modeling studies require a quantitative and precise understanding of soil hydraulic properties. That information is essential for a wide range of applications, such as research on soil and water conservation, irrigation scheduling, solute transport, virus and bacterial migration, plant growth, and plant stress. However, classical methods for direct measurement of soil hydraulic properties (Dane and Topp, 2002) are known to be costly, time consuming, and impractical for large-scale applications in which many samples are required to quantify the spatial and temporal variability of those properties. Hence, pedotransfer functions (PTFs) have been developed as an alternative to classical methods to indirectly estimate soil hydraulic properties from basic soil physical and chemical properties (Bouma, 1989; Vereecken et al., 1989; McBratney et al., 2002; Pachepsky and Rawls, 2004), thus overcoming some of the limitations mentioned earlier, especially when the objective is to characterise soil hydraulic properties at large scales.

Most of the available PTFs use soil-texture-based information as the main predictor to estimate the hydraulic behaviour of soils. This popular option is justified by the fact that soil texture characteristics are among the most easily measured soil properties, and also by the assumption that soil texture is the dominant soil variable in determining hydraulic properties, while other soil variables, such as bulk density or organic matter content, have a secondary effect (Twarakavi et al., 2010). The simplest texture based PTFs were developed to provide estimates of average soil water retention properties or hydraulic parameters for different texture classes (e.g. Wösten et al., 1995; Schaap and Leij, 1998; Bruand et al., 2003; Al Majou et al., 2008; Ramos et al., 2013a). More complex functions have also been developed by relating the particle size limits of the soil constituents to soil hydraulics using multiple regression analysis or data mining tools (e.g. Gupta and Larson, 1979; Saxton et al., 1986; Schaap et al., 2001; Nemes et al., 2006; Haghverdi et al.,

2012). Although the hierarchical approaches followed in many of those studies showed that the accuracy of PTFs improved considerably when other variables (usually bulk density), rather than soil texture information alone, were used also as predictors, texture based PTFs have been considered to also provide reasonably accurate estimates of soil hydraulic properties for many research and technical applications (Vereecken et al., 2010).

Soil texture is normally represented in a ternary diagram, function of sand, silt and clay percentages, where the limits of the texture classes vary according to the texture classification system used. However, the soil texture triangle has also had more applications than simply grouping texture information data, namely it has also been used as a tool to estimate soil hydraulic properties. Saxton et al. (1986) divided the soil texture triangle into grids of 10% sand and 10% clay content increments to develop texture based PTFs for generalized predictions of soil hydraulic properties in each grid cell. Later, Saxton and Rawls (2006) updated the previous work to further include the effect of organic matter, bulk density, gravel, and salinity in their model and provide a broadly applicable predictive system. The developed model has been successfully applied to a wide variety of analysis, particularly those related to agricultural hydrology and water management, since estimates do not involve complex mathematical methods, and the texture triangle serves as a familiar tool to users for estimating the soil water characteristics. Twarakavi et al. (2010) also focused on the relations between the texture triangle and soil hydraulic properties. Those authors estimated soil hydraulic properties throughout the entire soil texture triangle as a function of sand, silt, and clay contents using the ROSETTA PTFs (Schaap et al., 2001) such that the various soil texture possibilities (i.e., combinations of sand, silt, and clay percentages) were considered. They then concluded that although the soil texture triangle was qualitatively very similar to the soil hydraulic triangle, differences existed especially for soils where capillary forces dominate the flow throughout the soils. Bormann (2007) took those studies one step forward and performed water balance calculations for the entire space of the soil texture triangle, after dividing it into 1% grid cells and applying Rawls and Brakensiek (1985) PTFs for obtaining the soil hydraulic properties.

In this study, a geostatistical approach was used to spatial interpolate water retention values (the field capacity and wilting point) available in a soil database (Gonçalves et al., 2011) throughout the entire soil texture triangle. Kriging is generally considered to be the best method for spatial interpolation that also includes information on uncertainty (Goovaerts, 1999, 2001). Although

there are countless applications to its application in soil science, as far as we know the kriging estimator has never been used as a PTF to actually derive soil hydraulic properties from basic soil data. To proceed with this study, three very basic assumptions had to be validated:

(i) Soil texture and soil water retention properties available in the database were assumed as being determined in the same sample. This is usually not the case in most PTFs where the predictors used in their development, although measured in the same soil horizon, are not always determined directly on the soil samples used for measuring the hydraulic properties. As referred by Vereecken et al. (2010), this becomes more important as the spatial and temporal variability of additional soils information increase and the information content is not related anymore to the samples on which the hydraulic properties were determined. Thus, taking into account the size of the database used in this study, the error resulting from this assumption was not considered to be relevant.

(ii) Soil texture was assumed as the main predictor to estimate soil hydraulic properties. As mentioned earlier, this is the main assumption sustaining all texture based PTFs, since these two soil properties normally exhibit a high correlation.

(iii) The spatial continuity of soil hydraulic properties along the soil texture triangle could be described by means of a variogram. Taking into account that soil texture is the main soil property considered when grouping soils having similar water retention curves (Wösten et al., 1995; Bruand et al., 2003; Ramos et al., 2013a), and that the soil texture triangle and the soil hydraulic triangle can be relatively similar (Twarakavi et al., 2010), we assumed that there could be a spatial dependence of soil hydraulic properties, at least within the limits of each soil texture class. The percentage units that define the texture triangle were thus converted into metric units to allow the application of geostatistics.

The objective of this study is thus to develop ternary diagrams for estimating point specific water retention values (the field capacity and wilting point) of Portuguese soils using a geostatistical approach. The available water capacity was later computed from both ternary diagrams.

2. Material and Methods

2.1. The data set

The ternary diagrams were developed for estimating the field capacity and wilting point of Portuguese soils from particle size distribution. The field capacity and wilting point were here assumed to correspond to the water retention values at -33 and -1500 kPa, respectively. The data was extracted from the PROPSOLO soil database (Gonçalves et al., 2011), which gathers all information on soil hydraulic and pedological properties from soil profiles obtained from research projects and academic studies performed at the Portuguese National Institute of Agronomic and Veterinarian Research (former Estação Agronómica Nacional). This database contains practically all of the existing knowledge on the soil hydraulic properties of Portuguese soils (with the exception of a few specific retention points found in soil survey studies).

The data included information on soil texture and water retention properties of 742 horizons/layers studied in 346 soil profiles located in Portugal between 1977 and 2012 (Fig. 1). The soil reference groups (FAO, 2006) represented were Fluvisols (36.4%), Luvisols (29.5%), Vertisols (9.8%), Cambisols (8.7%), Calcisols (6.6%), Anthrosols (4.0%), Arenosols (1.4%), Podzols (0.9%), Regosols (0.9%), Ferralsols (0.6%), Leptosols (0.6%), and Planosols (0.6%).

The data was randomly divided in two subsets, a development set composed of two-thirds of the data (495 horizons/layers), and a validation set with the remaining one-third of the data (247 horizons/layers). Table 1 presents the main physical and chemical properties of the two datasets. The particle size distribution was obtained using the pipette method for particles having diameters <2 μm (clay) and between 20–2 μm (silt), and by sieving for particles between 200–20 μm (fine sand) and between 200–2000 μm (coarse sand). These textural classes follow the Portuguese classification system (Gomes and Silva, 1962) and are based on the International Soil Science Society (ISSS) particle limits (Atterberg scale). The organic carbon (*OC*) content was determined by the Walkley–Black method (Nelson and Sommers, 1982). The dry bulk density (ρ_b) was obtained by drying volumetric soil samples (100 cm^3) at 105 ºC for 48 h. The gravimetric water content at -33 kPa matric potential was determined on undisturbed soil samples (100 cm^3) using suction tables (Romano et al., 2002; used in 494 horizons/layers) or the pressure plate apparatus (Dane and Hopmans, 2002; used in 212 horizons/layers). The gravimetric water

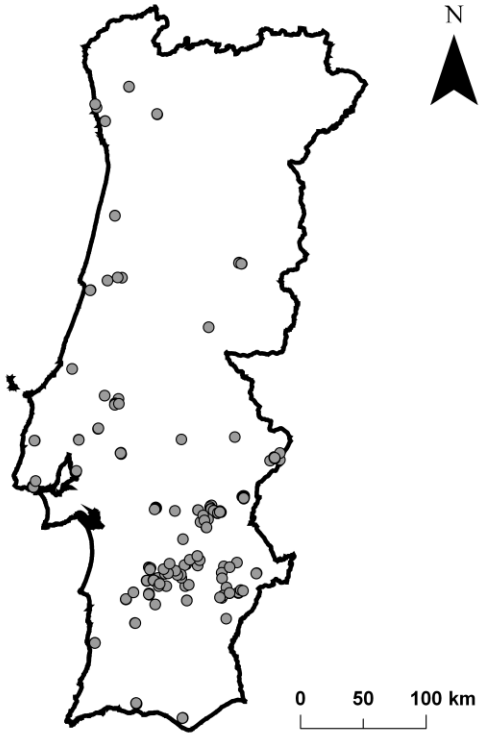

Fig 1. Location of the soil profiles.

Table 1. Main physical and chemical properties of the datasets used in the development and validation of the ternary diagrams.

Statistics	Particle size distribution				Organic carbon	Bulk density	Volumetric water contents	
	2000-200 µm	200-20 µm	20-2 µm	<2 µm			$\theta_{-33\ kPa}$	$\theta_{-1500\ kPa}$
	(%)				(g kg^{-1})	(g cm^{-3})	(cm^3 cm^{-3})	
Development set (n = 495)								
Mean	20.7	34.5	21.6	23.2	0.74	1.50	0.287	0.162
Std. Deviation	17.7	15.2	11.8	14.7	0.54	0.18	0.089	0.081
Minimum	0.1	0.7	1.1	0.6	0.00	0.91	0.029	0.007
Maximum	94.4	70.7	68.1	63.3	2.51	1.90	0.536	0.407
Validation set (n = 247)								
Mean	21.4	34.7	20.5	23.4	0.72	1.52	0.282	0.158
Std. Deviation	17.1	15.4	12.4	14.3	0.52	0.18	0.086	0.073
Minimum	0.1	0.8	0.9	0.1	0.00	0.92	0.029	0.006
Maximum	94.6	73.6	60.2	62.2	2.21	1.87	0.535	0.359

content at -1500 kPa matric potential was also determined on undisturbed soil samples (100 cm^3) using the pressure plate apparatus. Then, the volumetric water content for each horizon/layer and each matric potential was computed from the gravimetric water contents and the bulk density of the corresponding horizon/layer.

In the case of 36 soil horizons/layers where the volumetric water content at -33 kPa matric potential was not readily available, the missing values were estimated by introducing values derived from the fitted van Genuchten model (1980) to each individual water retention curve, also available in the soil database for all soil horizons/layers. The van Genuchten model describes the volumetric soil water content, θ (L^3 L^{-3}), as a function of matric potential, ψ (L), in the following form:

$$S_e(\psi)=\frac{\theta(\psi)-\theta_r}{\theta_s-\theta_r}=\frac{1}{\left(1+|\alpha\psi|^{\eta}\right)^{1-1/\eta}} \quad (1)$$

in which S_e is the effective saturation, θ_r and θ_s denote the residual and saturated water contents (L^3 L^{-3}), respectively, α (L^{-1}) and η (-) are empirical shape parameters. This procedure introduced an error to the subsequent calculations and model evaluations resulting from the non-perfect fit of the fitted model to the experimental data (RMSE = 0.012 cm^3 cm^{-3}), in line with published results (e.g. Nemes and Rawls, 2006; Ramos et al., 2013a). The errors were thus relatively small compared with the errors usually obtained using PTFs, and therefore, the fitted values were assumed as if they were measured.

2.2. Development of the ternary diagrams

The soil texture triangle was divided into a 1% grid of soil texture composition resulting in 4332 different soil textures (i.e., different combinations of sand, silt, and clay percentages). Figure 2 shows the textural distribution of the datasets used for the development of the ternary diagrams and for their validation. The soil texture triangle was converted into ternary diagrams by replacing the percentage units by metric units (cm were used for convenience), and by including the soil water retention values at -33 and -1500 kPa matric potentials in the coordinates given by the particles size distribution determined in the same soil samples. Measured $\theta_{-33\ kPa}$ and $\theta_{-1500\ kPa}$ within the same location (i.e., same particle size distribution) were averaged. The measured

volumetric water content values $\theta_{-33\ kPa}$ and $\theta_{-1500\ kPa}$ were then interpolated to the remaining areas of the ternary diagrams using ordinary kriging.

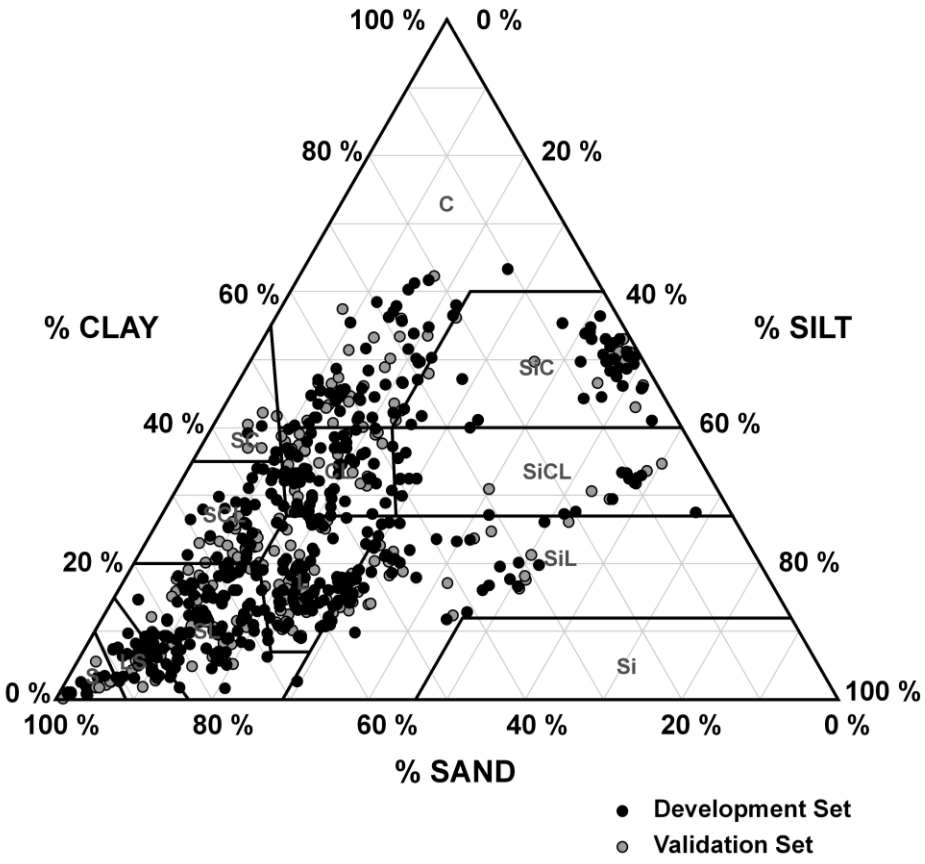

Fig. 2. Textural distribution of the datasets used in the development and validation of the ternary diagrams.

The spatial pattern of $\theta_{-33\ kPa}$ and $\theta_{-1500\ kPa}$ in each ternary diagram was first described from the semi-variance of the differences between measured values included in the development set using the experimental semivariogram (Goovaerts, 1997; Yates and Warrick, 2002), as follows:

$$\gamma_e(h) = \frac{1}{2\,n(h)} \sum_{i=1}^{n(h)} \left[Z(x_i) - Z(x_{i+h}) \right]^2 \qquad (2)$$

where $n(h)$ is the total number of pairs of observation points (x_i and x_{i+h}; i = 1, …, n) of the variable Z (i.e., $\theta_{-33\ kPa}$ and $\theta_{-1500\ kPa}$) that are separated by a distance h. The omnidirectional

semivariogram was computed, and hence the spatial variability was assumed to be identical in all directions. The variogram was defined by assigning pairs of measured values of $\theta_{-33\ kPa}$ and $\theta_{-1500\ kPa}$ to a lag interval of 5 cm ($h_i = i$ 5 cm), since data was irregularly distributed in the texture triangle (Fig. 2). A theoretical variogram was then fitted to the experimental semivariogram using a Gaussian model with nugget effect (Goovaerts, 1997; Yates and Warrick, 2002):

$$\gamma_t(h) = \begin{cases} C_0 + C_1 \left[1 - exp\left(\dfrac{-3\,h^2}{a^2} \right) \right] & for\ h \le a \\ C_0 + C_1 & for\ h > a \end{cases} \tag{3}$$

where C_0 is the nugget (-), C_1 is the sill (-), and a is the range (L). The nugget, C_0, is a measure of discontinuity at the origin of the semivariogram which mainly arises from various sources of unexplained errors, such as measurement errors or the existence of spatial variations at distances smaller than the shortest sampling interval. The sill, C_1, should be approximately equal to the variance of the data. Finally, the range, a, corresponds to the distance at which the semivariance approaches the sill, and represents the separation distance beyond which two values of the variable can be considered statistically independent.

Ordinary kriging was the geostatistical interpolation method selected (Goovaerts, 1997; Yates and Warrick, 2002). The kriging estimator, $Z^*(x)$, provided an estimate of $\theta_{-33\ kPa}$ and $\theta_{-1500\ kPa}$ at a location x_0 of the ternary diagram that contained no information. The estimator is written as a linear combination of the measured values, $Z(x_i)$, that is,

$$Z^*(x_0) = \sum_{i=1}^{n} \lambda_i Z(x_i) \tag{4}$$

where the observation at each location was weighted by λ_i. The value of λ_i depended on its proximity and orientation to x_0 and to the other sample locations, x_i. Since by definition,

$$E\left[Z^*(x_0)\right] = \sum_{i=1}^{n} \lambda_i \; E\left[Z(x_i)\right] \tag{5}$$

and

$$E\left[Z(x)\right] = m \tag{6}$$

the estimates will be unbiased (i.e., E[$Z(x) - Z^*(x_0)$] = 0). The following ordinary kriging system was solved in order to minimize the prediction variance:

$$\begin{cases} \sum_{i=1}^{n} \lambda_i \, \gamma\left(x_k - x_i\right) + \mu = \gamma\left(x_k - x_0\right) \\ \sum_{i=1}^{n} \lambda_i = 1 \end{cases} \tag{7}$$

where E[ ] is the expected value, m is the mean value of $Z(x)$, γ is the semivariance between data pairs, μ is the Lagrange parameter accounting for the constraint on the weights, and $k = 1, \ldots, n$.

The variograms calculation and fitting, and the implementation of the kriging method were carried out with the geoMS software package (CMRP, 2000).

2.3. Uncertainty analyses

The uncertainty of the ordinary kriging interpolation estimates was considered to be the estimation variance in each grid cell of the ternary diagrams. The estimation variance σ^2 gives an indication of the quality of the estimates and was computed as follows (Goovaerts, 1997; Yates and Warrick, 2002),

$$\sigma_k^2\left(x_0\right) = \sum_{i=1}^{n} \lambda_i \, \gamma\left(x_i - x_0\right) + \mu \tag{8}$$

The ternary diagrams were also validated by comparing measured $\theta_{-33\ kPa}$ and $\theta_{-1500\ kPa}$ values included in the validation dataset with ordinary kriging estimates using various quantitative measures of the uncertainty, such as the determination coefficient (R^2), the mean error (ME), and the root mean square error (RMSE), given by:

$$R^2 = \left[\frac{\sum_{i=1}^{n} \left(O_i - \bar{O}\right)\left(P_i - \bar{P}\right)}{\left[\sum_{i=1}^{n} \left(O_i - \bar{O}\right)^2\right]^{0.5} \left[\sum_{i=1}^{n} \left(P_i - \bar{P}\right)^2\right]^{0.5}} \right]^2 \tag{9}$$

$$ME = \frac{1}{n} \sum_{i=1}^{n} \left(P_i - O_i\right) \tag{10}$$

$$RMSE = \sqrt{\frac{\sum_{i=1}^{n}(P_i - O_i)^2}{n-1}} \quad (11)$$

where n is the number of observations, O_i are the measured values, P_i are the interpolation predictions, $\overline{O}$ is the average of the measured values, and $\overline{P}$ is the average of the interpolation predictions.

3. Results and Discussion

3.1. Spatial patterns of $\theta_{-33\ kPa}$ and $\theta_{-1500\ kPa}$

Figure 3 presents the experimental and theoretical semivariograms obtained for $\theta_{-33\ kPa}$ and $\theta_{-1500\ kPa}$. The fitted parameters of the Gaussian model are given in Table 2. The nugget value found for $\theta_{-33\ kPa}$ and $\theta_{-1500\ kPa}$ corresponded to 15.4 and 6.1% of the total variance (*Ct*), respectively. As referred above, these values can be explained by sampling or measurement errors, and by variability that occurs at scales too small to characterize, which in this case correspond to variability that cannot be explained only by variations in soil texture. This unexplained variability is surely attributed to the effect of bulk density, organic matter, soil structure, soil mineralogy, soil chemical composition, and land use and management on water retention properties. Like in the development of traditional PTFs, grouping data by considering the effect of those soil properties (Wösten et al., 2001) would likely be advantageous in order to reduce the unexplained variability found in the development of the ternary diagrams. However, that approach would require a much larger database than the one currently available. The larger nugget value found for the semivariogram of $\theta_{-33\ kPa}$ may be further related to the different methodologies used for measuring water retention at -33 kPa matric potential (Schaap and Leij, 1998).

The spatial continuity of $\theta_{-33\ kPa}$ and $\theta_{-1500\ kPa}$ reached a range of 39.7 and 24.6 cm in the ternary diagrams, respectively. Water retention values were thus correlated with samples located in neighbor texture classes, but more distanced areas of the texture triangle showed no correlation with those measured values. These findings seem to be very useful to understand the limitations of the simplest texture based PTFs, the class-PTFs (Wösten et al., 2001), when estimating water retention properties for different texture classes. These class-PTFs estimate average soil water

retention properties for different texture classes based on the arithmetic (e.g. Bruand et al., 2003; Al Majou et al., 2008; Ramos et al., 2013a) or geometric mean (e.g. Wösten et al., 1995, 1999) of the datasets. However, for most regions of the texture triangle water retention values are sometimes better correlated with data included in their vicinity which may well be included in a neighbor texture class.

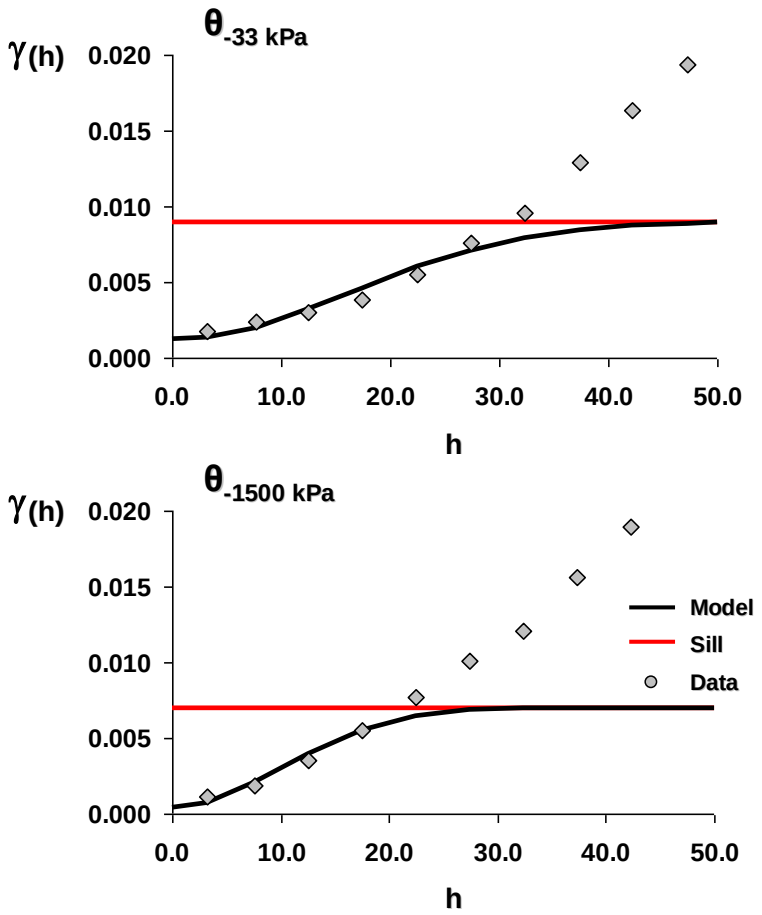

Fig. 3. Experimental semivariogram of $\theta_{-33\ kPa}$ (top) and $\theta_{-1500\ kPa}$ (bottom) with the Gaussian model fitted.

Table 2. Parameters of the Gaussian model fitted to the experimental semivariograms.

Volumetric water contents	Nugget C_0 (-)	Sill C_1 (-)	Total variance Ct (-)	Range a (cm)
$\theta_{-33\ kPa}$	0.0012	0.0078	0.009	39.745

$\theta_{-1500\ kPa}$	0.0004	0.0066	0.007	24.604

3.2. Ternary diagrams

Figure 4 presents the ternary diagram developed by ordinary kriging for estimating $\theta_{-33\ kPa}$ from particle size distribution. The resulting estimation variance is also shown in the same figure. Soil water retention values at -33 kPa matric potential were lower in the coarser texture classes and increased gradually with the increment of clay and silt contents. Basically, the ordinary kriging method calculated $\theta_{-33\ kPa}$ for all 4332 grid cells of the ternary diagram as a kind of weighted average of the measured values in the vicinity of each grid cell. The neighboring sample point values were weighted according to the semivariance as a function of distance to the prediction location. The kriging method also compensated for the effects of data clustering, by assigning individual points within a cluster less weight than isolated data points. This showed to be particularly useful when interpolating water content values to regions of the texture triangle where the information available in the development set was scarcer.

The mean and standard deviation values of the interpolated $\theta_{-33\ kPa}$ ternary diagram were 0.365 and 0.086 $cm^3\ cm^{-3}$, respectively. The mean value was thus higher than the one registered in the development dataset (0.287 $cm^3\ cm^{-3}$; Table 1). The difference found resulted from the fact that the interpolated ternary diagram estimated $\theta_{-33\ kPa}$ for all 4332 soil textures, including regions of the texture triangle where the development dataset had no information (e.g., the silty texture class, and the region of the texture triangle with clay content higher than 65%), thus producing significant differences in the classes of the interpolated histogram with higher water contents (not shown). The estimation variance was very high in those regions, and thus local estimates of $\theta_{-33\ kPa}$ were not realistic (Fig. 4). For the remaining regions of the ternary diagram, the estimation variance was low and estimates were considered to be accurate. In these regions, the mean value given by the kriging estimator (m = 0.338 $cm^3\ cm^{-3}$ where, for example, $\sigma^2 \leq 0.002$) and the mean value of the development dataset tended to be closer.

Figure 5 presents the interpolated $\theta_{-1500\ kPa}$ ternary diagram and the respective estimation variance. Soil water retention values at -1500 kPa matric potential were also lower in the coarser texture classes and increased progressively with the increase of clay content. However, soil water retention did not increase as gradually as registered for the $\theta_{-33\ kPa}$ ternary diagram, since there are

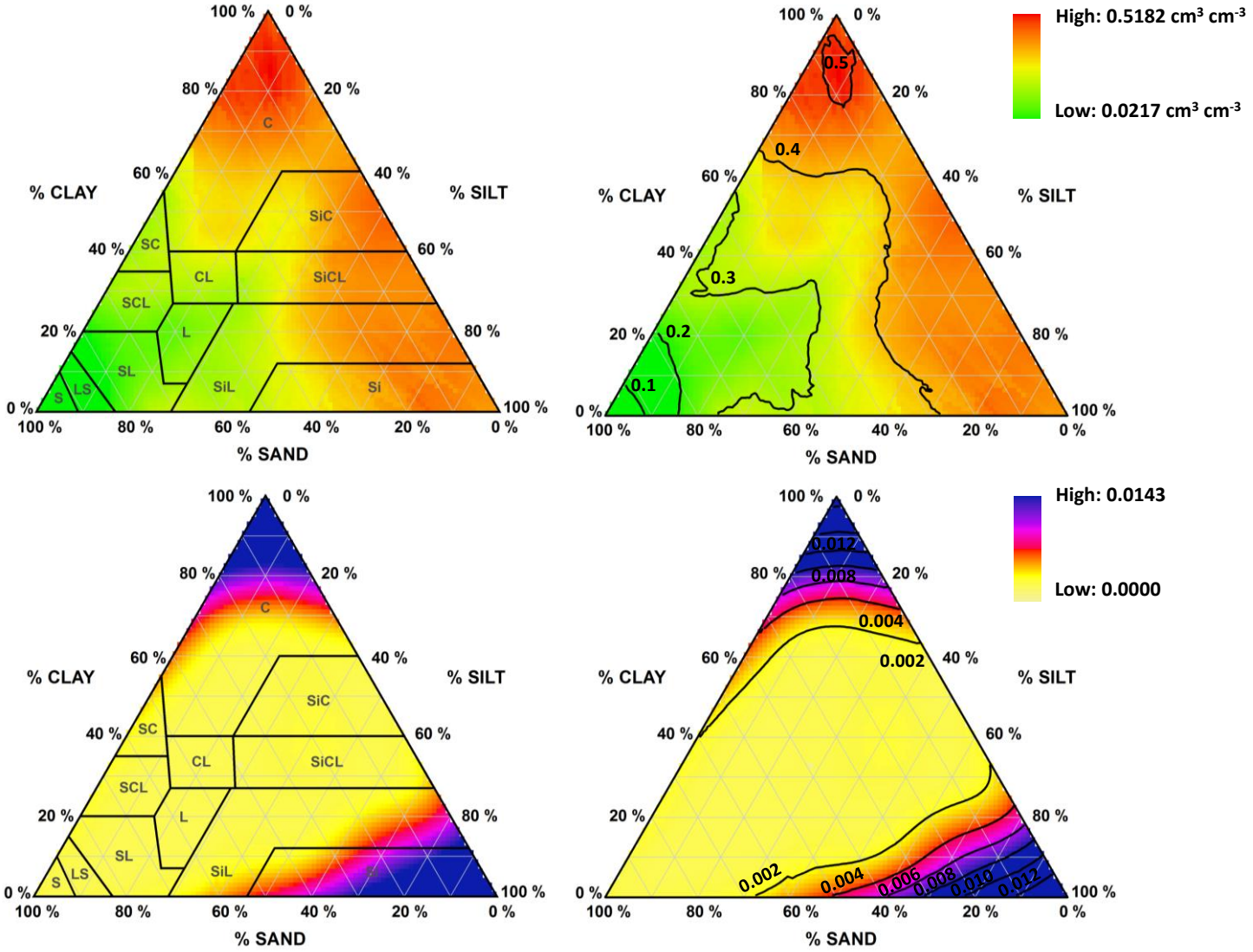

Fig. 4. Ternary diagrams soil water content values at -33 kPa matric potential estimated with ordinary kriging (top) and estimation variance (bottom) of those estimates (figures on the left show the ISSS texture classes; figures on the right show the contour plots of the estimates).

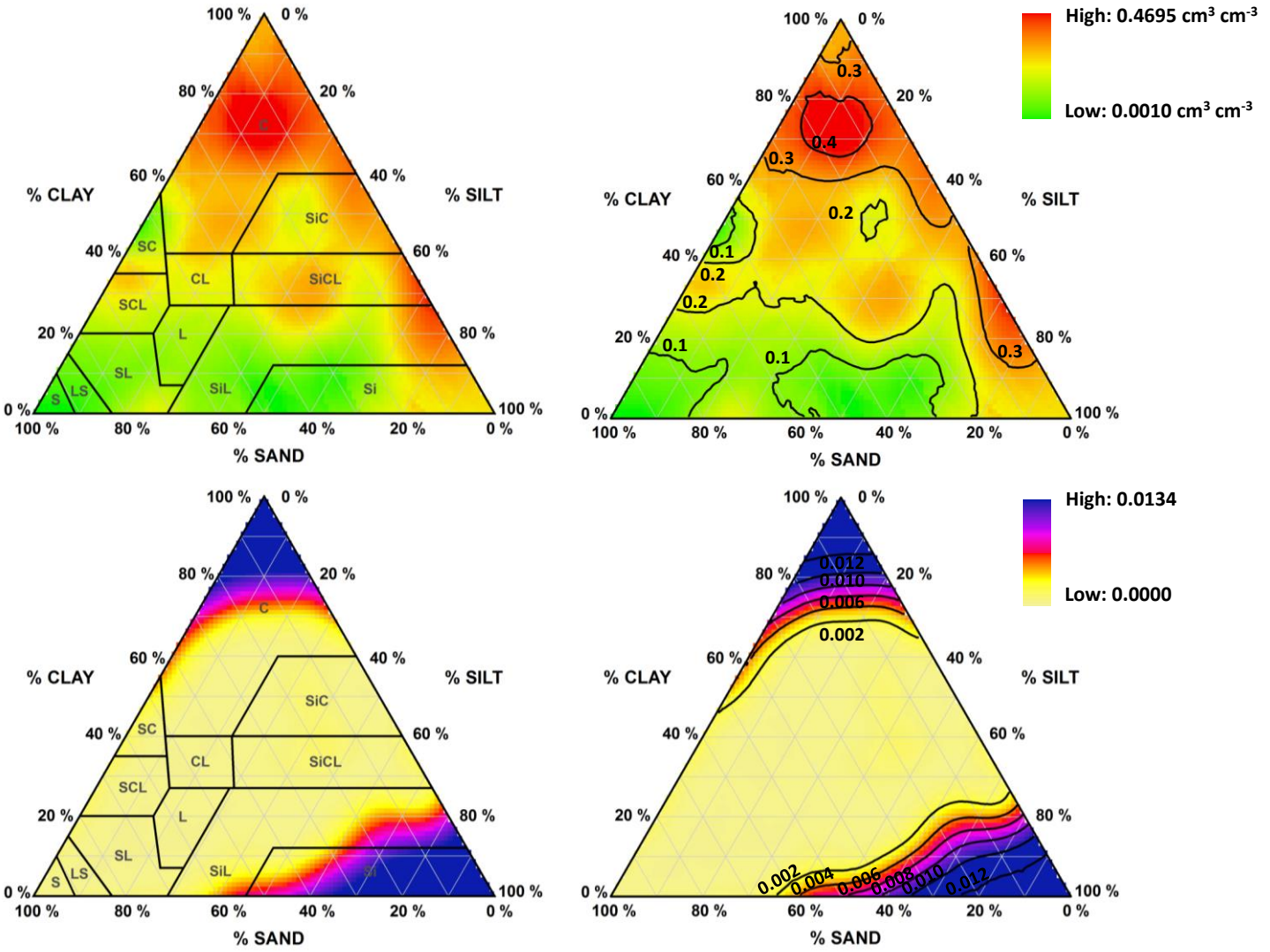

Fig. 5. Ternary diagrams soil water content values at -1500 kPa matric potential estimated with ordinary kriging (top) and estimation variance (bottom) of those estimates (figures on the left show the ISSS texture classes; figures on the right show the contour plots of the estimates).

a few regions of the texture triangle (e.g., the area in the vicinity of the soil texture with 50% clay, 32% silt, and 18% sand) that clearly needed more information when estimating $\theta_{-1500\ kPa}$. The mean and standard deviation values of the interpolated $\theta_{-1500\ kPa}$ ternary diagram were 0.216 and 0.101 $cm^3\ cm^{-3}$, respectively. The mean value was once again higher than the one in the development dataset (0.162 $cm^3\ cm^{-3}$; Table 1), but it was slightly lower where $\sigma^2 \leq 0.002$ (m = 0.204 $cm^3\ cm^{-3}$).

The results of the goodness-of-fit tests between measured and estimated water retention values at both matric potentials are presented in Table 3. Figure 6 shows the corresponding scatter plots between measured and estimated values. The kriging method produced an acceptable estimation of $\theta_{-33\ kPa}$ and $\theta_{-1500\ kPa}$, with ME values being very close to zero. RMSE values also showed that estimates were relatively accurate. RMSE were 0.040 and 0.033 $cm^3\ cm^{-3}$ for the estimates of $\theta_{-33\ kPa}$ and $\theta_{-1500\ kPa}$, respectively. The R^2 values were considerably high and identical for both water contents ($R^2 > 0.78$), indicating also a good agreement between measurements and predictions. However, data in the $\theta_{-1500\ kPa}$ scatter plot was found to be slightly more dispersing than for $\theta_{-33\ kPa}$.

Table 4 shows the accuracy of published PTFs that are available for estimating soil hydraulic properties of Portuguese soils, and which estimates can be compared with those obtained with the ternary diagrams. We limited our comparison to PTFs that used partially or the entire dataset used in this study. The class-PTFs developed by Ramos et al. (2013a) produced RMSE values that varied between 0.042 and 0.055 $cm^3\ cm^{-3}$ when estimating $\theta_{-33\ kPa}$, and between 0.037 and 0.048 $cm^3\ cm^{-3}$ when predicting $\theta_{-1500\ kPa}$. The best estimates, achieved with the class-PTFs developed after grouping data by ISSS texture classes and bulk density, can be comparable with the estimates given by the ternary diagrams. The point PTFs developed by Ramos et al. (2013b) yielded RMSE values of 0.040 and 0.036 $cm^3\ cm^{-3}$ also when predicting $\theta_{-33\ kPa}$ and $\theta_{-1500\ kPa}$, respectively, thus producing very similar predictions to those given by the kriging method. On the other hand, the parametric PTFs developed by Gonçalves et al. (1997), Wösten et al. (1999), and Ramos et al. (2013b) resulted in slightly higher RMSE values ($\geq 0.046\ cm^3\ cm^{-3}$) than those calculated with estimates given by the ternary diagrams. Hence, Table 4 shows that similar or even better predictions of $\theta_{-33\ kPa}$ and $\theta_{-1500\ kPa}$ can be obtained with the ternary diagrams. The only predictor needed is the particle size distribution, while the other comparable PTFs require relatively more predictors than the needs of those diagrams. In terms of number of predictors, the

ternary diagrams seem to be quite useful as they are the only PTFs that do not require bulk density, despite results are given in terms of volumetric water contents. Although this soil property is simple to measure, sampling undisturbed samples in different soil horizons/layers distributed over large areas in order to measure bulk density may be a very laborious task.

Table 3. Results of the statistical analysis between measured water retention values at -33 and -1500 kPa and ordinary kriging estimates.

Statistics	Volumetric water contents	
	$\theta_{-33\ kPa}$	$\theta_{-1500\ kPa}$
R^2 (-)	0.788	0.802
ME ($cm^3\ cm^{-3}$)	-0.001	0.001
RMSE ($cm^3\ cm^{-3}$)	0.040	0.033

Table 4. Accuracy of published pedotransfer functions in the estimation of water retention values at -33 and -1500 kPa included in the database.

PTFs	Predictors	RMSE ($cm^3\ cm^{-3}$)	
		$\theta_{-33\ kPa}$	$\theta_{-1500\ kPa}$
1. Class-PTFs			
Ramos et al. (2013a)	FAO texture classes	0.055	0.048
	FAO texture classes + depth	0.054	0.047
	FAO texture classes + ρ_b	0.049	0.047
	FAO texture classes + depth + ρ_b	0.047	0.046
	ISSS texture classes	0.049	0.039
	ISSS texture classes + depth	0.047	0.038
	ISSS texture classes + ρ_b	0.042	0.037
Wösten et al. (1999)	FAO texture classes + depth	0.063	0.051
2. Continuous PTFs			
2.1. Point PTFs			
Ramos et al. (2013b)	$Si_{20\ \mu m}$, C, ρ_b, Z	0.040	0.036
2.2. Parametric PTFs			
Gonçalves et al. (1997)	*CS*, *FS*, $Si_{20\ \mu m}$, C, ρ_b, Z, *OM*, *pH*	0.046	0.053
Wösten et al. (1999)	$Si_{50\ \mu m}$, C, ρ_b, *OM*, depth	0.049	0.045
Ramos et al. (2013b)	*CS*, *FS*, $Si_{20\ \mu m}$, C, ρ_b, Z	0.084	0.051

CS, coarse sand; *FS*, fine sand; $Si_{20\ \mu m}$, silt fraction at 20 µm; $Si_{50\ \mu m}$, silt fraction at 50 µm; C, clay; ρ_b, bulk density; Z, mean depth; *OM*, organic matter; depth, qualitative variable having the values 1 (topsoils) and 0 (subsoils).

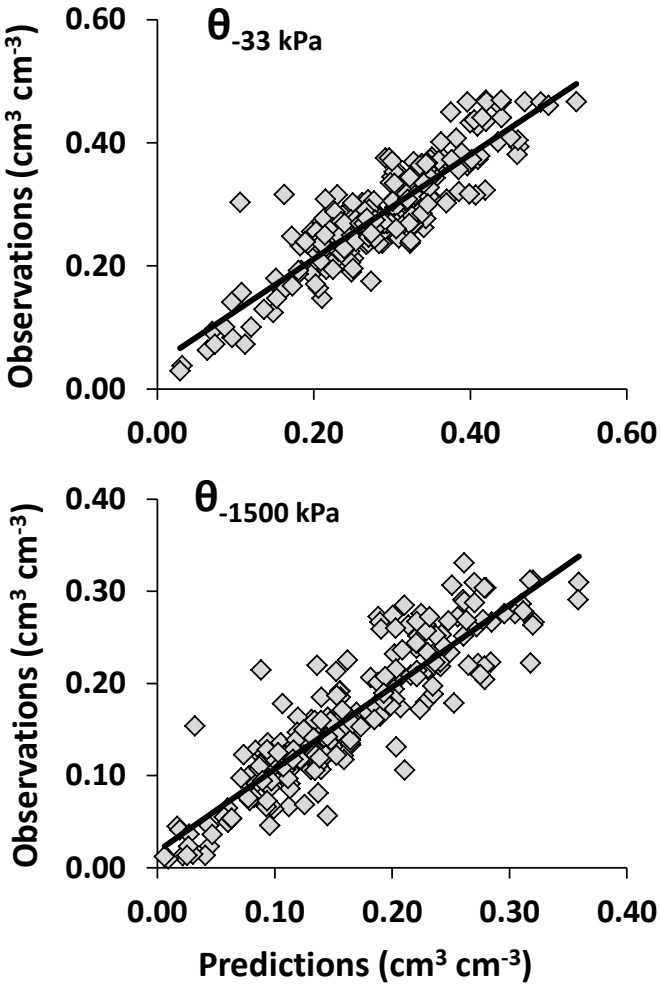

Fig. 6. Scatter plot of prediction of soil water content at -33 and -1500 kPa matric potentials with ordinary kriging versus measured values included in the validation dataset.

3.3. Available water capacity

Figure 7 shows estimates of the available water capacity (AWC), calculated as the difference between $\theta_{-33\ kPa}$ and $\theta_{-1500\ kPa}$, and setting soil depth to 1 m as reference for comparison between estimates. AWC was only calculated for areas of the ternary diagrams where the estimation variance of either $\theta_{-33\ kPa}$ or $\theta_{-1500\ kPa}$ was lower than 0.002. This value was chosen arbitrarily, but is much lower than the dataset total variance (Table 2). Therefore, we only considered estimates than may be considered reliable and avoided extrapolations produced by the kriging estimator.

The largest AWC estimates were obtained for the medium fine texture classes. The coarser texture classes and the soils with 65% clay content seem to present lower AWC. However, the low estimates found for these latter soils are produced in a region of the ternary diagram where the estimation variance increases rapidly with the increase of the clay content, i.e., those predictions are near the limits of a region where the kriging estimator starts to extrapolate information instead of interpolating it, and thus care should be taken when using that information. Nevertheless, the histogram presented in Fig. 8 shows that estimates of the AWC have an average value of 134.1 mm/m, a variance of 3150.7, and kurtosis (0.45) and skewness (0.83) close to zero. However, the Chi-Square and Kolmogorov-Smirnov (p value = 0.00 < 0.01) goodness-of-fit tests rejected the hypothesis that AWC is normally distributed at a level of 99% confidence since soil water content information in the very fine and medium fine texture classes is missing.

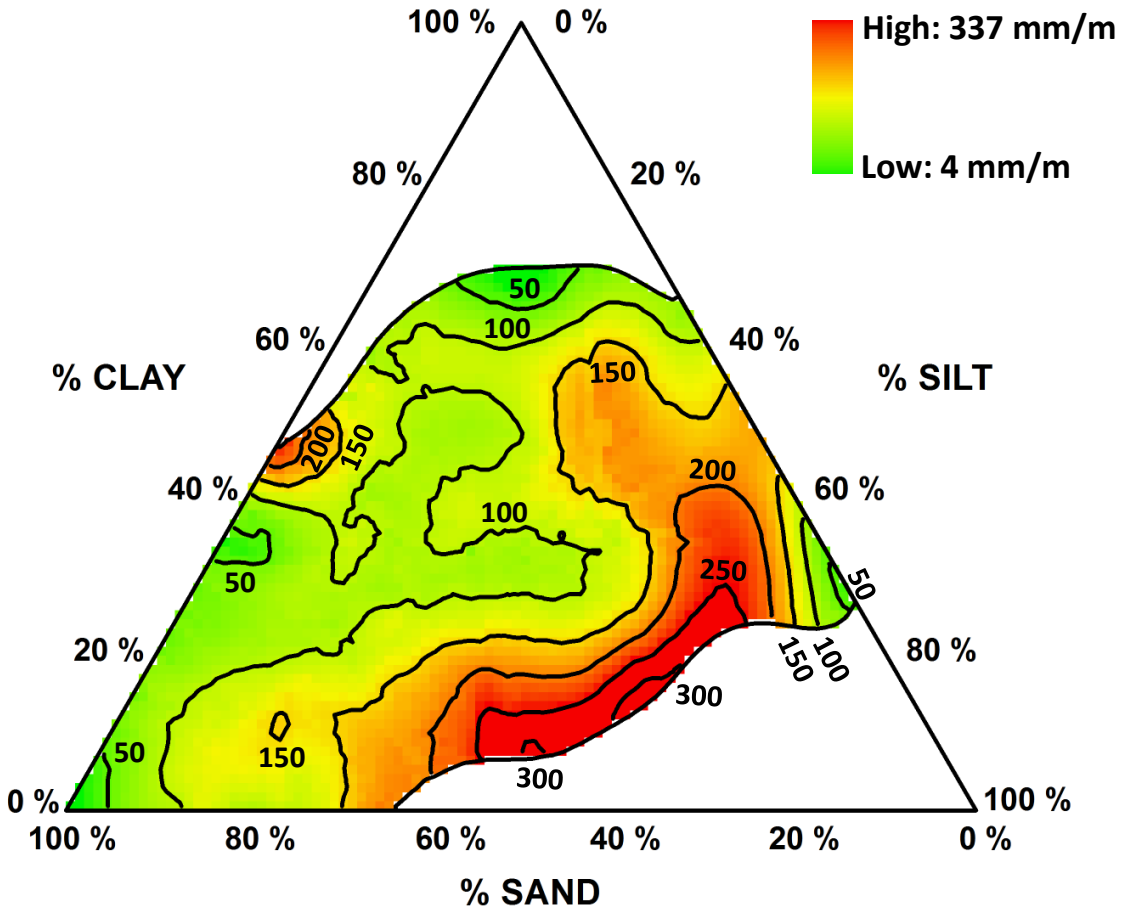

Fig. 7. Ternary diagram with estimates of the available water capacity (AWC).

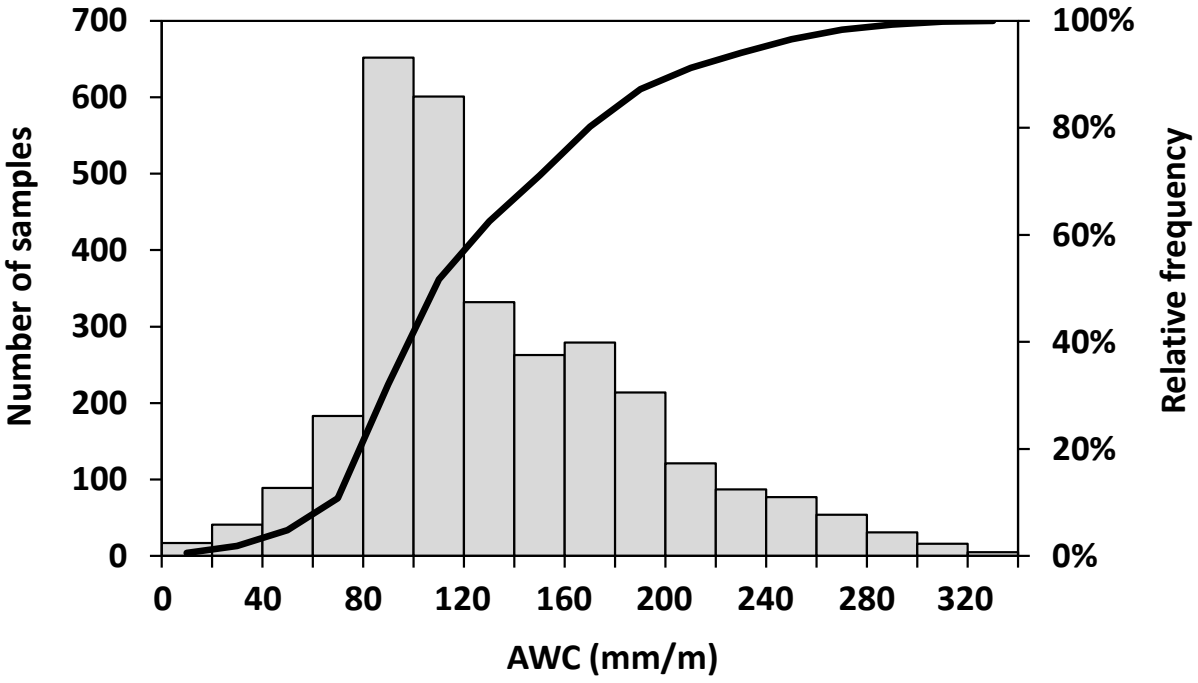

Fig. 8. Histogram with estimates of the available water capacity (AWC).

The ternary diagrams developed in this study ($\theta_{-33\ kPa}$, $\theta_{-1500\ kPa}$, and AWC) may potentially be useful for many scientific and technical domains, but they seem more relevant to agricultural water management, particularly irrigation management and scheduling. Various water balance models require the type of information provided by the ternary diagrams here developed at point scale (Liu et al., 1998; George et al., 2000; Chopart et al., 2007; Steduto et al., 2009; Khaledian et al., 2009; Rosa et al., 2012). Those that are associated to a geographical information system and are applied at field scale (Troch et al, 1993; Fortes et al., 2005; Ojeda-Bustamante et al., 2007) can make even further use of the ternary diagrams here developed for estimating soil water retention properties of Portuguese soils.

4. Conclusions

The geostatistical approach was able to provide reliable estimates of soil water retention at -33 and -1500 kPa matric potentials using only the relative proportion of different grain size particles (sand, silt, and clay) as input data. The ordinary kriging method was helpful to understand which

estimates of the soil water retention were valid based on the values of the estimation variance, and thus extrapolations were avoided.

The RMSE values were 0.040 and 0.033 cm^3 cm^{-3} when comparing the estimates provided by the $\theta_{-33\ kPa}$ and $\theta_{-1500\ kPa}$ ternary diagrams, respectively, and the measured values included in the validation dataset. Those values are comparable to the estimates provided by most of the available PTFs for estimating soil water retention properties of Portuguese soils. The ternary diagrams may thus serve as simplified tools for estimating those properties from particle size distribution and eventually serve as an alternative to the traditional statistical regression and data mining techniques used to derive PTFs.

Acknowledgments

This research was performed within the framework of the Project PTDC/AGR-AAM/098100/2008 of the Fundação para a Ciência e a Tecnologia (FCT). T. B. Ramos was funded by the FCT grant SFRH/BD/60363/2009.

References

Al Majou, H., Bruand, A., Duval, O., Le Bas, C., Vautier, A., 2008. Prediction of soil water retention properties after stratification by combining texture, bulk density and the type of horizon. Soil Use Manage. 24, 383-391, doi:10.1111/j.1475-2743.2008.00180.x.

Bormann, H., 2007. Analysis of the suitability of the German soil texture classification for the regional scale application of physical based hydrological model. Adv. Geosci. 11, 7-13, doi:10.5194/adgeo-11-7-2007.

Bouma, J., 1989. Using soil survey data for quantitative land evaluation. Adv. Soil Sci. 9, 177-213.

Bruand, A., Pérez Fernandez, P., Duval, O., 2003. Use of class pedotransfer functions based on texture and bulk density of clods to generate water retention curves. Soil Use Manage. 19, 232-242, doi:10.1111/j.1475-2743.2003.tb00309.x.

Chopart, J.L., Mézino, M., Aure, F., Le Mézo, L., Mété, M., Vauclin, M., 2007. OSIRI: A simple decision-making tool for monitoring irrigation of small farms in heterogeneous environments. Agric. Water Manage. 87, 128-138, doi:10.1016/j.agwat.2006.06.023.

CMRP (Centro de Modelização de Reservatórios Petrolíferos), 2000. Manual do geoMS v1.0. Instituto Superior Técnico, Lisboa, Portugal.

Dane, J.H., Hopmans, J.W., 2002. Pressure plate extractor. In: Dane, J.H., Topp, G.C. (Eds.), Methods of Soil Analysis, Part 4, Physical Methods, pp. 688-690. Soil Science Society of America book Series, Madison, Wisconsin.

Dane, J.H., Topp, G.C., 2002. Methods of soil analysis. Part 4, Physical methods. Soil Science Society of America book Series, Madison, Wisconsin.

FAO, 2006. World reference base for soil resources. A framework for international classification, correlation and communication. World Soil Resources Report 103, Food and Agriculture Organization of the United Nations, Rome, Italy.

Fortes, P.S., Platonov, A.E., Pereira, L.S., 2005. GISAREG – A GIS based irrigation scheduling simulation model to support improved water use. Agric. Water Manage. 77, 159-179, doi:10.1016/j.agwat.2004.09.042.

George, B.A., Shende, S.A., Raghuwanshi, N.S., 2000. Development and testing of an irrigation scheduling model. Agric. Water Manage. 6, 121–136, doi:10.1016/S0378-3774(00)00083-4.

Gomes, M.P., Silva, A.A., 1962. Um novo diagrama triangular para a classificação básica da textura do solo. Garcia da Orta 10, 171–179.

Gonçalves, M.C., Pereira, L.S., Leij, F.J., 1997. Pedo-transfer functions for estimating unsaturated hydraulic properties of Portuguese soils. Eur. J. Soil Sci. 48, 387-400, doi:10.1111/j.1365-2389.1997.tb00205.x.

Gonçalves, M.C., Ramos, T.B., Pires, F.P., 2011. Base de dados georreferenciada das propriedades do solo. In: Coelho, P.S., Reis, P. (Eds.), Agrorrural. Contributos Científicos, pp. 564-574. Instituto Nacional dos Recursos Biológicos, Oeiras, Portugal.

Goovaerts, P., 1997. Geostatistics for natural resources evaluation. Oxford University Press, New York.

Goovaerts, P., 1999. Geostatistics in soil science: state-of-the-art and perspectives. Geoderma 89, 1-45, doi:10.1016/S0016-7061(98)00078-0.

Goovaerts, P., 2001. Geostatistical modeling of uncertainty in soil science. Geoderma 103, 3-26, doi:10.1016/S0016-7061(01)00067-2.

Gupta, S.C., Larson, W.E., 1979. Estimating soil water retention characteristics from particle size distribution, organic matter content, and bulk density. Water Resour. Res. 15, 1633-1635, doi:10.1029/WR015i006p01633.

Haghverdi, A., Cornelis, W.M., Ghahraman, B., 2012. A pseudo-continuous neural network approach for developing water retention pedotransfer functions with limited data. J. Hydrol. 442-443, 46-54, doi:10.1016/j.jhydrol.2012.03.036.

Khaledian, M.R., Mailhol, J.C., Ruelle, P., Rosique, P., 2009. Adapting PILOTE model for water and yield management under direct seeding system: The case of corn and durum wheat in a Mediterranean context. Agric. Water Manage. 96, 757–770, doi:10.1016/j.agwat.2008.10.011.

Liu, Y., Teixeira, J.L., Zhang, H.J., Pereira, L.S., 1998. Model validation and crop coefficients for irrigation scheduling in the North China Plain. Agric. Water Manage. 36: 233-246, doi:10.1016/S0378-3774(97)00051-6.

McBratney, A.B., Minasny, B., Cattle, S.R., Vervoort, R.W., 2002. From pedotransfer functions to soil inference systems. Geoderma 109, 41–73, doi:10.1016/S0016-7061(02)00139-8.

Nelson, D.W., Sommers, L.E., 1982. Total carbon, organic carbon, and organic matter. In: Page, A.L., et al. (Eds.), Methods of soil analysis, Part 2, Chemical and microbiological properties, pp. 539–579. ASA and SSSA, Madison, WI.

Nemes, A., Rawls, W.J., 2006. Evaluation of different representations of the particle-size distribution to predict soil water retention. Geoderma 132, 47-58, doi:10.1016/j.geoderma.2005.04.018.

Nemes, A., Rawls, W.J., Pachepsky, Y.A., 2006. Use of a nonparametric nearest-neighbor technique to estimate soil water retention. Soil Sci. Soc. Am. J. 70, 327–336, doi:10.2136/sssaj2005.0128.

Pachepsky, Y.A., Rawls, W.J., 2004. Development of pedotransfer functions in soil hydrology. Elsevier, Amsterdam, The Netherlands.

Ojeda-Bustamante, W., González-Camacho, J.M., Sifuentes-Ibarra, E., Isidro, E., Rendón-Pimentel, L., 2007. Using spatial information systems to improve water management in México. Agric. Water Manage. 89, 81-88, doi:10.1016/j.agwat.2006.11.002.

Ramos, T.B., Gonçalves, M.C., Brito, D., Martins, J.C., Pereira, L.S., 2013a. Development of class pedotransfer functions for integrating water retention properties into Portuguese soil maps. Soil Research 51, doi:10.1071/SR12347.

Ramos, T.B., Gonçalves, M.C., Martins, J.C., Pereira, L.S., 2013b. Comparação de diferentes funções de pedotransferência para estimar as propriedades hidráulicas em Portugal. In: Gonçalves, M.C., Martins, J.C. (Eds.), Proceedings do Encontro Anual de Ciência do Solo, 26-28 Julho, Instituto Nacional de Investigação Agrária e Veterinária, Oeiras, Portugal.

Rawls, W.J., Brakensiek, D.L., 1985. Prediction of soil water properties for hydrologic modelling. In: Jones, E., Ward, T.J. (Eds.), Watershed management in the Eighties (Proceedings), pp. 293-299. ASCE, Denver, Colorado.

Romano, N., Hopmans, J.W., Dane, J.H., 2002. Suction table. In: Dane, J.H., Topp, G.C., (Eds.), Methods of Soil Analysis, Part 4, Physical Methods, pp. 692-698. Soil Science Society of America Book Series, Madison, Wisconsin.

Rosa, R., Paredes, P., Rodrigues, G.C., Alves, I., Fernando, R.M., Pereira, L.S., Allen, R.G., 2012. Implementing the dual crop coefficient approach in interactive software. 1. Background and computational strategy. Agric. Water Manage. 103, 8-24, doi:10.1016/j.agwat.2011.10.013

Saxton, K.E., Rawls, W.J., Romberger, J.S., Papendick, R.I., 1986. Estimating generalized soil water characteristics from texture. Soil Sci. Soc. Am. J. 50, 1031–1036, doi:10.2136/sssaj1986.03615995005000040039x.

Saxton, K.E., Rawls, W.J., 2006. Soil water characteristics estimates by texture and organic matter for hydrologic solutions. Soil Sci. Soc. Am. J. 70, 1569–1578, doi:10.2136/sssaj2005.0117.

Schaap, M.G., Leij, F.J., 1998. Database-related accuracy and uncertainty of pedotransfer functions. Soil Sci. 163, 765-779, doi:10.1097/00010694-199810000-00001.

Schaap, M.G., Leij, F.J., van Genuchten, M.Th., 2001. ROSETTA: a computer program for estimating soil hydraulic parameters with hierarchical pedotransfer functions. J. Hydrol. 251, 163-176, doi:10.1016/S0022-1694(01)00466-8.

Steduto, P., Hsiao, T.C., Raes, D., Fereres, E., 2009. AquaCrop — The FAO Crop Model to Simulate Yield Response to Water: I. Concepts and Underlying Principles. Agron. J. 101, 426-437, doi:10.2134/agronj2008.0139s.

Troch, P.A., Mancini, M., Paniconi, C., Wood, E.F., 1993. Evaluation of a distributed catchment scale water balance model. Water Resour. Res. 29, 1805–1817, doi:10.1029/93WR00398.

Twarakavi, N.K.C., Šimůnek, J, Schaap, M.G., 2010. Can texture-based classification optimally classify soils with respect to soil hydraulics? Water Resour. Res. 46, W01501, doi:10.1029/2009WR007939.

van Genuchten, M.Th., 1980. A closed form equation for predicting the hydraulic conductivity of unsaturated soils. Soil Sci. Soc. Am. J. 44, 892-898, doi:10.2136/sssaj1980.03615995004400050002x.

Vereecken, H., Maes, J., Feyen, J., Darius, P., 1989. Estimating the soil moisture retention characteristics from texture, bulk density, and carbon content. Soil Sci. 148, 389-403.

Vereecken, H., Weynants, M., Javaux, M., Pachepsky, Y., Schaap, M.G., van Genuchten, M.Th., 2010. Using pedotransfer functions to estimate the van Genuchten-Mualem soil hydraulic properties: a review. Vadose Zone J. 9, 795-820, doi:10.2136/vzj2010.0045.

Wösten, J.H.M., Finke, P.A., Jansen, M.J.W., 1995. Comparison of class and continuous pedotransfer functions to generate soil hydraulic characteristics. Geoderma 66, 227-237, doi:10.1016/0016-7061(94)00079-P.

Wösten, J.H.M., Lilly, A., Nemes, A., Le Bas, C., 1999. Development and use of a database of hydraulic properties of European soils. Geoderma 90, 169-185, doi:10.1016/S0016-7061(98)00132-3.

Wösten, J.H.M., Pachepsky, Y.A., Rawls, W.J., 2001. Pedotransfer functions: bridging the gap between available basic soil data and missing soil hydraulic characteristics. J. Hydrol. 251, 123-150, doi:10.1016/S0022-1694(01)00464-4.

Yates, S.R., Warrick, A.W., 2002. Geostatistics. In: Dane, J.H., Topp, G.C. (Eds.), Methods of Soil Analysis, Part 4, Physical Methods, pp. 81-118. Soil Science Society of America book Series, Madison, Wisconsin.

Chapter 8

Estimating soil hydraulic properties from limited data to improve irrigation management in agricultural soils of Santiago Island, Cape Verde

(Published in: Irrigation and Drainage. In press)

Estimating soil hydraulic properties from limited data to improve irrigation management in agricultural soils of Santiago Island, Cape Verde

Â. Moreno[1], T. B. Ramos[1], M. C. Gonçalves[1,2] and L. S. Pereira[1]

[1] CEER-Biosystems Engineering, Institute of Agronomy, Technical University of Lisbon, Tapada da Ajuda, 1349-017 Lisbon, Portugal

[2] Estação Agronómica Nacional, Instituto Nacional de Investigação Agrária e Veterinária, 2784-505 Oeiras, Portugal.

Abstract

The limited knowledge on the hydraulic properties of semi-arid Cape Verde soils makes the use of water balance models difficult. In this paper, water retention characteristics of agricultural soils of Santiago Island and the development of point pedotransfer functions (PTF) to improve irrigation management are investigated. Soil water retention curves were studied in 72 horizons of 31 soil profiles located in Santiago Island. Soil textures varied from coarse to medium classes. PTFs were, at the same time, developed by regression analysis to predict total porosity (φ) and water retention at -0.25, -1, -3.2, -10, -33, -100, and -1500 kPa. Due to the lack of available data from Cape Verde, PTFs were developed from 85 soil horizons specifically selected from a Portuguese database. The PTFs were then validated with the data determined in the 72 soil horizons studied in Santiago Island. Statistics showed a relatively good performance of Cape Verde PTFs with RMSE varying between 0.030 and 0.086 $cm^3\ cm^{-3}$. However, Cape Verde PTFs always underestimated the measured values by -0.014 to -0.075 $cm^3\ cm^{-3}$. When compared with three other published PTFs, the new Cape Verde PTFs provided acceptable results for use in modelling aimed at improving irrigation water management practices.

Keywords: field capacity; modelling; soil hydraulic properties; water retention curves; wilting point.

Resumé

La connaissance limitée des propriétés hydrauliques des sols semi-arides de Cap Vert rend difficile l'utilisation des modèles de bilan hydrique des sols cultivés. Cet article concerne l'étude de la rétention de l'eau des sols agricoles de l'île de Santiago et le développement de fonctions de pedotransfer (PTF) pour améliorer la gestion de l'irrigation et la conservation de l'eau. Des courbes caractéristiques de l´humidité du sol ont été mesurées pour 72 horizons de 31 profils de sol de l'île de Santiago. La texture du sol varie entre sablonneuse et limoneuse moyenne. Les PTFs ont été développées par l'analyse de régression pour estimer tant la porosité totale (φ) que la rétention de l'eau aux pressions effectives de -0.25, -1, -3.2, -10, -33, -100, et -1500 kPa. En raison de l'absence d'autres données disponibles au Cap Vert à part les observations citées plus haut, les PTFs ont été développés à partir de 85 horizons de sol spécifiquement choisis parmi ceux inclus dans une base de données portugaise. Les PTFs ont été alors validées avec les données mesurées aux 72 horizons de sol étudiés a l'île de Santiago. Les indicateurs statistiques ont montré une exécution acceptable des PTFs, avec RMSE entre 0.030 et 0.086 cm^3 cm^{-3}. Cependant, les PTFs ont toujours sous-estimé de -0.014 jusqu'à -0.075 cm^3 cm^{-3} les valeurs mesurées. Pourtant, si on compare ces PTFs avec trois autres PTFs publiés, on constate que ces nouvelles PTFs pour Cap Vert donnent des résultats bien acceptables en vue de leur utilisation pour l'application de modèles de gestion de l'eau en irrigation.

Mots Clés: capacité au champ; modélisation; propriétés hydrauliques; courbes de rétention de l'eau; point de flétrissement; porosité totale.

1. Introduction

Countries located in regions with arid, semi-arid, and even dry sub-humid conditions have generally to cope with water scarcity. In these regions, controlling environmental effects and increasing the performance of irrigation are among the top priorities for soil and water resources protection and sustainable use (Pereira et al., 2009a). In Cape Verde, annual evaporation rates usually exceed 1500 mm while precipitation averages about 320 mm (Ministère de l'Environnement, de l'Agriculture et de la Pêche (MAAP), 2004). In this semi-arid country, irrigation is playing a major role in terms of food security and improving living standards by

increasing crop yields and rural incomes. However, irrigation has also enhanced some local environmental vulnerabilities, such as soil erosion, human induced soil salinization, and overexploitation of groundwater resources (Pereira et al., 2009a; Santos et al., 2010).

Appropriate irrigation water management practices under scarcity must be implemented. Soil water balance modelling to estimate crop irrigation requirements and supporting irrigation scheduling, i.e., defining the appropriate irrigation dates and volumes to be applied, has been playing an important role in improving water use in water scarce regions (e.g., Liu et al., 2006; Raes et al., 2006; Chopart et al., 2007; Pereira et al., 2009b; Rosa et al., 2012). However, the implementation of such tools in Cape Verde has been restrained due to lack of information on soil hydraulic properties, mainly field capacity and wilting point, which are required as input to soil water balance models as those referred above.

Thus, the objective of this study was to gain knowledge on the hydraulic properties of the soils of Cape Verde and provide information for soil water balance modelling. Soil water retention curves were characterized in 72 horizons of 31 soil profiles located in Santiago Island. At the same time, Pedotransfer Functions (PTF) (Bouma, 1989; Wösten et al., 2001; Pachepsky and Rawls, 2004) for estimating point specific values of Cape Verde soil water retention characteristics were developed from the information available in a Portuguese soil database (Ramos et al., 2011). The new Cape Verde PTFs were then validated with the retention data from the 72 soil horizons determined in Santiago Island, and by comparing the accuracy of its predictions with estimations from three other published PTFs relative to the Portuguese soil database PROPSOLO (Paz et al., 2009), the World Inventory of Soil Emission Potentials (WISE) database (Batjes, 1996), and the ROSETTA PTFs (Schaap et al., 2001).

2. Material and Methods

2.1. Study area

Cape Verde is a 10 islands (4033 km^2) semi-arid to arid country located in the Atlantic Ocean, 640 km west from Dakar, Senegal. Santiago (991 km^2) is the main island and holds for more than 52% of the country's arable land (MAAP, 2004). São Domingos (30.51 km^2) and Ribeira Seca (71.27 km^2) watersheds were selected to study the hydraulic behaviour of the soils of Santiago Island. The watersheds are located in the southern region of Santiago (Figure 1). The main soils

are Fluvisols, Leptosols, and Kastanozems (Faria, 1970; Food and Agricultural Organization (FAO), 2006), which are typically the soil reference groups used for agriculture in Cape Verde (Figure 2).

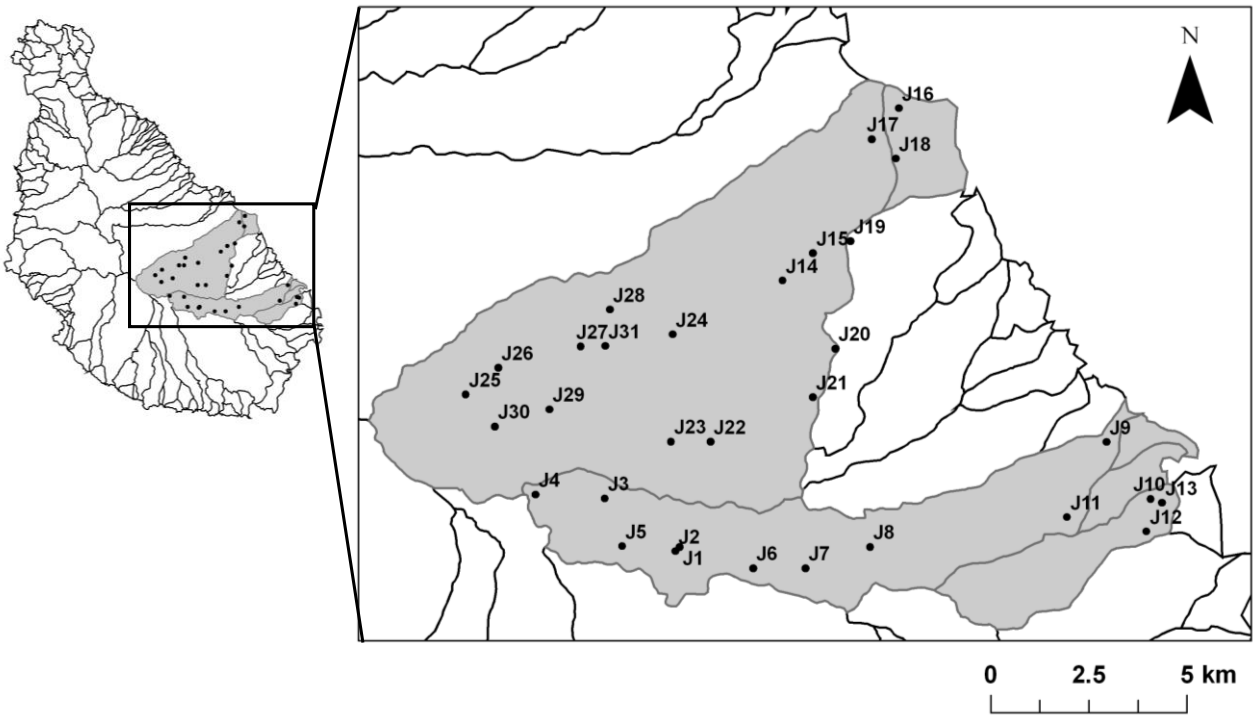

Fig. 1. Location of the studied watersheds and soil profiles.

2.2. Determination of soil water retention curves

Undisturbed samples (100 cm^3) were collected from 72 soil horizons of 31 soil profiles located in São Domingos and Ribeira Seca watersheds (Figure 1) to determine the soil water retention and the dry bulk density (ρ_b). The studied soil profiles were located mostly near the valley bottoms, with the exception of a few soil profiles studied in the upper (J4, J23, J25, and J28) and mid (J3, J7, J8, J21, J22, J26, J27, J29, and J31) slopes. Soil use was mostly associated with irrigated agriculture. Only a few profiles were studied in fields with rainfed agriculture (J8, J22, and J23) or agro-forestry systems (J4 and J7).

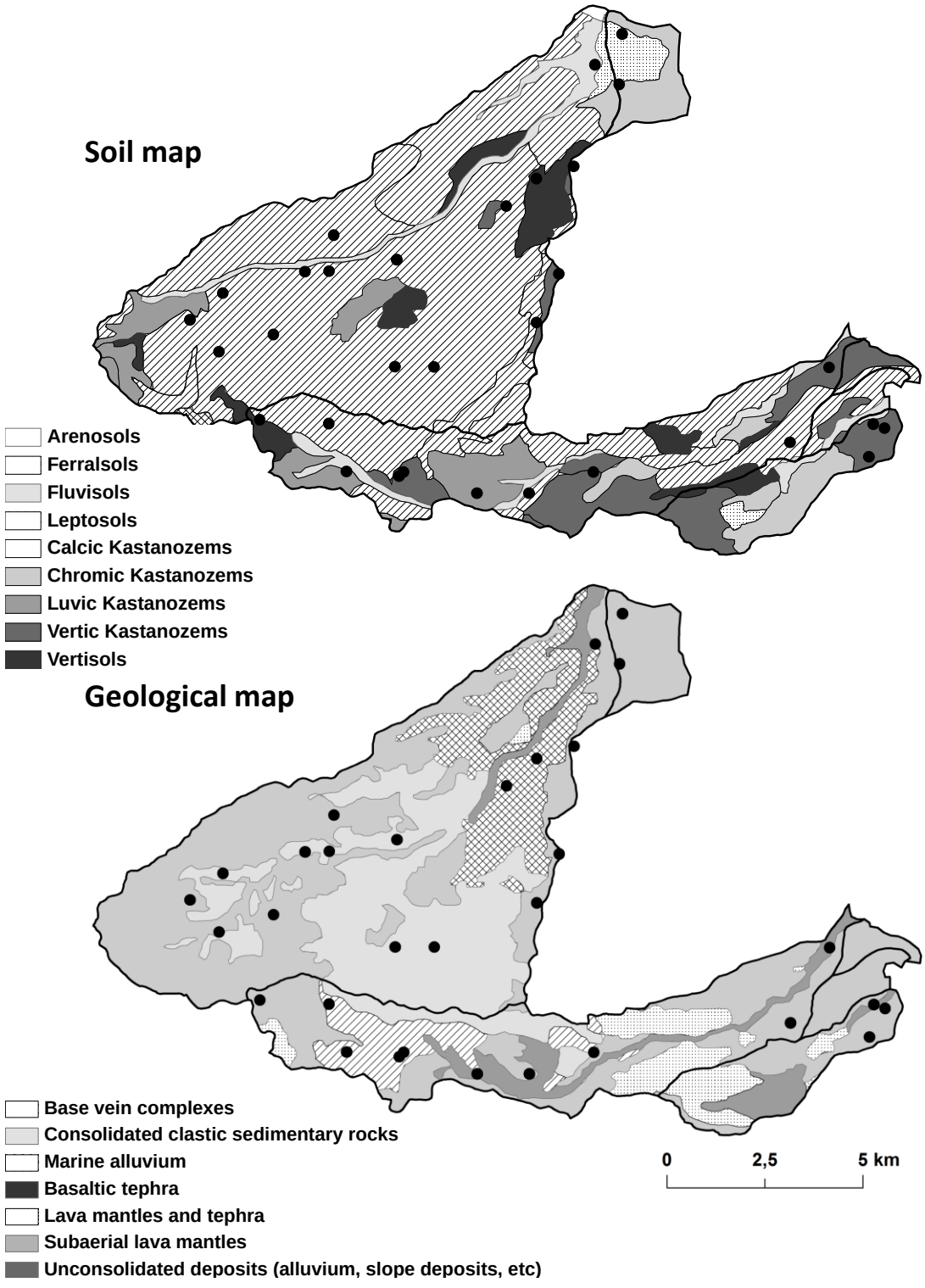

Fig. 2. Soil map (adapted from Faria, 1970) and geological map (adapted from Serralheiro et al., 1977) of the studied area, Santiago island. Dots refer to the sampling locations identified in Figure 1

For each soil horizon, water retention was determined in the laboratory on two separate 100 cm^3 samples using suction tables with sand for pressure heads of -0.25, -1, -3.2, and -10 kPa (Romano et al., 2002), while a pressure plate apparatus was used for pressure heads of -33, -100, and -1500 kPa (Dane and Hopmans, 2002). Soil water retention curves were described using the van Genuchten (1980) function:

$$S_e(h) = \frac{\theta(h) - \theta_r}{\theta_s - \theta_r} = \frac{1}{\left(1 + |\alpha h|^{\eta}\right)^{1-1/\eta}} \quad (1)$$

where S_e is effective saturation (-), θ_r and θ_s denote the residual and saturated water contents (L^3 L^{-3}), respectively, and α (L^{-1}) and η (-) are empirical shape factors. The water retention data were analyzed in terms of Eq. 1 using the RETC computer program (van Genuchten et al., 1991). The dry bulk density was obtained by drying volumetric soil samples (100 cm^3) at 105 ºC during 48 h. Total porosity (φ) was determined from the maximum gravimetric water contents of the soil samples and the bulk density. The particle size distribution was determined for 2, 20, 200 and 2000 µm, using the pipette method for particles having diameters <20 µm (clay, *C*, and silt, *S*, fractions), and by sieving for particles between 200 and 2000 µm (coarse sand, *CS*) and between 20 and 200 µm (fine sand, *FS*). These textural classes follow the Portuguese classification system (Gomes and Silva, 1962) and are based on international soil particle limits (Atterberg scale). Due to historical, social and cultural ties between Cape Verde and Portugal, this classification was also followed in this study. The organic carbon (*OC*) content was determined by the Walkley–Black method (Nelson and Sommers, 1982). The mean, minimum, maximum, and standard deviation values of the main physical and chemical properties of the soils of Cape Verde are given in Table 1.

2.3. Development of pedotransfer functions

Pedotransfer functions were developed to estimate total porosity (denoted by φ) and soil water contents at -0.25, -1, -3.2, -10, -33, -100, and -1500 kPa matric potentials of Cape Verde soils. Water retention values at -10, -33, and -1500 kPa were selected as they are the most important soil information required to parameterize soil-water balance models used for irrigation

Table 1. Mean, maximum, minimum and standard deviation values of the main physical and chemical properties of the Portuguese soils selected to derive Cape Verde pedotransfer functions (training set), and of the Cape Verde soils studied in Santiago island (testing set).

Parameter	Training set (Portuguese data)				Testing set (Cape Verde data)			
	mean	stdev.	min.	max.	mean	stdev.	min.	max.
CS (%)	27.1	18.3	0.1	91.2	30.2	12.1	5.5	65.9
FS (%)	38.8	15.5	3.9	69.1	31.5	10.4	12.0	63.9
Si (%)	20.4	13.6	3.4	68.1	19.1	5.7	6.1	36.1
C (%)	13.8	8.9	1.5	47.4	19.1	11.0	4.4	62.0
GPD	0.101	0.105	0.006	0.774	0.077	0.062	0.004	0.337
GSD	8.42	3.04	3.46	17.02	11.30	2.62	5.47	18.10
ρ_b (g cm^{-3})	1.41	0.17	1.00	1.73	1.25	0.15	0.97	1.75
OC (%)	0.78	0.53	0.03	2.83	1.28	0.90	0.19	5.53
Z (cm)	34.2	26.1	5.0	110.0	48.9	53.0	7.5	110.0
φ (cm^3 cm^{-3})	0.477	0.063	0.350	0.631	0.545	0.056	0.379	0.640
$\theta_{-0.25\ kPa}$ (cm^3 cm^{-3})	0.458	0.063	0.313	0.594	0.531	0.054	0.360	0.622
$\theta_{-1\ kPa}$ (cm^3 cm^{-3})	0.421	0.064	0.253	0.538	0.499	0.064	0.251	0.601
$\theta_{-3.2\ kPa}$ (cm^3 cm^{-3})	0.379	0.071	0.114	0.525	0.445	0.066	0.211	0.586
$\theta_{-10\ kPa}$ (cm^3 cm^{-3})	0.331	0.083	0.075	0.505	0.378	0.064	0.185	0.525
$\theta_{-33\ kPa}$ (cm^3 cm^{-3})	0.264	0.091	0.064	0.465	0.323	0.059	0.165	0.489
$\theta_{-100\ kPa}$ (cm^3 cm^{-3})	0.214	0.084	0.044	0.432	0.288	0.055	0.151	0.450
$\theta_{-1500\ kPa}$ (cm^3 cm^{-3})	0.127	0.067	0.012	0.360	0.213	0.049	0.109	0.378

CS – coarse sand; *FS* – fine sand; *S* – silt; *C* – clay; *GPD* – mean particle diameter; *GSD* – geometrical standard deviation; ρ_b – bulk density; *OC* – organic carbon; *Z* – mean soil depth; φ – total porosity; θ – soil water retention at different matric potentials.

management (Pereira et al., 1995). Soil water content at -10 and -33 kPa are normally associated with field capacity in coarse and medium textured soils, respectively, while soil water retention at -1500 kPa is generally accepted as the wilting point for most plants (Romano and Santini, 2002).

The term Pedotransfer Functions (PTFs) has been introduced by Bouma (1989) to define all predictive regression models that are used to obtain soil hydraulic properties (i.e. soil water retention and hydraulic conductivity points or model parameters) from basic soil physical and chemical properties usually easily available from soil survey studies (e.g. particle size distribution, bulk density, organic carbon content, soil structure and soil mineralogy).

In this study, a multiple regression analysis was followed to formulate PTFs for Cape Verde soils. The PTFs have the following general form:

$$y = a_0 + a_1 x_1 + a_2 x_2 + \ldots + a_n x_n \quad (2)$$

where y is the total porosity (φ) or water retention point ($\theta_{-0.25\ kPa}$, $\theta_{-1\ kPa}$, $\theta_{-3.2\ kPa}$, $\theta_{-10\ kPa}$, $\theta_{-33\ kPa}$, $\theta_{-100\ kPa}$, and $\theta_{-1500\ kPa}$) to be predicted; a_0, a_1, a_2, …, a_n are the regression coefficients; and x_1, x_2, …, x_n are the arguments of the PTFs, i.e., (i) soil texture (*CS*, *FS*, *S*, and *C*); (ii) mean particle diameter (*GPD*) and geometrical standard deviation (*GSD*), as defined by Shirazi and Boersma (1984); (iii) bulk density (ρ_b), (iv) organic carbon content (*OC*); and (v) mean soil depth (*Z*).

A few problems came up with the development of PTFs for Cape Verde soils. A first major obstacle in developing PTFs for Cape Verde was obviously the lack of information on soil hydraulic properties, namely soil-water retention characteristics of the soils in Santiago Island and other islands of Cape Verde. The lack of knowledge is in part justified by the inexistence of adequate laboratory equipment, high cost of analysis, and lack of trained technicians. The Portuguese database 'PROPriedades do SOLO' (PROPSOLO) was therefore selected as training set to derive PTFs for Cape Verde. The PROPSOLO database was created in 1997 and currently gathers 733 soil-water retention curves and 306 hydraulic conductivity curves determined in soil profiles of Portugal (Gonçalves et al., 1997, 1999; Ramos et al., 2011).

A second major obstacle for developing PTFs for Cape Verde was the well established fact that PTFs should not be used to make predictions for soils that are outside the range of soils used to derive the PTFs (Wösten et al., 2001). Most PTFs available in literature have been developed using databases with soil information collected in soils of temperate regions. Using those same PTFs in areas of the world with different soils and climates usually revealed unsatisfactory results (van den Berg et al., 1997; Tomasella and Hodnett, 1998; Wösten et al., 2001). The use of the Portuguese soil database for developing soil water retention PTFs for Cape Verde could lead to significant errors for the reasons cited above. However, the soil information available in PROPSOLO extends from dry temperate regions in southern Portugal's mainland to the volcanic Atlantic islands of Madeira and Azores. The database contains therefore a wider variety of information than the one normally found in other soil databases from temperate regions. In order to further reduce the error, only information for soil horizons that fell in the same texture range and having retention curves with similar shapes to the ones determined in the horizons of the soil profiles of Santiago Island (testing set) were selected for the training set.

The training set ended up gathering the information specifically selected from 85 soil horizons available in PROPSOLO. Table 1 lists the means, the minima and maxima, and the standard

deviation of the soils properties of those 85 horizons used as training set. The testing set was naturally composed by φ and soil water retention values at -0.25, -1, -3.2, -10, -33, -100, and -1500 kPa determined in the 72 soil horizons studied in Santiago Island.

2.4. Statistical analysis

The performance of PTFs developed for Cape Verde was assessed by using some of the standard criteria for evaluating the accuracy/reliability of the PTFs (Wösten et al., 2001; Schaap, 2004), such as the determination coefficient (R^2), the mean error (ME), the mean absolute error (MAE), the root mean square error (RMSE), and the mean relative error (MRE) defined as:

$$R^2 = \left[\frac{\sum_{i=1}^{N} \left(O_i - \bar{O} \right) \left(P_i - \bar{P} \right)}{\left[\sum_{i=1}^{N} \left(O_i - \bar{O} \right)^2 \right]^{0.5} \left[\sum_{i=1}^{N} \left(P_i - \bar{P} \right)^2 \right]^{0.5}} \right]^2 \quad (2)$$

$$ME = \frac{1}{N} \sum_{i=1}^{N} \left(P_i - O_i \right) \quad (3)$$

$$MAE = \frac{1}{N} \sum_{i=1}^{N} \left| P_i - O_i \right| \quad (4)$$

$$RMSE = \sqrt{\frac{\sum_{i=1}^{N} \left(P_i - O_i \right)^2}{N-1}} \quad (5)$$

$$MRE = \frac{1}{N} \sum_{i=1}^{N} \left| \frac{P_i - O_i}{O_i} \right| \quad (6)$$

where N is the number of observations, O_i are the measured values, P_i are the PTFs predictions, $\overline{O}$ is the average of the measured values, and $\overline{P}$ is the average of the PTFs predictions.

The predicting capabilities of the PTFs were further validated by comparing the error (R^2, ME, MAE, RMSE, and MRE) obtained when estimating φ and the soil water retention at the studied matric potentials with Cape Verde PTFs, and with the PTFs developed by Paz et al. (2009), Batjes (1996), and Schaap et al. (2001). Paz et al. (2009) developed PTFs (PTFs Portugal) for

point specific values of the water retention characteristics of Portuguese soils using the entire dataset of the same soil database. Thus, comparing the prediction errors of both models would assess if the new developed PTFs actually contributed significantly to improve water content estimations in Cape Verde soils. Batjes (1996) also developed PTFs (PTFs ISRIC) for point specific values of the water retention characteristics for the soil units shown on FAO's soil map of the world. Batjes (1996) used the International Soil Reference and Information Centre (ISRIC) database, which gathers information for soils from different regions of the world, including 1799 soil profiles from Africa. Thus, Batjes (1996) PTFs could actually provide better estimates of soil-water content than Cape Verde PTFs due to the extensive amount of data available from the soils of Africa. Finally, Schaap et al. (2001) developed PTFs (ROSETTA) for estimating model parameters in van Genuchten-Mualem functional relationships (van Genuchten, 1980). ROSETTA is likely to be one of the most used models to derive soil hydraulic properties. Therefore, the accuracy of its estimations for Cape Verde soils was also assessed. As we were comparing point specific values of the water retention characteristics, and not model parameters, the predictions of φ and soil water retention at -0.25, -1, -3.2, -10, -33, -100, and -1500 kPa matric potentials were calculated after first estimating soil water retention curve parameters of Cape Verde soils.

In order to apply Batjes (1996) and Schaap et al. (2001) PTFs, the particle size distribution of Cape Verde soils, which was determined based on the international soil particle limits (Atterberg scale), was converted into the USDA soil particle limits by loglinear interpolation (Leij et al., 1994; Nemes et al., 1999), as follows:

$$CP_n = CP_{n-1} + \frac{(-\phi_n)-(-\phi_{n-1})}{(-\phi_{n+1})-(-\phi_{n-1})}(CP_{n+1} - CP_{n-1}) \quad (7)$$

where *CP* is the cumulative percentage on the particle-size distribution curve, $-\Phi$ is the $\log_2$ value of the particle-size limits (in mm), and notations *n*, *n-1*, *n+1* are the missing particle-size limit, the preceding neighbouring limit and the succeeding neighbouring limit, respectively.

3. Results and Discussion

3.1. Soil water retention curves in Santiago Island

Table 2 presents the mean and standard deviation values obtained for total porosity and for soil water retention at -0.25, -1, -3.2, -10, -33, -100, and -1500 kPa. The results were grouped by textural classes. The soil textures found in 72 soil horizons studied in São Domingos and Ribeira Seca watersheds were mainly loam (*n*=31) and sandy loam (*n*=25) (Figure 3). Soil water retention presented high variability for each pressure head, with standard deviation values varying between 0.006 and 0.145 cm^3 cm^{-3}.

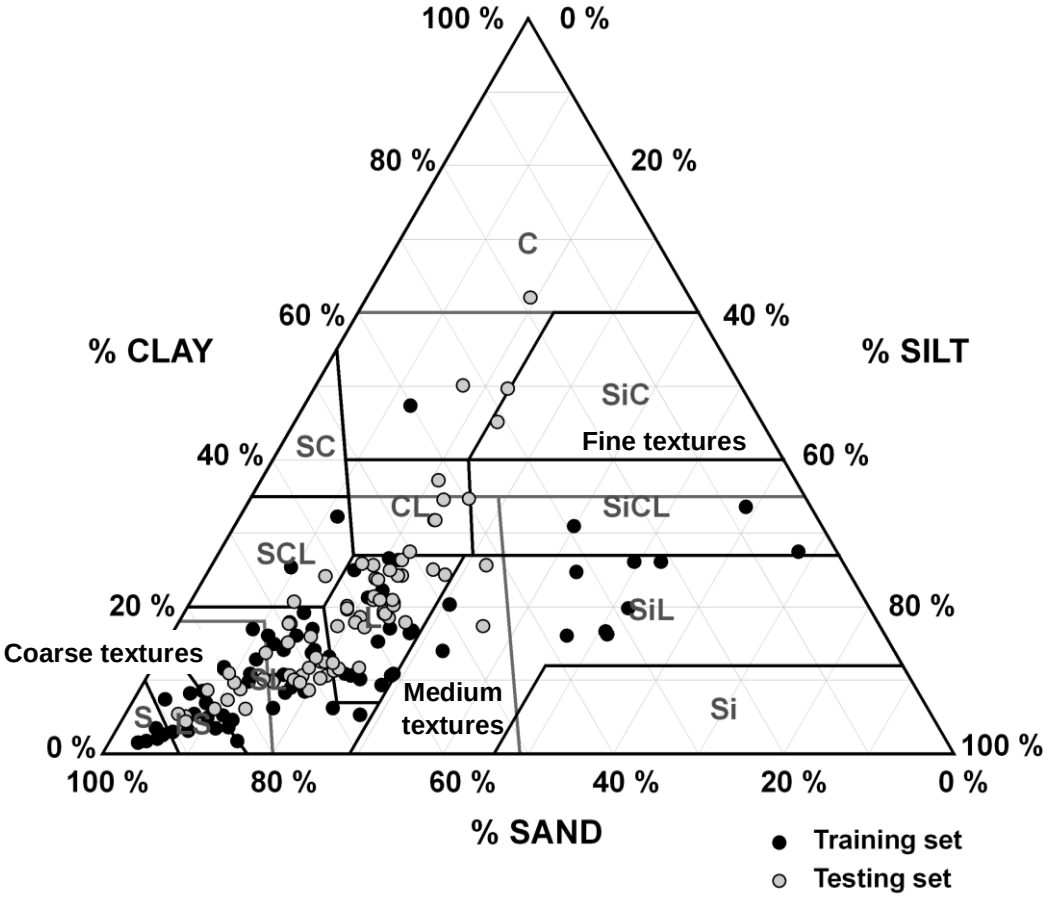

Fig. 3. Textural distribution of the 85 samples taken from the Portuguese database and used to develop pedotransfer functions (PTFs) for estimating point specific values of the water retention characteristics in Cape Verde soils (training set) and the 72 samples collected in Cape Verde and used to validate those

Table 2. Mean values and standard deviation (in brackets) of soil water retention at -0.25, -1, -3.2, -10, -33, -100 and -1500 kPa, and van Genuchten's parameters for Cape Verde soils.

Texture class	N	Volumetric water content							van Genuchten's parameters			
		$\theta_{-0.25\ kPa}$	$\theta_{-1\ kPa}$	$\theta_{-3.2\ kPa}$	$\theta_{-10\ kPa}$	$\theta_{-33\ kPa}$	$\theta_{-100\ kPa}$	$\theta_{-1500\ kPa}$	θ_r	θ_s	α	η
		($cm^3\ cm^{-3}$)							($cm^3\ cm^{-3}$)		(cm^{-1})	(-)
Loamy sand	3	0.518	0.450	0.414	0.307	0.250	0.224	0.175	0.174	0.531	0.138	1.614
		(0.060)	(0.122)	(0.145)	(0.074)	(0.048)	(0.046)	(0.034)	(0.046)	(0.050)	(0.194)	(0.172)
Sandy loam	25	0.516	0.479	0.429	0.358	0.296	0.261	0.191	0.128	0.529	0.115	1.354
		(0.068)	(0.075)	(0.075)	(0.065)	(0.054)	(0.050)	(0.046)	(0.075)	(0.070)	(0.128)	(0.188)
Sandy clay loam	2	0.569	0.553	0.513	0.446	0.399	0.370	0.309	0.164	0.576	0.066	1.315
		(0.058)	(0.053)	(0.074)	(0.111)	(0.128)	(0.114)	(0.098)	(0.102)	(0.060)	(0.038)	(0.327)
Clay	3	0.545	0.518	0.478	0.452	0.405	0.360	0.251	0.017	0.550	0.087	1.140
		(0.031)	(0.031)	(0.019)	(0.030)	(0.049)	(0.057)	(0.018)	(0.019)	(0.046)	(0.078)	(0.028)
Clay Loam	5	0.540	0.521	0.466	0.418	0.361	0.320	0.239	0.110	0.554	0.100	1.179
		(0.063)	(0.065)	(0.063)	(0.064)	(0.054)	(0.048)	(0.045)	(0.056)	(0.064)	(0.053)	(0.050)
Loam	31	0.536	0.508	0.447	0.381	0.329	0.295	0.217	0.128	0.553	0.127	1.276
		(0.044)	(0.048)	(0.052)	(0.053)	(0.045)	(0.042)	(0.043)	(0.071)	(0.047)	(0.123)	(0.159)
Silty Loam	2	0.544	0.515	0.459	0.417	0.372	0.330	0.252	0.131	0.561	0.136	1.170
		(0.006)	(0.012)	(0.024)	(0.029)	(0.011)	(0.014)	(0.011)	(0.081)	(0.015)	(0.087)	(0.033)
Silty Clay	1	0.557	0.544	0.485	0.391	0.342	0.301	0.198	0.078	0.576	0.078	1.200
		(-)	(-)	(-)	(-)	(-)	(-)	(-)	(-)	(-)	(-)	(-)

N – number of observations

Soil water retention values in the dry region of the soil-water retention curve presented unusually high values when compared with the soils from Portugal. In Cape Verde, water retention at -1500 kPa averaged, for example, 0.175, 0.191 and 0.217 cm^3 cm^{-3} in soils with loamy sand, sandy loam and loam textures, respectively. In Portugal, the corresponding average water retention values are much smaller, 0.0576, 0.1179, and 0.1418 cm^3 cm^{-3} (Ramos et al., 2011). The soil water retention values observed in Cape Verde at higher suctions were also larger when compared with typical soil water characteristics for different soil types reported by Allen et al. (1998).

The high water content values observed in the dry ends of the water retention curves of the soils of Cape Verde suggest that the different hydrological behaviour could be attributed to mineralogical and pedo-genetic factors. The geology of Santiago Island is mainly characterized by alkali basaltic rocks and respective pyroclastic products (Figure 2). Quaternary sediments and calcareous sedimentary rocks also occur (Faria, 1970; Serralheiro, 1977; Pinto, 2010; Marques et al., 2012). Magnetite/maghmites, hematites, pyroxens, and filossilicates are the most common minerals found in those soils. However, these minerals are quite common and do not justify the hydrological behaviour observed in Cape Verde soils per se. Therefore, a possible explanation would be the soil composition of an alkaline basalt chemical weathering process under dry and warm tropical conditions in combination with the spatial arrangement of the solid constituents in the soil matrix.

Soil water retention curves were well described with the van Genuchten's (1980) function (Eq. 1). The mean and standard deviation values of the van Genuchten's (1980) model parameters for each textural class are also given in Table 2. The hydraulic parameters obtained for the soils of Cape Verde follow the same tendencies reported by Schaap et al. (1998) and Ramos et al. (2011). Average values for θ_s increase from coarse to medium textures, while η decrease in the same direction. Similarly to Schaap et al. (1998) and Ramos et al. (2011), no tendency regarding α could be observed. As for θ_r, since the dry ends of the water retention curves of the soils of Cape Verde present relatively high water content values when compared with soils from temperate regions, θ_r also showed higher average values than those reported in literature (e.g., Carsel and Parish, 1988; Schaap et al., 1998; Ramos et al., 2011).

3.2. Pedotransfer functions for Cape Verde

Table 3 presents the PTFs to estimate total porosity (φ) and soil water retention at -0.25, -1, -3.2, -10, -33, -100, and -1500 kPa of Cape Verde soils. These coefficients were selected by stepwise regression and were chosen by their utility to predict φ and soil water retention from basic soil properties (*CS*, *FS*, *S*, *C*, ρ_b, etc). PTFs for φ and $\theta_{-0.25\ kPa}$ were similar, with both functions having the same four arguments (*FS*, *GPD*, ρ_b, and *Z*). The main difference in these PTFs was the lower constant value observed as the pressure head decreased. The PTFs developed for $\theta_{-3.2\ kPa}$ and $\theta_{-10\ kPa}$, and for $\theta_{-33\ kPa}$ and $\theta_{-100\ kPa}$ were also found to be similar, with the first two requiring the same four arguments (*CS*, *FS*, *GPD*, and ρ_b), and the last two the same five arguments (*FS*, *Si*, *C*, *GSD*, and ρ_b). The PTF developed for $\theta_{-1500\ kPa}$ needed six arguments (*CS*, *FS*, *Si*, *C*, *GSD* and ρ_b). Organic Carbon content was not statistically significant and was excluded from all functions by stepwise regression.

Table 3. Point pedotransfer functions for Cape Verde Soils.

PTFs Cape Verde	
$\varphi = 0.920 - 0.00067\ FS - 0.128\ GPD - 0.281\ \rho_b - 0.00022\ Z$	(R^2 = 83.2%)
$\theta_{-0.25\ kPa} = 0.901 - 0.00081\ FS - 0.165\ GPD - 0.276\ \rho_b - 0.00020\ Z$	(R^2 = 87.0%)
$\theta_{-1.0\ kPa} = 0.748 + 0.001\ Si - 0.180\ GPD - 0.233\ \rho_b$	(R^2 = 76.8%)
$\theta_{-3.2\ kPa} = 0.702 - 0.0016\ CS - 0.00077\ FS - 0.201\ GPD - 0.163\ \rho_b$	(R^2 = 69.1%)
$\theta_{-10\ kPa} = 0.697 - 0.0025\ CS - 0.00151\ FS - 0.192\ GPD - 0.156\ \rho_b$	(R^2 = 75.8%)
$\theta_{-33\ kPa} = 0.140 + 0.0013\ FS + 0.0047\ Si + 0.0032\ C + 0.0066\ GSD - 0.086\ \rho_b$	(R^2 = 79.6%)
$\theta_{-100\ kPa} = 0.108 + 0.00077\ FS + 0.0041\ Si + 0.003\ C + 0.0065\ GSD - 0.074\ \rho_b$	(R^2 = 82.0%)
$\theta_{-1500\ kPa} = -560.9 + 5.61\ CS + 5.61\ FS + 5.61\ Si + 5.61\ C - 0.0095\ GSD - 0.071\ \rho_b$	(R^2 = 80.9%)

CS – coarse sand; *FS* – fine sand; *S* – silt; *C* – clay; *GPD* – mean particle diameter; *GSD* – geometrical standard deviation; ρ_b – bulk density; *OC* – organic carbon; *Z* – mean soil depth; φ – total porosity; θ – soil water retention at different matric potentials.

Table 4 presents statistics R^2, ME, MAE, RMSE, and MRE to evaluate the accuracy of the PTFs developed for Cape Verde soils. ME values revealed that PTFs predictions underestimated all

measured water retention points by -0.014 ($\theta_{-10\ kPa}$) to -0.075 ($\theta_{-1\ kPa}$) $cm^3\ cm^{-3}$. The best estimates were for φ and $\theta_{-10\ kPa}$. Since field capacity ($\theta_{-10\ kPa}$ or $\theta_{-33\ kPa}$) and the wilting point ($\theta_{-1500\ kPa}$) estimation in Cape Verde PTFs produced a similar bias, the assessment of the available water holding capacity (AWC=FC-WP) may be relatively safe for irrigation scheduling modelling. Figure 4 shows the histogram of the residuals obtained from the difference between AWC values predicted with Cape Verde PTFs and observations. Field capacity was associated to $\theta_{-33\ kPa}$ and soil depth was set to 1 m to serve as reference for comparison. The histogram shows that the residuals follow a normal distribution, with an average value of 14.09 mm/m, and kurtosis (0.88) and skewness (-0.21) close to zero. The Shapiro-Wilks, Chi-Square, and Kolmogorov-Smirnov goodness-of-fit tests allow accepting the hypothesis that residuals are normally distributed at a level of 90% confidence. The normal distribution of the residuals helps sustaining the argument that AWC estimates from Cape Verde PTFs may be relatively safe, despite the fact that field capacity and the wilting point may be slightly underestimated.

Table 4. Accuracy of water retention PTFs developed for Cape Verde.

PTFs	φ	$\theta_{-0.25\ kPa}$	$\theta_{-1\ kPa}$	$\theta_{-3.2\ kPa}$	$\theta_{-10\ kPa}$	$\theta_{-33\ kPa}$	$\theta_{-100\ kPa}$	$\theta_{-1500\ kPa}$
Cabo Verde								
R^2	0.659	0.682	0.577	0.363	0.357	0.356	0.342	0.214
ME	-0.018	-0.021	-0.075	-0.034	-0.014	-0.024	-0.037	-0.038
MAE	0.030	0.031	0.079	0.050	0.045	0.047	0.052	0.052
RMSE	0.038	0.038	0.086	0.063	0.056	0.060	0.065	0.065
MRE	0.058	0.061	0.188	0.127	0.131	0.176	0.241	0.370
Portugal								
R^2	…	0.754	…	…	0.303	…	…	0.177
ME	…	-0.049	…	…	-0.024	…	…	-0.073
MAE	…	0.050	…	…	0.049	…	…	0.076
RMSE	…	0.057	…	…	0.059	…	…	0.088
MRE	…	0.106	…	…	0.142	…	…	0.626
ISRIC								
R^2	0.166	…	0.210	0.154	0.281	0.331	…	0.186
ME	-0.185	…	-0.155	-0.164	-0.110	-0.112	…	-0.086
MAE	0.188	…	0.159	0.165	0.112	0.113	…	0.087
RMSE	0.206	…	0.177	0.184	0.129	0.125	…	0.099
MRE	0.616	…	0.538	0.689	0.487	0.609	…	0.813
ROSETTA								
R^2	0.445	0.486	0.418	0.304	0.305	0.275	0.219	0.154
ME	-0.098	-0.085	-0.060	-0.032	-0.034	-0.073	-0.112	-0.119
MAE	0.099	0.086	0.070	0.054	0.056	0.081	0.116	0.119
RMSE	0.108	0.094	0.078	0.067	0.070	0.093	0.125	0.129
MRE	0.227	0.197	0.162	0.138	0.177	0.354	0.720	1.427

PTF – pedotransfer function, R^2 – coefficient of determination (-), ME – mean error (cm^3 cm^{-3}), MAE – mean absolute error (cm^3 cm^{-3}), RMSE – root mean square error (cm^3 cm^{-3}), MRE – mean relative error (cm^3 cm^{-3}).

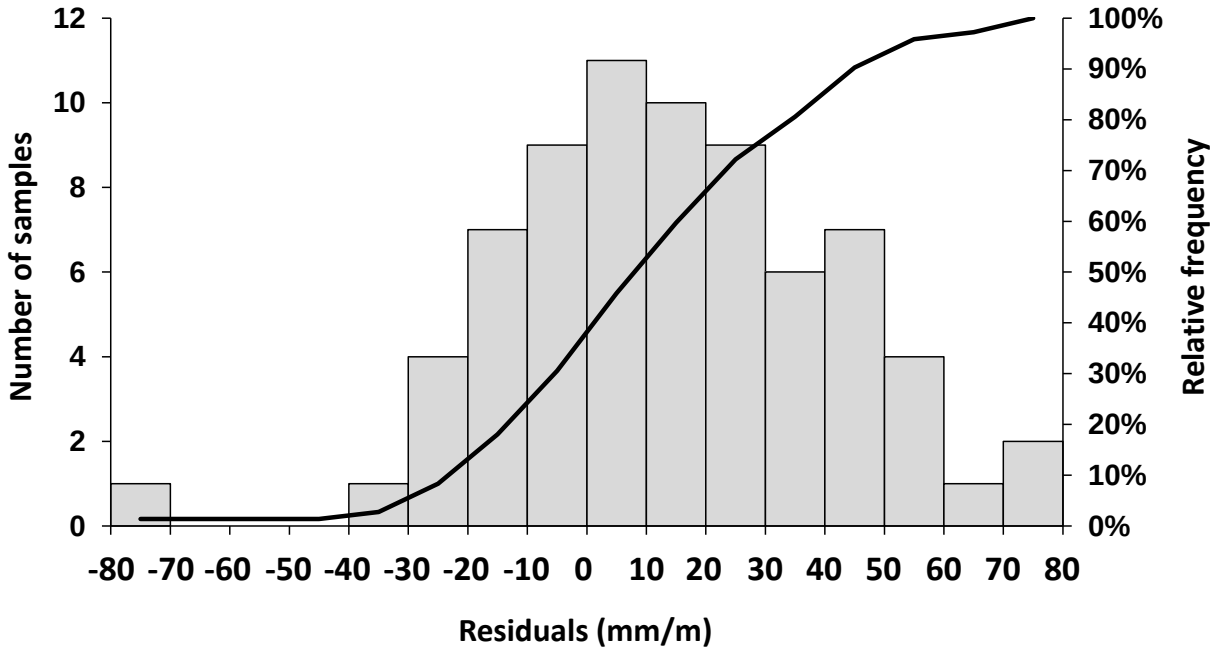

Fig. 4. Histogram of the residuals of the difference between available water capacity values predicted with Cape Verde PTFs and observations.

In terms of MAE, results showed a systematic error that increased while pressure heads decreased, i.e., φ, $\theta_{-10\ kPa}$, $\theta_{-33\ kPa}$, and $\theta_{-1500\ kPa}$ produced an increasing systematic error of 0.030, 0.045, 0.047 and 0.052 cm^3 cm^{-3}, respectively. RMSE also increased from 0.038 cm^3 cm^{-3} to 0.065 cm^3 cm^{-3}. The relative size of the systematic error (MRE) also increased from higher (MRE φ=5.8%) to lower pressure heads (MRE $\theta_{-1500\ kPa}$=37.0%). The higher MRE registered at lower pressure heads resulted normally from the bias observed in the dry ends of the water retention curves between the soils of Portugal and Cape Verde, since the latter were higher than the ones observed in the Portuguese soils. Figure 5 presents the deviations between measured values and PTFs predictions which help to understand the errors associated with the PTFs developed for Cape Verde.

Cape Verde PTFs provided better predictions of all water retention points than the PTFs published by Paz et al. (2009), Batjes (1996) and Schaap et al. (2001). These three PTFs also underestimated Cape Verde soil-water retention across the entire range of measured pressure heads (Figure 5) but with greater bias than Cape Verde PTFs. PTFs ISRIC (Batjes, 1996)

provided, in general, the worse results for all water retention points with ME varying between -0.086 and -0.185 $cm^3\ cm^{-3}$, and RMSE between 0.099 and 0.206 $cm^3\ cm^{-3}$. PTFs Portugal (Paz et al., 2009) and PTFs ROSETTA (Schaap et al., 2001) likewise resulted in worse estimations of the studied pressure heads than Cape Verde PTFs. ROSETTA provided the worst predictions for $\theta_{4.2}$ (RMSE = 0.129 $cm^3\ cm^{-3}$; ME = -0.119 $cm^3\ cm^{-3}$). However, as observer in Figure 5, the main problem with these two PTFs was their inability to reasonably predict Cape Verde soil water retention at lower pressure heads.

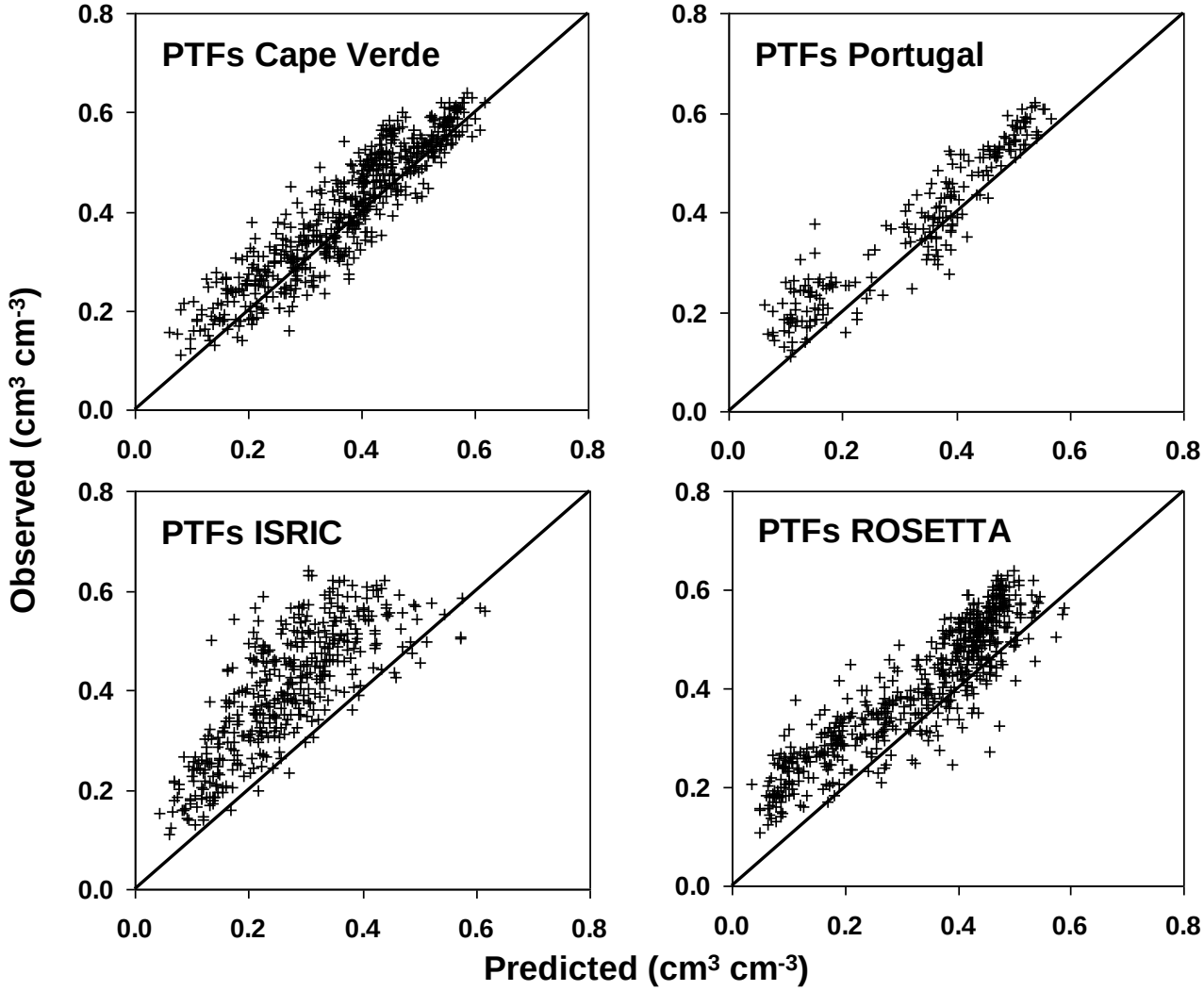

Fig. 5. Measured water retention values versus predictions obtained with PTFs Cape Verde, PTFs Portugal (Paz et al., 2009), PTFs ISRIC (Batjes, 1996), and PTFs ROSETTA (Schaap et al., 2001).

4. Conclusions

Agricultural areas of Cape Verde are mainly located in Santiago Island, in soils with coarse and medium textures. Soil water retention values at lower pressure heads presented unusually high values when compared with soils from temperate regions. The differences in hydrological behavior between soils in temperate regions and soils from dry tropical Cape Verde suggest the influence of mineralogical and pedo-genetic factors associated to the spatial arrangement of the solid constituents of these latter soils.

Pedotransfer functions (PTFs) were derived to predict total porosity (φ) and point specific values of the water retention characteristics at -0.25, -1, -3.2, -10, -33, -100, and -1500 kPa from basic soil properties, namely texture and bulk density. However, these PTFs are only valid for soils with coarse and medium textures. Statistics show a relatively good performance for those PTFs with RMSE varying between 0.038 (φ) and 0.086 ($\theta_{-1\ kPa}$) $cm^3\ cm^{-3}$. However, care should be taken to use the functions here developed for prediction of point specific values of the water retention characteristics since Cape Verde PTFs always underestimated the measured values by -0.014 ($\theta_{-10\ kPa}$) to -0.075 ($\theta_{-1\ kPa}$) $cm^3\ cm^{-3}$, and since the wilting point seem to fall outside the range of the original database used to develop the PTFs. Nonetheless, the PTFs here published provide an important basis to support the use of simulation models aimed at improving irrigation water management practices in Cape Verde since it provided better estimates than three other published PTFs.

Acknowledgments

This study was supported by Fundação para a Ciência e Tecnologia contracts SFRH/BD/60972/2009 and SFRH/BD/60363/2009.

References

Allen, R.G., Pereira, L.S., Raes, D., Smith, M., 1998. Crop Evapotranspiration. Guidelines for Computing Crop Water Requirements. FAO Irrig. Drain. Paper 56, Food and Agricultural Organization, Rome.

Batjes, N.H., 1996. Development of a world data set of soil water retention properties using pedotransfer rules. Geoderma 71, 31-52.

Bouma, J., 1989. Using soil survey data for quantitative land evaluation. Adv. Soil Sci. 9, 177-213.

Carsel, R.F., Parish, R.S., 1988. Developing joint probability distributions of soil and water retention characteristic. Water Resour. Res. 24, 755-769.

Chopart, J.L., Mézino, M., Aure, F., Le Mézo, L., Mété, M., Vauclin, M., 2007. OSIRI: A simple decision-making tool for monitoring irrigation of small farms in heterogeneous environments. Agric. Water Manage. 87, 128-138.

Dane, J.H., Hopmans, J.W., 2002. Pressure plate extractor. In: Dane, J.H., Topp, G.C. (Eds.). Methods of Soil Analysis, Part 4. Physical Methods, pp 688-690. Soil Science Society of America book Series, Madison, Wisconsin.

Food and Agricultural Organization (FAO), 2006. World Reference Base for Soil Resources. A Framework for International Classification, Correlation and Communication. FAO World Soil Resources Report 103, Rome, Italy.

Faria, F.X., 1970. Os Solos da Ilha de Santiago (Arquipélago de Cabo Verde). Estudos, Ensaios e Documentos nº 124. Junta de Investigação do Ultramar, Lisboa, p 157.

Gomes, M.P., Silva, A.A., 1962. Um novo diagrama triangular para a classificação básica da textura do solo. Garcia da Orta 10, 171-179.

Gonçalves, M.C., Pereira, L.S., Leij, F.J., 1997. Pedo-transfer functions for estimating unsaturated hydraulic properties of Portuguese soils. Eur. J. Soil Sci. 48, 387-400.

Gonçalves, M.C., Almeida, V.V., Pereira, L.S., 1999. Estimation of hydraulic parameters for Portuguese soils. In: van Genuchten, M.Th., Leij, F., Wu, L. (Eds). Characterization and Measurement of the Hydraulic Properties of Unsaturated Porous Media, Part 2, pp 1199-1209. USDA-ARS, US Salinity Laboratory and Dept. Environmental Sciences, University of California, Riverside.

Leij, F.J., Alves, W.J., van Genuchten, M.Th., Williams, J.R., 1994. Unsaturated Soil Hydraulic Database, UNSODA 1.0 User's Manual. Office of Research and Development. United States Environmental Protection Agency, Ada, OK.

Liu, Y., Pereira, L.S., Fernando, R.M., 2006. Fluxes through the bottom boundary of the root zone in silty soils: Parametric approaches to estimate groundwater contribution and percolation. Agric. Water Manage. 84, 27-40.

Ministère de l'Environnement, de l'Agriculture et de la Pêche (MAAP). 2004. Agriculture et Pêche: Stratégie de développement a l'horizon 2015 & Plan d'Action 2005-2008. Ministère de l'Environnement, de l'Agriculture et de la Pêche, et Organisation des Nations Unies pour l'Alimentation et l'Agriculture, Praia, Cap Vert.

Marques, R., Prudêncio, M.I., Rocha, F., Pinto, M.M.S.C., Silva, M.M., Silva, E.F., 2012. REE and other trace and major elements in the topsoil layer of Santiago Island. Cape Verde. J. African Earth Sci. 64, 20-33.

Nelson, D.W., Sommers, L.E., 1982. Total carbon, organic carbon, and organic matter. In: Page A.L. (Ed.). Methods of Soil Analysis, Part 2, Chemical and Microbiological Properties, pp 539-579. Agronomy monographs Nº 9. American Society of Agronomy and Soil Science Society of America, Madison, Wisconsin.

Nemes, A., Wösten, J.H.M., Lilly, A., Oude Voshaar, J.H., 1999. Evaluation of different procedures to interpolate particle-size distribution to achieve compatibility within soil databases. Geoderma 90, 187-202.

Pachepsky, Ya.A., Rawls, W.J., 2004. Development of Pedotransfer Functions in Soil Hydrology. Developments in Soil Science 30, Elsevier, Amsterdam, The Netherlands.

Paz, A.M., Cipriano, D., Gonçalves, M.C., Pereira, L.S., 2009. Funções de pedo-transferência para a curva de retenção da água no solo. Rev. Ciências Agrárias 32, 337-343.

Pereira, L.S., van den Broek, B., Kabat, P., Allen, R.G., 1995. Crop-Water Simulation Models in Practice. Wageningen Pers, Wageningen, The Netherlands.

Pereira, L.S., Cordery, I., Iacovides, I., 2009a. Coping with Water Scarcity. Addressing the Challenges. Springer, Dordrecht.

Pereira, L.S., Paredes, P., Cholpankulov, E.D., Inchenkova, O.P., Teodoro, P.R., Horst, M.G., 2009b. Irrigation scheduling strategies for cotton to cope with water scarcity in the Fergana Valley, Central Asia. Agric. Water Manage. 96, 723-735.

Pinto, M.M.S.C., 2010. Cartografia geoquímica da ilha de Santiago com uma densidade de amostragem média/baixa. PhD Thesis, Universidade de Aveiro. Portugal.

Raes, D., Geerts, S., Kipkorir, E., Wellens, J., Sahli, A., 2006. Simulation of yield decline as a result of water stress with a robust soil water balance model. Agric.l Water Manage. 81, 335-357.

Ramos, T.B., Gonçalves, M.C., Martins, J.C., Pires, F.P., Pereira, L.S., 2011. Propriedades hidráulicas dos solos para as diferentes classes texturais. Rev. Ciências Agrárias 34(2), 252-264.

Romano, N., Hopmans, J.W., Dane, J.H., 2002. Suction table. In: Dane, J.H., Topp, G.C. (Eds). Methods of Soil Analysis, Part 4, Physical Methods, pp 692-698. Soil Science Society of America Book Series, Madison, Wisconsin.

Romano, N., Santini, A., 2002. Water retention and storage. Field. In: Dane, J.H., Topp, G.C. (Eds). Methods of Soil Analysis, Part 4, Physical Methods, pp 721-738. Soil Science Society of America Book Series, Madison, Wisconsin.

Rosa, R.D., Paredes, P., Rodrigues, G.C., Fernando, R.M., Alves, I., Pereira, L.S., Allen, R.G., 2012. Implementing the dual crop coefficient approach in interactive software: 2. Model testing. Agric. Water Manage. 103, 62-77.

Santos, F.A.M., Gonçalves, R.M.D., Represas, P., Almeida, E.P., 2010. Cape Verde Santiago's island salt water origin?. Proceeding of SWIM21 21st Salt Water Intrusion Meeting (21-26 June, Azores, Portugal), pp. 85-88.

Schaap, M.G., Leij, F.L., van Genuchten, M.Th., 1998. Neural network analysis for hierarchical prediction of soil hydraulic properties. Soil Sci. Soc. America J. 62, 847-855.

Schaap, M.G., Leij, F.L., van Genuchten, M.Th., 2001. Rosetta: a computer program for estimating soil hydraulic parameters with hierarchical pedotransfer functions. J. Hydrol. 251, 163-176.

Schaap, M.G., 2004. Accuracy and uncertainty in PTF predictions. In: Pachepsky, Y.A., Rawls, W.J. (Eds.). Development of Pedotransfer Functions in Soil Hydrology. pp 33-43. Developments in Soil Science, vol. 30, Elsevier, Amsterdam, The Netherlands.

Serralheiro, A., 1977. Carta geológica da Ilha de Santiago (Cabo Verde) na escala 1:100 000. Junta de Investigação Cientifica do Ultramar. Laboratório de Estudos Petrológicos e Paleontológicos do Ultramar. Lisboa.

Shirazi, M.A., Boersma, L., 1984. A unifying quantitative analysis of soil texture. Soil Sci. Soc. Am. J. 48, 142–147.

Tomasella, J., Hodnett, M.G., 1998. Estimating soil water retention characteristics from limited data in Brazilian Amazonia. Soil Sci 163, 190-202.

van den Berg, M., Klamt, E., van Reeuwijk, L.P., Sombroek, W.G., 1997. Pedotransfer functions for the estimation of moisture content characteristics of Ferralsols and related soils. Geoderma 78, 161-180.

van Genuchten, M.Th., 1980. A closed form equation for predicting the hydraulic conductivity of unsaturated soils. Soil Sci. Soc. Am. J. 44, 892-898.

van Genuchten, M.Th., Leij, F.J., Yates, S.R., 1991. The RETC code for quantifying the hydraulic functions of unsaturated soils. Report No. EPA/600/2-91/065. R. S. Kerr Environmental Research Laboratory, U.S. Environmental Protection Agency, Ada, Oklahoma.

Wösten, J.H.M., Pachepsky, Y.A., Rawls, W.J., 2001. Pedotransfer functions: bridging the gap between available basic soil data and missing soil hydraulic characteristics. J. Hydrol. 251, 123-150.

Chapter 9

Discussion and conclusions

1. Discussion and conclusions

The study presented in Chapter 2 analyzed a field experiment carried out in Alvalade and Mitra where maize was irrigated with waters with different salt and nitrogen concentrations. The objective was to use the HYDRUS-1D software package to evaluate soil salinization and sodification risks in two agricultural fields irrigated with synthetic saline waters, and to quantify the effects of the salinity stress on nitrogen leaching. The model was further evaluated (i) to predict water contents and fluxes, (ii) to predict salinization and sodification risks by estimating the overall salinity given by the electrical conductivity of the soil solution (EC_{sw}), individual cations Na^+, Ca^{2+}, and Mg^{2+}, and sodium adsorption ratio (SAR), (iii) to quantify water uptake reductions due to the use of saline waters, and (iv) to predict N-NH_4^+ and N–NO_3^- concentrations in the soil and their leaching under field conditions.

The major ion chemistry (or UNSATCHEM) module of HYDRUS-1D successfully simulated the water regime (root mean square error, RMSE = 0.04 cm^3 cm^{-3}), EC_{sw} (RMSE = 0.87–2.35 dS m^{-1}), the concentration of soluble Na^+ (RMSE = 6.44–13.86 $mmol_c$ L^{-1}), Ca^{2+} (RMSE = 3.57–5.66 $mmol_c$ L^{-1}), Mg^{2+} (RMSE = 1.75–4.16 $mmol_c$ L^{-1}), and SAR (RMSE = 3.91–6.27 ($mmol_c$ L^{-1})$^{0.5}$) in different plots of each experimental field. RMSE were always lower in the soil with coarse texture of Mitra than in the soil with medium texture of Alvalade. The less favorable hydraulic conditions of Alvalade, as compared to Mitra, namely the lower saturated hydraulic conductivity (*Ks*) values of the soil with medium texture, were here decisive for not obtaining higher levels of performance in the goodness-of-fit tests for this soil.

HYDRUS-1D was able to predict root water uptake reductions due to water and osmotic stresses. Maize potential transpiration was reduced by about 39% in the experimental plots at Alvalade and 77% at Mitra, due to water stress. These water stress reductions were a consequence of the soil physical and hydrodynamic characteristics and plant type, but mostly of the irrigation schedule adopted. Potential transpiration was further reduced by about 59% at Alvalade and 83% at Mitra due to the effects of the osmotic stress in the plots irrigated with saline waters.

Root water uptake reductions obtained with the major ion chemistry module were then reproduced with the standard HYDRUS solute transport module in order to study the effect of salinity stress on nutrient uptake. HYDRUS-1D successfully modeled N–NH_4^+ (RMSE = 0.05–0.07 $mmol_c$ L^{-1}) and N–NO_3^- (RMSE = 2.01–2.60 $mmol_c$ L^{-1}) concentrations while either

assuming or neglecting the effect of the osmotic stress on nutrient uptake. According to HYDRUS-1D simulations, irrigation with saline waters led to root water and nutrient uptake reductions due to osmotic stress. Consequently, the fluxes of $N–NH_4^+$ and $N–NO_3^-$ through the bottom of the soil profiles increased. The simulated cumulative $N–NO_3^-$ fluxes across the bottom of the soil profile for example, in the plots irrigated with saline waters of Alvalade and Mitra differed by 220.0 and 70 kg ha^{-1}, respectively, when compared with the plots irrigated only with fresh irrigation waters.

In this experiment, EC_{sw} was simulated as a nonreactive tracer using the standard HYDRUS solute transport module, and by considering the concentrations of individual anions and cations in the soil solution using the UNSATCHEM module. Both modeling approaches produced similar results. The most significant differences were found at the end of each crop season, after irrigation ended. During these periods, the standard HYDRUS solute transport module simply increased EC_{sw} linearly as the soil dried out, while the UNSATCHEM module produced a nonlinear increase of EC_{sw} as a result of cation exchange. Thus, results show that EC_{sw} can be adequately simulated as a nonreactive tracer. However, this approach is only relatively precise in the absence of processes of precipitation/dissolution (e.g., gypsum, calcite) in the soil profile. If these processes are relevant, the major ion chemistry module of HYDRUS needs to be used instead. On the other hand, results clearly showed that the major cations (Na^+, Ca^{2+}, and Mg^{2+}) and SAR can only be successfully simulated when considering the various interactions between the multiple cations and competition for sorption sites, i.e., when using the approach available in the UNSATCHEM module. Simpler models based on adsorption isotherms would have failed to reproduce field data.

The study presented in Chapter 3 was a follow up of the previous application. The HYDRUS-2D was used to model nitrogen fate in a plot with sweet sorghum while considering different drip fertigation and water quality scenarios. Field data were again used to calibrate and validate HYDRUS-2D for predicting (i) soil water contents and fluxes, (ii) EC_{sw} (here simulated as a nonreactive tracer), (iii) water uptake reductions due to the use of saline waters, and (iv) $N\text{-}NH_4^+$ and $N\text{-}NO_3^-$ concentrations in the soil and leaching. The HYDRUS-2D model was able to consider water and solute fluxes, and pressure head and concentration gradients in the horizontal direction, which had been previously neglected in the one-dimensional approach. Additionally, the two-dimensional modeling approach was able to better describe the drip irrigation system

used in the experiment and the complex physical and chemical processes that took place in the soil profile under this irrigation system.

In this study, the water contents, EC_{sw}, $N\text{-}NH_4^+$ and $N\text{-}NO_3^-$ concentrations simulated continuously with HYDRUS-2D during the entire field experiment, compared well with collected experimental data, resulting in a RMSE of 0.030 $cm^3\ cm^{-3}$, 1.764 dS m^{-1}, 0.042 $mmol_c\ L^{-1}$, and 3.078 $mmol_c\ L^{-1}$, respectively. Potential transpiration was reduced due to water stress by 21.9–27.4%, as a function of the adopted irrigation schedule during each crop season. In addition, sweet sorghum showed to be tolerant to the levels of salinity reached in the soil solution during the first crop season. However, the continuous application of synthetic saline waters in the following years (2008–2009) led to increasingly higher root water uptake reductions due to the combined effects of water and salinity stresses, i.e., root water uptake reductions 2.3–4.7% (in 2008) and 4.6–7.0% (in 2009) higher than those found in the plots irrigated with fresh waters. Hence, soil salinization and the increase of the salinity stress was related to the continuous and increasing amount of synthetic saline waters being applied in each experimental plot. Nonetheless, these marginal waters showed to be viable for irrigating sweet sorghum during a limited time period.

The leaching of N out of the root zone depended closely on drainage, the amount of N applied, the form of N in the fertilizer, and the time and number of fertigation events. Based on model simulations, leaching of nitrogen occurred mainly in the $N\text{-}NO_3^-$ form, reaching 41–70% of the total amount of $N\text{-}NO_3^-$ available in the soil system. These values were significantly lower than those observed for maize (67–80%, also in Alvalade; Chapter 2) since this crop is less tolerant to salinity than sweet sorghum. Higher $N\text{-}NO_3^-$ uptakes (and lower nutrient leaching) were obtained when the number of fertigation events was larger. The effects of the salinity stress on nutrient uptake (and inversely on nutrient leaching) was relatively small since sweet sorghum has a medium to high tolerance to salinity, and consequently there were only small reductions in transpiration due to the increase of the osmotic stress. The cumulative N uptake (2007-2009) for example, between plots irrigated with the highest amount of synthetic saline waters and fresh irrigation waters was only 17.9 kg ha^{-1}.

The logarithmic function describing the relation between $N\text{-}NO_3^-$ uptake, as estimated with HYDRUS-2D, and measured dry biomass yield (R^2 = 0.71) predicted sweet sorghum N

requirements to be between 130–180 kg ha^{-1}. These optimum values were lower than estimated N uptakes (>200 kg ha^{-1}) for the scenario with the highest levels of applied nitrogen, revealing some luxury uptake in these plots. However, that relatively large interval shows that the modeling approach was not sufficient to optimize N requirements for sweet sorghum, and that a more traditional approach needed to be applied for estimating optimum N needs for sweet sorghum.

The study presented in Chapter 4 analyzed the combined effects of soil salinity and nitrogen application on sweet sorghum yield functions using a more traditional approach. This study related crop yield with applied factors (water, nutrients), but could not consider the actual nutrient uptake, as done in Chapter 3. Thus, sweet sorghum yield functions were determined in terms of biomass (total, stems, and leaves dry biomass), sugar content (reducing and non-reducing), and total sugar yields. Relationships between sweet sorghum yield and applied factors (nitrogen and sodium) during the irrigation cycles were evaluated by stepwise multiple regression analysis.

Sorghum dry biomass (and sugar yield) presented the same diminishing returns for each incremental change of N that had been reported in Chapter 3. The multiple regression analysis further showed that the higher the amount of Na^+ applied to the soil with the irrigation water, the lower the level of N necessary to achieve maximum yield. This effect was explained by an accumulation of salts in the root zone, increasing the osmotic stress, and reducing plant transpiration, N uptake, and crop yield in the plots irrigated with saline waters. Also, results showed that although total dry biomass decreased, stems dry biomass, sucrose content, and sugar yield progressively increased throughout the years. This was attributed to the increasing amounts of irrigation applied throughout the years, which somehow minimized the effect of the salinity stress on those yield functions. Unfortunately, as HYDRUS software package has no crop growth module incorporated it was not possible to further study the relations between soil processes and crop yield.

The salinization and sodification risks resulting from the irrigation scenarios described in Chapters 2 and 3, and the consequent effects on nutrient uptake and leaching are based on the agreement between measured data and model simulations. Possible causes of disagreements between model simulations and experimental data were related to field measurements, model

input data, and model structure errors, and were extensively discussed in both Chapters, showing HYDRUS advantages and limitations for similar application.

One of the most relevant limitations is that HYDRUS only accounts for N processes that can be described with sequential first-order decay chains, such as nitrification, denitrification, and volatilization. Other nitrogen reactions, with probable relevance for long-term applications such as those described in Chapters 2 and 3, simply cannot be accounted for using this approach. Examples of such reactions are nitrogen fixation from the atmosphere, mineralization of crop residues and other organic wastes, mineralization of the soil humus fraction, and so on. As a result, the previously reported RMSE obtained for $N–NH_4^+$ and for $N–NO_3^-$ reflect errors caused by not considering processes other than nitrification, which were apparently relevant for describing residual concentrations. However, from an agronomical perspective where the efficient use of the fertilizer applied is one of the main objectives to achieve, the approach available in HYDRUS can be considered adequate. On the other hand, if the objective is to minimize the environmental impacts of fertilization practices, that approach may be considered too limited.

Another important reason explaining the disagreement between model simulations and experimental data was that since the modeling approaches presented in Chapters 2 and 3 were process-based, rather than conceptual, our input parameters were obtained/measured independently. In general, it was considered that it was superior to measure input material parameters independently rather than fitting them. The correspondence between measurements and model predictions would have obviously been better, had the input parameters been fitted using numerical modeling. However, the model that can be successfully run with independently measured input parameters is more robust for practical applications than calibrated models. Moreover, with this approach not only the used modeling approach was validated but also applied laboratory methodologies and various involved experimental procedures.

Chapters 2 and 3 proved that, in spite of the considerable demand on input data, both one and two-dimensional versions of HYDRUS can be seen as an effective and versatile tool that may become very useful for irrigation management in regions with scarce water resources where suitable waters are not always available for irrigation. HYDRUS software package was able to analyze two of the most important soil processes (i.e., transport and reactions of salts and

nitrogen species in the soil profile) resulting in degradation of groundwaters in these regions in an integrated way. HYDRUS, after proper calibration and validation, should be considered to be a useful tool for establishing sound irrigation policies in order to mitigate soil salinization/sodification and non-point source pollution from agricultural applications of fertilizers in irrigated areas of countries located in regions with arid, semi-arid, and even sub-humid conditions.

The most important limitation to a wider application of vadose zone models such as the HYDRUS software package is, as previously referred, the considerable demand on input data. In this sense, the soil hydraulic properties and solute transport parameters are among the input data most difficult to obtain. The PROPSOLO database presented in Chapter 5 was thus organized to provide the necessary soil information for developing pedotransfer functions (PTFs) to indirectly estimate those input parameters. This database contains practically all of the existing knowledge on the soil hydraulic properties (with the exception of a few specific retention points found in soil survey studies) and solute transport parameters of Portuguese soils. The only mandatory requirement is that soil data must be obtained using international referenced methodologies, which regretfully have not been followed in most soil survey studies recently published. Moreover, it is important to understand that the data gathered in the database was determined with the same methodologies that were validated during the experiments reported in Chapters 2 and 3, thereby justifying the use of PTFs in vadose zone modeling. The database is also compatible with most international databases developed with the same purpose as PROPSOLO, namely the European HYPRES and EU-HYDI databases, since there is the need to exchange data from time to time.

Currently, the PROPSOLO database contains a considerable amount of information on soil water retention functions, $\theta(h)$, of Portuguese soils (819 soil horizons/layers). However, the information on the hydraulic conductivity function, $K(h)$, is much more limited (300 soil horizons/layers), restraining the development of more reliable PTFs for this physical parameter than those currently available. Thus, there is a need to gain more knowledge on $K(h)$ since this parameter, and especially Ks, is normally much more variable than are water retention properties. Also, since the soil hydraulic information available in the database was mostly collected in soil profiles located in the Alentejo region of southern Portugal, it seems only relevant to further extend the database to other regions.

The study presented in Chapter 6 describes a set of class-PTFs developed from the information available in the PROPSOLO database. These class-PTFs are very basic tools to obtain reliable information on water retention properties of Portuguese soils and can be used in multiple applications, including irrigation water management and watershed modeling. The class-PTFs were established after stratifying data by texture classes, soil horizon, and bulk density. The accuracy of the predictions varied between 0.039–0.057 cm^3 cm^{-3}. The best performances were obtained for the class-PTFs established after grouping the data by the 12 texture classes based on the International Soil Science Society (ISSS) particle limits and bulk density. The class-PTFs were also able to provide similar, or even better, estimates than those obtained by much more sophisticated functions. However, the main advantages of these class-PTFs are the reduced number of basic predictors necessary to estimate the water retention properties of Portuguese soils, and their suitability for predicting water retention properties at larger scales.

That was demonstrated by combining the available 1:25.000 national soil survey maps with the class-PTFs, and by deriving maps with different available water capacity (AWC) estimates according to the hydraulic information provided by the class-PTFs used. The AWC maps were then used for modeling the water balance in a small catchment area with the Soil Water Assessment Tool (SWAT). Contrarily to the HYDRUS software package, SWAT is a conceptual model, and thus less sensitive to soil hydraulic properties inputs. Nonetheless, the data inputs provided by the class-PTFs contributed to a better soil characterization than when using coarse-scaled information. Therefore, the approach presented in Chapter 6 is the simplest, cheapest, and most feasible technique available today to modelers without many resources for characterizing water retention properties at large scales.

Chapter 7 presents another simple approach for predicting water retention properties. The objective of this study was to develop ternary diagrams for estimating point specific water retention values (the field capacity and wilting point) of Portuguese soils using a geostatistical approach. However, the same approach can theoretically be applied for estimating the soil hydraulic parameters of any continuous function describing $\theta(h)$ or $K(h)$.

The geostatistical approach was able to provide reliable estimates of soil water retention at -33 (assumed as corresponding to the field capacity) and -1500 (wilting point) kPa matric potentials using only the relative proportion of different grain size particles (sand, silt, and clay) as input

data. Basically, the ordinary kriging method calculated $\theta_{-33\ kPa}$ and $\theta_{-1500\ kPa}$ for all 4332 grid cells of each ternary diagram as a kind of weighted average of the measured values in the vicinity of each grid cell. The neighboring sample point values were weighted according to the semivariance as a function of distance to the prediction location. The kriging method also compensated for the effects of data clustering, by assigning individual points within a cluster less weight than isolated data points. This showed to be particularly useful when interpolating water content values to regions of the texture triangle where the information available in the development set was scarcer. The ordinary kriging method was also helpful to understand which estimates of the soil water retention were valid based on the values of the estimation variance, and thus extrapolations were avoided.

The RMSE values were 0.040 and 0.033 $cm^3\ cm^{-3}$ when comparing the estimates provided by the $\theta_{-33\ kPa}$ and $\theta_{-1500\ kPa}$ ternary diagrams, respectively, and the measured values included in the validation dataset. Those values are comparable to the results provided by most PTFs available today for estimating soil water retention properties of Portuguese soils. The ternary diagrams may thus serve as simplified tools for estimating those properties from particle size distribution and eventually serve as an alternative to the traditional statistical regression and data mining techniques used to derive PTFs. The only predictor needed is the particle size distribution, while the other comparable PTFs require relatively more input parameters. In terms of number of predictors, the ternary diagrams seem to be quite useful as they are the only PTFs that do not require bulk density, despite results are given in terms of volumetric water contents. Although this soil property is simple to measure, sampling undisturbed samples in different soil horizons/layers distributed over large areas for measuring bulk density may be a very laborious task.

The ternary diagrams developed in Chapter 7 ($\theta_{-33\ kPa}$, $\theta_{-1500\ kPa}$, and AWC) may potentially be useful for many scientific and technical domains, but they seem more relevant to agricultural water management, particularly irrigation management and scheduling. Various water balance models require the type of information provided by the ternary diagrams here developed at point scale. Those that are associated to a geographical information system and are applied at field scale can make even further use of these tools. However, if this study is also extended to the soil hydraulic parameters describing $\theta(h)$ or $K(h)$, the ternary diagrams can then have further applications.

The PTFs today available for estimating the water retention properties of Portuguese soils offer a wide variety of alternatives in terms of input parameters and can be applied in many different agronomical and environmental applications. Chapter 8 presents a first attempt for developing the same tools for Cape Verde. The objective of this study was to first gain knowledge on the hydraulic properties of the soils of Cape Verde, and then develop PTFs for estimating point specific water retention values for Cape Verde soils.

The soil water retention values at lower pressure heads of Cape Verde soils presented unusually high values when compared with soils from temperate regions. The differences in the hydrological behavior suggested the influence of mineralogical and pedo-genetic factors associated to the spatial arrangement of the solid constituents of the soils from dry tropical Cape Verde.

PTFs were derived to predict total porosity and point specific values of the water retention characteristics at -0.25, -1, -3.2, -10, -33, -100, and -1500 kPa from basic soil properties, namely texture and bulk density. Statistics showed a relatively good performance for those PTFs with RMSE varying between 0.038–0.086 cm^3 cm^{-3}. However, care should be taken when using those functions since Cape Verde PTFs always underestimated measured values between 0.014–0.075 cm^3 cm^{-3}, and since the wilting point seems to fall outside the range of the original database used to develop the PTFs. Nonetheless, the Cape Verde PTFs provide an important basis to support the use of simulation models aimed at improving irrigation water management practices in Cape Verde since it provided better estimates than three other published PTFs.

Based on the conclusions of this Thesis, the future perspectives for this work are:

- To relate the soil processes described in Chapters 2 and 3 with yield functions by applying a crop growth model to simulate plant development under those conditions;
- To evaluate simpler modeling approaches capable of quantifying the impacts of irrigation water quality on soil salinization, crop yield, and groundwaters;
- To further extent the PROPSOLO soil database to other regions of Portugal, particularly those with greater agronomic relevance (e.g., Ribatejo Oeste, southwest Alentejo, and Beira Interior);
- To increase the information on $K(h)$ available in the database;

- To evaluate the functional behavior of the existing PTFs and to compare it with relevant international PTFs;

To gain further knowledge on the hydraulic behavior of the soils of Cape Verde and other regions of Africa, namely $\theta(h)$ and $K(h)$ functions and their relations with the mineralogical constituents of those soils.

Symbols and acronyms

Symbols	Description	Units
θ	soil water content	L^3L^{-3}
$\theta(h)$	soil water retention function	L^3L^{-3}
θ_r	residual water content	L^3L^{-3}
θ_s	saturated water content	L^3L^{-3}
θ_p	predicted water content	L^3L^{-3}
θ_m	measured water content	L^3L^{-3}
$\theta_{-33\ kPa}$	volumetric soil water content at -33 kPa matric potential	L^3L^{-3}
$\theta_{-1500\ kPa}$	volumetric soil water content at -1500 kPa matric potential	L^3L^{-3}
S_e	effective saturation	
K	hydraulic conductivity	LT^{-1}
K_s	saturated hydraulic conductivity	LT^{-1}
$K(h)$	hydraulic conductivity function	LT^{-1}
$K(\theta)$	hydraulic conductivity function	LT^{-1}
h	matric pressure head	L^{-1}
ψ	matric potential	L^{-1}
l	number of water potentials for each horizon	
H	number of horizons	
α	empirical shape parameter	L^{-1}
η	empirical shape parameter	
ℓ	pore connectivity/tortuosity parameter	
Φ	total porosity	L^3L^{-3}
ρ	soil bulk density	ML^{-3}
ρ_b	dry bulk density	ML^{-3}
CS	coarse sand	MM^{-1}
FS	fine sand	MM^{-1}
$Si_{20\ \mu m}$	Silt fraction at 20 µm	MM^{-1}
$Si_{50\ \mu m}$	Silt fraction at 50 µm	MM^{-1}
C	clay	MM^{-1}
P	percolation	L
q	flux boundary condition	LT^{-1}
q	volumetric flux density	LT^{-1}
q_r	components of the volumetric flux density	LT^{-1}
q_z	components of the volumetric flux density	LT^{-1}
$\|q\|$	volumetric flux density (absolute value)	LT^{-1}
v	mean pore-water velocity	LT^{-1}
D	hydrodynamic dispersion coefficient	L^2T^{-1}
D_{rr}	component of the dispersion tensor	L^2T^{-1}
D_{zz}	component of the dispersion tensor	L^2T^{-1}
D_{rz}	component of the dispersion tensor	L^2T^{-1}
D_0	molecular diffusion coefficient of the solute in free water	L^2T^{-1}
R	retardation factor	
λ	dispersivity	L
ε_L	longitudinal dispersivity	L
ε_T	transversal dispersivity	L
τ	tortuosity factor	
K_d	linear distribution coefficient	L^3M^{-1}
$K_{Ca/Na}$	Gapon selectivity coefficient	
$K_{Mg/Ca}$	Gapon selectivity coefficient	
$K_{Ca/K}$	Gapon selectivity coefficient	
ϕ	chemical reactions of solutes involved in a sequential first-order decay chain	$ML^{-3}T^{-1}$

Symbols and acronyms

μ_w	first-order rate constant for solutes in the liquid phase	T^{-1}
μ_s	first-order rate constant for solutes in the solid phase	T^{-1}
c	solute concentrations in the liquid phase	ML^{-3}
$\bar{c}$	solute concentrations in the solid phase	ML^{-3}
c_r	solute concentrations in the sink term	ML^{-3}
c_{root}	solute concentrations in the sink term	ML^{-3}
c_{max}	maximum concentration of the root uptake	ML^{-3}
c_{sum}	sum of the solute concentrations	ML^{-3}
S	sink term accounting for water uptake by plant roots	$L^3L^{-3}T^{-1}$
$S_p(z,t)$	potential root water uptake	$L^3L^{-3}T^{-1}$
$S(h, h_\phi, z, t)$	actual volume of water removed from unit volume of soil per unit of time	$L^3L^{-3}T^{-1}$
$\beta(z,t)$	normalized root density distribution function	L^{-1}
ET_0	reference evapotranspiration rate	LT^{-1}
ET_c	crop evapotranspiration rate	LT^{-1}
K_c	crop coefficient	
K_{cb}	basal crop coefficient	
K_e	soil evaporation coefficient	
$K_{cb\ ini}$	basal crop coefficient during crop initial stage	
$K_{cb\ mid}$	basal crop coefficient during crop mid-season stage	
$K_{cb\ mid}$	basal K_{cb} during mid-season when the LAI is smaller than for full cover conditions	
$K_{cb\ end}$	basal crop coefficient during crop end season stage	
$K_{cb\ full}$	basal K_{cb} during mid-season for vegetation having LAI>3	
$K_{c\ min}$	minimum K_c for bare soil	
$K_{c\ max}$	maximum value of K_c following rain or irrigation	
K_r	dimensionless evaporation reduction coefficient	
Z_e	thickness of evaporation soil layer	L
f_{ew}	fraction of the soil surface from which most evaporation occurs	
f_w	fraction of soil surface wetted by irrigation	
L_{ini}	length of crop initial stage	T
L_{dev}	length of crop development stage	T
L_{mid}	length of crop mid-season stage	T
L_{late}	length of crop end season stage	T
T_p	potential transpiration rate	LT^{-1}
T_a	actual transpiration rate	LT^{-1}
T	crop transpiration rate	LT^{-1}
E	soil evaporation rate	LT^{-1}
$\alpha(h)$	water stress	
$\alpha(h_\phi)$	osmotic stress	
P_a	passive root nutrient uptake	$ML^{-2}T^{-1}$
A_t	area of the soil surface associated with transpiration	L^2
L_R	root domain	L
Ω	root domain	L^3
r_m	maximum radius of the root zone	L
z_m	maximum depth of the root zone	L
z^*	location of the maximum root water uptake in vertical direction	L
r^*	location of the maximum root water uptake in horizontal direction	L
EC	electrical conductivity	dS m^{-1}
EC_{sw}	electrical conductivity of the soil solution	dS m^{-1}
EC_e	electrical conductivity of the saturation extract	dS m^{-1}
EC_{iw}	electrical conductivity of the irrigation water	dS m^{-1}
EC_T	salinity threshold	dS m^{-1}
$h_{\phi T}$	salinity threshold	L
C_2	medium-salinity water	
C_3	high-salinity water	

C_4	very high salinity water	
S_1	low-sodium water	
S_4	very high sodium water	
S_i	salinity gradient (i = 0, 1, 2)	
N_i	nitrogen gradient (i = 0, 1, 2, 3)	
k_{EC}	ratio of the electrical conductivity of the *in situ* soil water at field capacity	
s	root water uptake decline per unit increase in salinity above EC_T	
$s*$	root water uptake decline per unit increase in osmotic head below EC_T	
$pIAP$	negative logarithm of the ion activity product	
t	time	T
z	vertical space coordinate	L
r	radial space coordinate	L
Z	mean depth	L
W	fresh water	
W	width of crop leafs	L
L	Length of crop leafs	L
n	number of green leafs on each measured sorghum plant	
Y	sorghum yield	ML^{-2}
y	sorghum yield	ML^{-2}
Y_{total}	total dry biomass	ML^{-2}
Y_{stems}	stems dry biomass	ML^{-2}
Y_{leaves}	leaves dry biomass	ML^{-2}
Y_{TRS}	total reducing sugars content	MM^{-1}
$Y_{sucrose}$	sucrose content	MM^{-1}
Y_{sugar}	sugar yield	ML^{-2}
Y_1	dummy variable	
Y_2	dummy variable	
$n(h)$	number of pairs of observation points of the variable Z	
h	distance separating pairs of observation points in the semivariogram	L
C_0	nugget	
C_1	sill	
a	range	L
$Z^*(x)$	kriging estimator	
λ_i	weight of observations at each location i	
E[ ]	expected value	
m	mean value of $Z(x)$	L^3L^{-3}
γ	semivariance between data pairs	
μ	Lagrange parameter	
σ^2	estimation variance	
Ct	total variance	
CP	cumulative percentage on the particle-size distribution curve	MM^{-1}
$-\Phi$	$\log_2$ value of the particle-size limits notations	
O_i	observations	
P_i	model predictions	
N	number of observations	
$\overline{O}$	average of the measured values	
$\overline{P}$	average of the model predictions	
x_m	média	
σ	desvio padrão	
a_i	regression coefficients (i = 1, 2, …, n)	
x_i	arguments of the regression function (i = 1, 2, …, n)	

Subscripts **Description**

Symbols and acronyms

k	chemical species
k	data pairs used in the variogram
i	matric potential
i	time
j	horizon
n	missing particle-size limit
n-1	preceding neighbouring limit
n+1	succeeding neighbouring limit

Acronyms	**Description**	**Units**
AWC	available water capacity	LL^{-1}
CDE	convection–dispersion equation	
CEC	cation exchange capacity	MM^{-1}
DAS	days after sowing	T
DCS	Departamento de Ciência do Solo	
EAN	Estação Agronómica Nacional	
ESP	exchangeable sodium percentage	%
EU-HYDI	European Hydropedological Data Inventory	
FRS	free reducing sugars	MM^{-1}
GM	geometric mean	
GPD	mean particle diameter	L
GSD	geometrical standard deviation	L
HYPRES	Hydraulic Properties of European Soils	
ISSS	International Soil Science Society system	
LAI	leaf area index	L^2L^{-2}
LAI_{max}	maximum leaf area index	L^2L^{-2}
LSD	least significant difference	
MAE	mean absolute error	
ME	mean error	
MEP	mean error of predictions	
MRE	mean relative error	
NSE	coefficient of efficiency	
OC	organic carbon contente	MM^{-1}
PROPSOLO	Propriedades do solo	
PTF	pedotransfer function	
R^2	coefficient of determination	
RA	regression analysis	
REW	readily evaporable water	L
RH	relative humidity	%
RMSE	root mean square error	
SAR	sodium adsorption ratio	$(ML^{-3})^{0.5}$
SCF	soil cover factor	
SCS	Soil Conservation Services	
SIG	Sistema de Informação Geográfica	
SQL	Structured Query Language	
SSE	sum of squares due to error	
SSR	sum of squares due to regression	
SWAT	Soil and Water Assessment Tool	
TDR	Time Domain Reflectometry	
TEW	total evaporable water	L
TRS	total reducing sugars	MM^{-1}
UNSODA	Unsaturated Soil Hydraulic Database	
USDA	United States Department of Agriculture	

WISE	World Inventory of Soil Emission Potentials

Texture	**Description**
Ar	textura arenosa
ArF	textura areno-franca
FAr	textura franco-arenosa
F	textura franca
FL	textura franco-limosa
FAAr	textura franco-argilo-arenosa
FA	textura franco-argilosa
FAL	textura franco-argilo-limosa
AAr	textura areno-argilosa
AL	textura argilo-limosa
A	textura argilosa
C	coarse texture class
M	médium texture class
MF	medium fine texture class
F	fine texture class
VF,	very fine texture classe
S	sand
LS	loamy sand
SL	sandy loam
L	loam
SCL	sandy clay loam
CL	clay loam
SC	sandy clay
C	clay
SiC	silty clay
SiCL	silty clay loam
SiL	silty loam
Si	sillt